New Biocatalysts for Synthetically Useful Metabolites from Available Phenols

A thesis submitted to the University of Manchester for the Degree of Doctor of Philosophy in the Faculty of Science and Engineering

2018

Daniel Howard

School of Chemistry

Contents

Abbreviations

MeCN	Acetonitrile
Anydr.	Anhydrous
aq	Aqueous
Ar	Aryl
ax	Axial
BPDO	Biphenyl dioxygenase
BINAP	2,2'-bis(diphenylphosphino)-1,1'-binaphthyl
BDA	Butan-2,3-diacetal
CSA	Camphorsulfonic acid
^{13}C	Carbon-13 isotope
cat.	Catalytic
CDO	Catechol-2,3-dioxygenase
δ	Chemical shift - delta
$[RhCl(cod)]_2$	Chloro(1,5-cyclooctadiene)rhodium(I) dimer
$CHCl_3$	Chloroform
C or conc	Concentration
CuI	Copper(I) iodide
CuTC	Copper(I) thiophene-2-carboxylate
J	Coupling constant value
COTC	2-Crotonyloxymethyl-(4*R*, 5*R*, 6*R*)-4,5,6-trihydroxycylohex-2-enone
°C	degree Celsius
C_6D_6	Deuterated benzene
$CDCl_3$	Deuterated chloroform
CD_3OD	Deuterated methanol
DBU	1,8-Diazabicyclo[5.4.0]undec-7-ene
CH_2Cl_2	Dichloromethane
DAST	Diethylaminosulfur trifluoride
DIBAL	Diisobutylaluminium hydride
DIPEA	*N*,*N*-Diisopropylethylamine
2,2-DMP	2,2-Dimethoxypropane
DMAP	4-(Dimethylamino)pyridine

DMF	Dimethylformamide
MTT	3-(4,5-Dimethylthiazol-2-yl)-2,5-diphenyltetrazolium bromide
CDD	*cis*-Diol dehydrogenase
ES	Electrospray mass spectrometry
e.e.	Enantiomeric excess
eq	Equatorial
eq.	Equivalents
E. coli	*Escherichia coli*
EtOH	Ethanol
EtOAc	Ethyl acetate
GC	Gas chromatography
GSH	Glutathione
g	Gram(s)
IC_{50}	Half maximal inhibitory concentration
Hz	Hertz
HRMS	High resolution mass spectrometry
h	Hour(s)
^{1}H	Hydrogen-1 isotope
LC TOF/MS	Liquid chromatography time of flight mass spectrometry
LB	Lysogeny broth
m.p.	Melting point
CH_3SO_2Cl	Methanesulfonyl chloride
MeOH	Methanol
µL	Microlitre(s)
µM	Micromolar
mg	Milligram(s)
mL	Millilitre(s)
mmol	Millimole(s)
min	Minute(s)
M	Molar
MBH	Morita-Baylis-Hillman
nm	Nanometre(s)
nM	Nanomolar

NDO	Naphthalene dioxygenase
NMR	Nuclear magnetic resonance
OD	Optical density
p-TSA	*Para*-toluenesulfonic acid
log P	Partition coefficient
ppm	Parts per million
X % Pd/C	Percentage of palladium on carbon
$HClO_4$	Perchloric acid
Ph	Phenyl
P. putida	*Pseudomonas putida*
RDS	Rate-determining step
RT	Room temperature
RPMI	Roswell Park Memorial Institute
rpm	Rotations per minute
$NaBH_4$	Sodium borohydride
SDS	Sodium dodecyl sulphate
NaH	Sodium hydride
$NaHCO_3$	Sodium hydrogen carbonate
NaOH	Sodium hydroxide
$NaIO_4$	Sodium *meta*-periodate
THF	Tetrahydrofuran
ISP	Terminal iron-sulfur protein
TLC	Thin layer chromatography
TDO	Toluene dioxygenase
Tol	Tolyl
SOTol	(*p*-Tolylsulfinyl)methyl
Et_3N	Triethylamine
TESOTf	Triethylsilyl trifluoromethanesulfonate
TFA	Trifluoroacetic acid
TMSCl	Trimethylsilyl chloride
H_2O	Water

Abstract

Toluene dioxygenase (TDO) is a Rieske type non-haem enzyme found within the soil bacteria, *Pseudomonas putida* (*P. putida*) and is responsible for catalysing the enantioselective *cis*-dihydroxylation of aromatic substrates. This remarkable trait of the TDO enzyme has enabled its application in the preparation of over 400 novel *cis*-diol bioproducts using whole cell biocatalysis. Recently, a new and synthetically useful bioproduct, (4*S*,5*S*)-4,5-dihydroxy-3-iodocyclohex-2-en-1-one, has been identified from the TDO catalysed biotransformation of 3-iodophenol. The purpose of this project was to demonstrate the synthetic application of this new bioproduct in the synthesis of natural product analogues, which possess anti-proliferative activity against different cancer cell lines. This was achieved by developing methodology towards a key enone building block, which was successfully applied in the synthesis of an analogue of the natural product incarviditone. Furthermore, a robust computational docking model was developed using the Gold™ software, which showed significant correlation between the predicted docking outcome and the experimentally observed results for a series of monocyclic substrates. The docking model was also used to rationalise the major and minor binding modes of the 3-iodophenol substrate in the TDO enzyme active site. The project also sought to develop an alternative synthetic methodology using butan-1,2-diacetal (BDA) protected (-)-quinic acid, which would provide the same stereochemical outcome as the newly discovered bioproduct. This was achieved despite considerable synthetic challenges encountered when trying to control the diastereoselectivity of a key conjugate addition reaction. The antipodal compounds of the natural product analogues obtained using the 3-iodophenol bioproduct and BDA protected (-)-quinic acid were also synthesised using acetonide protected (-)-quinic acid. By reacting the enantiomers of a key hydroxyenone intermediate obtained using the two pathways, a novel heterodimerisation was reported to afford an analogue of the natural product, incarvilleatone. Finally, all the biological activities of the synthesised natural product analogues were evaluated using the MTT (3-(4,5-dimethylthiazol-2-yl)-2,5-diphenyltetrazolium bromide) assay: the results showed significant differences between the enantiomers of the incarviditone natural product analogues.

Declaration and Copyright Statement

No portion of the work referred to in this thesis has been submitted in support of an application for another degree or qualification of this or any other university or other institute of learning.

i. The author of this thesis (including any appendices and/or schedules to this thesis) owns certain copyright or related rights in it (the "Copyright") and s/he has given The University of Manchester certain rights to use such Copyright, including for administrative purposes.

ii. Copies of this thesis, either in full or in extracts and whether in hard or electronic copy, may be made only in accordance with the Copyright, Designs and Patents Act 1988 (as amended) and regulations issued under it or, where appropriate, in accordance with licensing agreements which the University has from time to time. This page must form part of any such copies made.

iii. The ownership of certain Copyright, patents, designs, trademarks and other intellectual property (the "Intellectual Property") and any reproductions of copyright works in the thesis, for example graphs and tables ("Reproductions"), which may be described in this thesis, may not be owned by the author and may be owned by third parties. Such Intellectual Property and Reproductions cannot and must not be made available for use without the prior written permission of the owner(s) of the relevant Intellectual Property and/or Reproductions.

iv. Further information on the conditions under which disclosure, publication and commercialisation of this thesis, the Copyright and any Intellectual Property and/or Reproductions described in it may take place is available in the University IP Policy (http://documents.manchester.ac.uk/DocuInfo.aspx?DocID=487), in any relevant Thesis restriction declarations deposited in the University Library, The University Library's regulations (http://www.manchester.ac.uk/library/aboutus/regulations) and in The University's policy on Presentation of Theses.

Acknowledgements

To Dr Roger Whitehead,

Thank you for giving me the opportunity to come and experience Manchester and to develop under your tutelage. Like all PhDs, there were testing challenges along the way; however, I have gained invaluable experience both professionally and personally. It was, without a shadow of a doubt, a pleasure to have completed a PhD within your research group. I hope along the way you came to love my St Helens twang and our, slightly crazy, lab atmosphere.

To Prof Ian Stratford, Prof Nicolas Turner and Dr Richard Bryce,

Thank you for providing me with the opportunity to expand my knowledge of cell biology, biocatalysis and computational chemistry. The multidisciplinary nature of this PhD has given me invaluable experience and a deeper appreciation of different scientific disciplines.

To Agata Brzeźniak,

One of the many highlights of this PhD has been the opportunity to develop new friendships. I could not imagine what this experience would have been like without you there in the lab. Thank you for stopping me from 'quitting' my PhD at least 30 times and thank you for all the amazing antics we got up to during our PhD. It has, however, taught me that we should be separated in the event of an office move, which requires the removal of computer cables. You are a true partner in crime and it was an experience I wouldn't trade for the world.

To Ali Raoof, Laura Johnson and Vikki Clayton,

The 'not so temporary' residents and my friends from Cancer Research UK. What a relief it was to find out that you were just as mad as the rest of us. Every cloud does have a silver lining, and despite the unfortunate circumstance that led you to joining our group, it was a pleasure to have shared the final year of my PhD with the lot of you.

To Yiwei Song and Ellie French,

Thank you both for helping me with my cell biology. Ellie I will miss your particular music choices and our everyday crazy antics.

To Mum, Dad, Nan and both Grandads,

This would of all not been possible without your support. There are no words that describe just how grateful I am to you all.

A special thank you to Christopher Lovett, the staff at the School of Chemistry and the Masters/PGT students over the years.

1.0 Introduction

The relevance of natural products in therapeutic drugs can be epitomised by the 2016 meta-review by Newman and Cragg, which showed that 42 % of clinically approved drugs between 1981 and 2014 were derived from natural products. This percentage increased to 56 % when synthetic drugs based on natural product pharmacophores were considered.[1] Natural product synthesis, however, can be complex and challenging because of the structural intricacy and multiple stereogenic centres. Nature's solution to these problems is to employ enzymes to carry out the necessary transformations, which can proceed regio- and stereoselectively under mild reaction conditions.

Unsurprisingly, the field of biocatalysis is rapidly expanding with significant impact already made in the production of food, fine chemicals and pharmaceuticals.[2] By applying an existing enzyme toolkit to natural product synthesis, in combination with mutagenesis (e.g. directed evolution), difficult or otherwise impossible chemical transformations can be accomplished. Furthermore, the bioproducts obtained from enzyme catalysed biotransformations can be used as synthetically useful chiral building blocks.

Herein is discussed the dioxygenase enzyme with specific focus on toluene dioxygenase (TDO). A new class of substrate for TDO is detailed, and its synthetic application towards analogues of the natural products: incarviditone, incarvilleatone, pseudohygrophorones and COTC was explored.

1.1 Dioxygenases

Dioxygenases (DO) are a family of oxidoreductase enzymes, which use molecular oxygen to oxidise a target substrate. They accomplish this transformation by incorporating both oxygen atoms into the resulting metabolite (see **Scheme 1**).

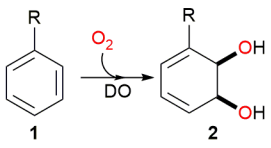

Scheme 1: The biotransformation of an arene substrate, of general structure **1**, to afford dihydroxylated bioproduct **2** using a dioxygenase (DO) enzyme.

These biocatalysts are ubiquitous in nature and are found in prokaryotic microorganisms, such as *Pseudomonas putida* (*P. putida*, toluene dioxygenase) and more complex

eukaryotic organisms such as humans (e.g. IDO, indoleamine-pyrrol 2,3-dioxygenase).[3] Remarkably, the dioxygenases can catalyse the regio- and enantioselective oxidation of aromatic substrates, whilst dearomatising the ring during the process. Synthetically this is a challenging reaction, and so far, there are no reported methods in the literature for the controlled incorporation of two oxygen atoms into an aromatic substrate. This can be attributed to the stabilisation provided by aromatic resonance, disruption of which would be thermodynamically unfavourable.

Most dioxygenases require a metal co-factor, the most prevalent of which are iron(II) and iron(III), to carry out the oxidative biotransformation. Iron containing oxygenases can be classified into three subgroups: haem-dependent, non-haem dependent and Rieske type.[4]

In the context of dioxygenases, the focal point of this thesis is toluene dioxygenase (TDO) from *Pseudomonas putida*. TDO is classified as a Rieske type non-haem iron dioxygenase, due to each α subunit containing a [2Fe-2S] cluster and a non-haem iron(II) core (see **Figure 1**).[5,6]

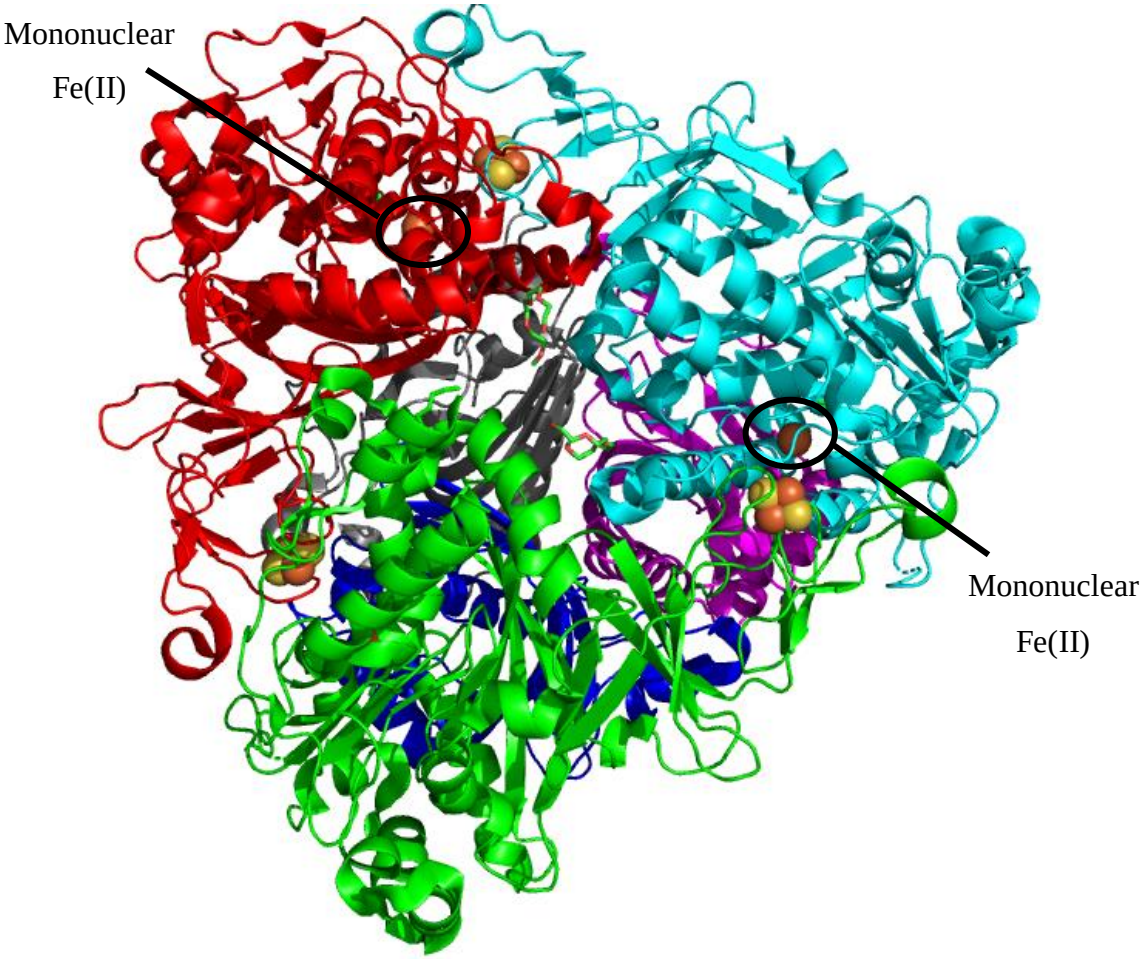

Figure 1: The protein structure of the heterohexamer TDO enzyme, showing the mononuclear iron(II) core and the Rieske [2Fe-2S] cluster. α-units = red, green and cyan; β-units = blue, grey and magenta; Fe = orange; S = yellow.[7]

TDO is commonly found in soil bacteria, namely *P. putida*, which have developed diverse metabolic biodegradation pathways to sustain their carbon source in various ecological niches.[8] *P. putida* is unique: it possesses a complex network of biodegradation pathways it can regulate at a transcriptional level. The Entner-Doudoroff (ED) pathway, responsible for the metabolism of glucose, is one example of a biodegradation pathway utilised by *P. putida*. (see **Scheme 2**).[9, 10, 11]

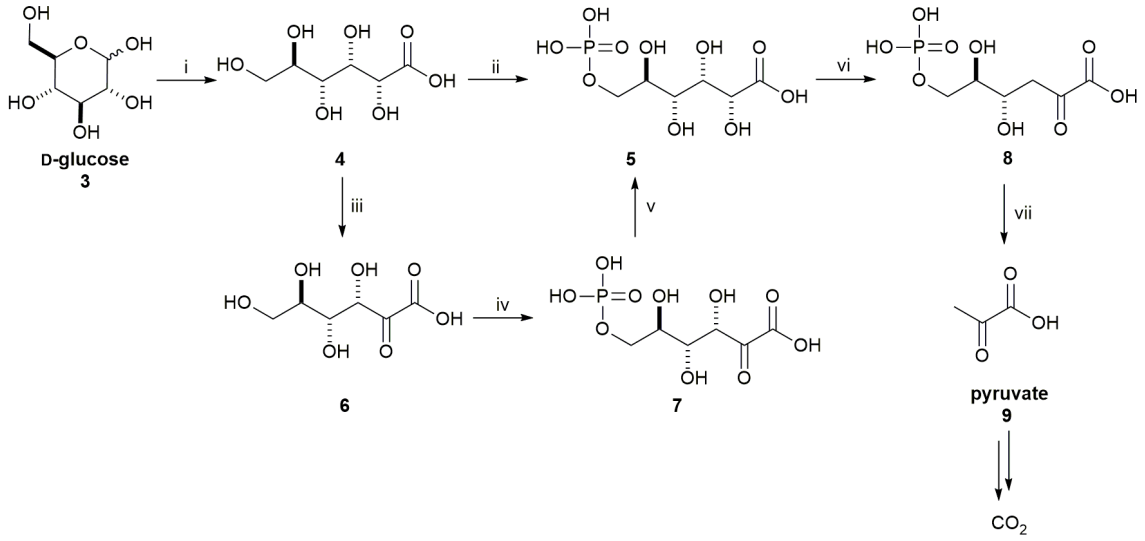

Scheme 2: The Entner-Doudoroff pathway. i = Glucose dehydrogenase; ii = gluconate kinase; iii = gluconate 2-dehydrogenase; iv = 2-ketogluconate kinase; v = 2-ketogluconate-6-*P* reductase; vi = 6-phosphogluconate dehydratase; vii = 2-keto-3-deoxy-6-phosphogluconate aldolase. **3** = glucose; **4** = gluconate; **5** = 6-*P*-gluconate; **6** = 2-ketogluconate; **7** = 2-ketogluconate-6-*P*; **8** = 2-keto-3-deoxy-6-phosphogluconate; **9** = pyruvate.

The ED pathway is atypical of glucose metabolism in many organisms, which characteristically proceed via the Embden-Meyerhof-Parnas (EMP) pathway. The EMP pathway, however, cannot operate in the *Pseudomonas* genus on account of the bacteria lacking the 6-phosphofructo-1-kinase enzyme. The major components of the ED pathway are the enzymes 6-phosphogluconate dehydratase and 2-keto-3-deoxy-6-phosphogluconate aldolase, which catalyse the conversion of **5** into **8** and **8** into pyruvate (**9**) respectively. This pathway also works alongside the anabolic pentose phosphate pathway, which also metabolises glucose. In the presence of aromatic substrates however, *P. putida* utilises an additional biodegradation channel, the catabolic dihydrodiol pathway, which employs a dioxygenase in the initial step (see **Scheme 3**).[12]

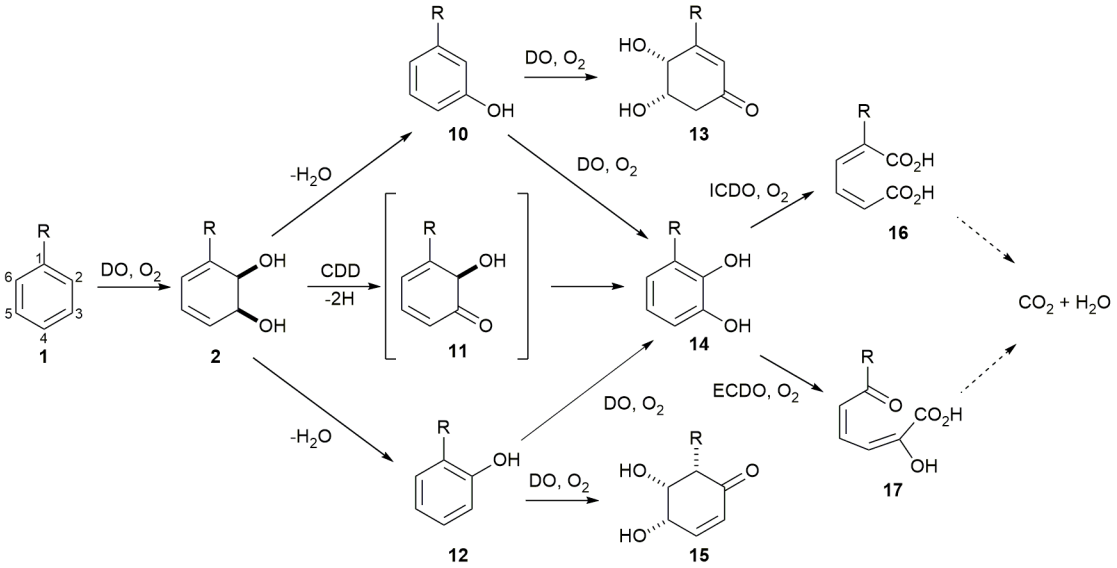

Scheme 3: The pathway of biodegradation for mono-substituted aromatic hydrocarbons. DO = dioxygenase, CDD = *cis*-diol dehydrogenase, ICDO = intradiol catechol dioxygenase, ECDO = extradiol catechol dioxygenase.[13]

The first key step is the dioxygenase (DO) catalysed *cis*-dihydroxylation of a mono-substituted arene of general structure **1** to afford *cis*-diol **2**. **2** can readily eliminate water to form the corresponding *meta* and *ortho* substituted phenols **10** and **12** respectively. Alternatively, the reaction of *cis*-diol **2** can be catalysed by the *cis*-diol dehydrogenase enzyme to form the intermediate α-ketol **11**, which readily tautomerises to form the more stable catechol **14**. *m*-Phenol **10** and *o*-phenol **12** can also form catechol **14** via the dioxygenase catalysed dihydroxylation across the 2,3-bond, followed by elimination of water. Conversely, **10** and **12** can be hydroxylated across the 5,6-bond to form β-ketols **13** and **15** respectively. Following the formation of **14**, two alternative pathways are used for further biodegradation. In the presence of O_2, intradiol catechol dioxygenase (ICDO) catalyses the ring opening to form *cis*-*cis*-muconic acid (**16**), whereas extradiol catechol dioxygenase (ECDO) catalyses the formation of hydroxymuconic semialdehyde (**17**). From here, these two bioproducts proceed into different downstream biodegradation pathways: **16** is biodegraded via the β-ketoadipic acid pathway and **17** by the hydroxymuconic semialdehyde hydrolase enzyme.[14,15] It is, however, the catalysed formation of *cis*-diol **2** that is the most remarkable step in the dihydrodiol biodegradation pathway. The dioxygenase selectively dihydroxylates at the 2,3-bond of the aromatic substrate (**1**) to form *cis*-diol metabolite **2** enantioselectively, simultaneously breaking the aromaticity of the ring.

In 1977, Gibson and co-workers were the first to suggest that the dioxygenase catalysed biotransformation of **1** to **2** requires a multicomponent system. At the time, they were unable to achieve the full purification of the distinct components, partly due to the instability of the cell extracts, but by comparison to similar enzymatic systems they concluded that it consists of a flavoprotein and two separate iron components. Furthermore, they determined that one of the iron components contains a ratio of 2 moles of iron to 2 moles of sulfur.[16] Continued studies by the Gibson research group formally confirmed the presence of a reductase flavoprotein, a ferredoxin and a Rieske [2Fe-2S] cluster, dubbed the iron-sulfur protein (ISP) (see **Scheme 4**).[17, 18]

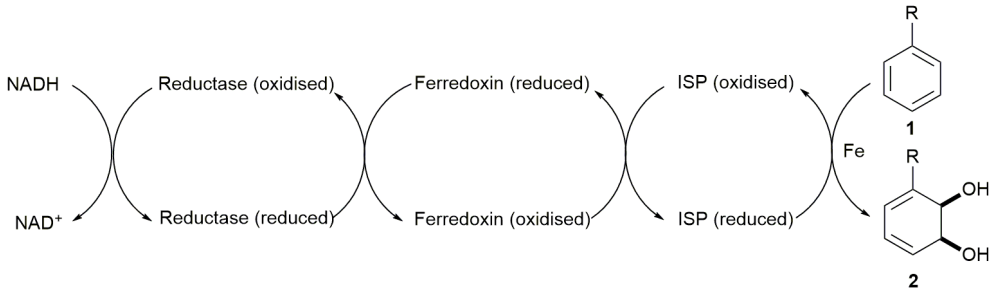

Scheme 4: The multi-component toluene dioxygenase catalysed dihydroxylation. ISP = terminal iron-sulfur protein.[19]

The cycle starts with the flavoreductase accepting two electrons from the coenzyme NADH. Studies by Subramanian and co-workers showed that a FAD co-factor was the only electron-transfer component within the reductase; therefore, ruling out the presence of a metalloflavoreductase which is present in similar systems (e.g. methane monooxygenase).[18] From here, the reductase facilitates a one-electron transfer to the ferreodoxin whose role is to link the reductant to the ISP. It was noted that the activity of TDO only occurred if all three components were present.[20] The ferredoxin then shuttles an electron to the ISP, which is comprised of a Rieske [2Fe-2S] cluster coordinated to two cysteine and two histidine residues, in addition to a His-His-carboxylate triad (**Figure 2**), which binds the mononuclear iron core responsible for *cis*-dihydroxylation.[21] The primary function of the His-His-carboxylate facial motif is to anchor the mononuclear iron core, and to leave three *cis*-orientated coordination sites available for the binding of a substrate and O_2.[22]

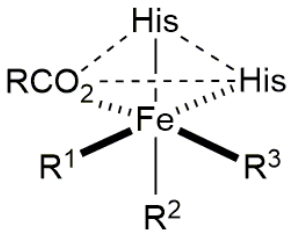

Figure 2: The His-His-carboxylate facial triad coordinated to a mononuclear iron core. R^1, R^2 and R^3 represent the available coordination sites.

The exact mechanism of how iron catalyses the formation of *cis*-diol **2** remains under dispute; however, Boyd and co-workers collated the suggested mechanisms for evaluation and these are shown in **Scheme 5**.[8, 23]

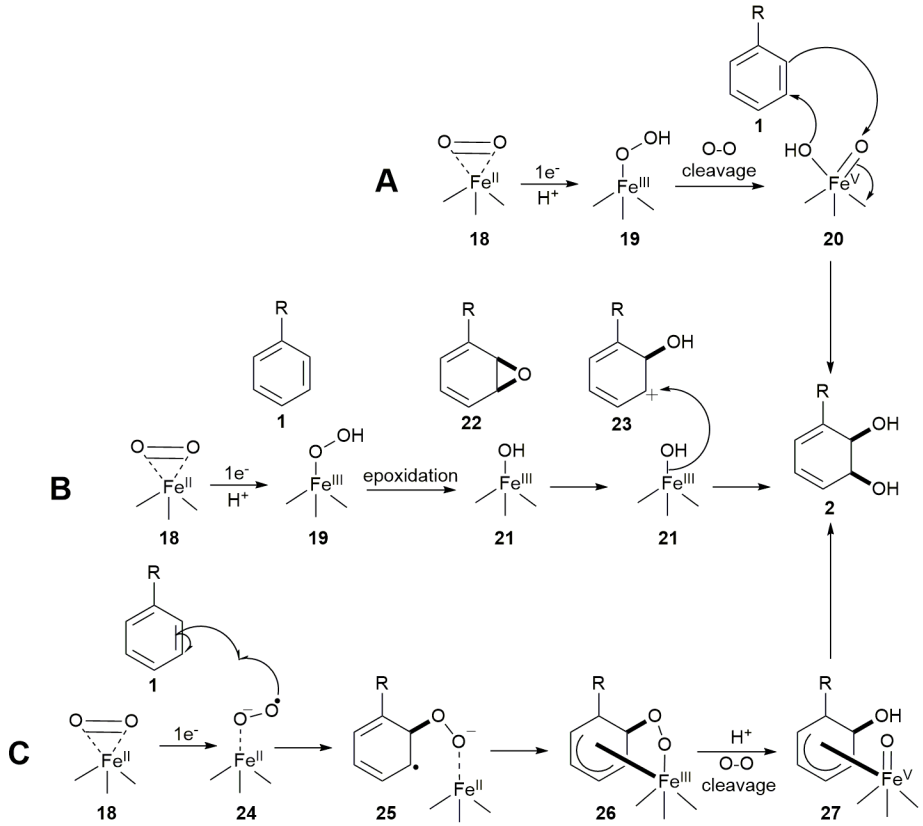

Scheme 5: The proposed mechanisms for the *cis*-dihydroxylation of mono-substituted arenes by the dioxygenase enzymes.

Much of the evidence for the dioxygenase mechanism is derived from naphthalene dioxygenase (NDO). TDO's instability outside the cell, coupled with the difficulty in obtaining a crystal structure, makes it unsuitable for mechanistic studies. There is a good agreement within the literature and between all three pathways that the mechanism is commenced with a one electron transfer from the Rieske [2Fe-2S] cluster to the mononuclear iron. This process cannot be carried out within the same α-subunit as the

distance between the mononuclear iron core and the Rieske [2Fe-2S] cluster in NDO enzyme is 43.5 Å, which is inadequate for an efficient one electron transfer. X-ray crystallography studies, however, have showed that the distance from one α subunit [2Fe-2S] cluster to a neighbouring α subunit mononuclear iron is 12 Å in NDO. This characteristic is also conserved in other dioxygenase enzymes, for instance in phthalate dioxygenase the same distance is approximately 10 Å; thus, implying that the close proximity of these two components from separate α domains is a vital aspect of the catalytic mode of action. The electron transfer pathway is facilitated by His_{104}-Asp_{205}-His_{208} (**28**), which connects the [2Fe-2S] cluster to the mononuclear iron as illustrated by **Figure 3**.[21]

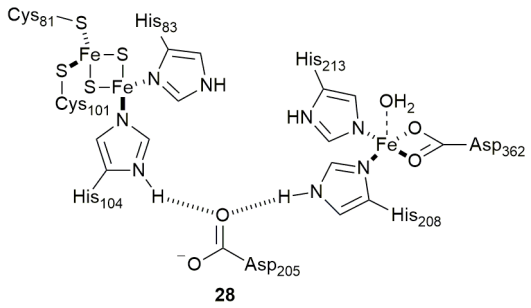

Figure 3: The one electron transfer pathway from an α subunit Rieske [2Fe-2S] cluster to a mononuclear iron core situated in a neighbouring α subunit.

The importance of this pathway was validated by site-directed mutagenesis, whereby the Asp_{205} residue was changed to alanine and all enzyme activity was lost.[21] Furthermore, it was established early on that both oxygen atoms from O_2 are incorporated into the final product. In 1970, Gibson and co-workers used ^{18}O labelling studies on the TDO catalysed dihydroxylation of benzene (**29**), in conjunction with mass spectrometry, to conclude that both oxygens were present in the bioproduct, *cis*-benzenediol **30** (**Scheme 6**).[24]

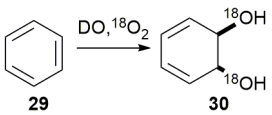

Scheme 6: Dioxygenase catalysed biotransformation of benzene (**29**) using $^{18}O_2$ to afford *cis*-benzenediol (**30**).

Finally, the one electron reduction of bound oxygen to a superoxide, which is postulated by some mechanisms to become protonated (Paths **A** and **B**, **18** to **19** in **Scheme 5**), is based on the NDO catalysed biotransformation of benzene (**29**). Benzene (**29**) is a partial uncoupling substrate for the NDO enzyme and becomes decoupled from the enzyme prior

to oxidation. Analysis of the uncoupled products indicated the presence of hydrogen peroxide. This observation has been noted in monooxygenase enzymes and P450 enzymes, which suggests that molecular oxygen must first be activated to the superoxide species (**18** to **19** or **18** to **24**).[25] Further validation for this proposal can be obtained from the ^{18}O labelled hydrogen peroxide 'shunting' experiments performed by Wolfe and Lipscomb.[26] Their hypothesis stated that if a peroxo intermediate (**19** or **24**) was active during the mechanism, then carrying out the NDO catalysed biotransformation of naphthalene (**31**) in the presence of ^{18}O labelled hydrogen peroxide and in the absence of O_2 should lead to the same bioproduct, naphthalene *cis*-diol **32** (see **Scheme 7**).

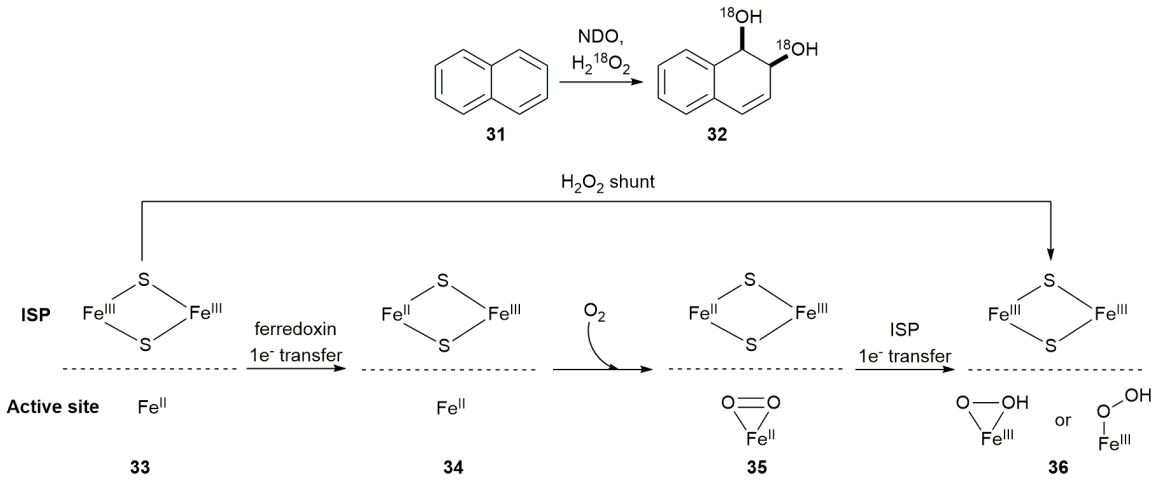

Scheme 7: The H_2O_2 'shunt' experiment, which by-passes the suggested biological route and renders the ISP in an oxidised state.

Wolfe and Lipscomb's studies confirmed this, and they noted the following: the reaction proceeded despite by-passing the initial one electron reduction (**33** to **34**) by the ferredoxin to the Rieske [2Fe-2S] cluster (ISP), which remained in an oxidised state as determined by electron paramagnetic resonance (EPR); both oxygen atoms originating from hydrogen peroxide were incorporated into the final product (**32**) and finally, an iron(III) species (**36**) was detected by EPR, which suggests that the mononuclear iron within the active site had been oxidised by the hydrogen peroxide. All these observations indicated the presence of a peroxo species within the mechanism.

From this point, the mechanistic proposal for the dioxygenase mechanism diverges. Wolfe and co-workers suggested that following the initial one electron reduction of **18** into **19**, an O-O cleavage occurs to afford iron(V)-oxo-hydroxy intermediate **20** (Path **A**, **Scheme 8**).[26]

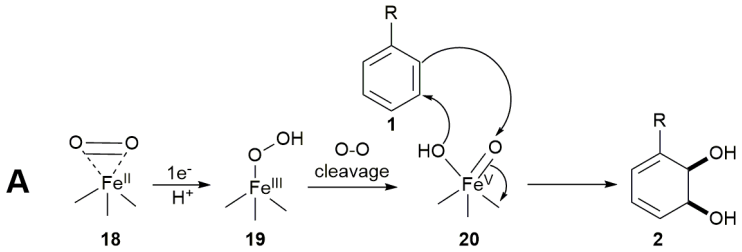

Scheme 8: The mechanism of DO catalysis suggested by Wolfe and Limpscomb (path **A**).

Their evidence was based on the P450 catalytic system (see **Scheme 9**), because they noted that NDO catalyses the same type of reaction as P450 enzymes. P450 enzymes were therefore considered a good model for mechanistic insight.[27]

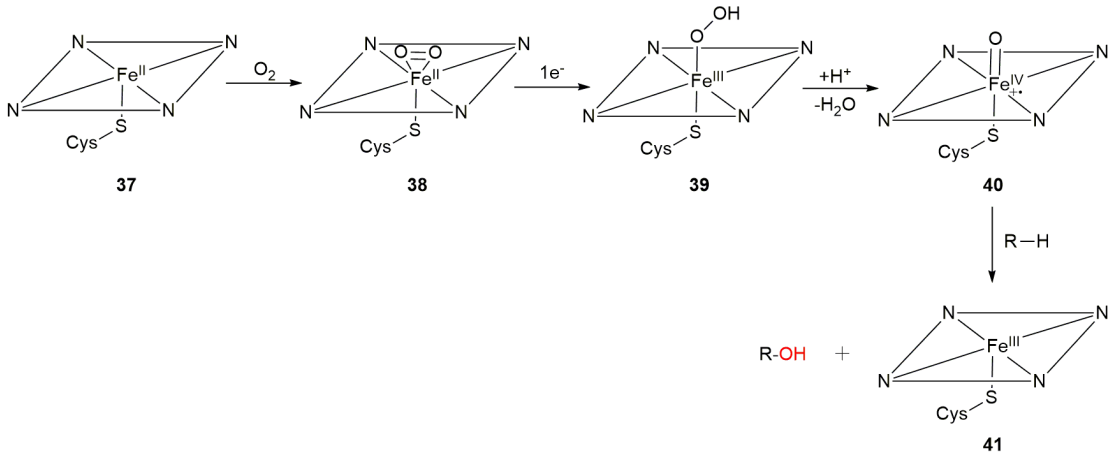

Scheme 9: The general P450 catalytic mechanism.

The mechanism of P450 enzymes involves a key O-O cleavage (**39** to **40**) in the oxygen activation process, which produces a high valent iron-oxo species (**40**).[28] The presence of a high valent iron(IV) species has also been observed in the methane monooxygenase enzyme, which was determined by Wallar and Lipscomb using Mössbauer spectroscopy.[29] At the time, this was the first confirmed non-haem iron biological system to stabilise a high valent iron centre, and supports the idea that such a system could be operating in the dioxygenase mechanism. Following the formation of **20**, it was then proposed that *cis*-diol **2** was formed in a similar manner to the dihydroxylation of an alkene using OsO_4. Despite there being a precedent in the literature for the formation of a high valent Fe species (e.g. **40**), computational studies based on the density functional theory (DFT) by Bassan and co-workers found that the activation energy for the O-O cleavage of **19** to **20** was 25.6 kcal/mol. Furthermore, the resulting product **20** lied 17.5 kcal/mol higher in energy than

reactant **19**. This was concluded to be too high of an energy barrier for an enzymatic process.[30]

During the same study, the Bassan research group proposed two alternative pathways that could be operating. They explored the possibility of an iron(IV)-oxo-hydroxy species, which was shown to have a 16.4 kcal/mol calculated activation energy for the O-O cleavage. This is approximately 10 kcal/mol lower than the corresponding iron(V)-oxo-hydroxy species (**20**) and would be favourable for an enzyme reaction; however, to generate an iron(IV) intermediate a second electron transfer must occur. Their suggestion is contradictory to the NDO single turnover studies conducted by Lipscomb and co-workers, whose research concluded that only one electron is required for the dioxygenase catalysed *cis*-dihydroxylation of a substrate and a second electron transfer was non-essential.[28] Although the single turnover studies do not rule out the possibility of an iron(IV) intermediate, it does discredit the idea that an iron(IV) intermediate is active either prior or during the *cis*-dihydroxylation. In lieu of the high activation energies accompanying the formation of a high valent iron species, the Bassan group propounded a second, alternative mechanism that involved an iron(III)-OOH intermediate (**19)** attacking the aromatic substrate to form an epoxide (**22**) (Path **B**, **Scheme 10**).

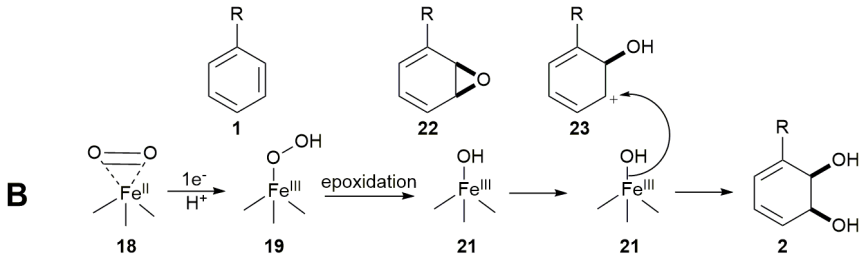

Scheme 10: The mechanism of DO catalysis suggested by Bassan and co-workers (path **B**).

This pathway was calculated to be the lowest energy pathway, with the O-O cleavage and the new C-O bond formation proceeding concertedly ($\Delta E^{\ddagger}$ = 17.5 kcal/mol). Following the formation of epoxide **22**, the C-O cleaves generating the intermediate carbocation species **23**. The remaining hydroxyl ligand of iron intermediate **21** can then bind to carbocation **23** by proceeding through a relatively low activation energy barrier ($\Delta E^{\ddagger}$ = 2.4 kcal/mol). The crux of this suggested mechanism is the formation of the proposed intermediate **23**, which would discriminate against electron-deficient substrates. It is well documented in the literature, however, that dioxygenase enzymes can efficiently catalyse electron-deficient

aromatic substrates (**Scheme 11**), which should otherwise destabilise a carbocation intermediate if this mechanism was proceeding.

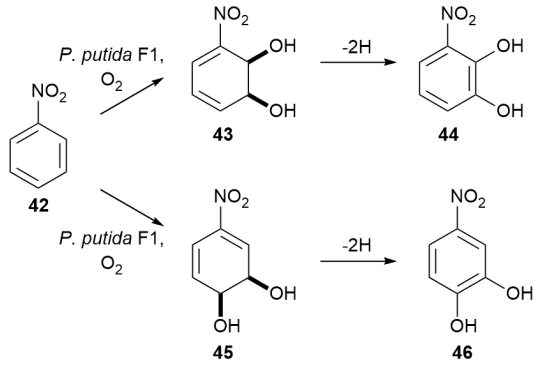

Scheme 11: The TDO catalysed *cis*-dihydroxylation of electron-deficient nitrobenzene (**42**) to afford catechols **44** and **46**.[31]

Currently, Path C is accepted as the best hypothesis for the dioxygenase mechanism (**Scheme 12**).

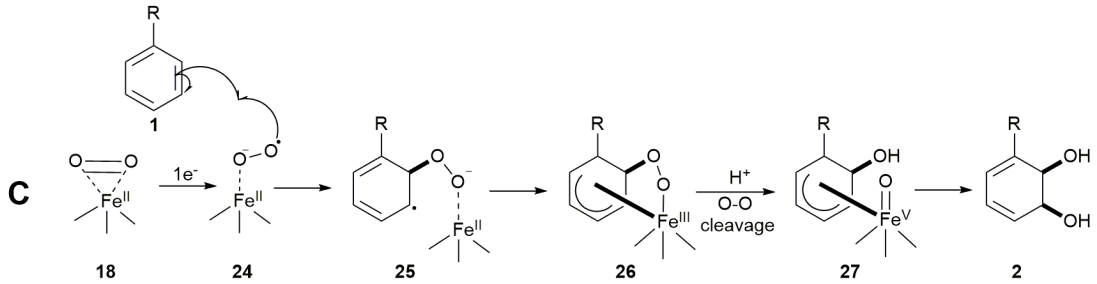

Scheme 12: The accepted hypothesis for the DO catalysis mechanism (path **C**).

NDO crystallography studies using indole as the substrate have shown an iron(III) peroxo species linked at the C3 position of the compound within the active site (**Figure 4**), which suggest that a peroxo species (**24**) attacks the double bond of the aromatic substrate (**1**).[32]

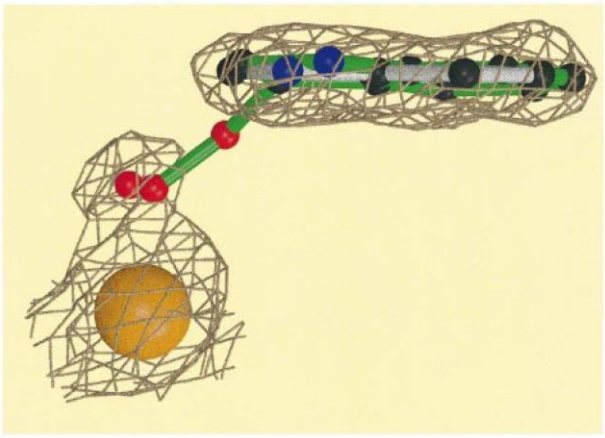

Figure 4: Comparison of the crystal structures with soaked indole superimposed onto the model indole adduct. Soaked indole crystals show peroxo binding at C3 of the indole.

Furthermore, Boyd and co-workers confirmed the presence of a substrate based delocalised radical intermediate (**25**) using ^{2}H labelled indene with TDO.[23] Analysis of the resulting product inden-1-ol revealed that the ^{2}H had equilibrated between C-1 and C-3, which is consistent with the formation of a stabilised allylic/benzylic carbon-centred radical. This radical was suggested to become stabilised by the iron centre (**26**), which has a basis within the literature, but requires close contact with the iron centre.[8]

In summary, what is clear is that there is no consensus on the exact catalytic mechanism of dioxygenase enzymes, but the evidence suggests that Path **C** is the most likely route. Nevertheless, a gap remains in the understanding of how the dioxygenase catalysed dihydroxylation occurs, and as a result further studies are required within this area.

1.1.1 TDO from *Pseudomonas putida*

The first reported whole-cell biotransformation using the TDO enzyme from *P. putida* was in 1968 by Gibson and co-workers using benzene (**29**) as a substrate (**Scheme 13**).[33]

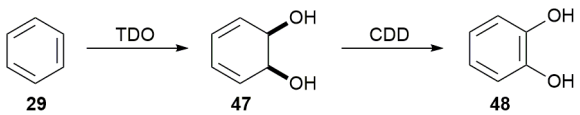

Scheme 13: The first biotransformation conducted using *P. putida* (Biotype B) and benzene (**29**) as a substrate to afford catechol **48**. CDD = *cis*-diol dehydrogenase.

Only catechol **48** was isolated during this experiment, which was a result of the *P. putida* biotype B strain possessing the *cis*-diol dehydrogenase enzyme, which catalysed the conversion of *cis*-diol metabolite **47** into **48**. It is now understood that *P. putida* biotype B, now referred to as *P. putida* F1 in consequence of a nomenclature change,[34] is a poor

representation of typical *P. putida* strains and is instead more closely related to *Pseudomonas fluorescens*.[35] This observation is consistent with the DNA sequence analysis of *P. putida* F1, which showed that this strain is phylogenetically closer to *P. fluorescens* than to *P. putida*.[36] It was shortly after this work in 1970 when the Gibson group successfully isolated *cis*-diol **47** using *P. putida* 39/D, a mutant strain derived from *P. putida* F1.[37] 39/D is a blocked mutant of F1, which removes the activity of the *cis*-diol dehydrogenase enzyme.[38] It was this variant that facilitated the isolation and application of these new and interesting *cis*-diol metabolites.

P. putida F1 formed the basis of this research due to its unique biodegradation pathway when compared to the broader *Pseudomonas* family (see **Scheme 14**).[39]

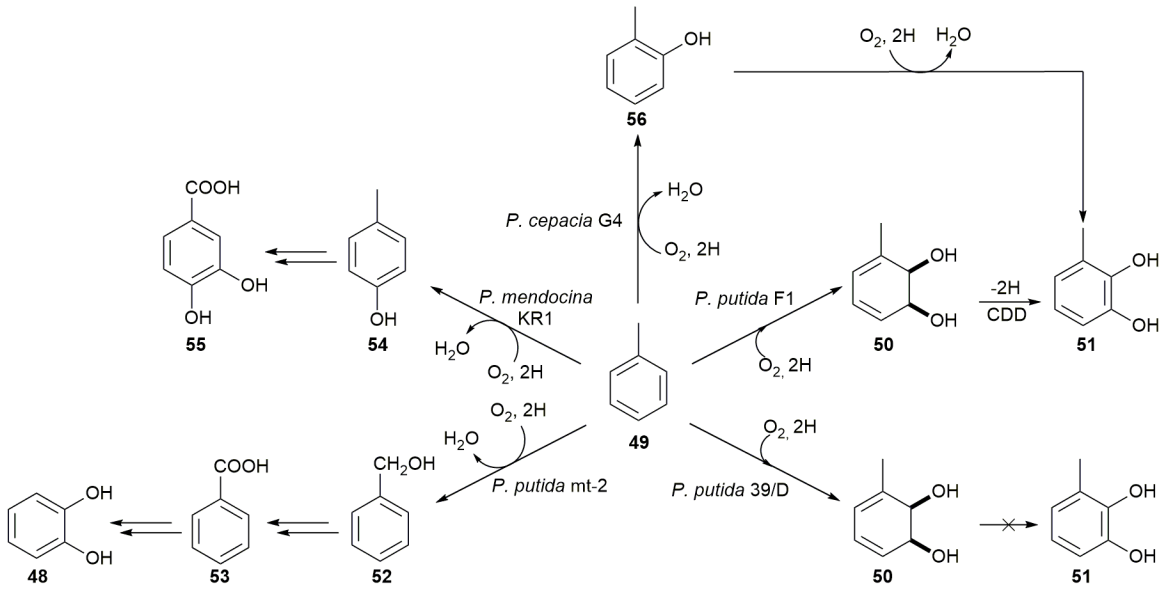

Scheme 14: The biodegradation pathways for toluene by different species of the genus *Pseudomonas*. CDD = *cis*-diol dehydrogenase.

With consideration of other examples from the *Pseudomonas* family, *P. putida* F1 is the only strain that produces the *cis*-diol metabolite as part of its biodegradation pathway (**49** to **50**). Furthermore, F1 can sustain its growth on aromatic substrates such as benzene and toluene as its sole carbon source, whereas other strains such as *P. cepacia* G4 and *P. putida* mt-2 are unable to do so.

The interest sparked by the discovery of the F1 mutant led to the discovery of another toluene dioxygenase expressing strain by Imperial Chemical Industries (ICI), the wild type *P. putida* NCIMB 11767.[40] Jenkins and Heald noted that like F1, NCIMB 11767 was able to catalyse the *cis*-dihydroxylation of aromatic substrates, but unlike F1 it was able to

sustain its growth on a wider variety of carbon sources, such as 2,4- and 2,5-dichlorophenol. Furthermore, the bioproducts obtained from the two strains differed in enantioselectivity when indene (**57**) was used as a substrate (see **Scheme 15**).[41, 42] This led the authors to conclude that the active site of the TDO enzyme must be significantly different between the two strains.

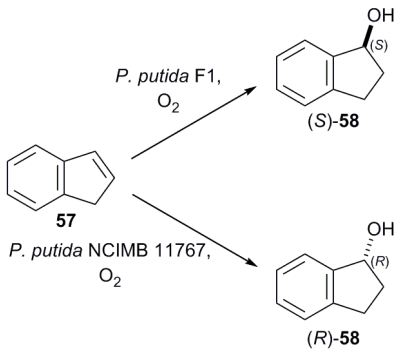

Scheme 15: The *P. putida* F1 and *P. putida* NCIMB 11767 catalysed hydroxylation of indene (**57**) to afford metabolites (*S*)-**58** and (*R*)-**58** respectively.

The conclusion regarding a disparity between the active sites of the TDO enzymes from the two *P. putida* strains, however, is likely not the correct explanation and rather an alternative, unknown mechanism is taking place. A recent publication by Allen and co-workers has revealed the full sequence identity of *P. putida* UV4, which is a blocked mutant variant of NCIMB 11767 that stops dehydrogenase enzyme activity similar to 39/D described previously.[43] Comparison of the genetic sequences responsible for the coding of the TDO enzyme in both F1 and UV4 revealed an identical match, thus ruling out Jenkins and Heald's original proposal of significant differences between the TDO active sites from the two strains. It is worth noting that these biotransformations are carried out in whole-cell, and therefore it would be conceivable that another component of the bacterial system may participate and give rise to the differing enantioselectivity. With regards to the formation of monohydroxylated products (*S*)-**58** and (*R*)-**58**, this has been shown to be the result of isomerisation of the *cis*-dihydroxylated product to the *trans* stereoisomer, followed by elimination of water.[23] Additionally, kinetic studies have showed that NCIMB 11767, in some cases, has a 20-fold higher rate of oxidation than the F1 strain, with multiple substrates acting as inducers for the TDO enzyme leading to high expression of this protein within the bacteria. These properties of the NCIMB 11767 strain in comparison to F1, make it more applicable in the preparation of enantiomerically pure products as well as other areas such as bioremediation.

1.1.2 Applications of TDO

The ability of *P. putida* to grow on hydrocarbons has attracted considerable attention from an environmental perspective. Hydrocarbon mixtures such as crude oil pose an environmental risk and often devastate a local ecosystem if allowed to spill. The ability of *P. putida* to use the TDO enzyme to biodegrade hydrocarbons, whether aromatic or aliphatic, designates the bacteria as useful tools in cleaning up pollutants from contaminated areas. In 1999, Raghavan and Vivekanandan documented the use of *P. putida* at the contaminated Bharat Heavy Electricals site located in Tiruchirappalli, India. After seeding with the bacteria, the authors reported the disappearance of crude oil components after 21 days.[44] It is to be noted that the bacteria had to be treated with fertiliser for efficient decontamination.

From a chemical synthesis point of view however, the TDO enzyme's most lucrative application is the biotransformation of a catalogue of arene substrates to form the resulting enantiomerically pure *cis*-diols. The *cis*-diol bioproducts are useful synthetic building blocks for complex, natural products and are otherwise highly difficult to obtain in high enantiomeric purity. Following the isolation of the blocked mutant strains *P. putida* UV4 and 39/D, these products became widely accessible to the chemistry field. The most extensively used *cis*-diol substrate precursors are the halogenated benzenes (**59-61**), which can be prepared on large scale with a >98 % e.e. (see **Scheme 16**).[45, 46, 47, 48]

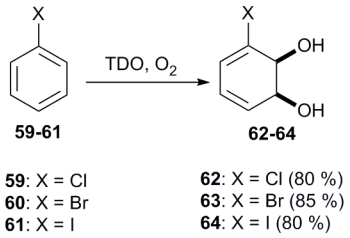

Scheme 16: The biotransformation of halogenated benzenes **59-61** to afford *cis* diols **62-64** using *P. putida* UV4 and the respective biotransformation percentage yields.

The presence of a halogen within the final product makes these bioproducts prime candidates as building blocks for the synthesis of medicinally active compounds. Arguably, iodobenzene (**61**) has proved to be the most valuable substrate. Its high reactivity towards dihydroxylation and potential for halogen substitution makes it a useful synthetic precursor. The bromo and iodo *cis*-diols **63** and **64** respectively can be obtained in particularly good yields, making them commercially useful and desirable entities.

Previous synthetic investigations carried out by the Whitehead group have utilised both bromo **63** and iodo **64** for the synthesis of shikimic acid (anti-bacterial agent, **65**), and 6-epi-COTC (glutathione inhibitor, **66**) respectively (**Scheme 17**).[49, 50]

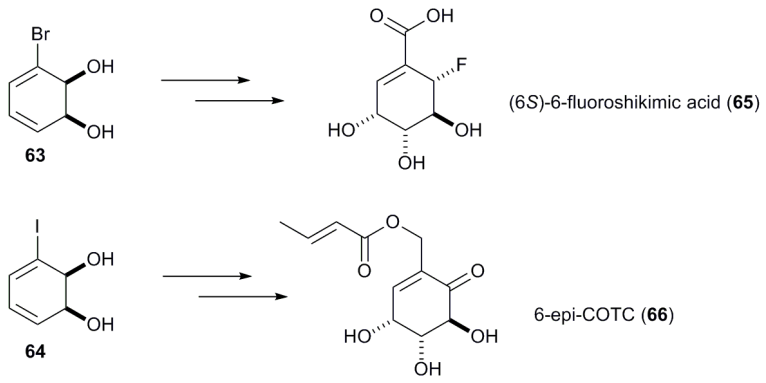

Scheme 17: The bromo **63** and iodo *cis*-diol **64** precursors to fluoroshikimic acid (**65**) and 6-epi-COTC (**66**) respectively.

In both examples, the *cis*-diol precursor acted as a useful chiral pool molecule. In the case of *cis*-diol **64**, the iodine provided an accessible route for installation of useful functionality via a palladium catalysed carbonylation reaction (**67** to **68**, **Scheme 18**).

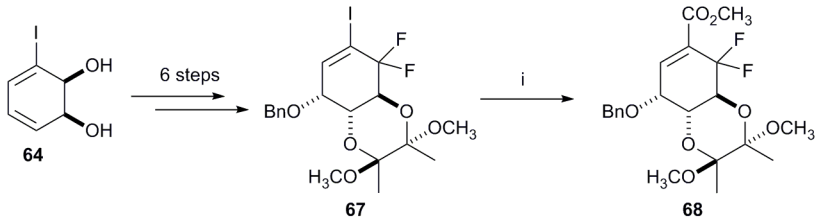

Scheme 18: *Reagents and conditions*: (i) $Pd(OAc)_2$, diisopropylethylamine, tri-2-furylphosphine, MeOH, CO, DMF, RT, 24 h, 56 %.

TDO is not just restricted to monosubstituted arenes; the substrate scope of the enzyme can extend beyond this substrate class. Hudlicky and co-workers completed the synthesis of the alkaloids, narciclasine (**73**) and 7-deoxypancratistatin (**78**) using two bioproducts obtained from the TDO catalysed biotransformation of 1,3-dibromobenzene (**69**) and 1-bromo-4-iodobenzene (**74**) respectively (**Scheme 19**).[51]

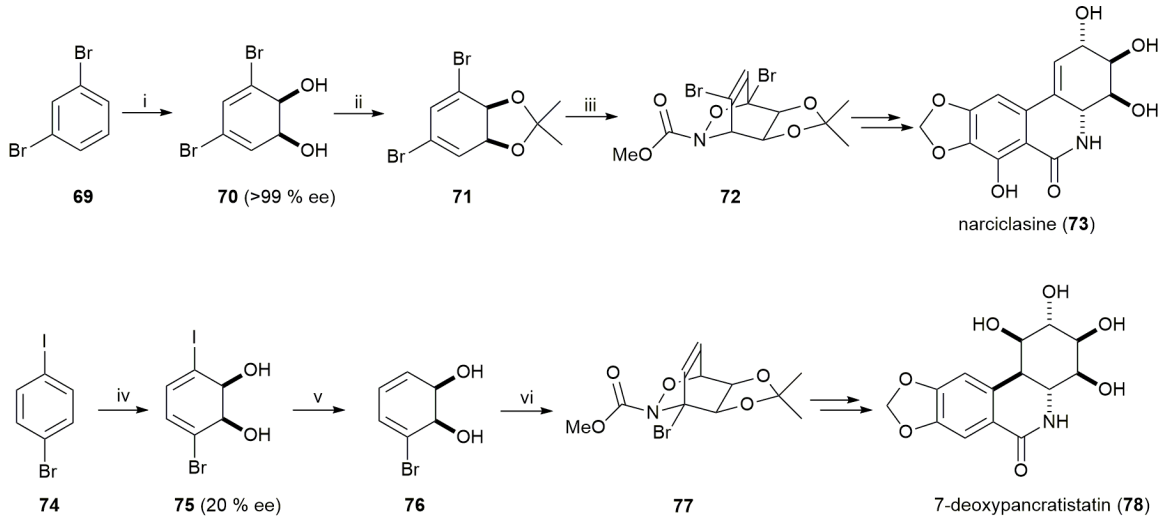

Scheme 19: The synthesis of the alkaloids narciclasine (**73**) and 7-deoxypancratistatin (**78**) using the TDO bioproducts **70** and **75** respectively. *Reagents and conditions*: (i) TDO, O_2; (ii) 2,2-DMP, cat. *p*-TsOH, RT; (iii) 2,2-DMP, $NaIO_4$, methyl carbamate in MeOH, RT, 16 H, 68 % over two steps; (iv) TDO, O_2; (v) Bu_3SnH, AIBN, 55 %; (vi) $NaIO_4$, *N*-hydroxymethyl carbamate, MeOH:H_2O, RT, 18 H, 70 %.

This total synthesis corroborates the synthetic application of the *cis*-diol metabolites. It is, however, not without limitations as shown by the biotransformation of 1-bromo-4-iodobenzene (**74** to **75**), which proceeded in low enantiomeric purity. Nonetheless, further research into TDO and *P. putida* has revealed a wealth of compatible substrates with unique and potentially useful functionalities (see **Scheme 20**).

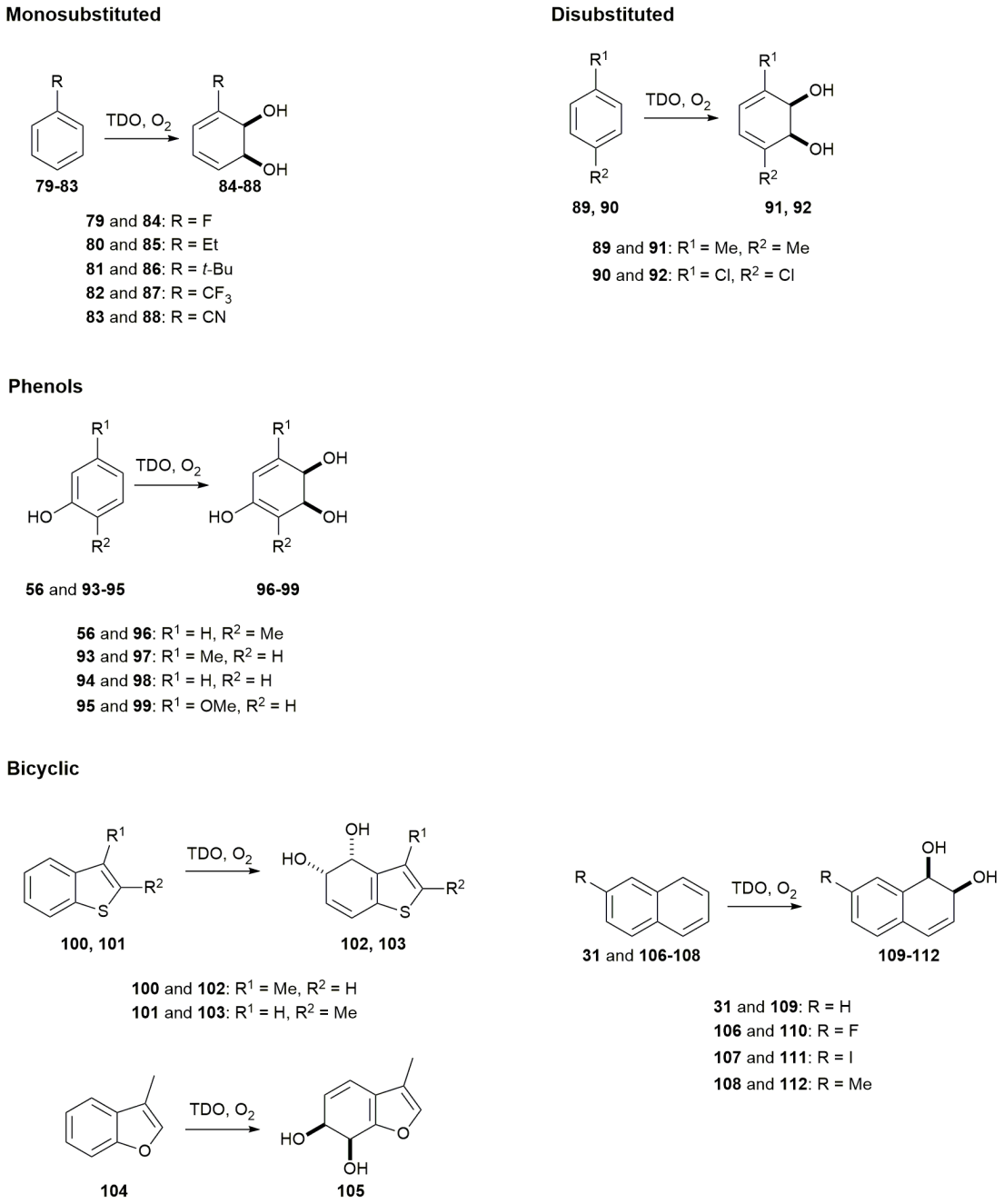

Scheme 20: Shown are examples of compatible substrates from different substrate classifications for *P. putida* UV4 and the corresponding *cis*-diol bioproducts. Only the major regioisomers are shown. [48, 52, 53, 54, 55]

The application of the TDO enzyme in the preparation of chiral *cis*-diols has been well documented since its isolation in 1968. There have now been over 400 different *cis*-diol products identified, which have been derived from arene substituents. Excitingly, a new class of bioproduct, as reported by Boyd and co-workers in 2009, has been identified using TDO and is henceforth described in the following section.

1.1.3 Keto *Cis*-Diols

Using *m*-iodophenol (**115**) as a substrate, the Boyd group were able to isolate the enantiomerically pure (≥98 % e.e.) iodo keto *cis*-diol **117** (see **Scheme 21**) using *P. putida* UV4. These bioproducts could have far reaching synthetic applications, which this project aimed to demonstrate.[56]

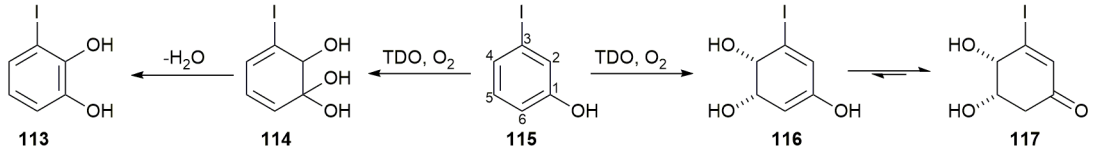

Scheme 21: The biotransformation of iodophenol (**115**) to give the iodo keto *cis*-diol **117** product and iodo catechol **113** side-product.

The iodo keto *cis*-diol **117** is formed via the enzyme catalysed *cis*-dihydroxylation of the 4,5-bond of the aromatic ring of **115** to give triol **116**. This is followed by tautomerisation to afford keto *cis*-diol **117**. This contrasts with the alternative regiochemistry of dihydroxylation across the 1,2-bond to afford triol **114**. Water is then eliminated to afford the corresponding catechol **113**, which is a competing biological pathway. The preference to form the favoured tautomer metabolite **117,** rather than eliminate water from **116,** demonstrates the remarkable regioselectivity of the TDO enzymes.[57]

In contrast to the *cis*-dihydroxylated products explored previously, which readily decompose when exposed to small amounts of acid, the keto *cis*-diols display a surprising stability. Iodo keto *cis*-diol **117** exhibited a $t_{1/2}$ for aromatisation of 10 hours in 5 M $HClO_4$ at 25 °C.[56] The biotransformation, however, proceeds in a relatively low yield. The major competing pathway leading to the formation of catechol **113** results in the inhibition and deactivation of the TDO enzyme. Furthermore, the phenolic substrates (e.g. **115**) act as antimicrobial agents and induce cell death.[57]Allen and co-workers at Queens Belfast University are currently investigating a new *E. coli* clone, which contains catechol-2,3-dioxygenase (CDO). It is proposed that CDO will further metabolise any catechol formed during the biotransformation and avoid the accumulation of this inhibiting bioproduct.

This biotransformation is not exclusive to the TDO enzyme; however, TDO exhibits the highest yield for keto *cis*-diol formation and the strongest preference for *m*-substituted phenols. This difference is illustrated by the catalysed dihydroxylation of *m*-phenyl phenol **118** using different dioxygenases (see **Table 1**).

Table 1: The relative ratios based on peak area of metabolites **119** and **120** using LC-TOF/MS analysis, from the biotransformation of **118** by different dioxygenases. BPDO = Biphenyl dioxygenase.[57]

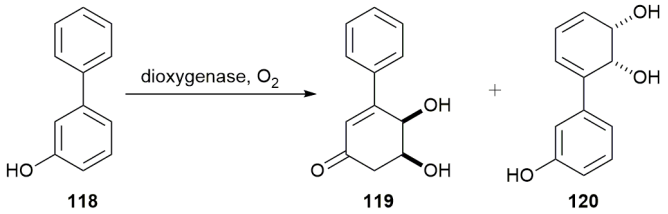

Dioxygenase	Keto-*cis*-diol **119**	*cis*-Dihydrodiol **120**
TDO	61	39
NDO	48	52
BPDO	29	71

TDO's stronger preference for *m*-phenols compared to the other dioxygenase enzymes can be suggested to be the result of the following binding interactions in the active site of the enzyme (**Figure 5**).

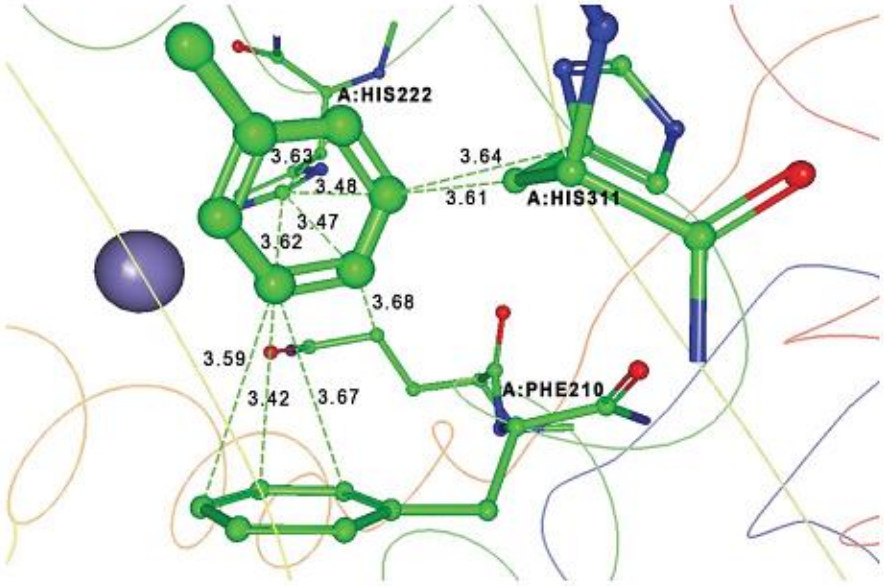

Figure 5: The active site of the toluene bound TDO as determined by x-ray crystallography. Purple = mononuclear non-heme iron atom.[58]

The active site is primarily comprised of hydrophobic residues, which in conjunction with Van der Waals forces, bind the toluene substrate into the active site. There is a further stabilising interaction from the π-stacking between the bound toluene and Phe_{210}. Crucially, the *ortho* and *meta* positions of the bound substrate are near the mononuclear non-haem iron. The adopted conformation of the bound substrate results in only one face of the aromatic ring facing towards the non-haem iron. This correlates with the observed regio- and stereoselectivity exhibited by dioxygenases. It is also noted that there is a basic

imidazole ring deriving from the His_{311} residue in close proximity to the *meta* position of the toluene, where the alcohol group would reside in a phenolic substrate. It is possible that a hydrogen bonding interaction could manifest itself between the imidazole side chain and the acidic hydrogen of the alcohol. This would provide a possible explanation for the observed decrease in formation of keto *cis*-diol **119** when using different dioxygenases, as this residue is not conserved (**Table 1**). For instance, in BPDO His_{311} is replaced by Asp_{204}, and in NDO it is replaced by Asn_{297}. The hydrogen bonding interaction between the phenolic alcohol and these residues would be comparatively weaker than with His_{311} present in TDO and would account for the lesser yields highlighted in **Table 1**. This interaction, however, has only been suggested through computational studies and does not yet have experimental validation.

Examples of the synthetic application of the keto *cis*-diol metabolites are few due to their relatively recent discovery, but a number of synthetic transformations have been carried out by Sharma, Boyd and co-workers (see **Scheme 22**).[56]

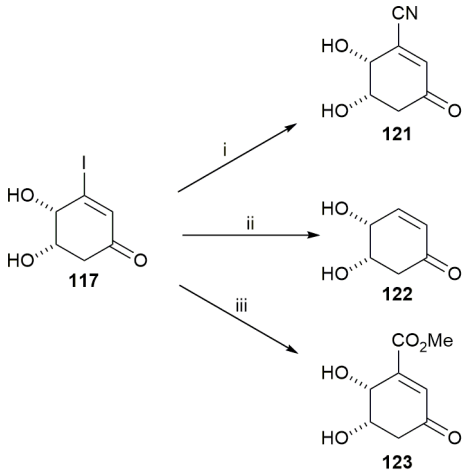

Scheme 22: *Reagents and conditions*: (i) Bu_3SnCN, $Pd(PPh_3)_4$, Et_3N, THF, 18 h, reflux, 48 %; (ii) 3 % Pd/C, Et_3N, MeOH, H_2, overnight, RT, 81 %; (iii) $Pd(OAc)_2$, $NaOAc.3H_2O$, MeOH, $CO_{(g)}$, 12 h, RT, 66 %.

Conclusively, their research shows the potential of iodo keto *cis*-diol **117** by demonstrating the lability of the iodo group towards different reaction conditions.

1.2 Incarviditone

(±)-Incarviditone (**124**), a benzofuranone dimer, and (±)-rengyolone (**125**) were each isolated as a racemic mixture in 2009 by Zhang and co-workers from the plant *Incarvillea delavayi* (**Figure 6**).[59]

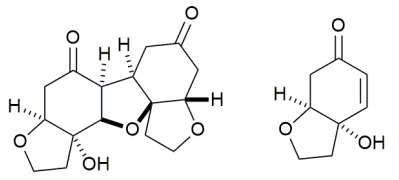

Figure 6: The originally proposed structure for incarviditone (**124**) and the structure of rengyolone (**125**).

The two compounds were tested across a range of cancer cell lines to assess their biological activity, as shown by **Table 2**.

Table 2: The biological results for (±)-incarviditone (**124**) and (±)-rengyolone (**125**). A549 = non-small cell lung cancer; LOVO = colon cancer; HL-60 = promyeloblast leukaemia; 6T-CEM = acute lymphocytic leukaemia; HepG2 = liver cancer.

	IC_{50} (μg/mL)				
Compound	A549	LOVO	HL-60	6T-CEM	HepG2
124	>30	>30	14.8 ± 0.3	22.2 ± 0.9	>30
125	16.2 ± 0.8	11.6 ± 0.6	5.7 ± 0.3	6.1 ± 0.4	20.2 ± 0.7

(±)-Rengyolone (**125**) exhibited a more potent bioactivity profile compared to (±)-incarviditone (**124**); however, this is to be expected due to the potential of the conjugated alkene to undergo a Michael addition. In a biological system, this would likely manifest itself via reaction with cysteine residues from proteins resulting in cell apoptosis. (±)-Incarviditone (**124**) on the other hand showed a more moderate bioactivity, however its intriguing structure and promising initial biological results prompted Whitehead and co-workers to synthesise a library of analogues of this compound for the investigation into structure-activity relationships.[60, 61]

In the original work published by Zhang and co-workers, the biosynthetic mechanism to the formation of **124** was not suggested. Nonetheless, it was noted that incarviditone (**124**) had exactly double the mass units of rengyolone (**125**), and it was postulated that **125** could dimerise to form **124**.

1.2.1 Biosynthetic Pathway to Incarviditone

In 2012, Wu, Tang and co-workers investigated the biosynthetic pathway to incarviditone (**124**) and suggested the following two routes, as illustrated by **Scheme 23**.[62]

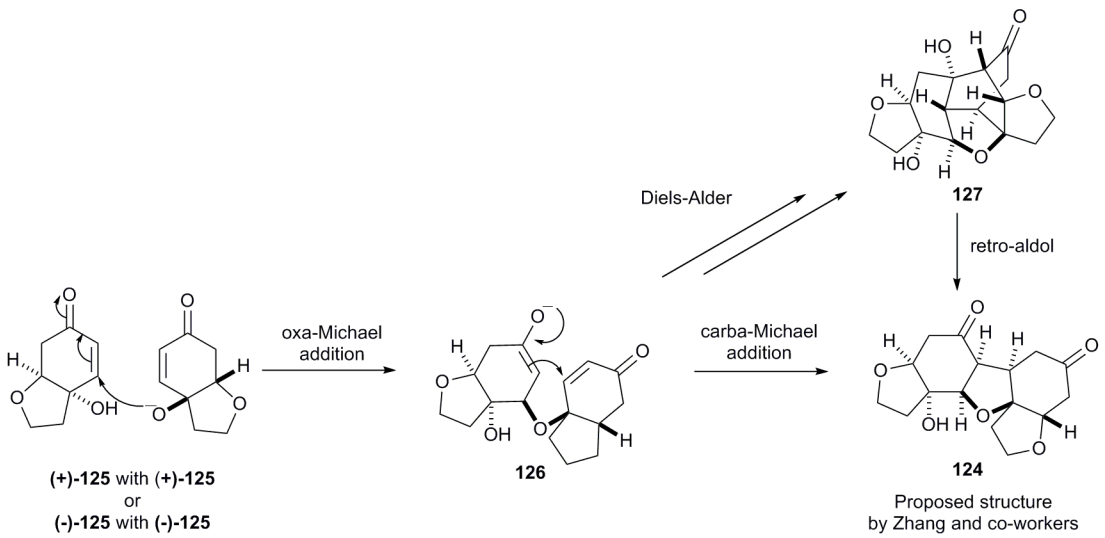

Scheme 23: The proposed biosynthetic mechanism for the formation of (±)-incarviditone (**124**).

It was proposed that the formation of incarviditone (**124**) initially starts with a homodimerisation between two molecules of rengyolone (**(+)-125**/**(+)-125** or **(-)-125**/**(-)-125**) via an oxa-Michael addition (**125** to **126**). From here, intermediate **126** could tautomerise, which would provide a basis for an intramolecular Diels-Alder (**127**) followed by a retro-aldol (**127** to **124**); or alternatively, **126** could undergo a carba-Michael addition to form the natural product **124**. Before embarking on a biomimetic synthesis, computational studies were carried out to determine the transition state energy for the oxa-Michael addition (**125** to **126**). It was during this study that a discrepancy was found with the originally proposed structure (see **Scheme 24**).[62]

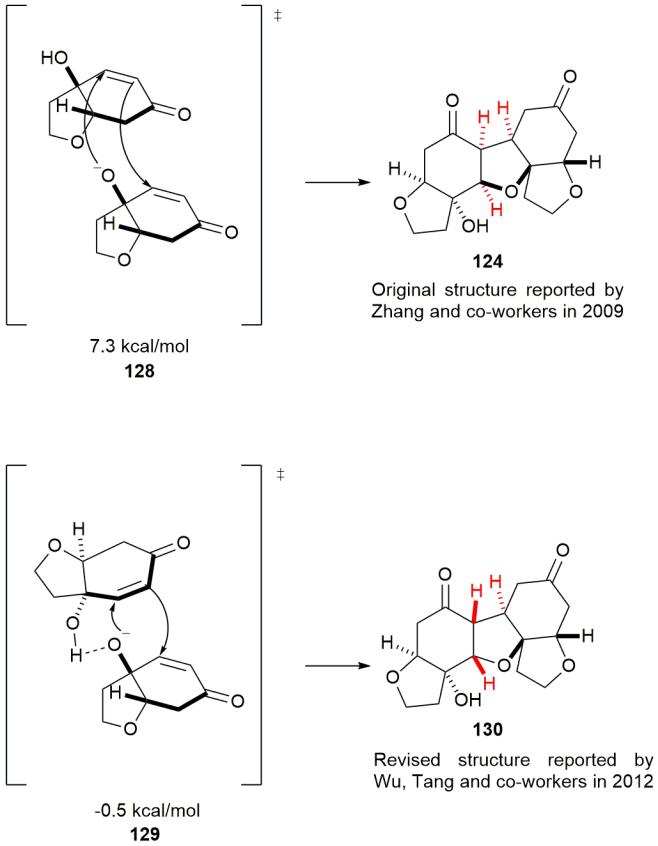

Scheme 24: The calculated transition state energies for the dimerisation of rengyolone (**125**) to afford the original structure (**124**) and the revised structure (**130**) of incarviditone.

The transition state (**128**) associated with the concave/convex nucleophilic attack leading to the originally proposed structure (**124**) was 7.8 kcal/mol less favourable than the transition state (**129**) corresponding to a convex/convex approach. Notably, in transition state **129** a crucial hydrogen bond interaction was proposed to occur between the nucleophilic oxygen and the hydroxy substituent on the recipient rengyolone molecule. The convex/convex approach, however, leads to a *trans* arrangement across the tetrahydrofuran ring (**130**) rather than the *cis* arrangement as originally proposed. To further probe their new findings, Wu, Tang and co-workers carried out biomimetic studies by starting with the synthesis of (±)-rengyolone (**125**) from the commercially available 2-(4-hydroxyphenol)ethanol (**131**).[62] The original synthetic approach was modified to the following procedure shown in **Scheme 25** on account of the poor overall yield on scaling up.

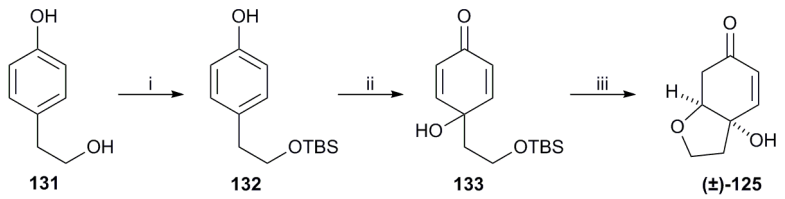

Scheme 25: *Reagents and conditions:* (i) TBSCl, imidazole, THF, 1 h, 0 °C; (ii) $PhI(OAc)_2$, $MeCN/H_2O$ (1:1), 1 h, 0 °C (65 % over 2 steps); (iii) TBAF, THF, 12 h, 0 °C, 76 %.

With the synthetic (±)-rengyolone (**125**) in hand, a biomimetic approach was employed whereby **125** was treated with NaH in CH_2Cl_2 to afford (±)-incarviditone (**130**) in 40 % yield (**Scheme 27**). Coincidentally, at the same time, Lawrence and co-workers published their proposed biosynthetic pathway to (±)-incarviditone (**130**), hypothesising that the pathway proceeded via an oxa-Michael, carba-Michael cascade to afford **130**.[63] Furthermore, they offered a plausible biosynthesis to (±)-rengyolone (**125**) (see **Scheme 26).**

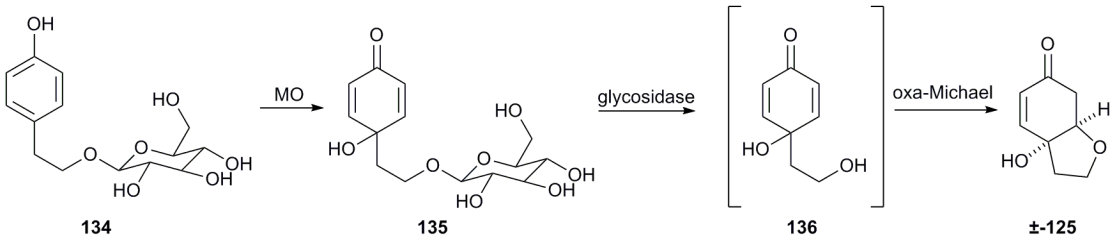

Scheme 26: The biosynthesis of (±)-rengyolone (**125**) as suggested by Lawrence and colleagues. MO = salidroside monooxygenase.

They envisaged that rengyolone (**125**) is derived from salidroside (**134**), which in turn is biosynthesised from either tyrosine or tyramine.[64] Interestingly, the conversion of salidroside (**134**) to cornoside (**135**) is facilitated by salidroside monooxygenase, which hydroxylates at the C-4 position. Studies into the biological mechanism of the salidroside monooxygenase enzyme have revealed that it is mediated by a radical intermediate at the C-4 position, which draws parallels with the most accepted hypothesis for the dioxygenase mechanism (see **Section 1.1.1**).[65] Following monooxygenation (**134** to **135**), the glycosidic bond of cornoside (**135**) is hydrolysed by a glycosidase enzyme to form diol **136**, which effectuates a 4-*exo*-trig oxa-Michael ring closure to afford racemic (±)-rengyolone (**125**). Lawrence and co-workers' incarviditone mechanism proposal concurred with the previously described work by Wu and Tang, and the dimerisation conditions utilised by both the groups are summarised in **Scheme 27**.

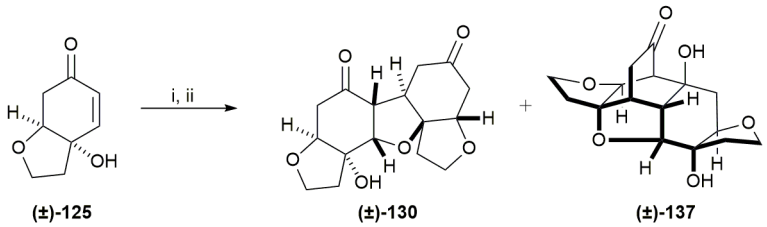

Scheme 27: The dimerisation of (±)-rengyolone (**125**) to afford (±)-incarviditone (**130**) and (±)-incarvilleatone (**137**). *Reagents and conditions*: (i) NaH (1.0 eq.), CH_2Cl_2, 12 h, RT, **(±)-130** (40 %), **(±)-137** (38 %).[62] (ii) K_2CO_3 (0.1 eq.), DCE, 18 h, 70 °C, **(±)-130** (19 %), **(±)-137** (23 %).[63]

Conclusively, the combined research determined that incarviditone arises from the homodimerisation of two monomers of rengyolone (**125**) possessing identical stereochemistry (+/+ or -/-). Evidence for the newly revised structure (**130**) was provided by ^{1}H-^{1}H NOESY (**Figure 7**) and X-ray crystallography experiments (**Figure 8**), which explicitly showed a *trans*-relationship across the tetrahydrofuran ring.

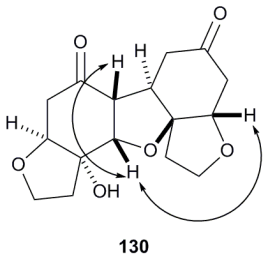

Figure 7: The ^{1}H-^{1}H NOESY correlations for the revised incarviditone structure (**130**).

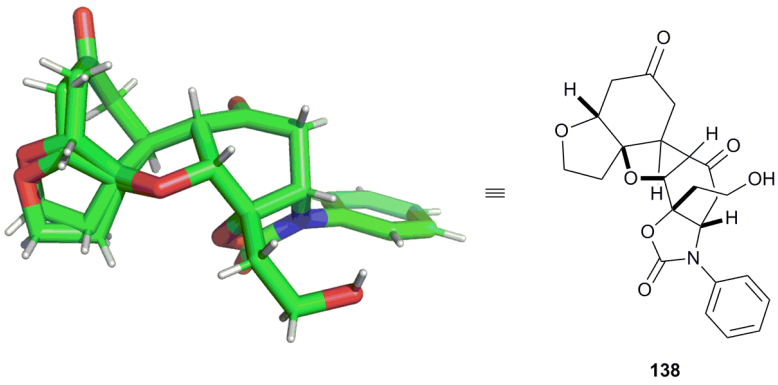

Figure 8: The X-ray crystal structure of the incarviditone oxazolidinone derivative **138**.

During the original work on *Incarvillea delavayi*, another 'caged like' structure was observed, which was the incarvilleatone natural product (see **Scheme 27**, **137**). Like incarviditone (**130**), it was proposed that incarvilleatone (**137**) arose from the dimerisation of rengyolone (**125**). The structural deviation depended on whether the product was a result of homodimerisation (**130**: +/+ or -/-) or heterodimerisation (**137**: +/- or -/+). In nature,

rengyolone (**125**) exists as a racemate; therefore, a mixture of both (±)-incarviditone (**130**) and (±)-incarvilleatone (**137**) are biosynthesised.

1.2.2 Related Research

The interesting biological activity of both rengyolone (**125**) and incarviditone (**130**) make these molecules desired entities for medicinal chemistry studies, and as such synthetic routes to analogues of these compounds would be an asset. Currently, there are limited methods described within the literature involving the synthesis of a dimeric benzodifuranone related to incarviditone (**130**) and even less that possess the desired *trans* relationship across the THF ring.

In 2014, the Whitehead group happened upon a serendipitous discovery of a cascade approach to synthesising perhydrodibenzofuranones of the general structure **139** (**Figure 9**), which are structurally related to incarviditone (**130**).[66]

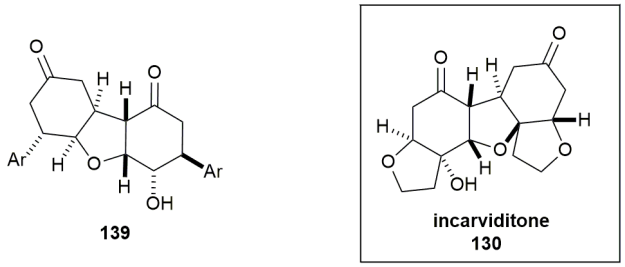

Figure 9: The general structure of perhydrodibenzofuranones (**139**) related to incarviditone (**130**), which is shown for comparison.

At the time, the Whitehead group were investigating hybrid analogues of the natural products COTC (**176**) and antheminone A (**191**) (see **Section 1.5**), during which side-chain functionality was installed via a rhodium catalysed conjugate addition. The conjugate adducts (**140**) were then exposed to basic conditions to remove the ketal protecting group and form the desired hydroxyenone product (**141**); however, it was noted that an unexpected dimerisation occurred when the adducts were exposed to these conditions for a prolonged time (ca. 18 hours) (**Scheme 28**).

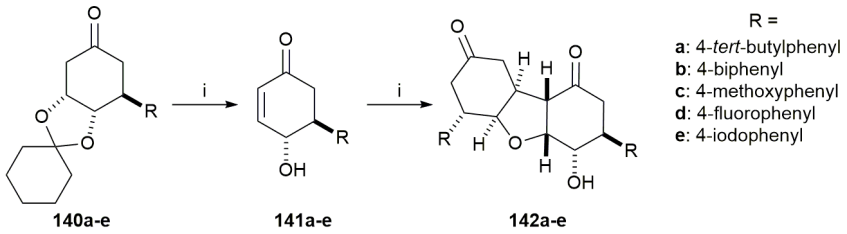

Scheme 28: The dimerisation of conjugate adducts **140a-e** to afford incarviditone analogues **142a-e**, as reported by the Whitehead group. *Reagents and conditions*: (i) 0.5 M $NaOH_{(aq)}$, THF, RT, 18 h.

The reaction proceeded via an isolatable hydroxyenone intermediate (**141**), which bares structural similarity to rengyolone (**125**). All the synthesised analogues were tested in MTT assays against various cancer cell lines, the results of which are discussed in **Section 2.9.3.2**.

Prior to this research and the discovery of incarviditone (**130**), Carreño and Ribagorda published their findings detailing the stereoselective trimerisation of *p*-quinols and *p*-quinamines.[67] Intriguingly, their work bears significant parallels with the Whitehead group's research described previously (**Scheme 29**).

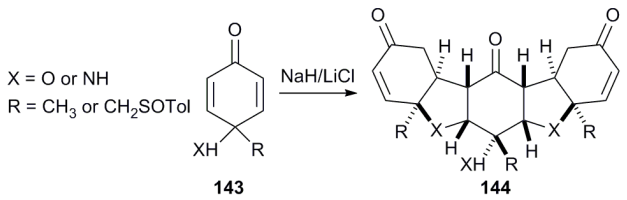

Scheme 29: The stereoselective trimerisation of *p*-quinols and *p*-quinamines of general structure **143** to afford trimers of general structure **144**. SOTol = (*p*-tolylsulfinyl)methyl.

The important aspect of this work was the diastereoconvergent approach: the trimerisation proceeded via four conjugate addition reactions, which gave excellent stereocontrol around the tetrahydrofuran or pyrrolidine ring. This resulting trimeric structure **144** possessed a *cis-trans-cis* relationship across the skeletal core, which is analogous to incarviditone (**130**) and its analogues (**139**). Carreño and Ribagorda were also curious to test their system using a single enone precursor (**145**, **Scheme 30**).[67]

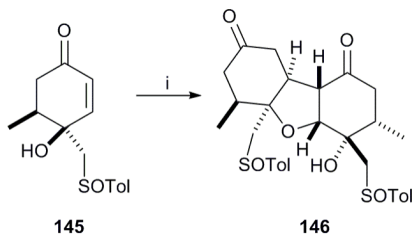

Scheme 30: The dimerisation of the single enone system **145** to afford dimer **146**. *Reagents and conditions*: (i) NaH, CH_2Cl_2, 24 h, RT, 57 %.

As shown, the excellent stereocontrol was also retained in the single enone system. Their rationale for the stereocontrol encompassing the above examples is illustrated in **Scheme 31**.

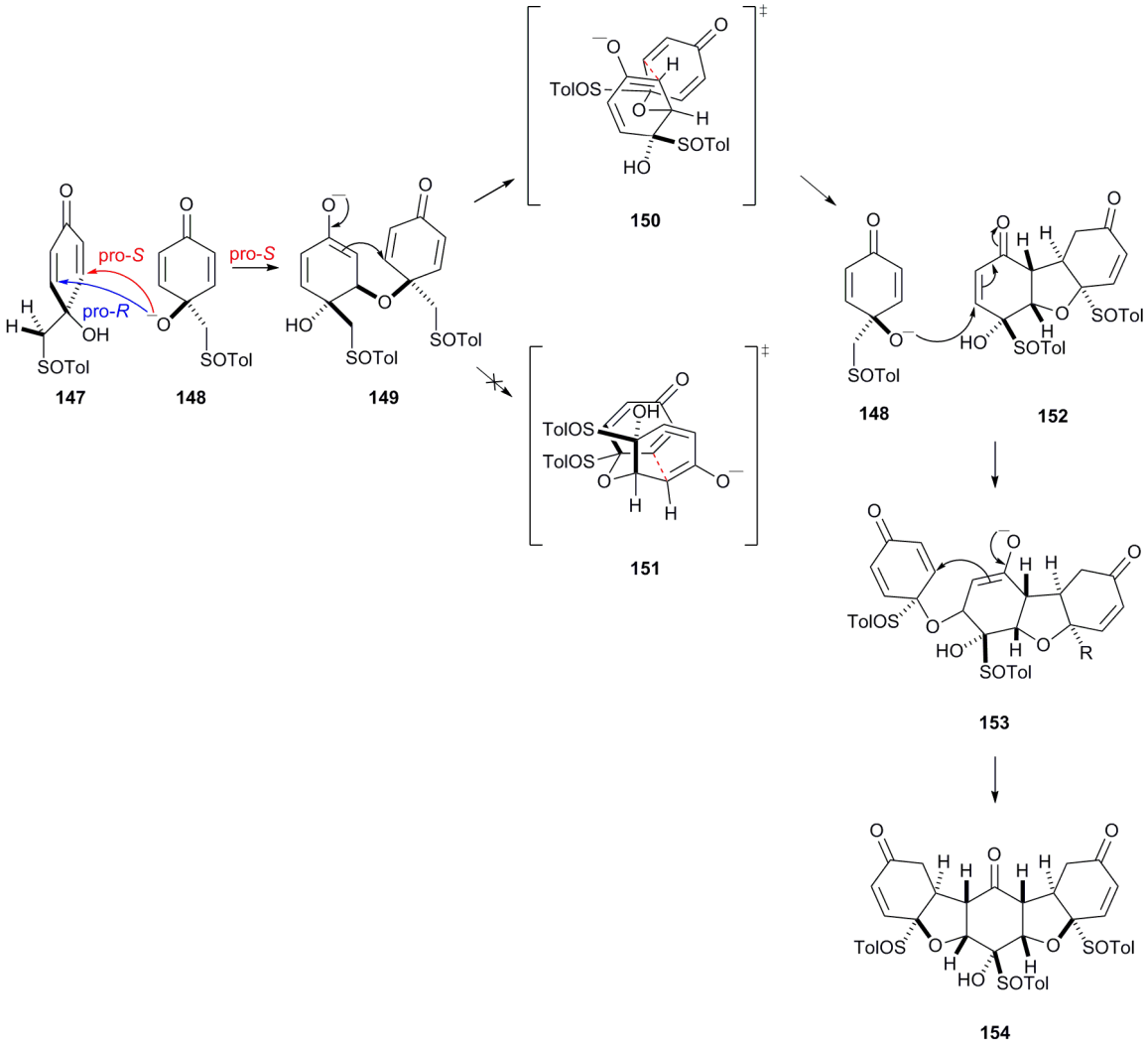

Scheme 31: The suggested mechanism for the dimerisation and trimerisation reported by Carreño and Ribagorda. For simplicity, only the pro-*S* route is shown; however, the pro-*R* also proceeds.

The initial attack of alkoxide **148** occurs on the least hindered face of **147**, which bears the hydroxyl group to afford intermediate **149**. The 1,4-addition can occur at both prochiral

positions on hydroxydiene **147**; however, for simplicity only the pro-*S* route is shown. An internal cyclisation then occurs in intermediate **149** to afford dimer **152**. The diastereoselectivity of the cyclisation can be rationalised by the transition state **150**; the alternative transition state **151** is destabilised by a 1,3-diaxial interaction and does not occur. Following cyclisation, a second molecule of alkoxide **148** can react with dimer **152**. Again, this occurs on the least hindered face supporting the free OH, which affords intermediate **153**. **153** can then subsequently cyclise to give the final product, trimer **154.** Nowhere in their explanation do the authors allude to any hydrogen bonding interaction occurring between the two alkoxide molecules; nevertheless, in light of the work carried out by Wu, Tang, Brown and co-workers, it is plausible that such a mechanism might be taking place. Furthermore, it is interesting to note that both the dimerisation and trimerisation can proceed with nitrogen as the nucleophilic element. This represents further possible structural analogues of incarviditone (**130**), which may be of chemical and biological interest.

In 2010, Spivey and co-workers developed their own dimerisation synthetic pathway, one that was also structurally related to incarviditone (**130**) but lacked the absolute stereocontrol described by the Whitehead group and Carreño and Ribagorda (**Scheme 32**).[68]

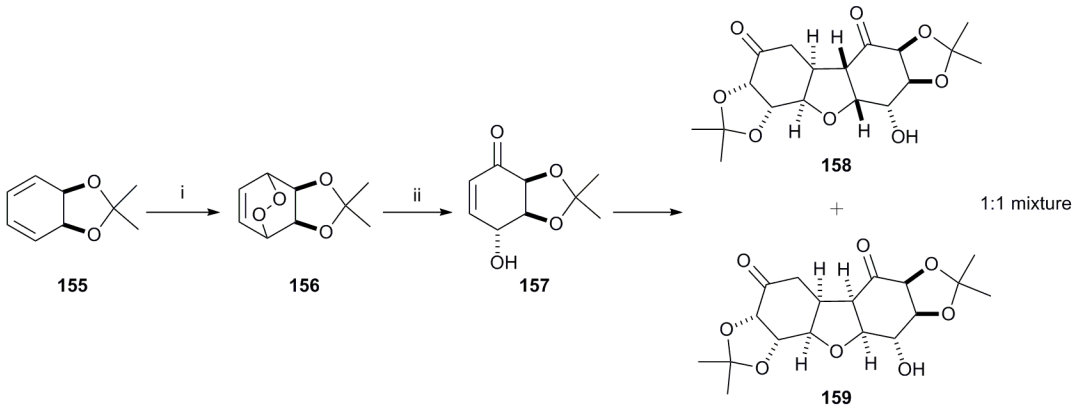

Scheme 32: The dimerisation conditions described by Spivey and co-workers to give the hydrodibenzofurans **154** and **155** as a 1:1 mixture. *Reagents and conditions*: (i) O_2, CCl_4, TPP (5 mol %), 300 W sun lamp, 7.5 h, RT, 95 %; (ii) *i*PrNEt, CH_2Cl_2 or DMF, >40 min, RT.

The diene **155** was prepared via a four-step synthesis starting from the commercially available 1,3-cyclohexadiene. With **155** in hand, a photooxygenation reaction afforded endoperoxide **156**. Treatment of **156** with Hunig's base prompted the Kornblum-DeLaMare rearrangement to give hydroxyenone **157**, and prolonged exposure under the

same conditions resulted in the dimerisation to afford the *cis-trans-cis* and the *cis-cis-cis* decahydrodibenzofurans **158** and **159** respectively, as a 1:1 inseparable mixture. The suggested mechanism for the formation of dimers **158** and **159** resonated with the proposed biosynthetic pathway to incarviditone (**130**) in the form of a double Michael cascade. Interestingly, there appeared to be no facial selectivity with the initial oxa-Michael addition, but excellent facial selectivity with the 5-*exo*-trig carba-Michael cyclisation to form the THF ring. This contrasts with the full selectivity exhibited by the Whitehead group's dimerisation using hydroxyenone intermediates of general structure **141** and Carreño and Ribagorda's *p*-quinol and *p*-quinamine trimerisations. Interestingly, Spivey and colleagues failed to report of any additional product that could be related to heterodimerisation despite the presence of both enantiomers in the dimerisation reaction. It is also worth noting that during their research, the initial 4 step synthesis to diene **155** could have been avoided by utilising the benzene *cis*-diol bioproduct **47** obtained from the *P. putida* UV4 biotransformation of benzene (**29**), followed by an acetonide protection (see **Section 1.1.1**, **Scheme 13**).

1.3 Incarvilleatone

In 2012, (±)-incarvilleatone (**137**, **Figure 10**) was isolated by Zhang and co-workers from the plant *Incarvillea younghusbandii* as a racemic mixture.[69]

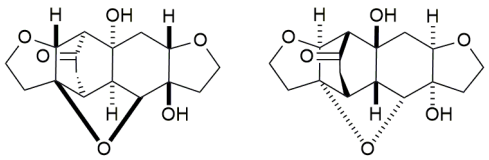

Figure 10: The structures of (+)- and (-)-incarvilleatone (**137**).

NOESY, X-ray crystallography and electronic circular dichromism were used to determine the structure and the absolute stereochemistry of the enantiomers of incarvilleatone (**137**). Later studies by Wu, Tang and colleagues found their data to be in agreement with the aforementioned.[62]

Both incarvilleatone enantiomers (**137**) were tested in a lipopolysaccharide (LPS)-induced RAW 264.7 macrophage assay: this was to assess incarvilleatone's inhibition of nitric oxide (NO) release, which is an important compound involved in the inflammatory

process. NO is a signalling molecule that can induce an anti-inflammatory effect under normal physiological conditions, or conversely induce inflammation in abnormal situations such as disease or injury.[70] Compounds that can target NO production are therefore of great therapeutic interest. The LPS-induced RAW 264.7 macrophage assay results are summarised in **Table 3**.

Table 3: The biological results for the (+) and (-) enantiomers of incarvilleatone (**137**).

Compound	Doses (μM)	Inhibition of NO (%)
(-)-**137**	6.3	22.4
	12.5	37.7
	25.0	49.2
	50.0	45.6
(+)-**137**	6.3	7.0
	12.5	18.1
	25.0	30.5
	50.0	25.3

The initial biological results showed that the enantiomer **(-)-137** exhibited a higher potency than **(+)-137** towards NO inhibition. This suggests that there is a degree of selectivity towards an unidentified biological target, and therefore synthetic methods to obtain analogues of these compounds are of great interest.

1.3.1 Biosynthetic Pathway to Incarvilleatone

As with incarviditone (**130**), there have been two proposals regarding the biosynthetic pathway to incarvilleatone (**137**), which are illustrated in **Scheme 33**.

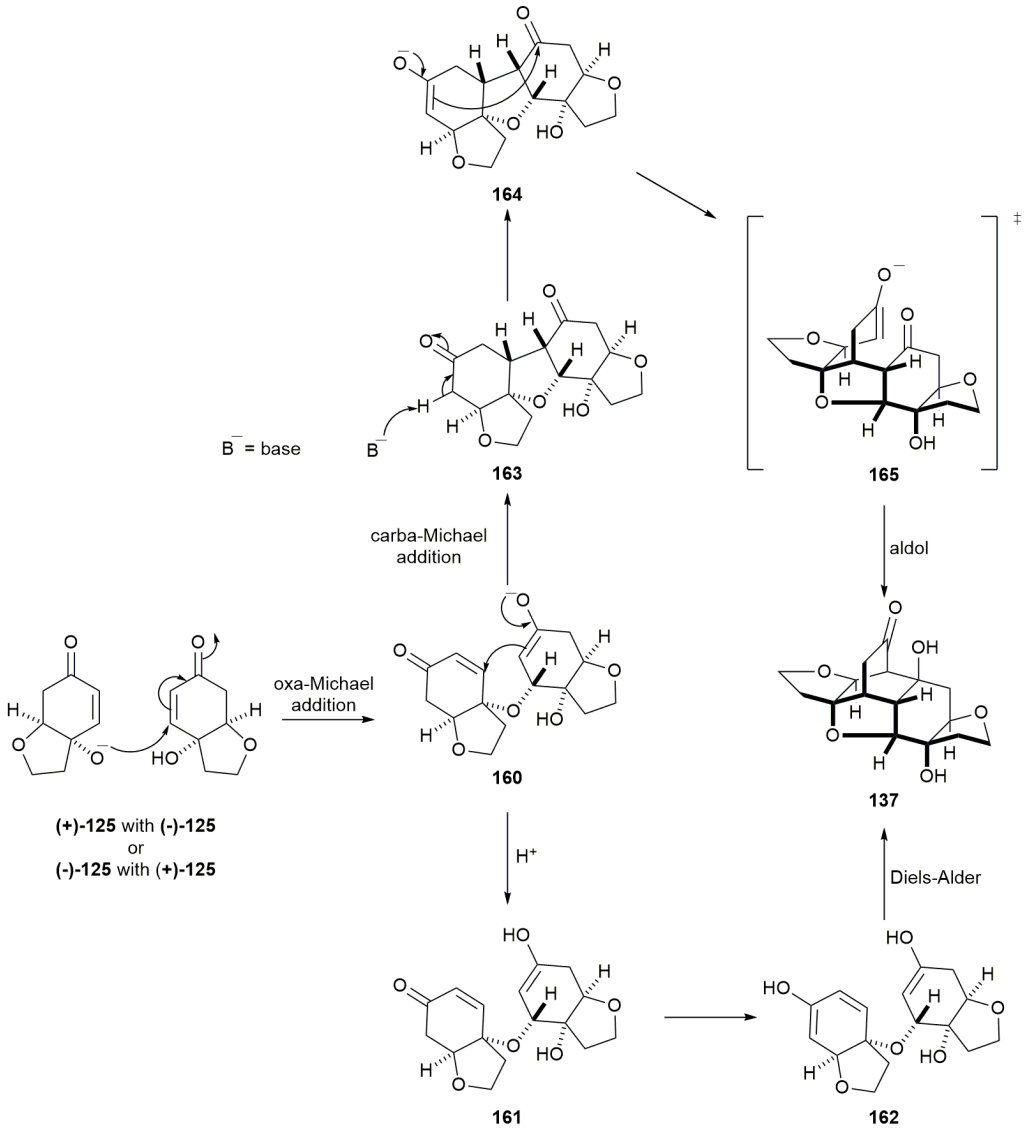

Scheme 33: The proposed biosynthetic pathways to incarvilleatone (**137**).

Zhang and co-workers originally conceived that two rengyolone (**(+)-125**/**(-)-125** or **(-)-125**/**(+)-125**) monomers come together via an oxa-Michael addition to form intermediate **160**. From here, a protonation occurs to form enol **161**, followed by tautomerisation to form enol **162**. **162** can then undergo an intramolecular Diels-Alder reaction to afford incarvilleatone (**137**).[69] Conversely, Wu, Tang and colleagues, in addition to the Lawrence group, envisaged that the likely biosynthetic pathway would have a carba-Michael addition succeeding the oxa-Michael addition to form dibenzofuranone **163**. Thereupon, enolate **164** is generated, which adopts transition state **165** prior to the 6-*exo*-trig intramolecular aldol to form incarvilleatone (**137**).[62, 63] Distinctly, both groups suggested that incarvilleatone (**137**) was formed via the heterodimerisation of two monomers of rengyolone (**125**) with the opposite stereochemistry. The diversification of the two

pathways leading to either incarviditone (**130**) (homodimerisation) or incarvilleatone (**137**) (heterodimerisation) was suggested to be the result of the transition state **165** adopted during the heterodimerisation, which brings the enolate in close proximity to the neighbouring carbonyl. Furthermore, computational studies have showed that an intermolecular hydrogen bond interaction (**166**), like that for incarviditone (**130**), was important during the oxa-Michael addition for energetic favourability of heterodimerisation (**Figure 11**).[62]

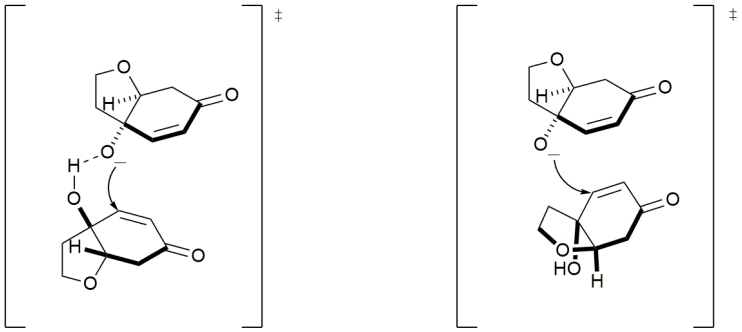

Figure 11: The calculated transition state energies for the oxa-Michael addition of the heterodimerisation of rengyolone (**125**) to afford incarvilleatone (**137**).

1.4 Pseudohygrophorones

Pseudohygrophorones, isolated by Arnold and co-workers in 2016, are naturally occurring cyclohexenones isolated from the fungus, *Hydrophorus abieticola* (**Figure 12**).[71]

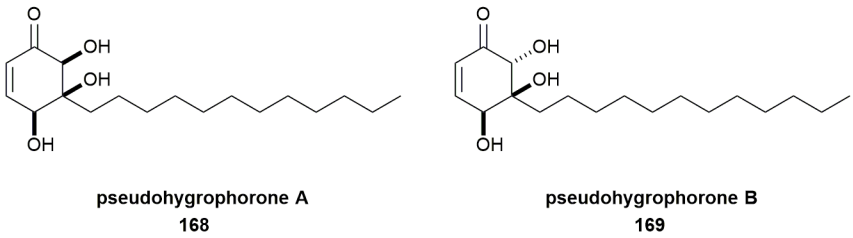

Figure 12: The structures of pseudohygrophorones A (**168**) and B (**169**) respectively.

It was first noted in 2004 that pathogenic fungi rarely infected species of the genus *Hygrophorus*.[72] It was postulated that compounds, such as **168** and **169**, are biosynthesised by these species as a method of defence to protect their fruiting bodies and to allow for the distribution of their spores.[71] As such, pseudohygrophorones A (**168**) and B (**169**) were biologically tested to evaluate their anti-fungal activity; the commercially available fungicide, dodine (**170**, **Figure 13**) was also tested to provide a comparison.

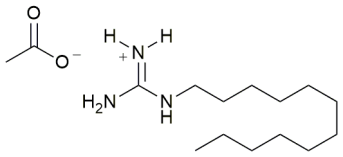

170

Figure 13: The structure of the commercially available fungicide, dodine (**170**).

Table 4: The biological results of pseudohygrophorones A (**168**) and B (**169**) against different pathogenic plant fungi. The commercial fungicide dodine (**170**) was used as a reference compound.

	IC_{50} (μM)		
Compound	*B. cinerea*	*S. tritici*	*P. infestans*
168	18.0 ± 2.6	17.5 ± 2.6	7.6 ± 0.5
169	19.0 ± 1.2	24.5 ± 3.2	4.3 ± 0.4
170	9.4 ± 0.6	2.8 ± 0.2	43.8 ± 5.6

In summary, for the fungi *B. cinera* and *S. tritici*, pseudohygrophones A (**168**) and B **(169**) displayed a slightly higher IC_{50} value in relation to the commercial fungicide, dodine (**170**); however, for *P. infestans* significantly more potent activities for **168** and **169** were observed. The likely mode of action for these compounds could entail an interaction with the cell membrane, in relation to their amphiphilic nature.

Their modest anti-fungal activity, cyclohexenone core and chirality make this class of compounds desirable candidates to demonstrate the synthetic versatility of iodo keto *cis*-diol **117**, which inherently possesses many of the desired structural features.

1.4.1 Biosynthetic Pathway to Hygrophorones

The biosynthetic pathway to pseudohygrophorones A (**168**) and B (**169**) has not been investigated; however, extensive research on the structurally related hygrophorone B (**171**, **Figure 14**) is believed to offer a plausible biosynthetic pathway that can be applied.

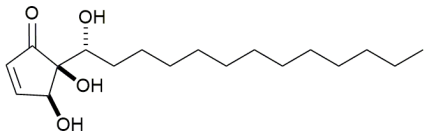

hygrophorone B

171

Figure 14: The structure of hygrophorone B (**171**).

Arnold and co-workers were able to decipher the biosynthetic pathway of hygrophorone B (**171**) by using ^{13}C labelled glucose. Their findings are shown in **Scheme 34**.[73]

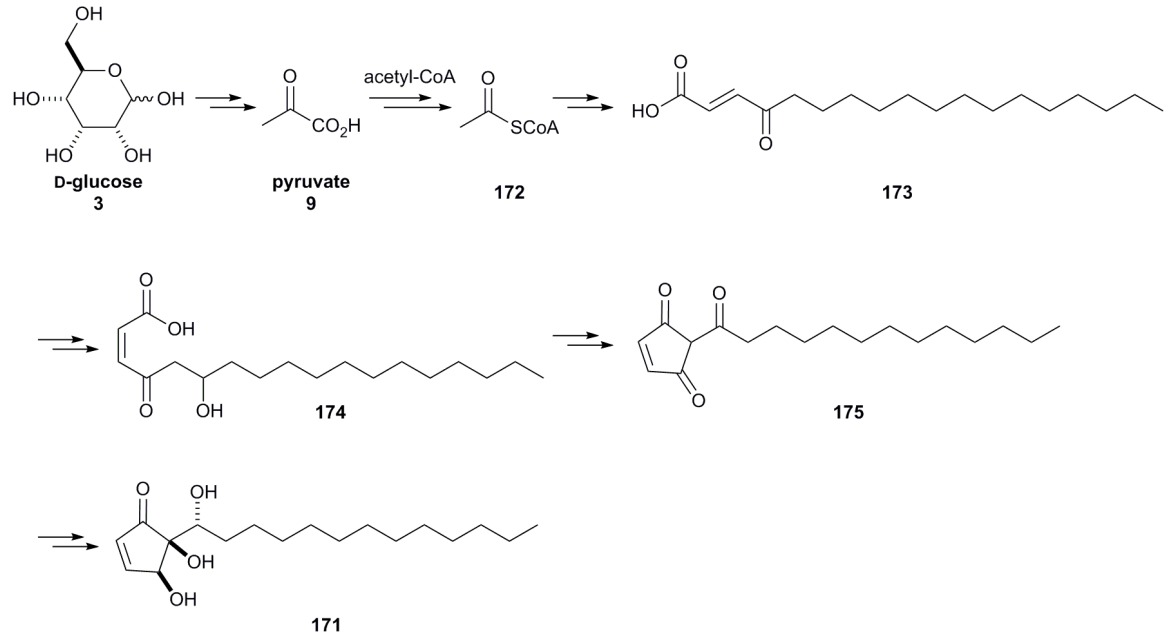

Scheme 34: The biosynthetic pathway for the formation of hygrophorone B (**171**).

Glucose (**3**) is first converted into pyruvic acid (**9**) via glycolysis, which undergoes oxidative decarboxylation to form coenzyme A derivative **172**. **172** then undergoes fatty acid polyketide biosynthesis to afford **173**, which is followed by an *E/Z* isomerisation and a hydroxylation of the aliphatic chain to give compound **174**. From here, the authors envisaged that an intramolecular aldol or lactonisation reaction occurs to form β,β'-triketone **175**. Finally, a stereoselective reduction of the carbonyl followed by an enantioselective hydroxylation, or vice versa, occurs to afford hygrophorone B (**171**). It was suggested that other cyclopentenone containing hygrophorones might follow an analogous pathway, however its relation to the biosynthesis of pseudohygrophorones A (**168**) and B (**169**) remains up for debate. Nonetheless, the hygrophorone B (**171**) biosynthesis provides a platform for further investigative research.

1.5 COTC

COTC (**176**, **Figure 15**) was first isolated in 1975 by Takeuchi and colleagues from the bacterium *Streptomyces griseosporeus*, and the absolute configuration was later confirmed by Chimura and co-workers.[74, 75]

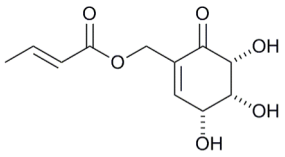

COTC
176

Figure 15: The structure of 2-crotonyloxymethyl-(4*R*, 5*R*, 6*R*)-4,5,6-trihydroxycyclohex-2-enone (COTC, **176**).

On isolation, it was noted that COTC (**176**) had significant inhibitory effects on HeLa and EHRLICH ascites carcinoma cells. Furthermore, it had potent reactivity with sulfhydryl compounds such as reduced glutathione, an antioxidant involved in detoxification. *In-vitro* studies on mice were carried out to evaluate the anti-proliferative activity of COTC (**176**), and the results are summarised in **Table 5**.[74]

Table 5: The effect of COTC (**176**) on subcutaneous solid tumours of EHRLICH carcinoma.

Dose (mg kg^{-1} day^{-1}) for 10 days	Tumour weight (mg)
0.00	1780 ± 110
0.32	1530 ± 330
0.63	1070 ± 200
1.25	1040 ± 100
2.50	1110 ± 130
5.00	980 ± 150
10.00	680 ± 250

It was observed that dosages above 10 mg/kg/day resulted in the death of the mice. On evaluation, this gave COTC (**176**) a relatively low toxicity (LD_{50} = 90 mg/kg). Aside from EHRLICH carcinoma, *in-vitro* studies were also carried out on L-1210 leukaemia cells; however, **176** showed only weak inhibition. The original hypothesis for the cytotoxic mechanism was inhibition of the glyoxalase I enzyme, which results in cell apoptosis.[74]

1.5.1 Glyoxalase System

The glyoxalase system (**Scheme 35**) is responsible for the catalytic conversion of cytotoxic methylglyoxal (**178**) to D-lactate (**181**) via *S*-D-lactoylglutathione (**180**). Glutathione (GSH, **177**, **Figure 16)** plays a pivotal role in this process and therefore has become a favoured biological target for oncological investigation.

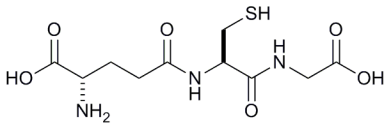

glutathione
177

Figure 16: The structural representation of γ-L-Glutamyl-L-cysteinylglycine (GSH, **177**).

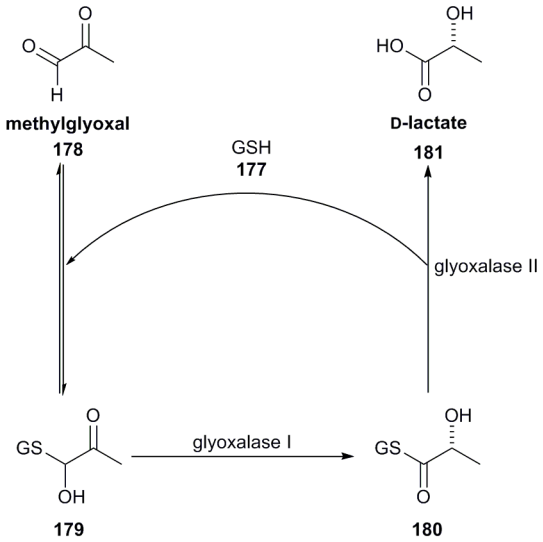

Scheme 35: The glyoxalase system.

The glyoxalase system starts with the non-enzymatic reaction of methylglyoxal (**178**) with reduced glutathione (GSH, **177**) to afford monohemithioacetal **179**. **179** is then converted to **180** via the glyoxalase I enzyme catalysed isomerisation. **180** then undergoes the catalysed hydrolysis by the glyoxalase II enzyme to afford D-lactate (**181**). The hydrolysis of the thioester of **180** to give **181** releases GSH (**177**), which can then be recycled to participate in another cycle with methylglyoxal (**178**). The blocking of this system results in the accumulation of methylglyoxal (**178**), which causes irreversible modification to the proteins and leads to cell apoptosis.[76]

Glutathione (**177)** plays a key role in the body's detoxification mechanisms, the glyoxalase system being one example as shown by **Scheme 35**. It is a tripeptide consisting of the amino acid residues: glycine, cysteine and glutamic acid and can act as both nucleophile and reductant. This property makes GSH (**177**) highly efficient at detoxifying xenobiotics. It also prevents the oxidative stress caused by cellular metabolism by reacting with the free radical by-products, which could damage the cell DNA.[77] The multi-cellular roles of GSH (**177**) are summarised in **Scheme 36**.

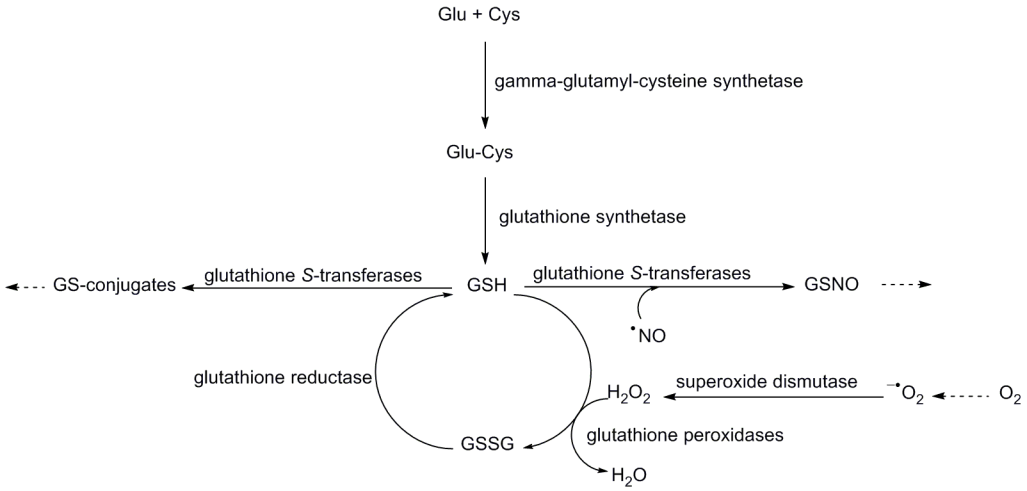

Scheme 36: The biological systems involving GSH (**177**). GSSG = oxidised GSH; GSNO = *S*-Nitrosoglutathione.[77]

COTC's (**176**) ability to detoxify drugs means it plays a prevalent role in anti-cancer drug resistance (e.g. cisplatin).[78] Cancer cell lines that exhibit resistance to alkylating agents have been noted to have an increased level of GSH (**177**) concentration within the cell and an overexpression of glyoxalase I.[79] Co-administering a GSH inhibitor with cancer-resistant drugs may provide a possible mechanism for reversing drug resistance without the need to develop new cancer agents.

1.5.2 COTC Mechanism

COTC (**176**) is an attractive therapeutic target, because of its synergistic effect with cancer drugs on cell lines that have become resistant to a drug treatment. Kamiya and co-workers first demonstrated the sequestering effect COTC (**176**) has on GSH (**177**) using apoptosis resistant human pancreatic adenocarcinoma (AsPC-1).[78] After dosing the AsPC-1 cell line with COTC, they reported that the intracellular concentration levels of GSH dropped to 40 % of their initial concentration after 1-2 hours. Following their confirmation that COTC decreased the GSH levels within a cancer cell line, Kamiya and co-workers co-administered Melphalan™ (**182**), an anti-cancer alkylating agent (**Figure 17**), with COTC and reported that the GSH underwent conjugate addition at a faster rate with COTC than with Melphalan™ (**182**), which was then free to act on the cancer target. This potentially opens new opportunities for a combined chemotherapeutic approach against resistant cancer cells. Finally, Kamiya and co-workers postulated that the conjugate product from

the reaction of COTC with GSH went on to inhibit the glyoxalase I. This resulted in cell apoptosis due to a build-up of cytotoxic compounds.[78]

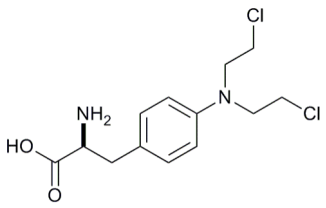

182

Figure 17: The chemical structure of Melphalan™ (**182**).

The initial proposed mechanism of inhibition by COTC (**176**), as proposed by Takeuchi and co-workers, is shown in **Scheme 37**. This proposal was based on reacting the natural product **176** with sulfhydryl compounds (**183**) to investigate the resulting products.

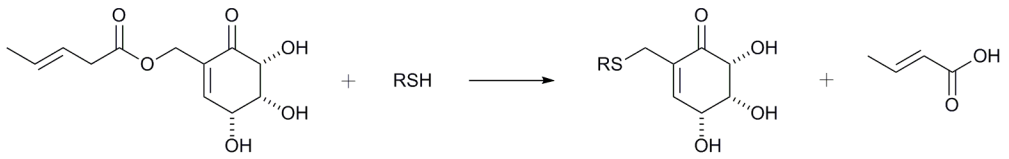

176 183 184 185

Scheme 37: The reaction of sulfhydryl compounds of general structure **183** with COTC (**176**) to probe the mechanism of inhibition.

According to their proposal, COTC (**176**) underwent nucleophilic attack by sulfhydryl containing compounds (**183**), which displaced the crotonyl group to form adduct **184**. The crotonyl group, which acted as a good leaving group, afforded crotonic acid (**185**) on displacement. The adduct **184** was then believed to inhibit glyoxalase I.

In 2000, Ganem and co-workers carried out the synthesis of compound **184** and reported that it was only a modest inhibitor of the glyoxalase I enzyme; thus, contradicting what was originally thought to be the biological mode of action.[80] In 2002, Ganem and co-workers also proposed a new hypothesis using COMC (**186**), a structural analogue of COTC (**176**) (**Scheme 38**).[81]

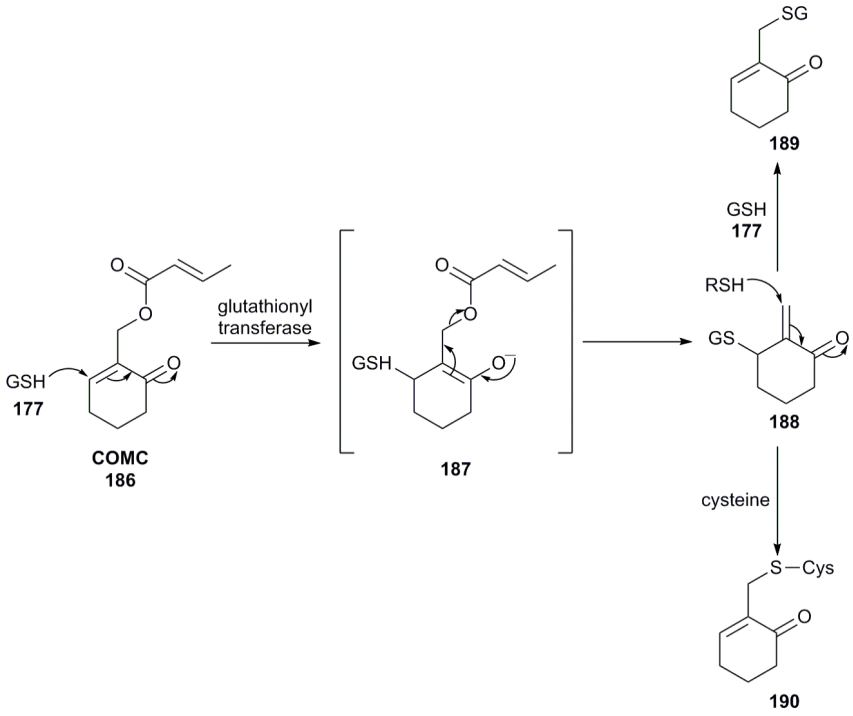

Scheme 38: The proposed biological mechanism for COTC (**176**) inhibition using the structural analogue COMC (**186**).

Ganem and colleagues proposed that the initial step was a glutathionyl transferase catalysed Michael addition of GSH (**177**) with COMC (**186**) to afford exocyclic enone **188** via the intermediate **187**. The exocyclic enone **188** was isolated during the study, which validated this initial step. From here, the highly reactive Michael acceptor **188** was suggested to induce cytotoxicity by undergoing a second Michael addition with GSH (**177**) to afford adduct **189**, or by alkylation from the proteins critical for cellular function (**190**).[82] The above mechanism is currently the accepted rationalisation for COTC (**176**) inhibition.

1.5.3 Antheminones

The antheminones are a class of compounds structurally related to COTC (**176**). They possess a similar cyclohexenone core and have been shown to target multi-drug resistant tumours.[83]

Collu and co-workers first isolated the antheminones from the leaves of *Anthemis maritium* in 2008. They characterised three new antheminone natural products, A (**191**), B (**192**) and C (**193**) (**Figure 18**).

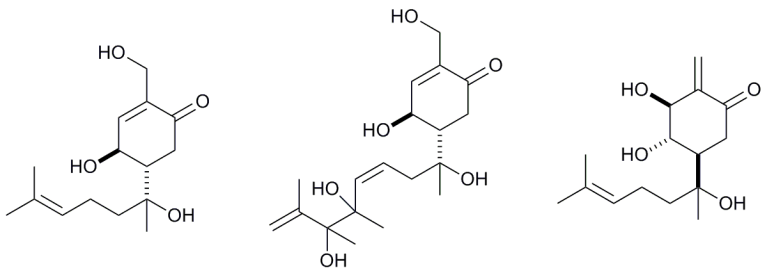

Figure 18: The chemical structures of antheminones A (**191**), B (**192**) and C (**193**).

The cytotoxicities of these compounds were evaluated against human cancer cell lines, and the results are summarised in **Table 6**.

Table 6: The biological results for antheminones A (**191**), B (**192**) and C (**193**). HCT-116 = colorectal carcinoma; CaCo-2 = Colorectal adenocarcinoma; MCF-7 = non-aggressive breast cancer; HL-60 = promyeloblast leukaemia; U-937 = histiocytic lymphoma; Jurkat T = acute T cell leukaemia.

	IC_{50} (μM)					
Compound	HCT-116	CaCo-2	MCF-7	HL-60	U-937	Jurkat T
191	15.0 ± 2.0	11.0 ± 1.0	21.0 ± 2.0	7.6 ± 0.6	6.2 ± 3.0	9.0 ± 0.4
192	29.0 ± 4.0	24.0 ± 3.0	29.0 ± 5.0	11.0 ± 0.9	12.0 ± 0.4	14.0 ± 2.0
193	19 ± 2.0	9.4 ± 1.1	15.0 ± 1.0	3.2 ± 0.6	7.4 ± 1.3	8.4 ± 0.3

It is generally accepted that the mechanism of cytotoxicity for antheminones A (**191**) and B (**192)** proceeds in a similar fashion to that of COMC (**186**). That is, the compounds react with GSH (**177**) leading to adducts that can become alkylated by intracellular proteins or nucleic acids. Antheminone C (**193**) lacks the cyclohexenone core, which is crucial for the proposed mechanism of GSH inhibition. Nonetheless, antheminone C (**193**) exhibited far more potency compared to A (**191**) and B (**192**) across most of the cell lines. Collu and co-workers rationalised that the exocyclic enone moiety in antheminone C (**193**) could undergo direct alkylation by the nucleic acids and by-pass activation by GSH (**177**).[83]

2.0 Results and Discussion

2.1 Project Aims

2.1.1 Development and Application of the Iodo Keto *Cis*-Diol

The major focus of this project was to develop synthetic methods for the synthesis of natural product analogues using the bioproduct, iodo keto *cis*-diol **117** (**Figure 19**). This bioproduct would be supplied by the project collaborators Höering and Allen.[84]

Figure 19: The structure of iodo keto *cis*-diol **117**.

Initial investigations would aim to develop: the acetonide protecting conditions for the *cis*-diol moiety, hydrogenolysis of the C-I bond and installing functionality at the β-position via a rhodium catalysed conjugate addition reaction. This would build upon the chemical groundwork set out by Boyd and co-workers (see **Section 1.1.3**, **Scheme 22**).[56] Following successful synthetic development, these conditions would then be applied to the synthesis of an analogue of the natural product incarviditone (**130**). This would be an appropriate target in consideration of incarviditone's promising biology and complex structure, which bears seven contiguous stereocentres. Furthermore, efforts would be made to demonstrate the reproducibility of the TDO catalysed biotransformation reaction by using the substrates 3-iodophenol (**115**) and bromobenzene (**60**). These biotransformations would initially be carried out on a small scale to determine optimum conditions before committing larger quantities.

In addition to the synthetic component of the project, a computational docking model would be developed for the TDO enzyme. Initial studies would begin with the docking of known substrates into the TDO enzyme active site and comparing the output with the observed experimental results. Providing a good correlation can be obtained, the computational docking studies would then be expanded to assess the model's ability to predict the biotransformation outcome of unknown substrates. The ultimate objective of this research is to develop a tool, which can reliably predict the potential bioproducts of

undocumented substrates and allow for the prediction of likelihood of success of a given biotransformation.

2.1.2 Alternative Synthetic Routes

In consequence of the poor yield for the biotransformation of 3-iodophenol (**115**) using *P. putida* UV4, the supply of bioproduct **117** was limited. An additional aim of this project therefore, was to develop alternative synthetic routes which would give the same stereochemical outcome as that accessible from iodo keto *cis*-diol **117**. This would be achieved by using the chiral pool molecule (-)-quinic acid (**194**) and protecting the *trans*-diol as a butan-1,2-diacetal (BDA, **195**, **Scheme 39**). This synthetic route would expand on the Whitehead group's previously reported results using the BDA protecting group.[85] It was also envisaged that by employing the substitute (-)-quinic acid route in parallel with the iodo keto *cis*-diol route, a direct comparison could be made to showcase the advantages of using diol **117** as a chiral building block.

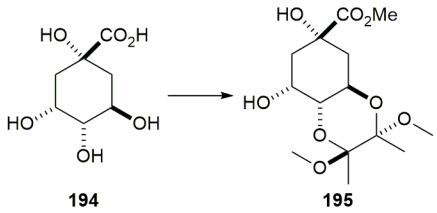

Scheme 39: The protection of the *trans*-diol in (-)-quinic acid (**194**) as the butan-1,2-diacetal (BDA) **195**.

Furthermore, (-)-quinic acid (**194**) would also be used to synthesise the antipodal compounds to those obtainable from iodo keto *cis*-diol **117** and the butan-1,2-diacetal protected (-)-quinic acid **195**. This would be accomplished by selective protection of the vicinal *cis*-diol as either a cyclohexylidene ketal (**196**) or acetonide moiety (**197**) (**Scheme 40**).

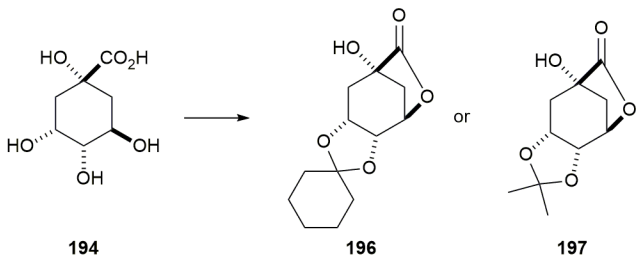

Scheme 40: The protection of the *cis*-diol in (-)-quinic acid (**194**) as either cyclohexylidene **196** or acetonide **197**.

The compounds synthesised using this methodology would serve to investigate the biological differences between the enantiomers of the incarviditone analogues as well as allowing for the synthesis of analogues of the related natural product incarvilleatone, which is formed by the heterodimerisation of two opposite monomeric enantiomers (see **Section 1.3**). The antipodal series would also be used for the synthesis of analogues of the natural products COTC and antheminone A: this would be with the purpose of developing and demonstrating a synthetic route towards an additional natural product target, which could be accessed from iodo keto *cis*-diol **117.**

In addition to the incarviditone and incarvilleatone natural product analogues, a model compound (**198**) would be used to develop the synthetic methodology (**Figure 20**) towards analogues of pseudohygrophorones A (**168**) and B (**169**).

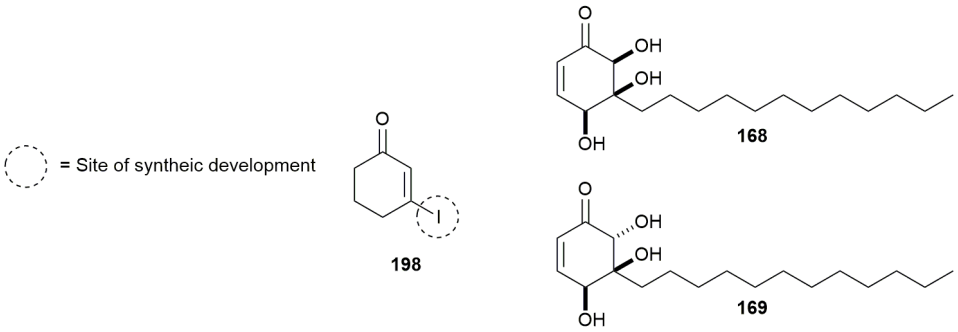

Figure 20: The structures of pseudohygrophorones A (**168**) and B (**169**), and 3-iodocyclohexenone (**198**); the model system for iodo keto *cis*-diol **117**.

Preliminary investigations would involve development of cross-coupling conditions for installation of aromatic and long alkyl side-chains. Following successful demonstration of these conditions on the model system, further studies would then look to apply the optimised reaction conditions using iodo keto *cis*-diol **117**.

2.1.3 Biological Studies

Following completion of the aims described above, the natural product analogues would then be assessed for their anti-proliferative activities using an MTT assay against the four cancer cell lines: A549, MDA-MB-231, FaDu and PNT2. Furthermore, the most potent incarviditone analogues would be subjected to structure-activity relationship (SAR) studies. The focus of these SAR studies would be to change key structural features of the incarviditone core to determine the effect this would have on the anti-proliferative activity.

This would provide information on the structural features responsible for the biological mode of action, which remains unknown.

2.2 Computational Docking

Prior to investigation of synthetic applications of iodo keto *cis*-diol **117**, a computational docking model was developed for TDO using the Gold™ docking software. The initial purpose of this work was to rationalise the binding modes of 3-iodophenol (**115**) in the TDO active site, which give rise to the desired iodo diol **117** and catechol side-product **113** (**Scheme 41**).

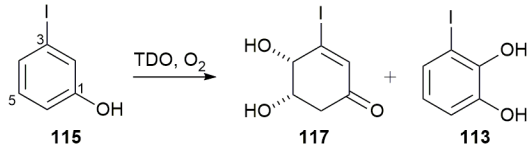

Scheme 41: The TDO catalysed biotransformation of 3-iodophenol (**115**) using *P. putida* UV4 to afford the desired iodo keto *cis*-diol **117** and the catechol side-product **113**.

Currently, there is only one available crystal structure for TDO, which was obtained from *P. putida* F1 with toluene bound into the active site in the absence of O_2.[7] As previously mentioned, however, the amino acid sequence of TDO in both F1 and UV4 is identical, (**Section 1.1.1**) and therefore the results of the computational studies can be assumed to apply across both *P. putida* strains. The active site of TDO is shown in **Figure 21**.

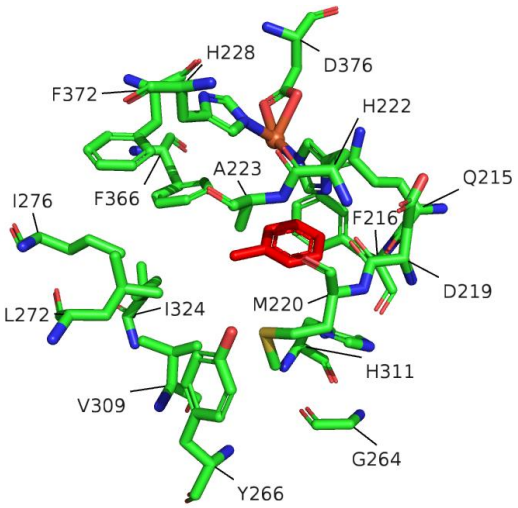

Figure 21: The TDO active site from *P. putida* F1 with toluene (red) bound. The active site consists of 17 amino acid residues.[7] The Fe (orange) is bound by the residues: Asp_{376}, His_{222} and His_{228}.

The active site is comprised of 17 amino acid residues, which create an ellipse-shaped substrate pocket. These mostly non-polar residues stabilise the toluene substrate through van der Waals and hydrophobic interactions. The active site of TDO bares significant similarity to the active site of biphenyl dioxygenase (BPDO), as there is only one amino

acid difference within the active site (Val_{309} in TDO, Ala_{311} in BPDO). This similarity assisted with the determination of the location of the methyl group of bound toluene, as the crystal structure resolution for the TDO enzyme (3.2 Å) was not sufficient to map its exact location.[7] As a result of the low resolution, all docking results reported herein are suggestive, and are otherwise a guide for future development.

Preliminary steps were taken before computational docking to "prepare" the crystal structure, which comprised of adding hydrogen atoms to the protein and removing all water molecules from within the structure. It is not believed any water molecule partakes in the dioxygenase mechanism, as indicated by the prior mechanistic evaluation described in **Section 1.1.1** and the absence of water in the active site. To support this assumption, a comparative docking of 3-iodophenol (**115**) was carried out using the TDO crystal structure with and without water molecules: in both systems the results were identical, thus supporting this assumption.

Following the preparation of the crystal structure for docking, an appropriate scoring function (a mathematical method) was required to predict the binding affinity of the docked substrate. Gold™ contains four scoring functions: GoldScore, ChemPLP, ASP and ChemScore, which differ by a set of predefined parameters (e.g. van der Waals energy and protein ligand atom clash). To determine the optimum scoring function for TDO, the bound ligand within the crystal structure, in this instance toluene, had to be extracted from the crystal structure and re-docked to ascertain the scoring function which best mimicked the natural binding mode (see **Figure 22**).

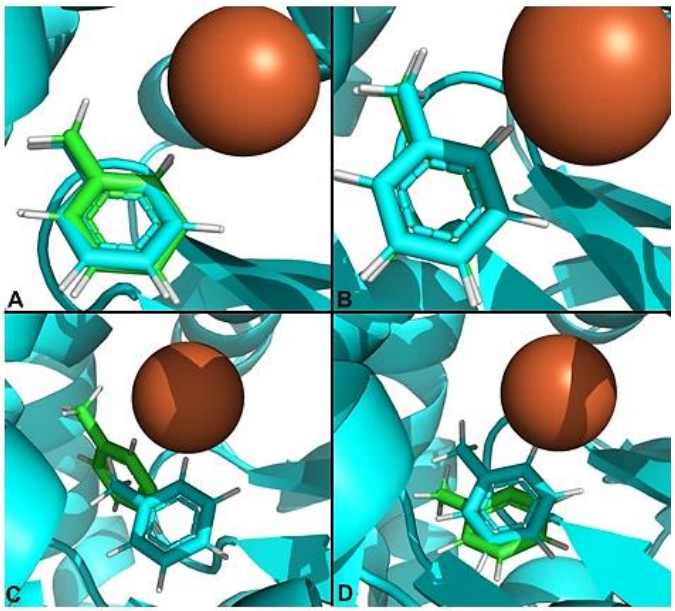

Figure 22: The determination of the best scoring function by extracting and redocking toluene. Cyan = original crystal structure; green = docked solution; A = ASP; B = ChemPLP; C = ChemScore; D = GoldScore.

Immediately, ChemScore (**C**) and GoldScore (**D**) were discarded as evident by the off-set positioning between the re-bound toluene and the original crystal structure. ASP (**A**) and ChemPLP (**B**) gave excellent consistency, with the latter being chosen as the preferred scoring function. Internal studies by the Cambridge Crystallographic Data Centre have demonstrated that ChemPLP is consistently the most effective scoring function for pose prediction and outperforms ASP on all accounts.[86] The ChemPLP scoring function is defined by **Equation 1**, which was developed by Exner and co-workers in 2008.[87] The definitions for the terms in **Equation 1** are shown in **Table 7**.

$$\int ChemPLP = \int plp + \int hb + \int hb - ch + \int hb - CHO + \int met + \int met - coord + \int met - ch + \int met - coord - ch + \int clash + \int tors + c_{site}$$

Equation 1: The definition for the ChemPLP scoring function.

Table 7: Definitions for the ChemPLP terms.

Abbreviation	Term	Definition
plp	Piecewise linear potential	Models the steric complementarity of the ligand and the protein active site
hb, hb-ch, hb-CHO	Hydrogen bonding	The distance and angle dependent hydrogen bonding terms. Hb = Both atoms are uncharged or exactly one atom is charged; hb-ch = charged donor and charged acceptor; hb-CHO = all hydrogen bonding pairs containing an oxygen-acceptor
met, met-coord, met-ch, met-coord-ch	Metal interactions	Distance and angle dependent metal interactions. Met = ligand acceptor and metal interaction; met-coord = fits the coordination polyhedra of the metal atom; met-ch = charged acceptor atom and metal interactions
clash	Ligand clash potential	A term to avoid internal ligand clashes. The term considers ligand atom pairs which are at least three bonds away
tors	Ligand torsional potential	Calculates the torsional potential for all rotatable bonds available in the ligand
c_{site}	Additional contributions	A quadratic potential which forces the ligand to interact with the predefined binding site and avoids areas outside of the binding sphere

The next goal was to establish whether the output from the newly developed model corresponded to the observed experimental results. Unfortunately, the docking pose of 3-iodophenol (**115**) with the highest fitness score (i.e. best docked pose) predicted the formation of catechol **113**. This is contradictory to the reported experimental outcome, with the formation of iodo keto *cis*-diol **117** being the major product and catechol **113** as the minor side-product.

Re-evaluation of the model revealed a shortcoming with regards to the absence of O_2 in the binding site. Due to the pivotal role of molecular oxygen in the mechanism, it was deemed critical to develop a model that encompassed this component. To achieve this, the O_2 bound crystal structure of NDO was used,[88] with the view that the similarity between the

two enzymes' active sites (see **Figure 23**) would allow for a reliable mapping of molecular oxygen into the TDO enzyme.

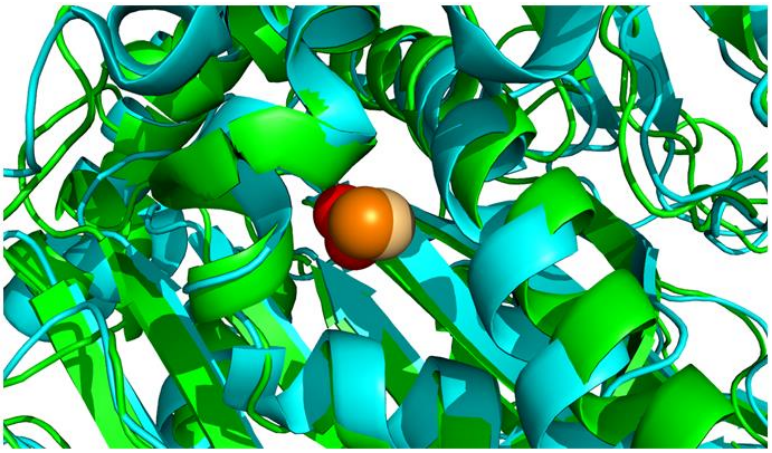

Figure 23: The TDO and NDO crystal structures overlaid using PyMol (v 2.0.4). Green = TDO; cyan = NDO; red = O_2; orange = Fe from NDO; light orange = Fe from TDO.

The root mean square deviation (R.M.S.D) of the overlaid dioxygenases shown above was 1.24 Å; thus, showing an excellent degree of homology between the two proteins. Furthermore, the relative position of the mononuclear iron in both active sites differed by only 0.9 Å. Based on this data, O_2 was successfully mapped into the TDO crystal structure, retaining its relative coordinates with respect to NDO. The newly devised model for TDO was then used in all the docking studies described herein.

2.2.1 Docking of 3-Iodophenol

To understand the remarkable ability of TDO to regio- and enantioselectively dihydroxylate halogenated phenols, 3-iodophenol (**115**) was docked to identify the key amino acid residues responsible for this transformation. Pleasingly, in the new model, the strongest predicted binding mode coincided with the major product **117** from the biotransformation using *P. putida* UV4 (**Figure 24**). The predicted outcome was determined by the closest distance from the nearest two carbons of the substrate to the mononuclear iron, rather than O_2. This was because O_2 was not inherent to the original crystal structure, and its relative position would be expected to deviate from the defined coordinates during the biological mechanism. Rather, O_2 was added to mimic the space filling and electrostatic interactions which would be present in the natural system.

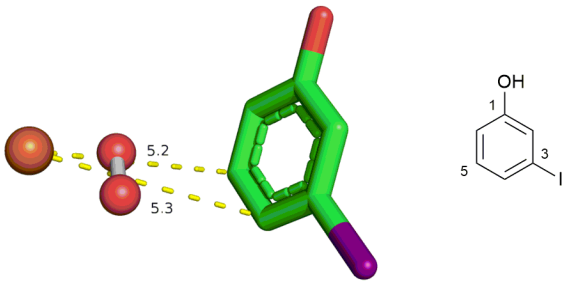

Figure 24: The major predicted binding pose with the highest fitness score of 3-iodophenol (**115**), corresponding to 4,5-dihydroxylation to give iodo keto *cis*-diol **117**. Orange = Fe; red = O; purple = iodine. Measurements to Fe are in Å.

As depicted, the best binding pose determined by the computational docking positions the 4,5-bond closest to the iron catalytic centre. Furthermore, the substrate is bound in a way that the iron faces only one side of the aromatic ring, which is suggestive for the possible enantioselectivity observed experimentally. The predicted stereochemistry of the bioproduct **117** (4*S*, 5*S*) was also consistent with the experimental data, which suggests that the docking pose depicted in **Figure 24** could represent the natural pose. The amino acids suggested to be involved in stabilising this pose are illustrated in **Figure 25** and **Figure 26**.

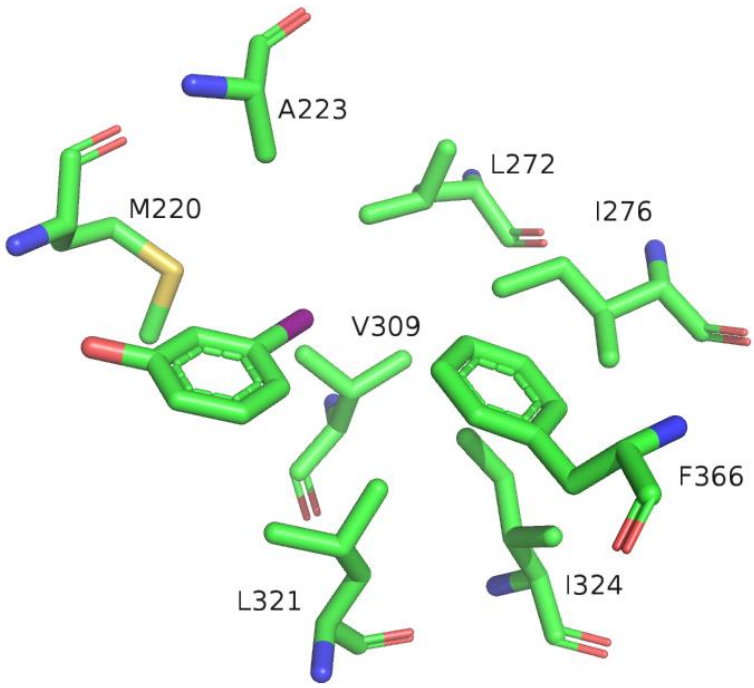

Figure 25: The amino acid residues within 5 Å of the iodine atom (purple) are shown.

The iodine atom is encapsulated inside a hydrophobic pocket, which is comprised of the key residues: Ala_{223}, Leu_{272}, Ile_{276}, Val_{309}, Leu_{321}, Ile_{324} and Phe_{366}; it is postulated that

these amino acid side-chains stabilise the iodine atom through hydrophobic and van der Waals interactions.

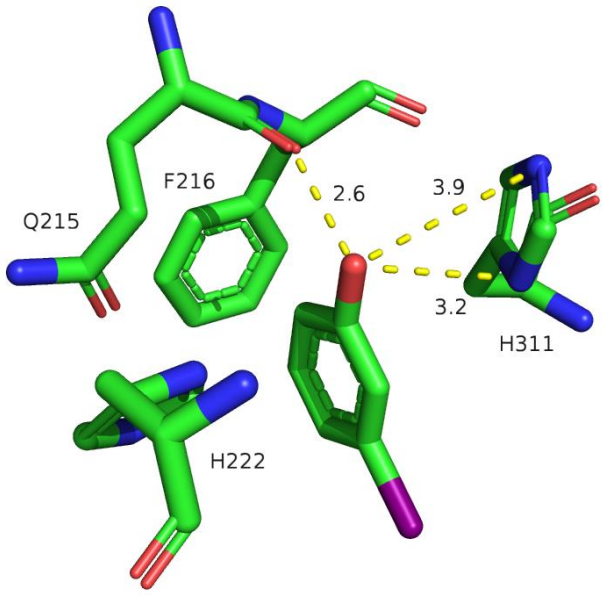

Figure 26: The T-faced interaction of His_{222} and Phe_{216}, and the hydrogen bonding distance measurements (Å) of His_{311} and Gln_{215} with 3-iodophenol (**115**).

The aromatic ring of 3-iodophenol (**115**) is positioned in a manner that suggests two T-faced interactions could be occurring with the His_{222} and Phe_{216} residues.[89, 90] T-faced interactions are one preferred orientation for the interaction between aromatic groups; it is proposed that T-faced interactions limit π-π repulsion; however, this idea is disputed within the literature. In 2011, Allen and co-workers proposed that the favoured formation of iodo keto *cis*-diol **117** is driven by a key hydrogen bonding interaction between the hydroxyl group of the substrate and His_{311}.[57] As shown in **Figure 26**, the nitrogen atom from His_{311} is 3.2 Å away from the hydroxyl oxygen atom of substrate **115**. This is not within the range for a strong hydrogen bond and suggests that his is not a key interaction. It should be noted that due to the resolution of the crystal structure, carbon and nitrogen atoms within the histidine side-chain cannot be distinguished. Furthermore, the exact tautomeric state of the histidine residues can also not be determined, so measurements to both His_{311} nitrogen atoms are consequently shown. Interestingly, the docking revealed a stronger predicted hydrogen bonding interaction (2.6 Å) between the carbonyl backbone of Gln_{215} to the hydroxyl of substrate **115**. The importance of this interaction has not been highlighted in previous studies, and therefore its role cannot be understated with respect to the preferential *cis*-dihydroxylation of the 4,5-bond of 3-iodophenol (**115**). Further research, therefore, should look to validate the importance of the Gln_{215} role.

Overall, 80 % of the observed poses led to diol **117** as the product and 20 % successfully predicted the formation of the minor side-product catechol **113**; the major and minor products are consistent with the reported experimental outcome. The minor binding pose is shown in **Figure 27**.

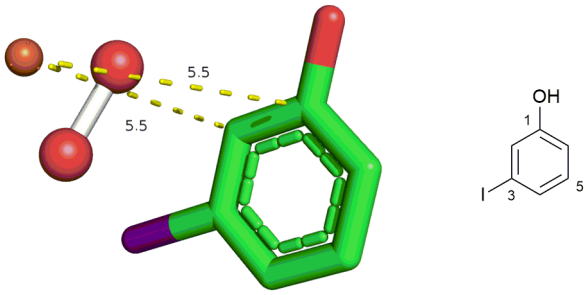

Figure 27: The minor predicted binding pose of 3-iodophenol (**115**), corresponding to the 1,2-dihydroxylation to give catechol **113**. Measurements to Fe are in Å.

The Fe is now positioned across the 1,2-bond, which would result in the formation of the intermediate triol **114** prior to the elimination of water to form catechol **113** (see **Section 1.1.3**, **Scheme 21**). The position of the iodine atom with respect to the major pose is retained and continues to occupy the hydrophobic pocket consisting of the key residues illustrated in **Figure 25**. Likewise, His_{222} and Phe_{216} are suggested to non-covalently bind the substrate via the same T-faced interactions described for the major docking pose. The hydrogen bonding interactions, however, are reduced in the minor binding pose, as illustrated by **Figure 28**.

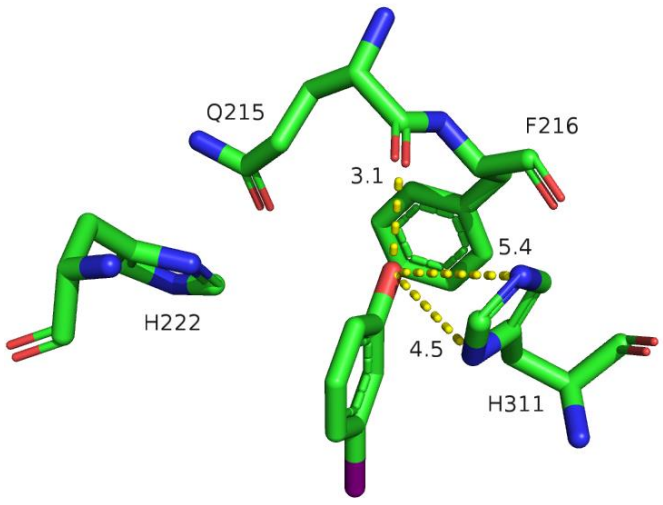

Figure 28: The T-faced interactions of His_{222} and Phe_{216} and the hydrogen bonding distance measurements (Å) between the hydroxyl functionality of **115** with the nitrogen atoms of His_{311} are shown.

With comparison to the major pose, the hydroxyl functionality of **115** is orientated away from His_{311}, which increases the relative distance from 3.2 Å (**Figure 26**) to 4.5 Å (**Figure 28**). This was also the case for the carbonyl backbone interaction between Gln_{215} and **115**, which increased from 2.5 Å to 3.1 Å. The increased distances observed in the minor binding pose were suggested to result in weaker hydrogen bonding interactions between the substrate and the protein and is a plausible explanation for why catechol **113** is formed as the minor side-product from the biotransformation.

The agreement between the predicted binding pose and the observed experimental outcome provide a basis for understanding the biotransformation of 3-iodophenol (**115**). The results, however, remain suggestive without experimental data. Nevertheless, with the model in hand, the next objective was to apply the model to other known substrates for TDO to verify its reliability in predicting the experimental outcomes. It was envisaged that if this could be established, then unknown substrates could be docked to predict potential bioproducts and the likely success of a biotransformation.

2.2.2 Docking of Halogenated Benzenes

The halobenzenes are amongst some of the best reported substrates for TDO, with excellent yields and stereoselectivity observed for most of the halogens. The reported experimental and computational docking results are summarised in **Table 8**. The percentage of binding poses reflects the number of poses that would lead to a predicted metabolite based on the shortest distance from the Fe centre to the nearest two adjacent carbon atoms from the substrate.

Table 8: The experimentally reported biotransformation products and yields for the halogenated benzene substrates **59-61** and **79** using *P. putida* UV4. The percentage of binding poses corresponding to the reported products **62-64** and **84** are shown. † = No reported yield.

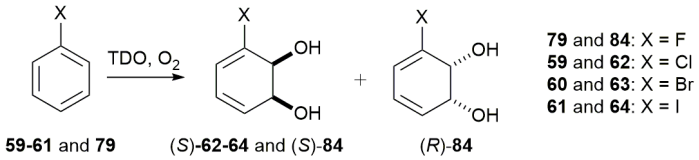

Substrate	Reported product(s)	Yields (e.e, %)	Percentage of binding poses (%)
79	(*S*)-**84** and (*R*)-**84**	†N.A (ca. 60 %)[91]	(*S*)-**84** (7 %), (*R*)-**84** (0 %)
59	(*S*)-**62**	80 % (>98 %)[48]	98 %
60	(*S*)-**63**	77 % (>98 %)[46]	99 %
61	(*S*)-**64**	85 % (>98 %)[46]	96 %

For the substrates **59**-**61**, the stereochemistry (1*S*, 2*S*) for the reported products was identical to the predicted outcomes obtained from the computational docking. The high yield associated with these substrates may be attributed to the preferential adoption of one major binding pose, which is illustrated in **Figure 29** using bromobenzene (**60**) as an example.

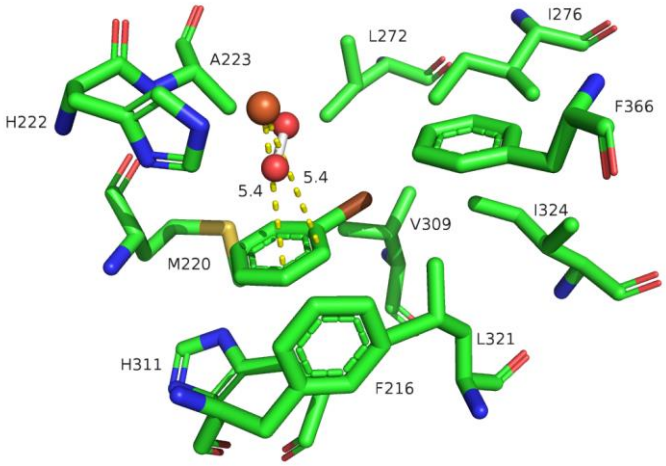

Figure 29: The major binding pose for bromobenzene (**60**). The amino acid residues within 5 Å of the substrate are shown. Brown = bromine. Measurements to Fe are in Å.

There is a clear preference in the model system for the non-polar functionalities of the halogenated benzenes (i.e. the halogen atom) to occupy the hydrophobic pocket described previously for 3-iodophenol (**115**). The T-faced interactions observed previously are also conserved and this binding mode was also consistent for chloro- (**59**) and iodobenzene (**61**). With regard to fluorobenzene (**79**), a reduction of the non-polar interactions within the hydrophobic pocket could be a major contributor to the poor regioselectivity reported for the formation of *cis*-diol metabolite (*S*)-**84**. To illustrate this, the space filling models for bromo- (**60**) and fluorobenzene (**79**) were compared as shown in **Figure 30**.

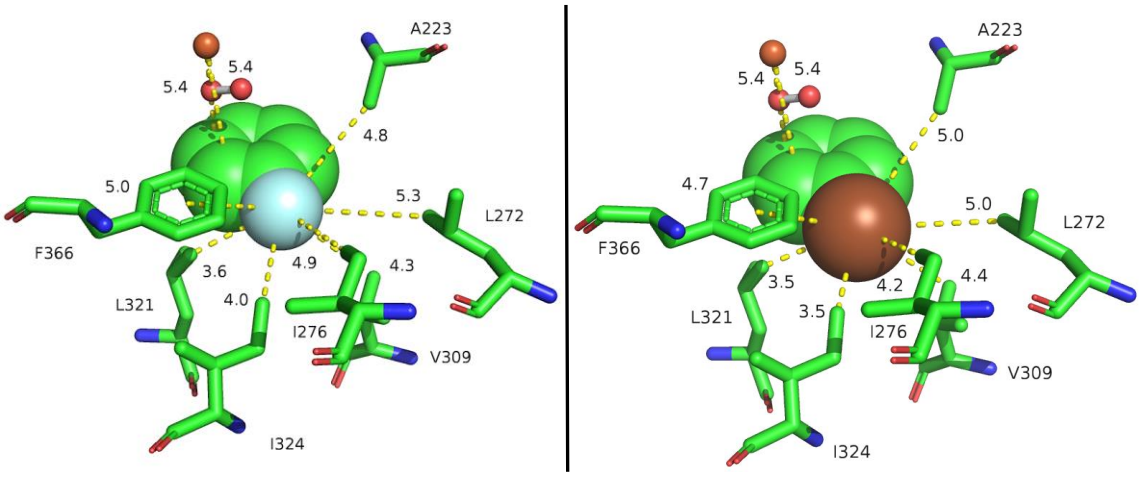

Figure 30: The space filling models of fluorobenzene (**79**) and bromobenzene (**60**) in the hydrophobic pocket of the TDO active site. The measurements (Å) shown are to the closest amino acid side-chains and to Fe. Light blue = fluorine; brown = bromine.

The fluoro group has a net loss of interaction with the hydrophobic pocket in comparison with the bromine atom, as supported by increased distances from the key amino acid residues. Only 7 % of the total docked results for fluorobenzene assumed this pose, with the remaining 93 % being orientated for effective dihydroxylation of the 1,2-bond, as shown by **Figure 31**. Once formed, the resulting diol formed would be expected to eliminate to regain aromaticity.

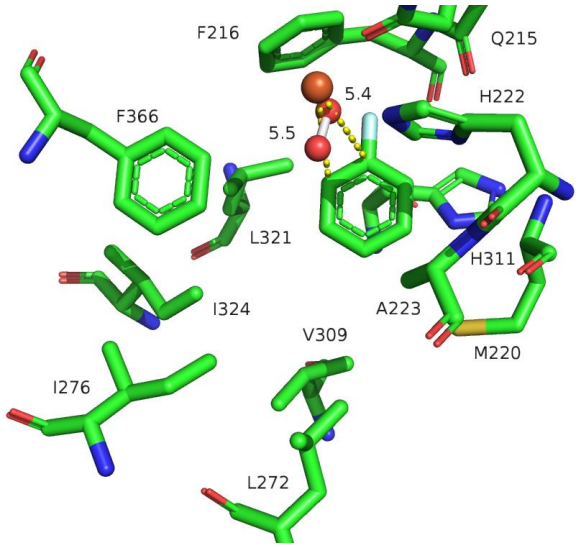

Figure 31: The highest fitness score pose for fluorobenzene (**79**), representing 97 % of the total docked poses. The amino acid residues within 5 Å of substrate **79** are shown. The measurements to Fe are in Å.

As shown by the major pose, fluorobenzene (**79**) is flipped with respect to the major docking poses of chloro- (**59**), bromo- (**60**) and iodobenzene (**61**). The smaller van der Waals radius of the fluorine atom (r_w = 147 pm), which can be likened to that of a

hydrogen atom (r_w = 120 pm),[92] presumably allows for a greater rotation of the substrate in the active site. Experimentally, there was no evidence for any formation of the bioproducts that could be linked to this pose, however it is important to note that formation of the catechol metabolites is rarely observed when using *P. putida* UV4, due to the further biodegradation by other enzymes. The existence of such metabolites, therefore, cannot be precluded particularly in the absence of a reported yield for the fluorobenzene biotransformation (**Table 8**).[91] On the other hand, both enantiomers of *cis*-diol metabolite **84** were isolated by Boyd and co-workers, and the pose presented in **Figure 31** would correlate well with the opposite stereochemistry depicted in **Figure 30**, providing the hydroxylation occurred at the 2,3-bond.

To conclude, the developed model has been shown to correlate with the experimental outcome of the TDO biotransformations of halobenzenes. Fluorobenzene (**79**) highlighted a shortcoming of this model with respect to predicting the bioproduct based on the shortest distance to the iron centre. This method, despite being adequate for a static model, detracts from the fact that the system is dynamic, and therefore such measurements would be expected to deviate from those defined by the docking studies. Consequently, the binding mode shown in **Figure 31** could be a plausible representation for the formation of *cis*-diol (*R*)-**84**. Nevertheless, in a broader sense, the model was predictive for a relatively poor biotransformation output for the substrate fluorobenzene, which is supported by the experimental results reported in the literature.

2.2.3 Docking of Bicyclic Systems

The substrate compatibility of the TDO enzyme extends beyond substituted monocyclic aromatics. In the literature, TDO has been reported to catalyse the dihydroxylation of a multitude of naphthalene and quinoline derivatives, examples of which are shown in **Table 9** along with the percentage of docked poses as determined by the shortest distance of the mononuclear Fe to the nearest two adjacent carbon atoms of the substrate.

Table 9: The experimentally reported biotransformation products and yields for a series of naphthalene and quinoline substrates (**199**-**203**) using *P. putida* UV4. The percentage of binding poses corresponding to the reported products (**204**-**215**) are shown. The metabolites **212**-**214** and **215** are unique to the naphthalene and quinoline biotransformations respectively. All the reported products possessed >98 % e.e.† = Relative yields for all the quoted bioproducts; no isolated yields were reported.

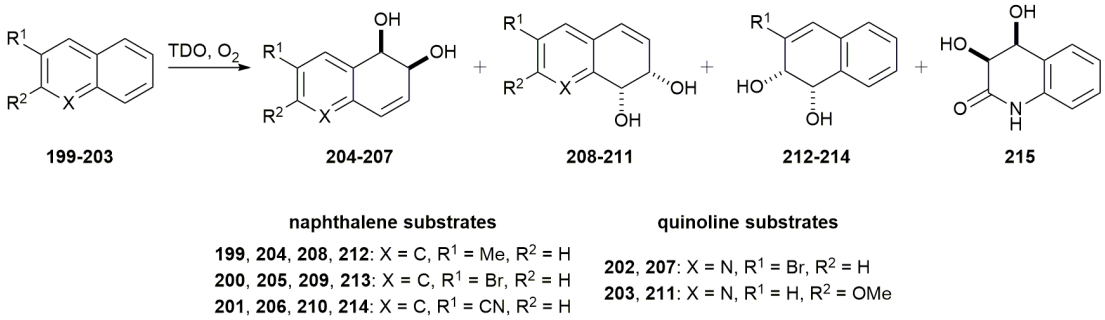

Substrate	Reported products	Reported yields (%)	Percentage of binding poses (%)
199	**204**, **208** and **212**	†**204** (60 %), **208** (10 %), **212** (30 %)[52]	**204** (97 %), **208** (0 %), **212** (0 %)
200	**205**, **209** and **213**	†**205** (33 %), **209** (40 %), **213** (27 %)[52]	**205** (98 %), **209** (0 %), **213** (0 %)
201	**206**, **210** and **214**	†**206** (15 %), **210** (57 %), **214** (28 %)[52]	**206** (61 %), **210** (8 %), **214** (4 %)
202	**207**	**207** (23 %)[93]	**207** (89 %)
203	**211** and **215**	**211** (7 %), **215** (13 %)[93]	**211** (85 %), **215** (7 %)

The computational docking studies of 6,6-bicyclic systems gave variable results concerning the ability of the model to predict the experimental outcome. Beginning with the naphthalene derivatives, 2-methylnapthalene (**199**) proved to be a moderate success, with 97 % of the predicted poses corresponding to the major bioproduct **204** from the biotransformation. The docking, however, failed to account for the minor metabolites **208** and **212**. The major binding pose for 2-methylnaphthalene (**199**), which corresponds to metabolite **204**, is shown in **Figure 32**.

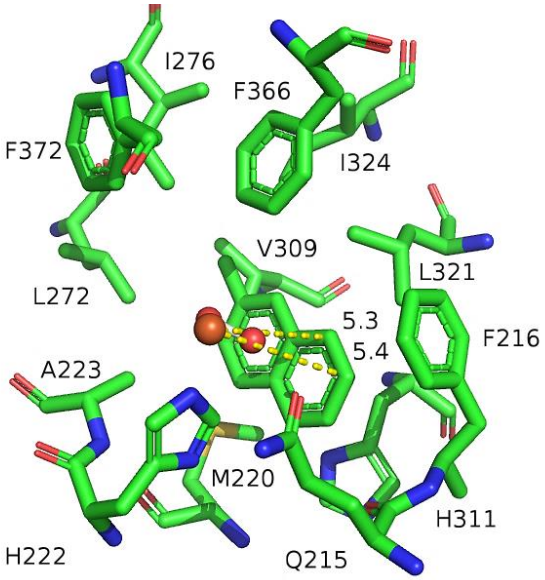

Figure 32: The major binding pose for 2-methylnaphthalene (**199**). All amino acid residues within 5 Å of the substrate are shown. The measurements to Fe are in Å.

As expected, the methyl group occupies the hydrophobic pocket with no additional interactions observed other than those previously described. 1 % of the docking poses did equate with the regiochemistry of **212**; however, the predicted stereochemical outcome was for the incorrect (*R*)-enantiomer. The binding mode shown in **Figure 32** was conserved for the major poses of 2-bromonaphthalene (**205**, 98 %), 2-cyanonaphthalene (**206**, 61 %), 3-bromoquinoline (**207**, 89 %) and 2-methoxyquinoline (**211**, 85 %).

The docking of 2-bromonaphthalene (**200**) gave no indication that all three regioisomers (**205**, **209** and **213**) would be formed in a similar relative amount, as was observed experimentally. Rather, the docking predicted a predominant formation of **205**. 2-Cyanonaphthalene (**201**) yielded a more complicated scenario: more than 10 different bioproducts were predicted by the computational docking, all of which were represented by relatively low percentage of poses (ca. 1-4 %). Interestingly, the major binding pose (**206**) of 2-cyanonaphthalene (**201**) situated the nitrile group inside the hydrophobic pocket, which would be unexpected considering the polar nature of this functionality. Instead, it would be anticipated that this pose would be energetically unfavourable, and as such would produce bioproduct **206** as a minor metabolite of the biotransformation. Experimentally, metabolite **206** was obtained in the lowest relative yield (15 %), which supports this proposal.

Conversely, 3-bromoquinoline (**202**) proved to be a good substrate for the docking model. 89 % of the docked poses predicted bioproduct **207**, which was the only isolated *cis*-diol

metabolite from the biotransformation. The introduction of a more polar side-chain, in this instance 2-methoxyquinoline (**203**), yielded less accurate results, with 85 % of the predicted poses corresponding to the minor metabolite (**211**) and only 7 % to the major (**215**). As with 2-cyanonapthalene (**201**), the predicted docking poses for **211** and **215** orientated the methoxy group into the hydrophobic pocket.

In addition to the 6,6-bicyclic aromatics described above, docking was also performed on 6,5-hetereoaromatic substrates, and the results are summarised in **Table 10.**

Table 10: The experimentally reported biotransformation products and relative yields for a series of benzothiophene (**100** and **216**) and benzofuran (**104** and **217**) substrates using *P. putida* UV4. The percentage of binding poses corresponding to the reported products are shown. Only the relative yields are quoted. All reported products possessed >98 % e.e.[53]

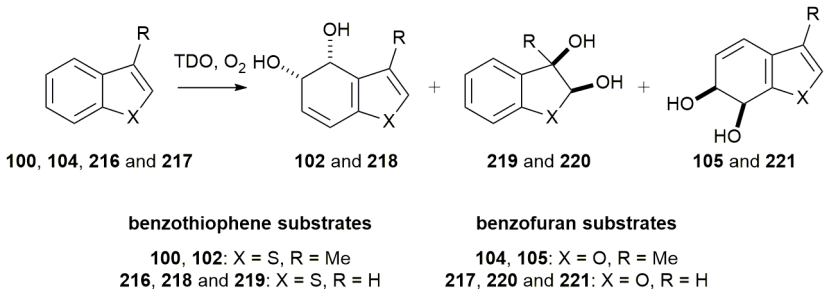

Substrate	Reported products	Relative reported yields (%)	Percentage of binding poses (%)
100	**102**	**102** (100 %)	**102** (95 %)
216	**218**, **219**	†**218** (12 %), **219** (71 %)	**218** (1 %), **219** (95 %)
104	**105**	**105** (75 %)	**105** (1 %)
217	**220**, **221**	†**220** (39 %), **221** (35 %)	**220** (61 %), **221** (2 %)

The docking of benzothiophene substrates **100** and **216** showed an excellent link between the predicted binding poses and reported products. The major metabolite for benzofuran (**217**) was also predicted; however, 35 % of the docking corresponded to the incorrect (*R*)-enantiomer of metabolite **220** and only 2 % predicted the formation of **221**. The results became progressively worse for 3-methylbenzofuran (**104**), as only 1 % of the docking poses corresponding to the major bioproduct **105**. The major binding poses of 3-methylbenzothiophene (**100**) and benzofuran (**217**) are shown in **Figure 33.**

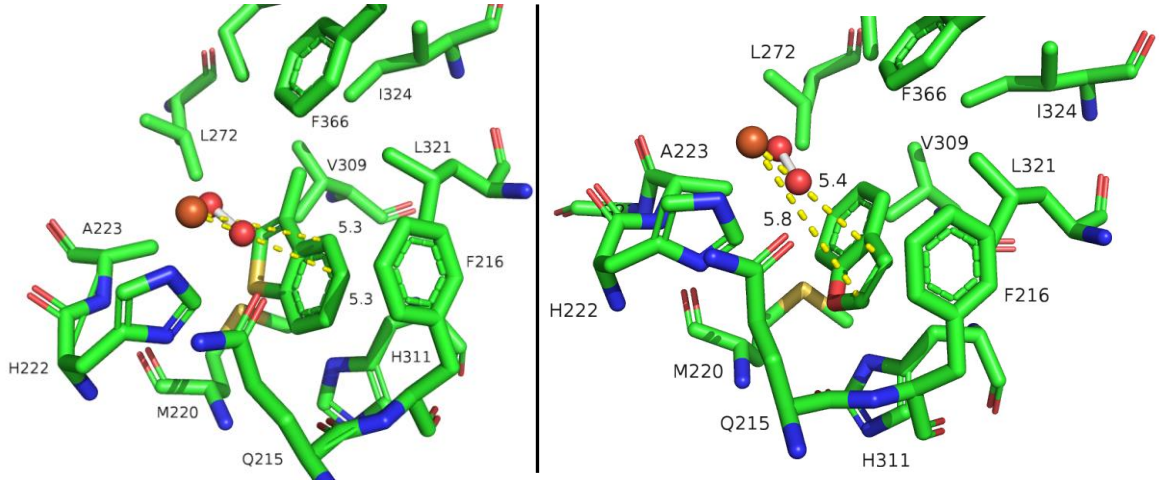

Figure 33: The major docking poses for 3-methylbenzothiophene (**100**) and benzofuran (**217**). The measurements to Fe are in Å.

To summarise, the docking model for 6,6-bicyclic systems functions reasonably well for non-polar substituted naphthalene and quinoline derivatives. In all cases, the docking successfully predicted the presence of an observed metabolite. Furthermore, with respect to 2-methylnaphthalene (**199**) and 3-bromoquinoline (**202**), the model predicted the major *cis*-diol metabolites **204** and **207** respectively. With regards to the 6,5-heteroaromatic systems, the docking proceeded well with the benzothiophene derivatives (**100** and **216**), but poorly with the benzofuran substrates (**104** and **217**). The model did, however, still predict the major metabolite for the majority of cases. It is apparent that the docking accuracy for the bicyclic systems is not as good as that for the monocyclic substrates. It was therefore postulated that a contributing factor to this inconsistency could be the rigidity of the amino acid side-chains. Gold™ factors in the flexibility of the protein backbone when docking the substrates, but retains the orientation of the amino acid side-chains from the original crystal structure. The original crystal structure, however, reflects the binding mode of toluene and makes no accommodation for the larger bicyclic substrates. With that in mind, if the key amino acid residues were allowed to rotate in the active site, it would be presumed that this would allow for poses that would better mimic the natural binding modes. This is discussed further in the following section.

2.2.4 His_{311} Pocket

During the final stages of the docking studies, an additional interaction occurring to His_{311} was suggested by the Belfast collaborators, which had not been considered in previous docking studies. Moreover, an empty pocket situated behind the His_{311} residue was

identified, which was suggested to allow for significant rotation of the histidine side-chain within the active site (see **Figure 34**).

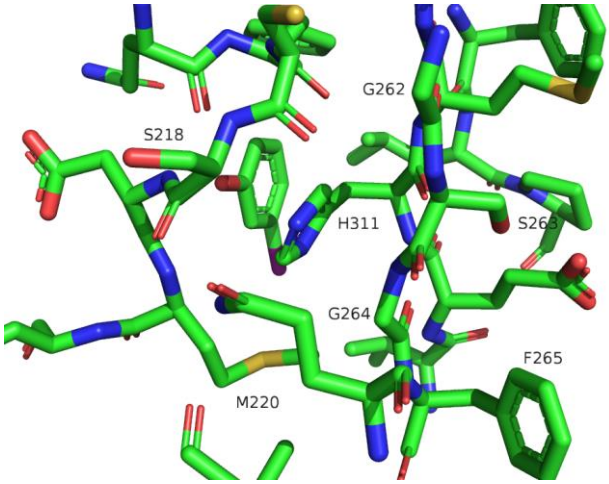

Figure 34: The empty pocket behind the His_{311} residue. All the amino acid residues shown are within 5 Å.

The first indication of this pocket was the presence of Gly_{264} within the active site. Glycine serves no functional role with regards to substrate interaction and is more commonly observed as maintaining the structural integrity of the protein. It was therefore postulated that the role of Gly_{264} is to create space for His_{311} to be able to rotate within the active site. Further support for this suggestion can be seen from the relative orientation of the amino acid side-chains: Ser_{218}, Ser_{263} and Phe_{265}, which outline the empty pocket and appear to point outwards from the cavity. As a consequence of this pocket, it was hypothesised that His_{311} would be able to adopt a pose that would allow for a push-pull interaction originating from Met_{220}. This interaction would arise via hydrogen bonding of the sulfur from Met_{220} to the protonated imidazole nitrogen from His_{311}. This would in turn increase the hydrogen bond acceptor properties of the remaining nitrogen within the imidazole ring, which would result in a stronger hydrogen bonding interaction with the hydroxyl moiety of the substrate. The basis for such a suggestion was made on analysis of conserved amino acids in different dioxygenase enzymes. There is, however, no experimental evidence to support such a claim and remains a new theory.

This interaction would not have been observed in the described computational docking model, as Gold™ only allows the protein backbone to flex and keeps the orientation of the amino acid side-chains static. Furthermore, the crystal structure utilised for the docking was co-crystallised with toluene in the active site, which does not possess a suitable hydrogen bond donor for this interaction to bind to. To test this theory, therefore, 3-

iodophenol (**115**) was re-docked into the model with Met_{220} and His_{311} allowed to freely rotate; the major docking pose from this model is shown in **Figure 35**.

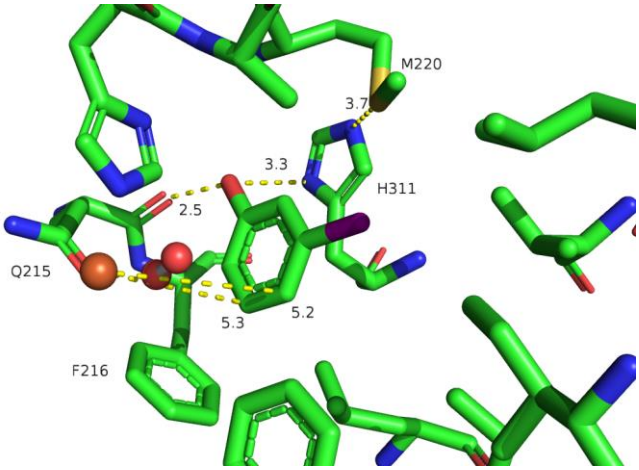

Figure 35: The major docking pose for 3-iodophenol (**115**). His_{311} and Met_{220} were allowed to freely rotate. The measurements to Fe are in Å.

The major predicted bioproduct **117** remained unchanged with comparison to previous docking results; however, critically the sulfur from the thioether of Met_{220} was aligned with the protonated nitrogen from the imidazole ring of His_{311}. Given the multitude of conformations that this docking could have adopted given such rotation, it is notable that the push-pull interaction was observed. To investigate further, phenol (**94**) was docked into the model with His_{311} and Met_{220} allowed to rotate freely. This was to discover whether a simple phenolic substrate would also adopt a similar pose in the absence of a hydrophobic substituent, which would significantly influence the binding pose. The major binding pose for phenol (**94**) using the model accounting for the rotation of His_{311} and Met_{220} is shown in **Figure 36.**

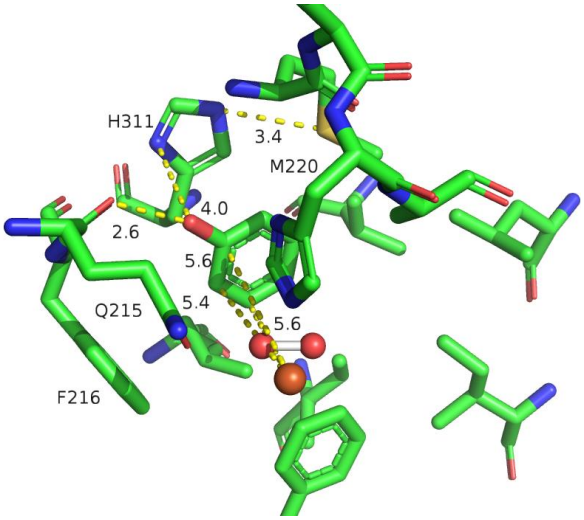

Figure 36: The major docking pose of phenol (**94**). His_{311} and Met_{220} were allowed to freely rotate. The measurements are in Å.

As with 3-iodophenol (**115**), the alignment of the sulfur from Met_{220} with the protonated nitrogen from His_{311} was observed even in the absence of a hydrophobic side chain. The docking results for phenol (**94**) using both the original static model and the newly revised His_{311}/Met_{220} rotation model were analysed and compared; the results are summarised in **Table 11**.

Table 11: The experimentally reported biotransformation products and relative yields for the substrate phenol (**94**) using *P. putida* UV4. The percentage of binding poses from the two docking models corresponding to the reported products are shown. Static model = No rotation in the amino acid side-chains. † = Catechol **48** and hydroquinone (**224**) are formed by the elimination of water from **222** and **223**; and **98** respectively.

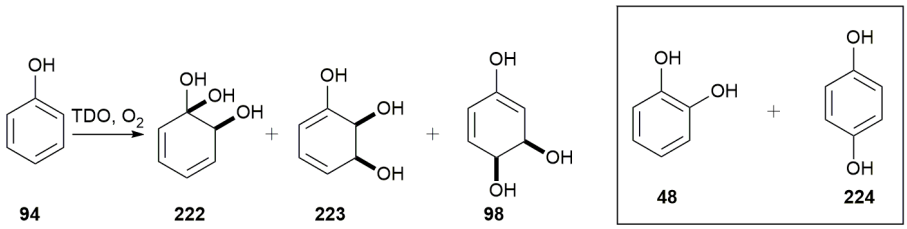

Reported products (relative % yield)	Docking model	Percentage of binding poses (%)
†**48** (<5 %), **224** (95 %)[94]	Static	**222** (98 %), **223** (1 %), **98** (1 %)
	His_{311}, Met_{220} rotation	**222** (28 %), **223** (66 %), **98** (1 %)

The predominant product from the biotransformation of phenol (**94**) using *P. putida* UV4 was hydroquinone (**224**, 95 % relative yield). In both models, only 1 % of the docked poses corresponded to hydroquinone precursor **98**. Rather, the docking models predicted the major formation of catechol **48** precursors **222** (static) and **223** (His_{311}/Met_{220} rotation). The two models' output differed by the regiochemistry of the dihydroxylation, yet

elimination of water from **222** and **223** would yield the same product. It is, however, important to note that the major bioproduct obtained from the biotransformation of phenol (**94**) using the *P. putida* F1 strain was catechol **48**. Moreover, there was no reported presence of hydroquinone (**224**), which is contrary to the experimental results for the *P. putida* UV4 strain shown in **Table 11**.[95] The apparent change in regiochemistry from F1 to UV4, despite both strains possessing the same TDO enzyme, likely indicates another, unidentified enzyme participating in the metabolism pathway. Furthermore, as previously mentioned (**Section 2.2.2)** the relative yield for the formation of catechol **48** when using *P. putida* UV4 is not a true representation, due to further biodegradation of the catechol metabolite. It was therefore difficult to substantiate the validity of both docking models on account of the multiple variables of the substrate phenol (**94**). In light of this, a further study was carried out using 2,5-xylenol (**225**), which was previously identified to be a poor substrate for the docking model. It was envisaged that any improvement for the model accounting for the described rotations on the previous results obtained, which used the original model (static amino acid side-chains), would be attributable to the allowed rotation of the His_{311} and Met_{220} residues. The results from the two models are summarised in **Table 12**.

Table 12: The experimentally reported biotransformation products and yields for the substrate 2,5-xylenol (**225**) using *P. putida* UV4. The percentage of binding poses corresponding to the reported products from the two docking models are shown. Static model = No rotation in the amino acid side-chains. † = Isolated bioproducts **230**, **231** and **232** are formed from **226**, **227** and **228**; and **229** respectively.[56]

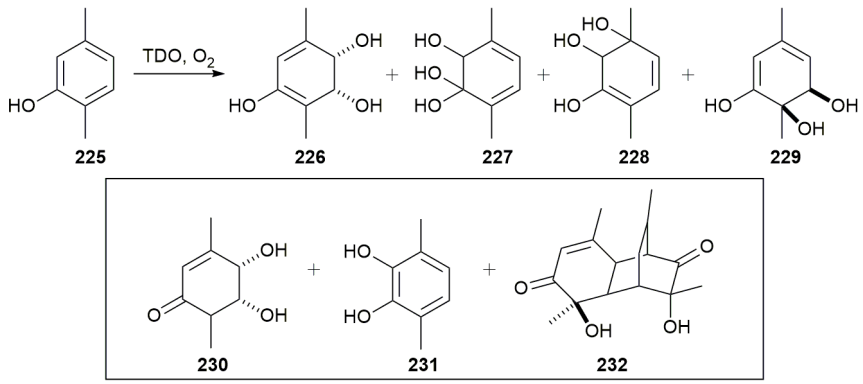

Reported products (% yield)	Docking model	Percentage of binding poses (%)
†**230** (17 %), **231** (9 %), **232** (7 %)	Static	**230** (1 %), **231** (8 %), **232** (90 %)
	His_{311}, Met_{220} rotation	**230** (2 %), **231** (22 %), **232 (**70 %)

The docking model comparison showed a minor improvement in the predicted docking outcome. In the model where His_{311} and Met_{220} were allowed to rotate freely, a greater proportion of poses corresponded to the second most abundant metabolite **231**. Yet the

overall outcome of the docking remained the same, with a major percentage of poses predicting metabolite **229**, which tautomerises prior to the dimerisation to form **232** as the minor bioproduct. Neither docking model predicted **230** as the major metabolite.

The dataset was then expanded to include the poorest performing bicyclic substrates docked in **Section 2.2.3**. One of the major outcomes from the docking of the bicyclic compounds was the inability of the crystal structure to accurately reflect the experimental outcome, which was suggested to be the result of the static side-chains. The re-docked results are shown in **Table 13**.

Table 13: The experimentally observed biotransformation products and relative percentage yields for 2-bromonaphthalene (**200**) and 2-cyanonaphthalene (**201**) using *P. putida* UV4. The percentage of binding poses corresponding to the reported products from the two docking models are shown. Static model = No rotation in the amino acid side-chains.

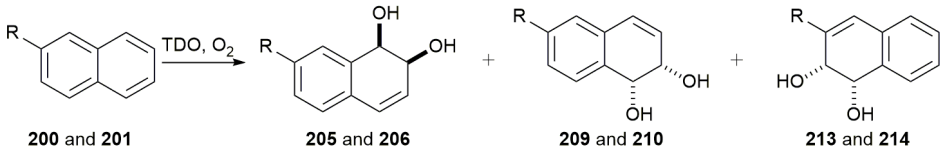

200, **205**, **209** and **213**: R = Br
201, **206**, **210** and **214**: R = CN

Substrate	Reported products (relative % yield)	Docking model	Percentage of binding poses (%)
200	**205** (33 %), **209** (40 %), **213** (27 %)	Static	**205** (98 %), **209** (0 %), **213** (0 %)
		His_{311}, Met_{220} rotation	**213** (38 %), **209** (38 %), **213** (3 %)
201	**206** (15 %), **210** (57 %), **214** (28 %)	Static	**206** (61 %), **210** (8 %), **214** (4 %)
		His_{311}, Met_{220} rotation	**206** (14 %), **210** (18 %), **214** (9 %)

The most significant change was observed for 2-bromonaphthalene (**200**). The His_{311}/Met_{220} rotation model allowed for the prediction of the poses that were otherwise unobtainable in the static model. The results were less pronounced for 2-cyanonaphthalene (**201**), yet the rotation model now correctly identified bioproduct **210** as the major metabolite. It is, however, evident that the rotation of the His_{311} and Met_{220} residues does not fully account for all of the binding poses, particularly for the formation of (**213** and **214**), and so the B-factors for the protein active site were visualised to determine additional areas of interest (**Figure 37**).

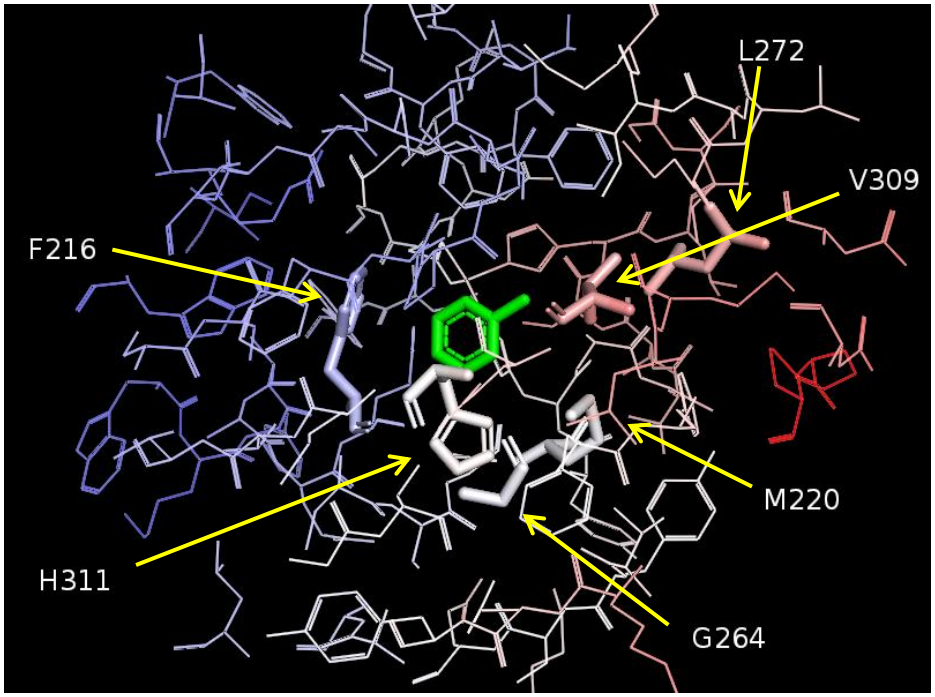

Figure 37: The visualisation of the protein B-factors of TDO using PyMol (v 2.0.4). The key amino acids are shown as stick models. Blue = low, grey = medium, red = high.

The B-factor is a measure of fluctuation of an atom about its relative position. It can therefore be used to highlight the amino acid residues that exhibit a high flexibility, as they would possess a high B factor (shown as red in **Figure 37**).[96] The visualisation in **Figure 37** shows little flexibility around Phe_{216}, indicating that this position is relatively conserved. Around His_{311} and Met_{220}, there appears to an area of flexibility, which would support the idea of the histidine pocket. Interestingly, the greatest variation was observed in the hydrophobic pocket (Val_{309}, Leu_{272}). With regards to the docking therefore, incorporating the flexibility of this hydrophobic pocket into the model might further refine the results described previously. It is, however, important to note that the B-factors can be influenced by the resolution of the crystal structure (3.2 Å for PDB code: 3EN1), and so this visualisation may not be an accurate representation of the dynamics of the protein.

2.2.5 Addition Docking and Summary

In addition to the sixteen substrates described in the previous sections, which were docked using a static crystal structure, an additional five are presented in **Table 14** using the same model. In summary, over 2100 poses have been individually evaluated to validate the docking model.

Table 14: The experimentally reported biotransformation products and percentage yields for various aromatic substrates using *P. putida* UV4. The percentage of docked poses for the reported bioproducts are shown.

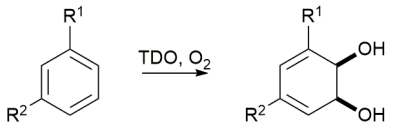

49, **93**, **95**, **233** and **234** → **50**, **97**, **99**, **235** and **236**

49 and **50**: R^1 = Me, R^2 = H
93 and **97**: R^1 = Me, R^2 = OH
95 and **99**: R^1 = OMe, R^2 = OH
233 and **235**: R^1 = 2-pyridine, R^2 = H
234 and **236**: R^1 = 1-pyrazole, R^2 = H

Substrate	Percentage yield for major bioproduct (%)	Percentage of docked poses for major bioproduct (%)
49	**50** (60 %)[97]	100 %
93	**97** (15 %)[56]	81 %
95	**99** (38 %)[98]	75 %
233	**235** (1 %)[99]	99 %
234	**236** (12 %)[99]	98 %

In all cases, the docking predicted the outcome of an experimentally observed metabolite. With regards to the monocyclic compounds, out of the 1200 poses analysed for the 12 substrates docked, 70 % were correctly orientated for the predicted major bioproduct. It is evident that the described docking model functions well for the substrates of this type. The deficiency of this system appears to be the bicyclic substrates, with 50 % of the 900 poses analysed for the nine bicyclic substrates corresponding to the observed major bioproduct. It is, however, important to reiterate that in the cases where the docking predicts a catechol metabolite in significant proportions, the observed experimental data would not accurately reflect this due to further biodegradation by *P. putida* UV4.

In addition to the static docking, Gold™ has been used to support the suggestion of a 'push-pull' interaction between Met_{220} and His_{311}. Allowing the Met_{220} and His_{311} residues to freely rotate has shown that the major poses for 3-iodophenol (**115**) and phenol (**94**) possessed this supposed interaction. Furthermore, a key pocket situated behind His_{311} has been identified possessing a glycine residue (Gly_{264}), which has been proposed to allow for the rotation of the His_{311} residue within the active site. Research by Pentlavalli and co-workers suggested that in light of this key His_{311} residue, it can be hypothesised that TDO may have evolved to biodegrade phenolic substrates. They carried out an analysis of ring hydroxylating dioxygenases, which revealed that His_{311} was highly conserved between the different dioxygenases. This indicates that this residue may play an important role in the dioxygenase catalysis. Furthermore, other key amino acids present in the active site have been identified as conserved residues, which include: Phe_{216}, Asp_{219}, Met_{220}, His_{222}, Ala_{223}

His_{228}, Gly_{264} and Phe_{366}.[100] Notably, the presence of Met_{220} and Gly_{264} within these conserved amino acids supports the idea of the His_{311} interaction and rotation pocket.

Utilising the idea of the interaction of Met_{220} with His_{311}, previously analysed substrates have been redocked into a crystal structure allowing for the free rotation of these key amino acid residues. The results showed a marginal improvement in the predicted outcome, yet the model still fell short of accurately predicting the experimental outcome for the poorest performing substrates. The B-factors for TDO have therefore been visualised to highlight additional areas of flexibility, which may further refine the docking model.

Despite the good correlation with the experimental data, further research is required to validate the theories put forward. Without experimental validation, the suggestions and poses suggested are tentative, and should be treated as a basis for future research.

2.3 Application of the Iodo Keto *cis*-Diol

The iodo keto *cis*-diol bioproduct **117** was supplied by the project collaborators (Allen and Höering, Queens Belfast University), however there was a limited supply due to the capricious nature of the whole-cell biotransformation using *P. putida* UV4. In consideration of this and the insufficient synthetic examples using diol **117**, it was decided that bioproduct **117** would be utilised for the synthesis of the novel incarviditone analogue **236** (**Figure 38**), as the chemistry for this synthetic route was already partially developed. Analogue **237** would then be tested for its anti-proliferative activity against different cancer cell lines, before being compared to incarviditone analogues previously synthesised by the Whitehead group and those described herein, with the aim to investigate structure-activity relationships. The synthesis would be achieved by applying the synthetic procedure previously developed by the Whitehead group (**Section 1.2.2**).[66]

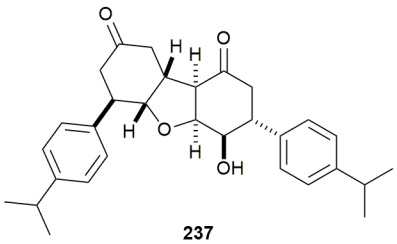

237

Figure 38: The structure of isopropylphenyl incarviditone analogue **237**.

The isopropylphenyl analogue **237** was selected based on previous IC_{50} data of different non-polar side chains collected by the Whitehead group on different cancer cell lines using the MTT assay. At the time, the trend of the data suggested that non-polar side-chains exhibited the highest anti-proliferative activity (**237**, miLogP = 6.26)[101], and this trend is discussed further in **Section 2.9.3.2**. It was therefore envisaged that the isopropylphenyl functionality would afford a relatively potent bioactive compound (i.e. **237**). Furthermore, the application of iodo keto *cis*-diol **117** in combination with the Whitehead group's procedure starting from (-)-quinic acid (**194**) described in **Section 2.4**, enables the synthesis of both enantiomers of analogue **237**. This would therefore allow for the investigation into any enantiomeric differences exhibited by incarviditone analogues **237** and ***ent*-237** in *in-vitro* studies using a panel of cancer cell-lines.

The proposed synthetic route (**Scheme 42**) necessitated the formation of the key enone building block **239**, which could then be functionalised with the isopropylphenyl side-chain prior to dimerisation. This synthetic route would also apply the hydrogenolysis conditions previous disclosed by Boyd and co-workers.[56]

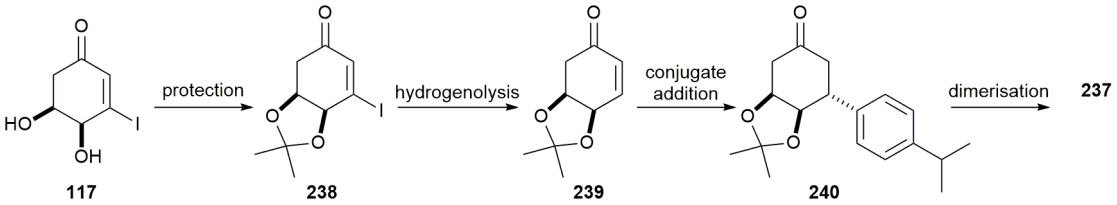

Scheme 42: The proposed synthesis for isopropylphenyl incarviditone analogue **237** using iodo keto *cis*-diol **117**.

Iodo keto *cis*-diol **117** was received as a crude biotransformation mixture in an aqueous phosphate buffer to ensure the stability of **117**. Initial attempts to extract the bioproduct using ethyl acetate in a separating funnel resulted in an intractable emulsion. The emulsion resisted all attempts to obtain a defined separation. To circumvent this, the crude mixture was first concentrated to 50 % of its original volume to remove excess water, before being slowly 'rolled' in ethyl acetate at 40 °C on a rotary evaporator. Temperature control was critical for the extraction as the product precipitated out from the phosphate buffer at a low temperature. The extracted material required purification by flash silica chromatography, with the major impurity being the iodo catechol **113** side-product of the biotransformation (**Figure 39**).

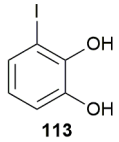

113

Figure 39: The structure of iodo catechol **113**.

2.3.1 Diol Protection and Hydrogenolysis

With purified diol **117** in hand, early experiments focused on protecting the *cis*-diol moiety. Prior work by the Whitehead group employed the cyclohexylidene group to protect *cis*-diols in similar systems, however the acetonide group was chosen in preference in view of its better carbon efficiency. The reaction conditions are shown in **Scheme 43**.

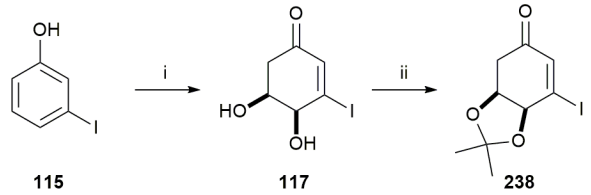

115 **117** **238**

Scheme 43: *Reagents and conditions*: (i) TDO, O_2; (ii) 2,2-dimethoxypropane, *p*-TSA, anhydr. acetone, 0 ºC, 75 min, 65 %.

The acetonide protection using 2,2-dimethoxypropane in the presence of the acid catalyst *p*-toluenesulfonic acid proceeded well, affording protected iodo diol **238** in 65 % yield.[102] Focus then turned to removing the iodine from iodo enone **238** using the conditions Boyd and co-workers had previously applied to iodo keto *cis*-diol **117** (**Scheme 44**).[56]

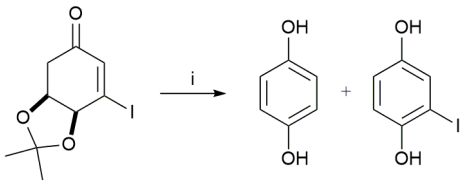

238 **224** **241**

Scheme 44: *Reagents and conditions*: (i) Et_3N, 5 % Pd/C, H_2, MeOH, RT, 20 h.

No formation of *des*-iodo enone **239** was observed and the reaction failed to progress. Following column chromatography, the only products isolated were hydroquinone (**224**) and iodohydroquinone **241**. What was particularly interesting about this result was that there was still iodine remaining in one of the products (**241**). This suggested that prolonged exposure of enone **238** to triethylamine, in combination with the good leaving properties of the acetonide protecting group, resulted in aromatisation of the compound. This route therefore was abandoned in favour of carrying out the hydrogenolysis first, followed by

cis-diol protection. This was with the view that the leaving group of *cis*-diol **242** would be hydroxide rather than acetone, which is less labile. As such, it was proposed that aromatisation should occur at a slower rate compared to the desired hydrogenolysis (**Scheme 45**)

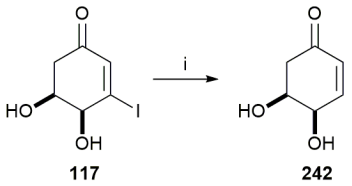

117 **242**

Scheme 45: *Reagents and conditions*: (i) 5 % Pd/C, H_2, Et_3N, MeOH, RT, 20 h, 90 %

Though isolated in good yield (90 %), scale-up of the hydrogenolysis reaction beyond 100 mg proved to be more challenging. Using the conditions outlined in **Scheme 45** on a larger scale resulted in both removal of the iodine atom and reduction of the double bond to afford saturated *cis*-diol **243** (**Figure 40**).

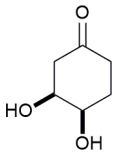

243

Figure 40: The structure of saturated *cis*-diol impurity **243**.

Further experiments reduced the catalyst loading to 3 % Pd on activated carbon, but this also led to the formation of saturated *cis*-diol **243** on scale-up. The outcome of all the hydrogenolysis experiments are summarised in **Table 15**.

Table 15: The summary of the hydrogenolysis reaction conditions. [a] No isolated yield of pure product could be obtained due to an inseparable mixture of **242** and **243.**

Amount of starting material **117** (mg)	Catalyst	Time (h)	% yield of **242**	% yield of **243**
100	5 % Pd/C	20	90 %	0
200	5 % Pd/C	20	0	90 %
150[a]	5 % Pd/C	20	N/A	N/A
200[a]	5 % Pd/C	4	N/A	N/A
200	3 % Pd/C	20	48 %	0
150	3 % Pd/C	7	0	70 %
150	3 % Pd/C	4	0	70 %

The results in **Table 15** show no defined trend and demonstrated the capricious nature of this heterogeneous reaction, despite all efforts to maintain consistent reaction conditions.

Attention turned away from utilising Pd/C and focused on alternative hydrogenolysis methods. In 2008, Heravi and co-workers described a reductive dehalogenation using zinc with ammonium chloride as a hydrogen source on a range of aliphatic and aromatic substituents.[103] Though no halocyclohexenones were tested, aryl and alkyl halides possessing aldehyde functionality were investigated. Considering the functional group tolerance of the reaction conditions, a small-scale trial reaction was attempted on the acetonide protected iodo diol **238** (**Scheme 46**).

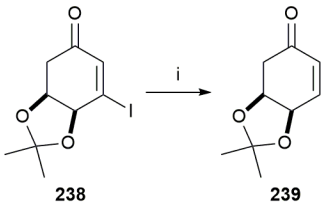

Scheme 46: *Reagents and conditions*: (i) zinc dust, sat. NH_4Cl, THF, 2.5 h, RT.

Formation of the desired product **239** was observed by analysis of the crude mixture using ^{1}H NMR spectroscopy; however, the product could not be isolated due to the presence of several unidentified products of similar polarity. This route was therefore abandoned due to its unsatisfactory reaction profile. Attention turned to reaction conditions that have been demonstrated on structurally similar compounds to iodo keto *cis*-diol **117**. In 1985, Ohno and co-workers carried out a reductive dehalogenation reaction using 1,4-dihydronicotinamide (BNAH, **248**) and a catalytic amount of $RhCl(PPh_3)_3$ on 3-iodocyclohexenone **198** (**Scheme 47**).[104]

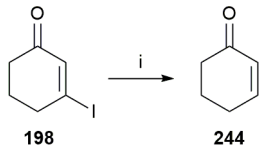

Scheme 47: *Reagents and conditions*: (i) BNAH, $RhCl(PPh_3)_3$, MeCN, 70 °C, 2.5 h, 100 % as reported by Ohno and co-workers.

To test these conditions, BNAH (**248**) was first synthesised over two steps starting from the commercially available nicotinamide (**245**) and benzyl bromide (**246**) (**Scheme 48**).

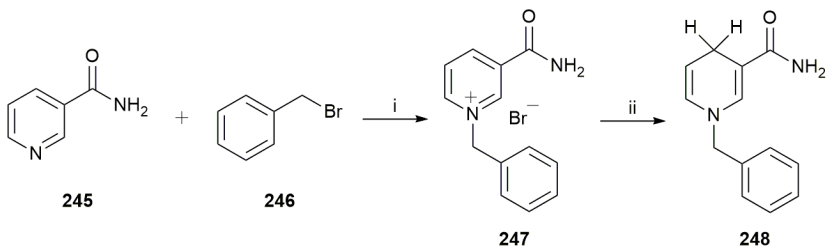

Scheme 48: *Reagents and conditions*: (i) MeCN, reflux, 15 h, 98 %; (ii) $NaHCO_3$, $Na_2S_2O_2$, H_2O, RT, 3 h, 85 %.

The role of BNAH (**248**) in the dehalogenation reaction is to act as a mimic of NAD(P)H (**Figure 41**, **249**) and function as a reducing agent.

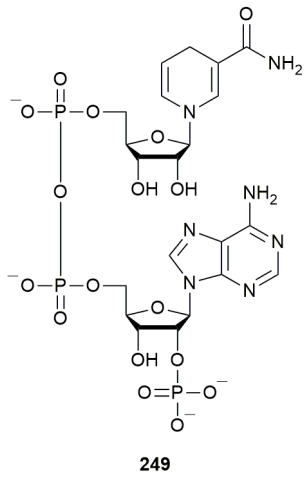

Figure 41: The structure of NAD(P)H (**249**).

248 acts as an electron donor to the transition metal, which catalyses the dehalogenation. With BNAH (**248**) in hand, Ohno and co-workers' reaction conditions were trialled on iodo keto *cis*-diol **117** (**Scheme 49**).

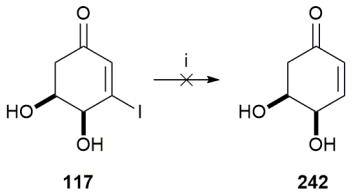

Scheme 49: *Reagents and conditions*: (i) $RhCl(PPh_3)_3$, **248**, MeCN, 40 °C to 70 °C, 48 h.

Concerned about the stability of both bioproduct **117** and the expected product **242** under the high temperatures used in the original procedure, the initial reaction conditions started at 40 °C. The reaction was monitored via TLC and no product was observed after 24 h.

The temperature was increased to 70 °C for a further 24 h, however no product was formed and starting material was recovered.

Due to the lack of progress trialling different reactions, focus returned to the Pd/C hydrogenolysis conditions with a view to optimising the reaction conditions for scale-up. The reaction time varied, with aliquots taken from the reaction mixture every 10 minutes. The optimal reaction conditions are shown in **Scheme 50.**

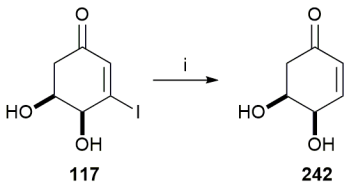

117 **242**

Scheme 50: *Reagents and conditions*: (i) 5% Pd/C, H_2, Et_3N, MeOH, 11 min, RT, 69 %.

Surprisingly, the reaction was completed in 11 minutes. This was in stark contrast to the small-scale trial and the conditions reported by Boyd and co-workers, which took 24 hours to afford a higher yield of *des*-iodo product **242** (**Scheme 45**).

The explanation for this result was only presented later in the project when receiving further crude TDO biotransformation reactions of iodo keto *cis*-diol **117**. It was observed that the hydrogenolysis reaction conditions to afford **242** varied across all the biotransformation reactions and were not consistent. This was due to the delicate nature of the biotransformation itself. Communication with the collaborators Allen and Höering revealed that the impurity levels varied between biotransformation batches depending on: the fluctuation in temperature and pH, the timing of feedstock addition and when the biotransformation was stopped. Though no specific impurity has been implicated to cause these inconsistent results, it can be assumed that side-products from the biotransformation were interfering with the Pd catalysis. On a number of occasions, this unidentified impurity appeared to stall hydrogenolysis and addition of extra Pd/C led to no further progression. To circumvent this issue, additional purification was required prior to the hydrogenolysis. Following the original purification by flash silica chromatography, iodo keto *cis*-diol **117** was then recrystallised from hexane:EtOAc (2:1), which resulted in the hydrogenolysis reaction proceeding in a reproduceable fashion.

Following the optimisation of the hydrogenolysis, *des*-iodo compound **242** was protected as its acetonide (**Scheme 51**).

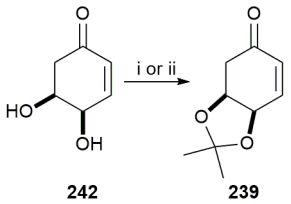

Scheme 51: *Reagents and conditions*: (i) 2,2-dimethoxypropane, *p*-TSA, anhydr. acetone, 0 °C, 30 min, 76 %. (ii) 2,2-dimethoxypropane, CSA, acetone, 0 °C, 75 mins, 62 %.

The original reaction conditions described previously (**Scheme 43**) proved to be inconsistent when repeated. Though a favourable yield of 76 % was achieved on one occasion, the acid sensitivity of *cis*-diol **242** and enone **239** made replication of this result difficult, yielding the product in just 7 % in one instance. *para*-Toluenesulfonic acid (pKa ~ -2.8) was identified to be too strong an acid for this reaction and therefore was substituted for the milder acid, camphorsulfonic acid (pKa ~ 1.2). The observed level of decomposition to **224** was lower and this led to a less capricious reaction overall, which allowed for the efficient preparation of the key enone **239**.

2.3.2 Conjugate Addition

With the synthetic route to the key building block **239** developed, synthesis of the (+)-isopropylphenyl incarviditone analogue (**237**, **Figure 38**) commenced with the installation of the isopropylphenyl functionality via a rhodium catalysed conjugate addition onto enone **239** to afford adduct **240** (**Scheme 52**).

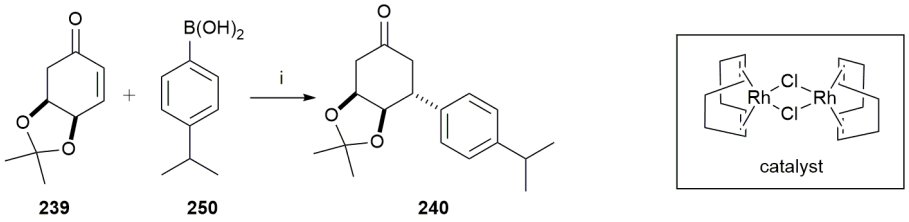

Scheme 52: *Reagents and conditions*: (i) $[RhCl(cod)]_2$ (5 mol %), Et_3N, dioxane:H_2O (10:1), RT, 18 h, 62 %

The reaction proceeded well and in reasonable yield of 62 %. One of the main advantages of using rhodium as the catalyst is that water can typically be used as a co-solvent. With respect to a 1,4-Michael addition, the most prevalent catalyst to facilitate this type of reaction is copper, in combination with an organometallic component namely: a diorganozinc, an organolithium or a Grignard reagent.[105] Despite significant advances in this area,[106, 107] these types of reactions frequently require low temperatures and anhydrous conditions. Furthermore, the organometallic reagents are prone to undergo unwanted side-

reactions and functional group incompatibility can become an issue. In the system described in **Scheme 52**, rhodium is used in conjunction with an organoboron nucleophile to deliver the isopropylphenyl functionality via a 1,4-addition. The first reported instance of a rhodium catalysed 1,4-addition of an aryl boronic acid to an α,β-unsaturated carbonyl system was in 1997 by Miyaura and co-workers (see **Scheme 53**).[108] The reaction outlined in **Scheme 53** is referred to as the Hayashi-Miyaura reaction.

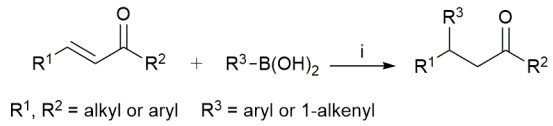

Scheme 53: Rh catalysed 1,4-addition of organoboronic acids to linear aliphatic enones. *Reagents and conditions*: (i) Rh(acac)CO_2/dppb, organic solvent:H_2O, 50 °C.

Overall, Miyaura and co-workers demonstrated that the reaction proceeded in high yields, with the best outcome generally observed when a methanol:water (6:1) solvent mixture was applied. For cyclohexenone (**244**) however, this solvent mixture produced only a trace amount of conjugate adduct **252**. Significant improvements in yield were observed when the reaction was conducted in cyclohexane:water (6:1), which signifies that there is a strong solvent effect associated with the Hayashi-Miyaura reaction.

Shortly after this work in 1998, Hayashi and co-workers reported the first enantioselective Hayashi-Miyaura reaction on a number of cyclic and aliphatic enones (**Scheme 54**).[109]

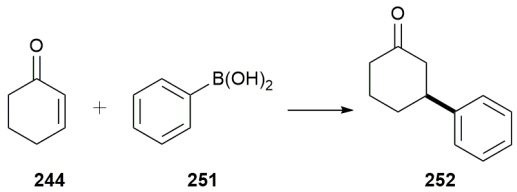

Scheme 54: The Rh catalysed enantioselective conjugate addition of $PhB(OH)_2$ (**251**) to cyclohexenone (**244**). *Reagents and conditions*: (i) Rh(acac)$(C_2H_4)_2$ (3 mol %), **253** (5.0 eq.), (*S*)-binap, dioxane:H_2O (10:1), 100 °C, 5 h, > 99 % (97 % e.e.).

The high yields and selectivity reported by Hayashi and co-workers were achieved by modifying the original procedure and using a 3 mol % catalyst loading. The solvent was changed to dioxane:water (10:1) and the reaction temperature was increased to 100 °C to afford a yield of >99 % and 97 % e.e for the reaction of cyclohexenone (**244**) with phenyl boronic acid (**251**). The caveat of these conditions, however, was the hydrolytic deboronation of the organoboron reagent **251**, which necessitated an excess of the boronic acid (5.0 eq.).

The catalytic cycle for the Hayashi-Miyaura reaction is shown in **Scheme 55**.[110]

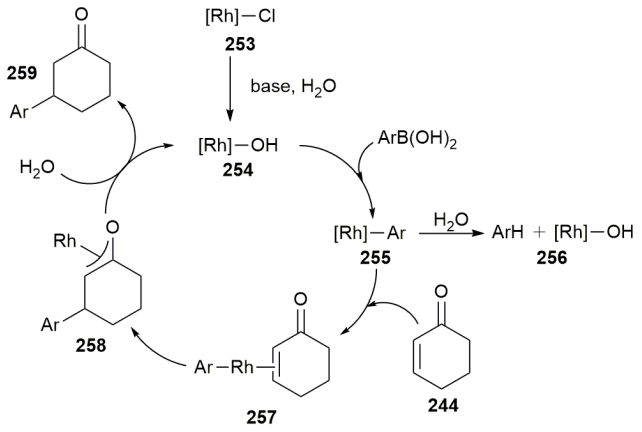

Scheme 55: The catalytic cycle for the Rh catalysed 1,4-addition of an aryl boronic acid to a cyclic enone as suggested by Hayashi and co-workers.

The [Rh]-Cl precatalyst **253** is first converted to the more active hydroxyrhodium species **254**. Mechanistic studies by Hayashi and co-workers have shown the *in-situ* formation of the [Rh]-OH species **254** by treatment of [Rh]-Cl **253** with KOH. Though it has been observed that transmetalation can occur to the Rh-Cl complex **253**, the reaction with Rh-OH **254** has been shown to occur at a significantly faster rate (see **Scheme 56**).[110]

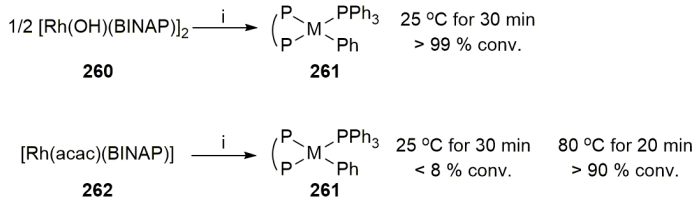

Scheme 56: The rates of reaction between activated [Rh]-OH **260** and [Rh]-acac **262**. *Reagents and conditions*: (i) $PhB(OH)_2$ (2.0 eq.), PPh_3, THF.

The activated rhodium-hydroxy complex then undergoes transmetalation by the organoboron reagent to afford **255**. Complex **255** can then undergo two alternative pathways; the first pathway is the hydrolysis of the rhodium-carbon bond leading to protonation of the aryl group (**255** to **256**). In the reaction described in **Scheme 52**, there was no observation of isopropylbenzene in the reaction mixture, however there was presence of homocoupled dimer **263,** which was confirmed by ^{1}H NMR (**Figure 42**).

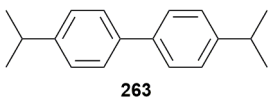

Figure 42: The chemical structure of isopropylphenyl dimer **263** side-product.

It has been observed that boronic acids, instead of water, can participate in this pathway; thus, accounting for the formation of **263**.[111] The second pathway continues with the catalytic cycle by means of binding of the alkene to the [Rh]-Ar complex (**257**). The Ar group is delivered to the β-position of the cyclic enone and an oxa-π-allyl rhodium complex is formed (**258**). Protonolysis of rhodium enolate **258** liberates the desired product **259** and consequently frees the catalyst for another cycle.

The observed *anti*-selectivity arises from the directing *cis*-diol protecting group. Past research conducted by the Whitehead group firmly established that cyclohexylidene is a suitable moiety to direct the diastereoselectivity of the conjugate addition,[66, 112] however little work had been done using the described rhodium catalysis on an acetonide system. Many examples within the literature focus on cuprate additions to enone **239**. Though good diastereoselectivity was observed in many of these cases, the yields typically suffered particularly for aromatic cuprates.[113] Pleasingly, the characterisation of adduct **240** showed that the acetonide moiety provided good diastereoselective control as determined by the vicinal proton coupling between the C4 and C5 hydrogens. The rationale for the diastereoselective control is illustrated in **Figure 43**.

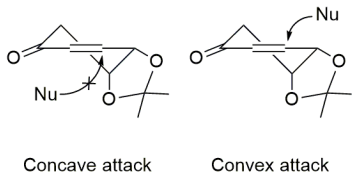

Figure 43: The mechanism for the diastereoselective control of the conjugate addition reaction.

The steric hindrance caused by the acetonide group disfavours nucleophilic attack on the concave face. As a result, the incoming nucleophile attacks the convex face, which affords the *anti* product.

2.3.3 (+)-Isopropyl Incarviditone Analogue

Conjugate adduct **240** was subjected to basic conditions to facilitate the dimerisation to afford isopropylphenyl incarviditone analogue **237** (**Scheme 57**).

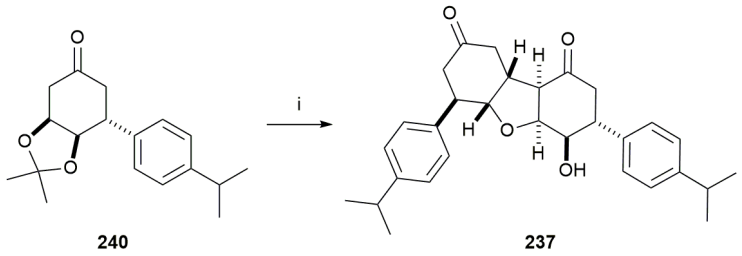

Scheme 57: *Reagents and conditions*: (i) 0.5 M $NaOH_{(aq)}$, THF, RT, 19 h, 73 %.

The conditions used in **Scheme 57** were developed previously by the Whitehead group. They were serendipitously discovered when conjugate adducts related to **240** were treated with sodium hydroxide for a prolonged period of time (24 h); this resulted in a cascade homodimerisation to afford the perhydrodibenzofuranones product (see **Section 1.2.2**).[66] The suggested mechanism for this process is shown in **Scheme 58**.

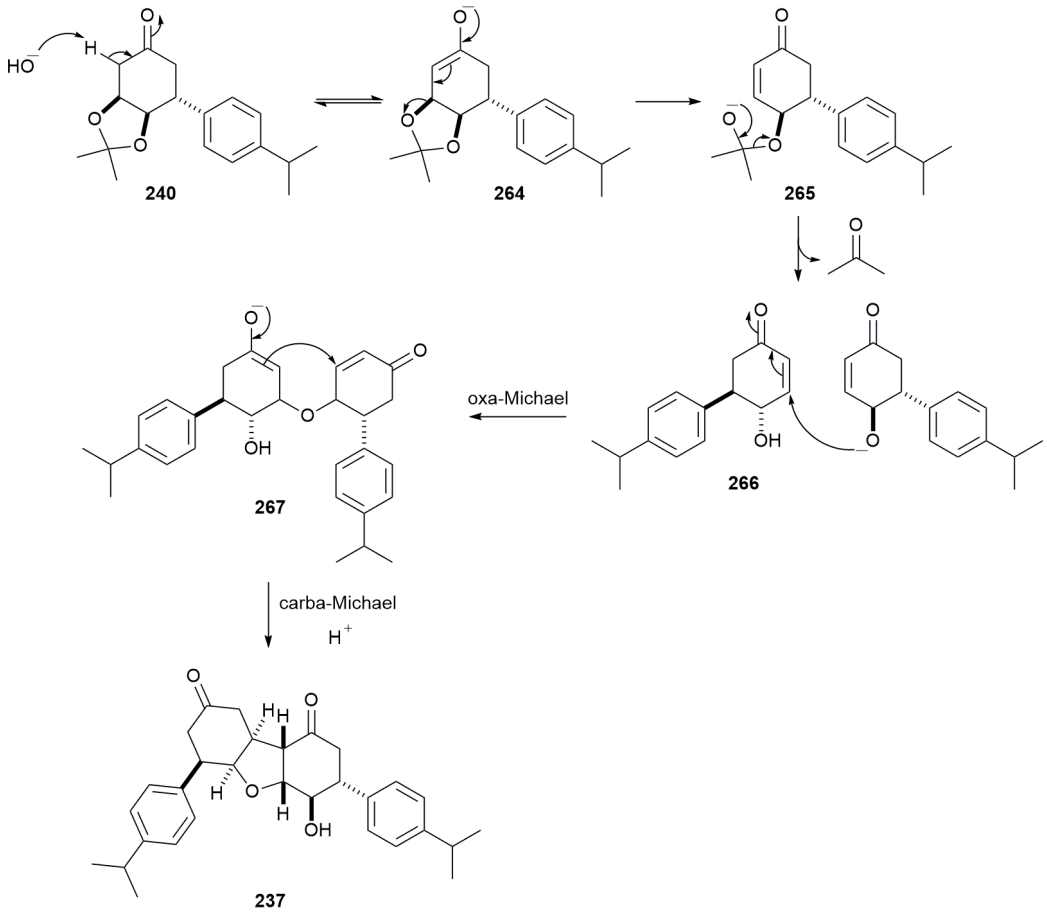

Scheme 58: The conjugate adduct dimerisation mechanism.

The initial step is the base mediated deprotection of conjugate adduct **240** to afford hydroxyenone **266** and acetone as the by-product. Hydroxyenone **266** was an isolable entity and further mechanistic studies are described in **Section 2.4.7**. From here, it was

envisaged that dimerisation would proceed in a similar manner to the incarviditone biosynthetic pathway (**Section 1.2.1**). Following a cascade sequence, two molecules of **266** react via an oxa-Michael addition to give intermediate **267**, before fusing the tetrahydrofuran ring with a carba-Michael addition to afford the final product **237**. The successful synthesis of analogue **237** allowed for the anti-proliferative activities for this compound to be evaluated, the results of which are discussed in **Section 2.9.3.1.**

2.3.4 Biotransformation of 3-Iodophenol and Bromobenzene

Prior to this project, the biotransformations using *P. putida* UV4 had exclusively been carried out by the project collaborators (Allen, Boyd and co-workers, Queens Belfast University). In the interest of demonstrating that the biotransformation could be conducted elsewhere, a lysogeny broth (LB) plate containing *P. putida* UV4 bacterial colonies was provided by Allen and Höering.

Before commencing the biotransformation studies, the activity of TDO in the bacterial culture was determined. The expression of TDO within *P. putida* UV4 can be lost, particularly if the culture is allowed to over-grow, and therefore a visual colorimetric test with the substrate indole was required. Two separate MSM (minimum salt medium) plates were prepared, one of which contained indole as shown by **Figure 44**.

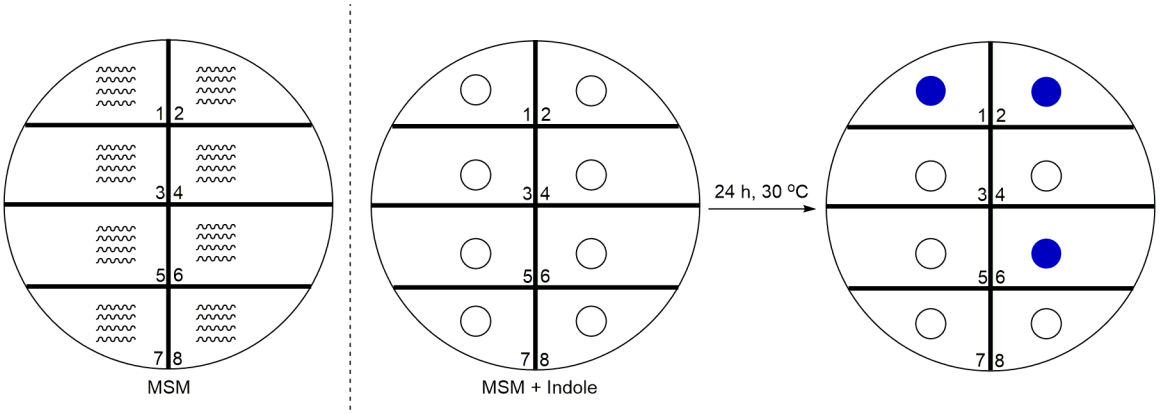

Figure 44: The indole test plates.

A single colony of *P. putida* UV4 was streaked four times on the MSM plate and then spotted on the MSM + indole plate. This process was repeated eight times before the indole plates were incubated at 30 °C for 24 hours.

The biotransformation of indole by *P. putida* UV4 is shown in **Scheme 59.**

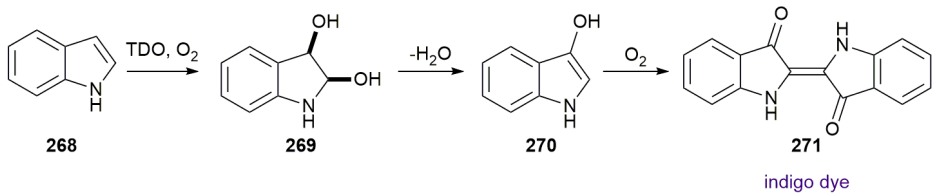

Scheme 59: The TDO catalysed biotransformation of indole (**268**) by *P. putida* UV4 to give metabolite **269**, which eliminates (**270**) and then oxidises to give indigo dye **271**.

Active colonies of *P. putida* UV4 expressing TDO appeared as a dark blue/purple colour on the MSM + indole plate. This is due to the formation of indigo dye **271**, which can be used as a spectrophotometric assay for dioxygenase enzyme activity. Following the *cis*-dihydroxylation of indole (**268**) to give **269**, the metabolite rapidly undergoes dehydration to give indoxyl **270**. Following exposure of **270** to a mild oxidising agent such as atmospheric O_2, indigo dye **271** is formed *in-situ*.[114] Active colonies identified through the indole test were subsequently used in the biotransformation.

A trial biotransformation was first performed using 100 mg of 3-iodophenol (**115**) (**Scheme 60**).

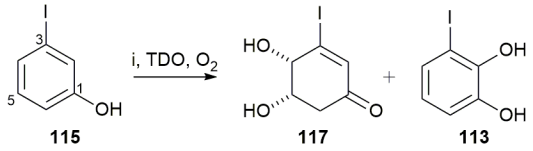

Scheme 60: *Reagents and conditions*: (i) *P. putida* UV4, 30 °C, 150 rpm, pH 7.0, 1.5 M PBS, 2 h.

GCMS proved to be an insufficient technique for measuring the progress of the biotransformation as only the starting material **115** and iodo catechol **113** could be detected; therefore, LCMS was used as the analytical method for monitoring the biotransformation. The biotransformation was stopped after 2 hours, and the crude aqueous reaction was extracted with CH_2Cl_2 after centrifugation. Surprisingly, the ^{1}H NMR spectrum showed no indication of iodo keto *cis*-diol **117** and revealed only 3-iodophenol (**115**) and catechol **113**. Perplexed by the formation of side-product **113** in the absence of diol **117**, the crude aqueous was re-extracted with EtOAc. The ^{1}H NMR spectrum of the concentrated extract is shown in **Figure 45.**

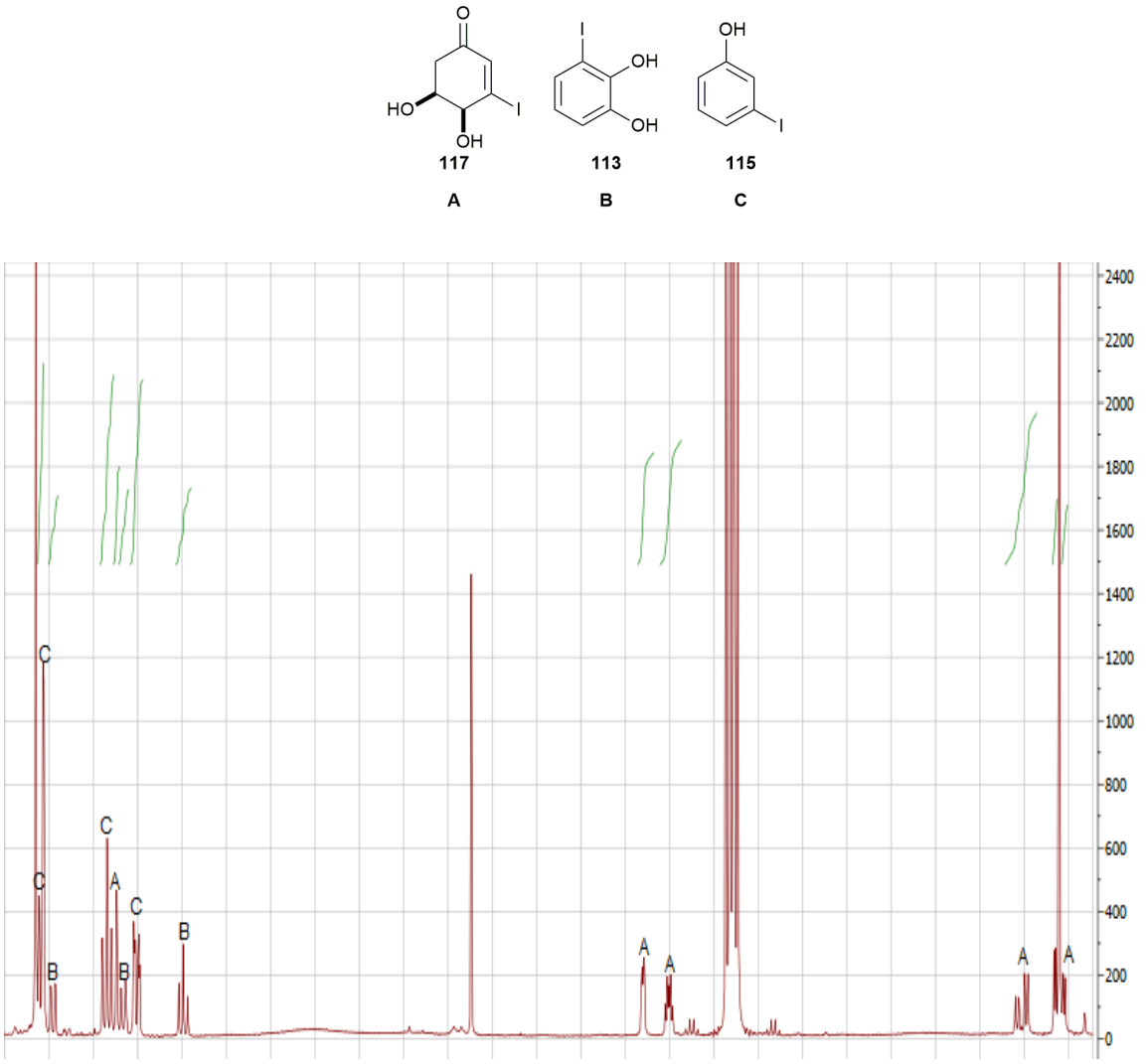

Figure 45: The crude ^{1}H NMR of the small-scale biotransformation using 3-iodophenol (**115**). The relative ratios of **117**(A):**113**(B):**115**(C) (1:0.7:1.7) are shown.

The presence of iodo keto *cis*-diol **117** demonstrated that the trial biotransformation was a partial success. Furthermore, it also appeared that an effective method for removing excess starting material **115** and catechol **113** with a CH_2Cl_2 extraction had been discovered.

Satisfied with the initial progress, the biotransformation was scaled up to 500 mg of 3-iodophenol (**115**). The biotransformation was left to proceed for 3 hours instead of 2 hours in an attempt to reduce the amount of unreacted starting material and increase the overall yield. The consequence of this however was the isolation of only catechol **113**, with no evidence of the desired diol **117**. Consultation with the project collaborators revealed the precarious nature of the biotransformation, which is a compromise between the maximum product concentration and product degradation. The desired keto *cis*-diol **117** reaches a maximum concentration on average after approximately 2 hours,[115] however this is unique

to each biotransformation. From here on, the product is degraded at a detrimental rate by other enzymes present within the whole-cell system. The presence of catechol **113** in the extract indicated that the TDO enzyme was active, and therefore intrinsically diol **117** must have also been formed. It is plausible therefore that the prolonged biotransformation duration led to the degradation of product **117**.

Nevertheless, interest still remained in demonstrating a scaled-up biotransformation using *P. putida* UV4 and so a more efficient substrate, bromobenzene (**60**) was used. Bromobenzene (**60**) was selected based on its excellent reported biotransformation profile, in addition to the synthetic utilities of bromo *cis*-diol metabolite **63** for future studies (see **Scheme 61**).

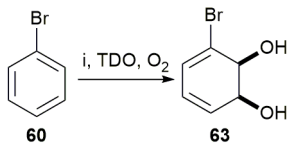

Scheme 61: *Reagents and conditions*: (i) *P. putida* UV4, 30 °C, 150 rpm, pH 7.0, 1.5 M PBS, 3 h, 28 %.

The biotransformation proceeded well, with only the crystalline product **63** and starting material **60** isolated. In conclusion, the proof of concept that the biotransformation of 3-iodophenol (**115**) can be conducted outside the hands of the project collaborators has been demonstrated, as testified by the small-scale trial. The isolation of catechol **113** on scale-up revealed the delicate nature of the biotransformation. Furthermore, substitution of 3-iodophenol (**115**) for bromobenzene (**60**) allowed for the isolation of a *cis*-diol metabolite **63** on a large scale using *P. putida* UV4, which satisfied the original aim.

2.3.5 Docking of 4’-Isopropyl-[1,1’-biphenyl]-3-ol

In addition to the synthesis, efforts were also made to scope potential new substrates for the synthetic route for the synthesis of isopropylphenyl analogue **237** using the previously described docking model (**Section 2.2**). This was with the view that future work would conduct the biotransformation to test the validity of the docking model and experimental support. It was conceived that 4’-isopropyl-[1,1’-biphenyl]-3-ol (**272**) could be used as a potential precursor to conjugate adduct **240** or analogue **237**, which would help to determine whether *P. putida* UV4 could be exploited for the production of synthetically useful intermediates with preinstalled side-chain functionality (**Scheme 62**).

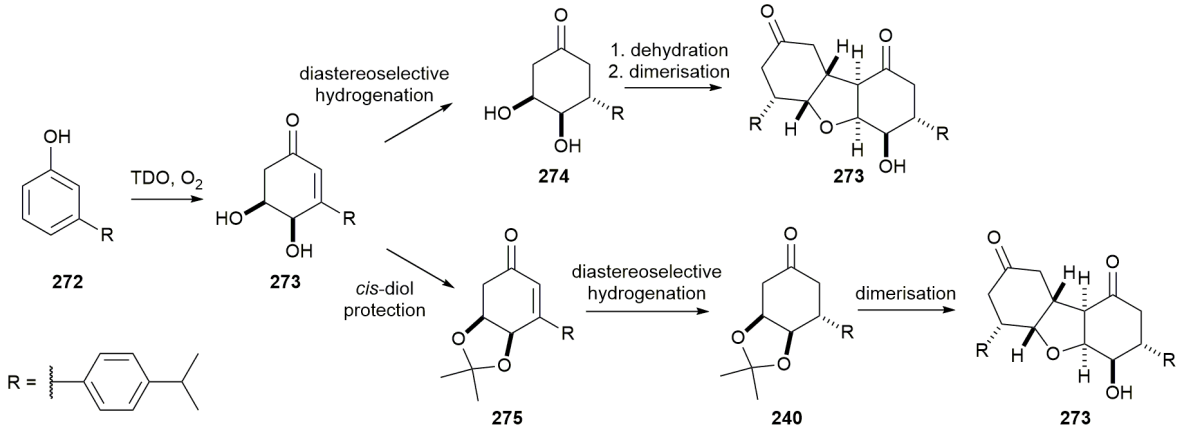

Scheme 62: Proposed synthetic route for the application of the conceived 4'-isopropyl-[1,1'-biphenyl]-3-ol metabolite **273**.

The docking results for 4'-isopropyl-[1,1'-biphenyl]-3-ol (**272**) are shown in **Scheme 63** using the TDO static model. Each product is represented by a percentage of the total binding poses.

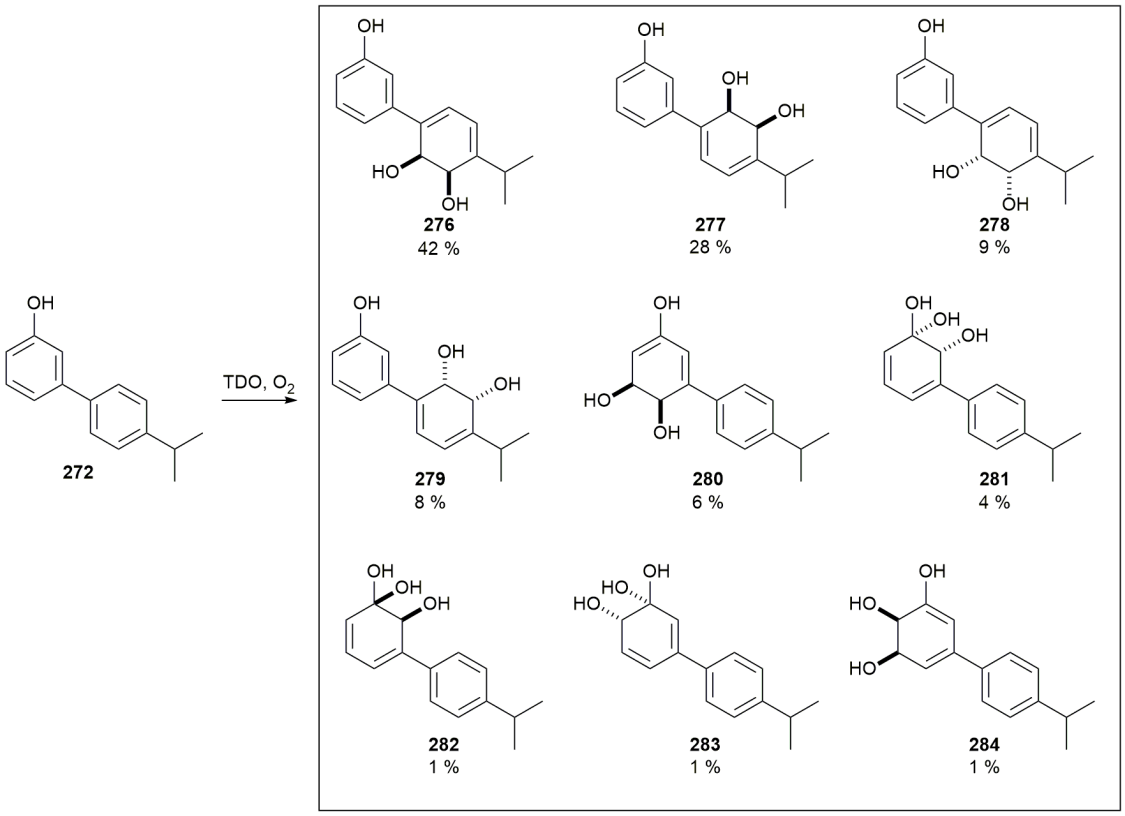

Scheme 63: The computational docking results for the biotransformation of 4'-Isopropyl-[1,1'-biphenyl]-3-ol (**272**) using *P. putida* UV4. The predicted bioproducts are represented as a percentage of the total binding pose.

Unfortunately, only 6 % of the docking poses predicted the desired *cis*-dihydroxylation regiochemistry on the phenolic ring to afford **280**. The major predicted product **276** (42 %)

corresponded to the undesired hydroxylation of the phenyl ring in substrate **272** and the suggested major binding pose is shown in **Figure 46**.

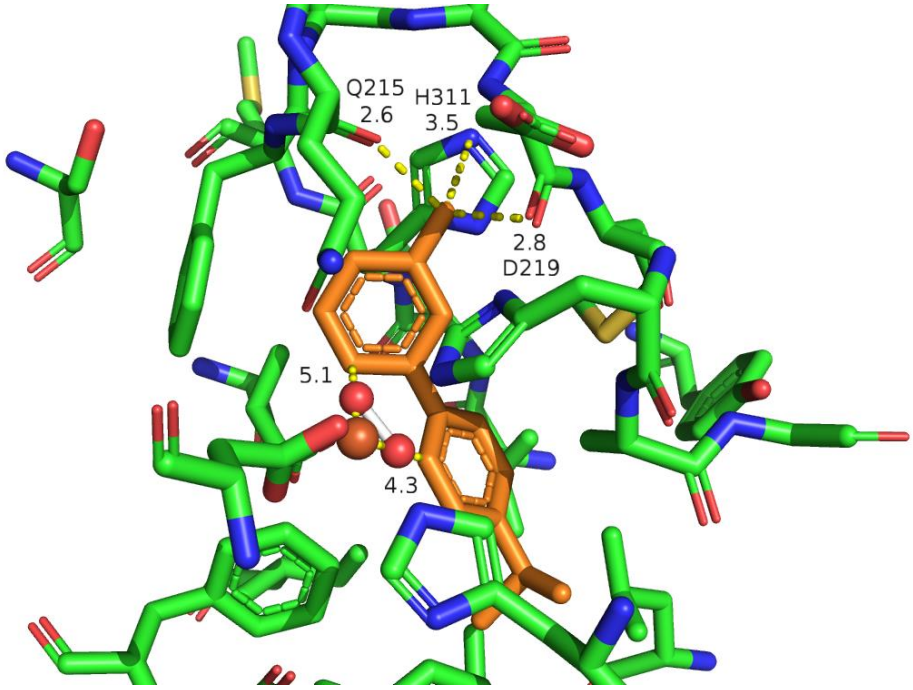

Figure 46: The major binding pose for 4'-isopropyl-[1,1'-biphenyl]-3-ol (**272**) shown in orange. The measurements to the Fe and hydrogen bonding distances to Gln_{215}, Asp_{219} and His_{311} are in Å. All the amino acid residues shown are within 5 Å of the substrate.

The isopropyl substituent is positioned in the hydrophobic pocket, which is discussed in detail in **Section 2.2**. Notably, the docking predicts a potential third hydrogen bonding interaction not previously mentioned, which is between the hydroxyl of the substrate and the carbonyl backbone of Asp_{219} (2.8 Å). The energetically favoured staggered conformer of substrate **272** positions the phenyl ring (4.3 Å) closer to the iron centre than the phenol ring (5.1 Å), which results in the anticipated hydroxylation on the phenyl side-chain functionality.

Based on the computationally derived biotransformation outcome, it is expected that *P. putida* UV4 cannot be exploited for the preparation of diol **280** using isopropyl-[1,1'-biphenyl]-3-ol (**272**). Nonetheless, the experimental results would still be of interest for the continued development of the docking model.

2.4 Preparation of the Incarviditone Analogues

With the synthesis of isopropylphenyl incarviditone analogue **237** complete using iodo keto *cis*-diol **117**, attention turned to the preparation of antipodal compound ***ent*-237** as well as three additional enantiomeric pairs of incarviditone analogues: **237b-d** and ***ent*-237a-c**, starting from the commercially available (-)-quinic acid (**194**) (**Scheme 64**).

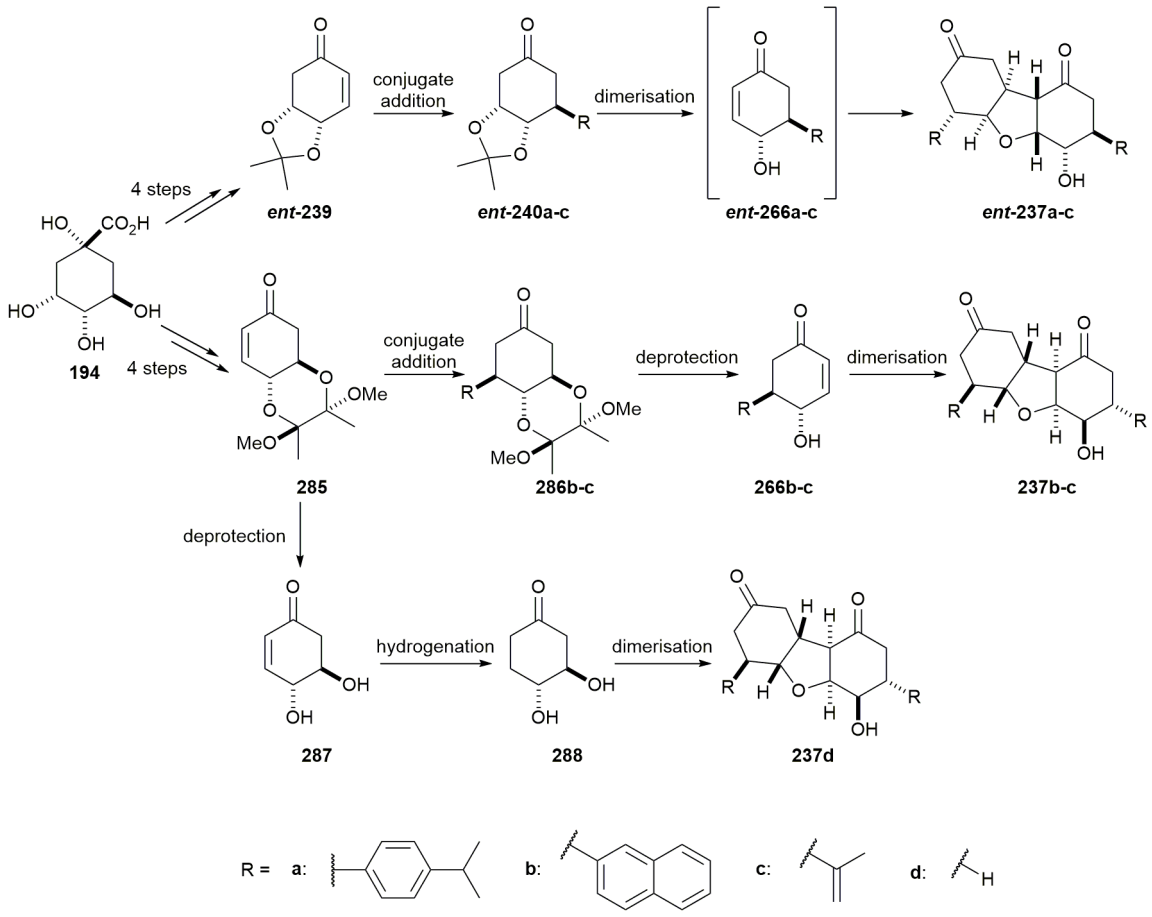

Scheme 64: The synthetic overview for the synthesis of dimers: **237b-d** and ***ent*-237a-c** using (-)-quinic acid (**194)**.

The successful synthesis of the compounds above would allow for the first biological evaluation of incarviditone analogues, which would allow comparison of the anti-proliferative activities between the optical isomers and potentially reveal any differences which may occur using *in-vitro* studies. Based on previous internal studies which indicated a relatively low IC_{50} for analogue ***ent*-237b**, naphthyl analogue **237b** was of particular interest.[61] Past incarviditone analogue syntheses however, have focused primarily on aromatic side chains and therefore the isopropenyl moiety (**237c** and ***ent*-237c**) was investigated to evaluate the biological activity of compounds containing aliphatic side-chains. The isopropenyl conjugate adduct ***ent*-240c** could also be exploited in the

preparation of the isopropyl analogue via hydrogenation of the double bond; the synthesis of which was undertaken by Matthew Usher, a fourth year project student.[116] Finally, incarviditone core **237d** was investigated to determine the effect of having no side-chain functionality. Taking into consideration the limited supply of iodo keto *cis*-diol **117**, butan-1,2-diacetal (BDA) protected quinic acid **195** was used in its place for the syntheses described herein. This allowed for the exemplification of alternative synthetic routes to those utilising diol **117**, with the benefit of demonstrating the synthetic utility of the biotransformation product **117**.

2.4.1 Protection of (-)-Quinic acid

The original procedure developed by the Whitehead group for the synthesis of incarviditone analogues employed the cyclohexylidene protecting group, which was also initially used for the purpose of this project.[66] The reaction conditions for the installation of this protecting moiety were adapted from a procedure reported by Gero and co-workers in 1971.[117] The two sets of reaction conditions are shown in **Scheme 65**.

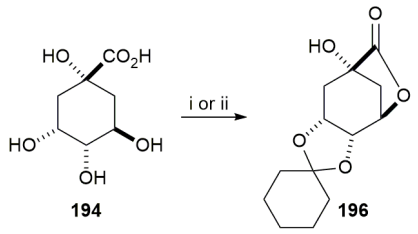

Scheme 65: *Reagents and conditions*: Gero and co-workers conditions: (i) cyclohexanone, Amberlite® IR 120 (H^+), *N*,*N*-dimethylformamide, benzene, Dean and Stark, reflux, 4 h, 86 %; Whitehead procedure: (ii) cyclohexanone, Amberlite® 120 (H^+), toluene, Dean and Stark, reflux, 6 h, 43 %.

Under the modified conditions, *N*,*N*-dimethylformamide was removed and benzene was replaced with the less toxic toluene. The yields for this adapted procedure however, were poorer than those quoted by Gero and co-workers and were exacerbated on reaction scales greater than 10 g.

In the interest of using a more carbon efficient protecting group, which would improve scalability, cyclohexylidene was replaced with the acetonide protecting group. In 1951, Grewe and Nolte were the first to report the acetonide protection of (-)-quinic acid (**194**) using hydrogen chloride and acetone.[118] An alternative procedure developed by Keiji and co-workers in 1998 however, was used in favour due to milder reaction conditions (see **Scheme 66**).[119]

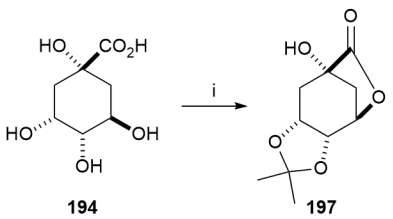

Scheme 66: *Reagents and conditions*: (i) 2,2-dimethoxypropane, *p*-TSA monohydrate (10 mol %), acetone, reflux, 6 h, 77 %.

The reaction proceeded well in 77 % yield on a 10 g scale, which demonstrated that scaling up the reaction did not influence the isolated yield. Furthermore, the addition of excess 2,2-dimethoxypropane had the added effect of acting as a dehydrating agent,[120] which pushed the reaction equilibrium in favour of the formation of product **197**. The mechanism is shown in **Scheme 67**.

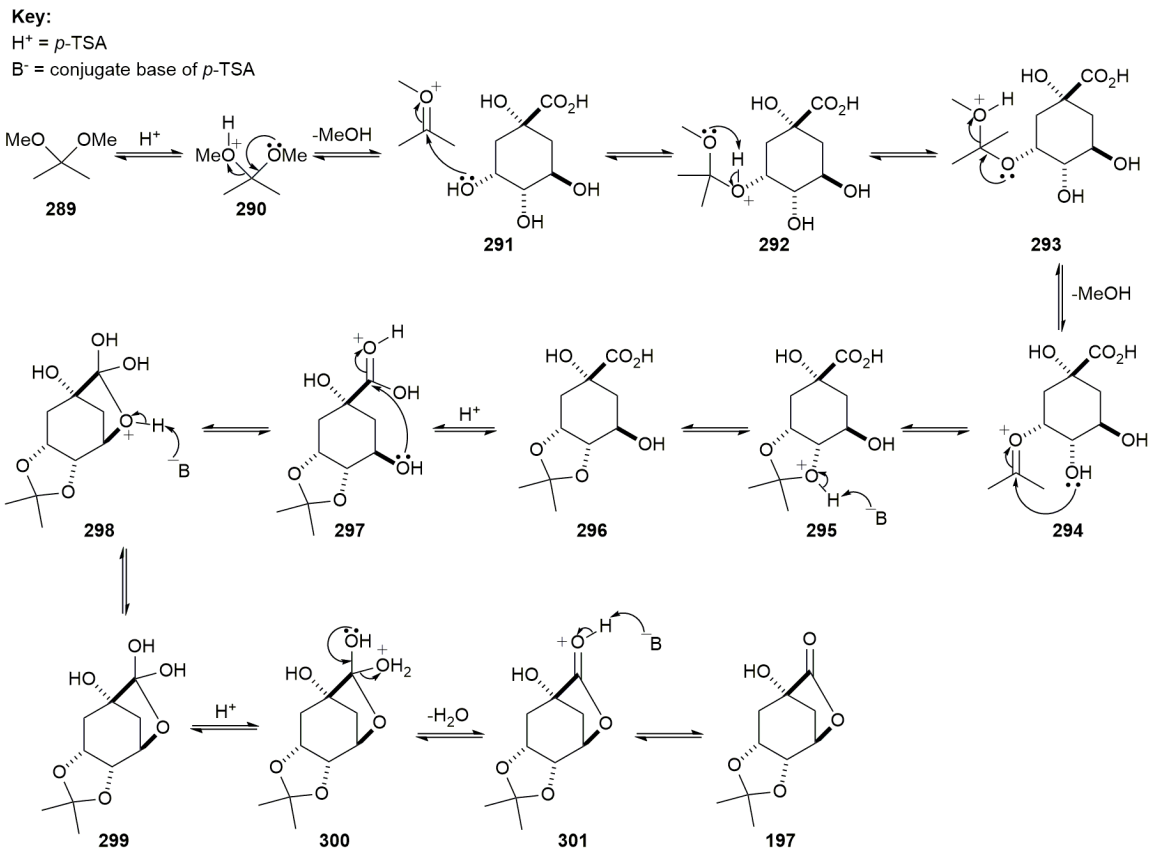

Scheme 67: The mechanism of the 1,2-*cis*-diol acetonide protection and lactonisation of (-)-quinic acid (**194**) to afford lactone **197**.

The protection of the vicinal *cis*-diol and formation of the lactone was confirmed by analysis of the ^{1}H NMR and infra-red spectra, which confirmed the presence of the carbonyl lactone at 1772 cm^{-1}. Though in **Scheme 67** the *cis*-diol protection is shown preceding the lactonisation (**296**), the order of reactivity is undetermined. If the diol

protection was to occur initially, then intermediate **296** would have to ring flip to adopt a high energy conformer that would facilitate the lactonisation (**Scheme 68**).[121]

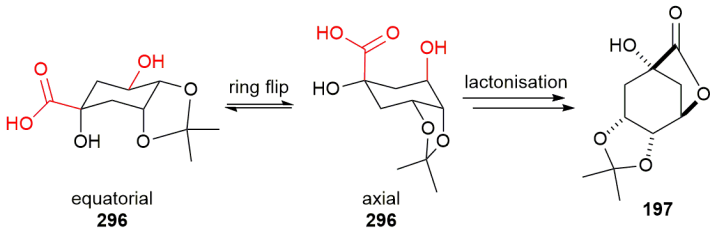

Scheme 68: Ring flipping of intermediate **296** to facilitate lactonisation.

In addition to the 1,2-*cis*-diol protection, an alternative synthetic route was sought for the synthesis of the incarviditone analogues, which would enable the same enantiomeric outcome as iodo keto *cis*-diol **117**. In 1996, Frost and co-workers reported the protection of the vicinal diequatorial diol of (-)-quinic acid (**Scheme 69**)[122] using adapted procedures originally reported by Ley and colleagues.[123, 124, 125]

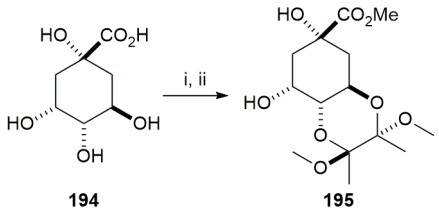

Scheme 69: *Reagents and conditions* as reported by Frost and co-workers: (i) MeOH, Dowex® 50 H^+, reflux, 15 h; (ii) 2,2,3,3-tetramethoxybutane, trimethyl orthoformate, CSA, MeOH, reflux, 22 h, 87 %.

The Whitehead group developed an improved procedure based on the conditions described by Ley and Frost (**Scheme 70**), whereby the *trans*-diol was protected using butan-2,3-dione to form the butan-1,2-diacetal (BDA).

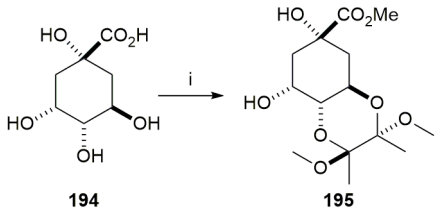

Scheme 70: *Reagents and conditions*: (i) butan-2,3-dione, trimethyl orthoformate, CSA, MeOH, reflux, 18 h, 88 %.

The *trans*-diol protection of (-)-quinic acid proceeded well and was accompanied by the esterification of the carboxylic acid to the methyl ester to afford product **195**. The mechanism for this process is shown in **Scheme 71**.

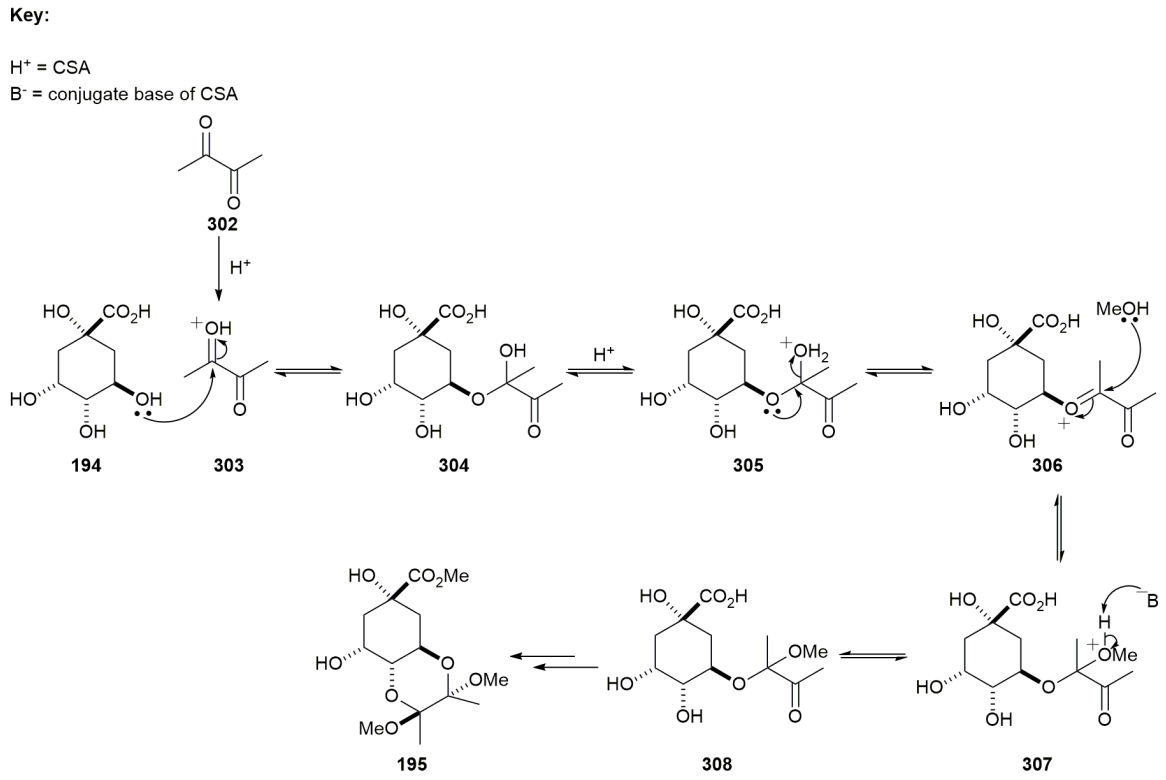

Scheme 71: The mechanism of the *trans*-diol BDA protection of (-)-quinic acid (**194**) to afford ester **195**.

The vicinal equatorial diol selectivity can be attributed to the conformation of the resulting product (**Figure 47**).

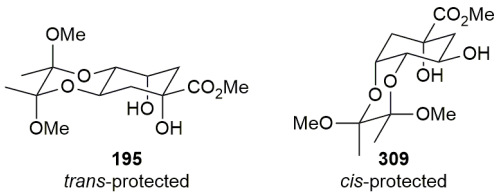

Figure 47: The trans- and *cis*-diol BDA protected (-)-quinic acid **195** and **309** respectively.

The sterically less demanding *trans*-ring junction and the axial arrangement of the methoxy groups situated on the BDA protecting moiety led to the thermodynamically stable *trans*-product **195**. Furthermore, González-Bello and co-workers proposed that due to the steric hindrance present within the *cis*-protected product **309**, the BDA ring would be forced to flatten leading to partial loss of the anomeric stabilisation.[126]

2.4.2 Sodium Borohydride Reduction

With compounds **195** and **197** in hand, the lactone/ester functionalities were reduced using $NaBH_4$ in the presence of EtOH/MeOH to form triols **310** and **311** respectively (see **Scheme 72**).[50, 127]

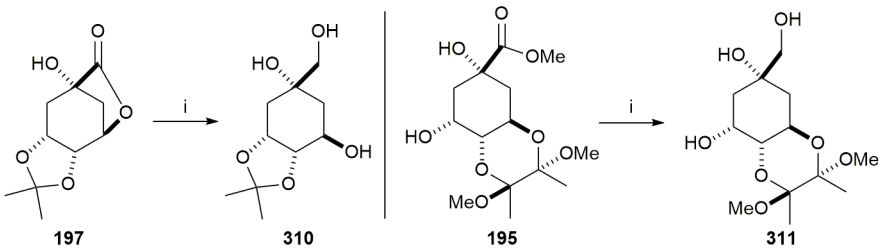

Scheme 72: The sodium borohydride reduction of lactone **197** and ester **195** to afford triols **310** and **311** respectively. *Reagents and conditions*: (i) $NaBH_4$, EtOH (**310**)/MeOH (**311**), 0 °C to RT, 20 h.

It is well established that reduction of esters typically requires a strong reducing agent such as lithium aluminium hydride. There are however examples of the comparatively weaker reductant sodium borohydride converting esters to the corresponding primary alcohols, as illustrated by **Scheme 72**. In 1961, Schenker analysed these anomalous reactions and concluded that in most cases a neighbouring functional group was present and was participating in the reduction, yet no mechanism was suggested.[128, 129] In the system depicted above, it was suggested that the α-hydroxyl group contributed by withdrawing electron density away from the carbonyl ester, thus increasing the propensity of the ester towards reduction. There are however reports of neighbouring hydroxyl groups directing the reduction through an internal coordination. Dalla and co-workers suggested that coordination of the borohydride to the α-hydroxyl results in a five-membered transition state, which delivers the hydride intramolecularly to the carbonyl ester (see **Scheme 73**).[130]

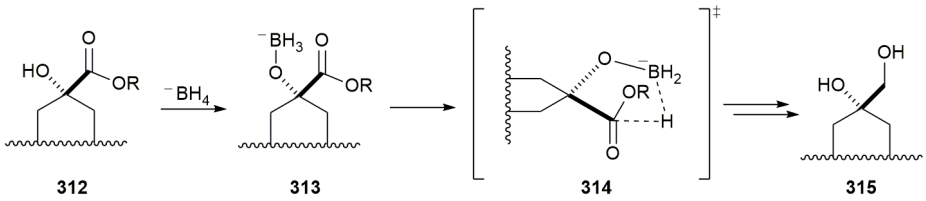

Scheme 73: The intramolecular reduction of ester/lactone by $NaBH_4$ via the five-membered transition state **314** proposed by Dalla and co-workers.

Despite the clear precedent regarding the active role of the α-hydroxyl in the reduction of (-)-quinic acid protected derivatives, it has been demonstrated that the reduction of an ester by $NaBH_4$ does not require neighbouring functional group participation to facilitate the reaction.[131] Rather, the *in-situ* formation of alkoxyborohydride intermediates by the reaction of sodium borohydride with the MeOH/EtOH solvent system (**Scheme 74**), produces a more reactive reducing agent, which is capable of slow reduction of esters.

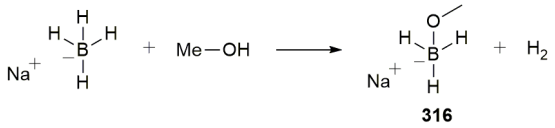

Scheme 74: The formation of the alkoxyborohydride intermediate **316** by the reaction of $NaBH_4$ with an alcohol solvent (e.g. MeOH).

Davis and Gottbrath proposed that the electron release from oxygen onto boron increases the hydridic character of the borane hydrogen atom, thus producing a more potent reductant.[132] In summary, it can be suggested that a combination of all three factors discussed facilitated the ester/lactone reduction.

On completion, the reaction was quenched by the addition of saturated ammonium chloride, which produced a large volume of gas. The mixture was then concentrated *in vacuo*, which produced a viscid, white solid that was difficult to wash with organic solvent. The organic washes used to extract products **310** and **311** typically contained unknown impurities, however they did not interfere with the following steps and the triols were therefore carried through crude.

2.4.3 Oxidative Cleavage

The crude triols **310** and **311** were oxidised using silica supported sodium *meta*-periodate to afford hydroxyketones **317** and **318** respectively (**Scheme 75**).[50, 133]

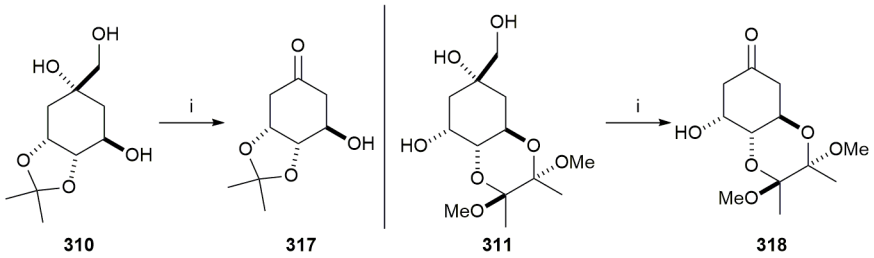

Scheme 75: The oxidative cleavage of triols **310** and **311** to give hydroxyketones **317** and **318** respectively. *Reagents and conditions*: (i) $NaIO_4$, silica gel, CH_3Cl (**317**)/CH_2Cl_2 (**318**), RT, 2 h, 85 % over two steps (**317**), 64 % over two steps (**318**).

Sodium *meta*-periodate is known for its poor solubility in non-polar organic solvents.[134] Hodge and co-workers developed a method to overcome this issue by supporting $NaIO_4$ on chromatographic grade silica gel.[135] Their methodology required an aqueous solution of $NaIO_4$ in the presence of silica gel to be concentrated at 120 °C to afford the supported $NaIO_4$ as a free-flowing powder. The supported silica gel had an approximate $NaIO_4$ loading of 10 % and was compatible with non-polar organic solvents. This was however

considered a tedious preparative procedure and was later supplanted by a more efficient method developed by Doumas and co-workers.[136] Their method comprised of adding a fresh solution of sodium *meta*-periodate in water to a stirring suspension of silica gel in CH_2Cl_2, followed by a drop-wise addition of the diol starting material in CH_2Cl_2. Despite the improvement in efficiency, the reaction had to be vigorously stirred, and the silica gel readily formed a colloid within the reaction vessel, which impeded the stirring of the reaction. In 1997, Zhong and Shing reported a refinement of Doumas' method, which involved dissolving the $NaIO_4$ reagent in a minimum amount of hot water prior to addition of silica gel to the solution to afford the supported reagent. The application of the supported $NaIO_4$ allowed for a simple filtration and organic wash for product purification, and the authors reported that the modified reagent was stable for up to 1 month with negligible loss of activity.[137] These conditions were applied to the oxidative cleavage of triols **310** and **311**, which proceeded with ease. The reaction mechanism is shown in **Scheme 76**.

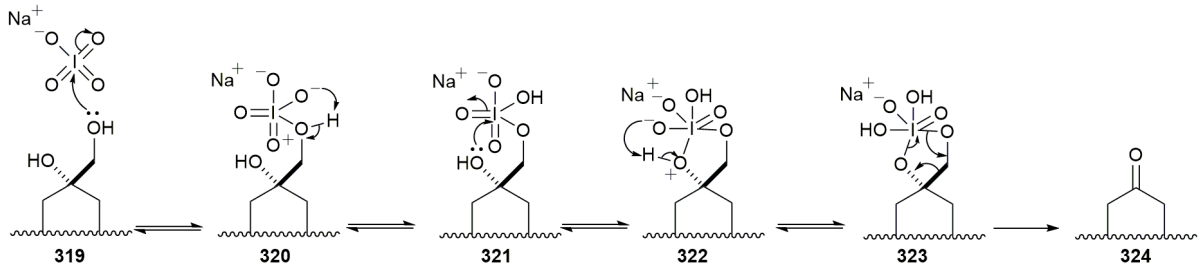

Scheme 76: The oxidative cleavage mechanism of vicinal diols by $NaIO_4$.[134, 138]

2.4.4 Dehydration

Treatment of hydroxyketones **317** and **318** with methanesulfonyl chloride in the presence of triethylamine yielded dehydrated products ***ent*-239** and **285** in good yields (**Scheme 77**).[50, 139]

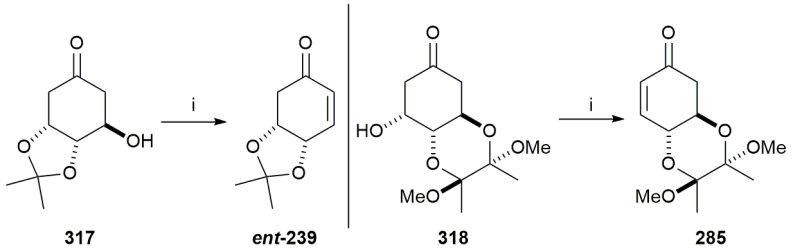

Scheme 77: The dehydration of the hydroxyketones **317** and **318** to afford enones ***ent*-239** and **285** respectively. *Reagents and conditions*: (i) Et_3N, MsCl, CH_2Cl_2, 0 °C to RT, 5 h (***ent*-239**)/4 h (**285**), 76 % (***ent*-239**), 83 % (**285**).

The reaction proceeds via an intermediate sulfene species (**327)**, which activates the hydroxyl group prior to elimination (**Scheme 78**).

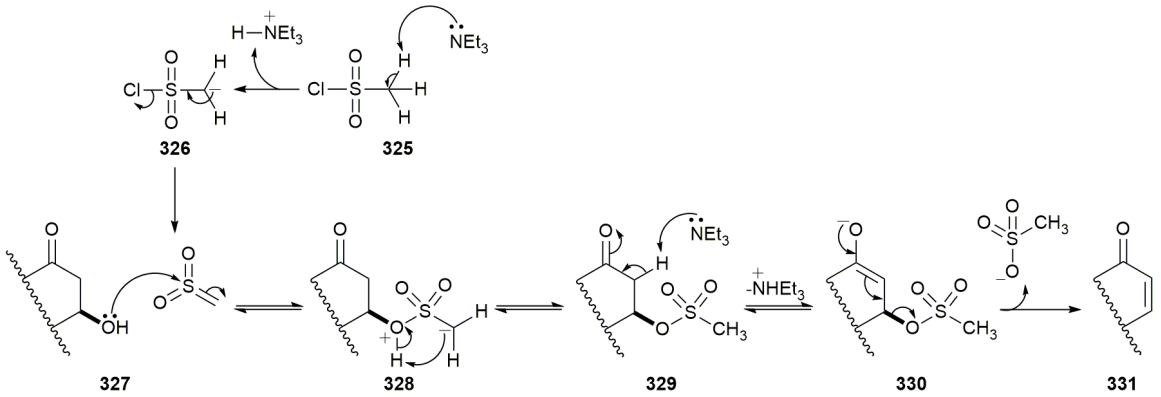

Scheme 78: The dehydration mechanism for hydroxyketones **317** and **318** by MsCl and Et_3N.[140]

The activation of the β-hydroxyl group by a sulfene (**327)** has precedent in the literature. Truce and co-workers used deuterium labelling studies to determine the formation of an intermediate carbanion on the sulfonyl chloride by proton-deuterium exchange.[141] Furthermore, King and co-workers used pH kinetic profiles in conjunction with nucleophilic trapping studies to confirm the formation of a reactive sulfene species.[142]

The stability of acetonide enone ***ent*-239** under the basic conditions and long-term storage proved to be problematic in comparison to BDA enone **285**. This can be rationalised by the propensity for enone ***ent*-239** to undergo elimination to form hydroquinone (**224**), which can oxidise to form *para*-benzoquinone (**334**) (**Scheme 79**).

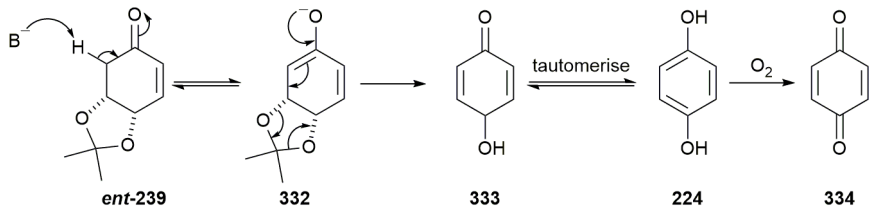

Scheme 79: The decomposition of acetonide enone ***ent*-239** to form hydroquinone (**224**) and *para*-benzoquinone (**334**).

To counteract the decomposition of enone ***ent*-239**, the crude reaction mixture was rapidly purified following the reaction quench, and elevated temperatures (>35 °C) were avoided when handling the product. The purified enone ***ent*-239** was stored at -18 °C under an inert N_2 atmosphere to ensure the stability of the product during storage. BDA enone **285** was not susceptible to decomposition under the reaction conditions due to the diequatorial

location of the protecting group, which disfavours elimination. As such, BDA enone **285** was not subjected to the same stringent handling requirements as acetonide enone ***ent*-239**.

2.4.5 Rhodium Catalysed Conjugate Addition

With the synthesis of key enone building blocks ***ent*-239** and **285** complete, the focus turned to the installation of side-chain functionalities at the β-position using rhodium catalysis. This was achieved using the reaction conditions described in **Section 2.3.2** (**Scheme 80**). The installation of the isopropenyl moiety was achieved using an alternative approach, described in **Section 2.4.6**, due to reported decomposition of the isopropenyl boronic acid reagent via protodeboronation, oxidation and/or polymerisation.[143]

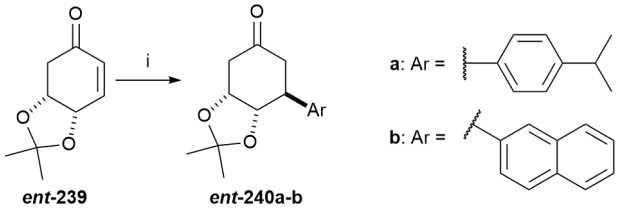

Scheme 80: *Reagents and conditions*: (i) 4-isopropylphenylboronic acid or 2-naphthylboronic acid, $[RhCl(cod)]_2$ (5 mol %), Et_3N, dioxane:H_2O (10:1), RT, 18 h, ***ent*-240a** (76 %), ***ent*-240b** (71 %).

Both conjugate adducts ***ent*-240a** and ***ent*-240b** were isolated in good yields of 76 % and 71 % respectively. Efforts were also made to optimise the reaction conditions and the results of these are shown in **Table 16** using the conjugate addition of 2-naphthylboronic acid to enone ***ent*-239**.

Table 16: The effect of reducing the Et_3N equivalents on the percentage yield of the rhodium catalysed conjugate addition of 2-naphthylboronic acid to enone ***ent*-239**. *Reagents and conditions*: (i) 2-naphthylboronic acid, $[RhCl(cod)]_2$ (5 mol %), Et_3N, dioxane:H_2O (10:1), RT, 18 h.

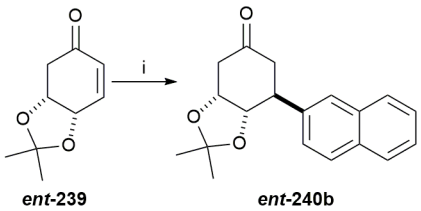

Equivalents of Et_3N (eq.)	% yield
1	62 %
0.5	71 %

The Whitehead group has previously investigated the effect of varying the catalyst and boronic acid loading, but has otherwise maintained the addition of 1.0 equivalent of triethylamine.[61] The decision to vary this parameter was prompted by the presence of the

corresponding hydroxyenone product **335**, which was formed by elimination of the conjugate adduct on prolonged exposure to triethylamine (**Figure 48**).

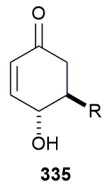

335

Figure 48: The general structure of hydroxyenone **335**.

The rate of elimination varied depending on the side-chain functionality, and in some instances the hydroxyenone rapidly accumulated in less than 6 hours (e.g**.** 4-(trifluoromethyl)phenyl).[144] With respect to 2-naphthyl adduct ***ent*-240b**, lowering the amount of triethylamine resulted in a modest improvement in the isolated yield, which can be attributed to a decrease in hydroxyenone ***ent*-266b** formation.

The synthesis of antipodal naphthyl adduct **286b** was achieved by subjecting the BDA enone **285** to the same conjugate addition reaction conditions described for the acetonide protected adducts. Furthermore, to establish a comparison with the synthetic route utilising iodo diol **117** (see **Section 2.3.2**), the conjugate addition of 4-isopropylphenylboronic acid was trialled on enone **285**. It was envisaged that as both synthetic routes provide the same stereochemical output, a comparison could be used to highlight the advantages of applying bioproduct **117**, which previously afforded the desired *anti*-diastereomer exclusively in 62 % yield (**Table 17**).

Table 17: *Reagents and conditions*: (i) 2-naphthylboronic acid or 4-isopropylphenylboronic acid, $[RhCl(cod)]_2$ (5 mol %), Et_3N, dioxane:H_2O (10:1), RT, 18 h.† = The ratio of diastereomers was determined by ^1H NMR. ‡ = Diastereomers were not separated, quoted yield is for the product mixture following purification.

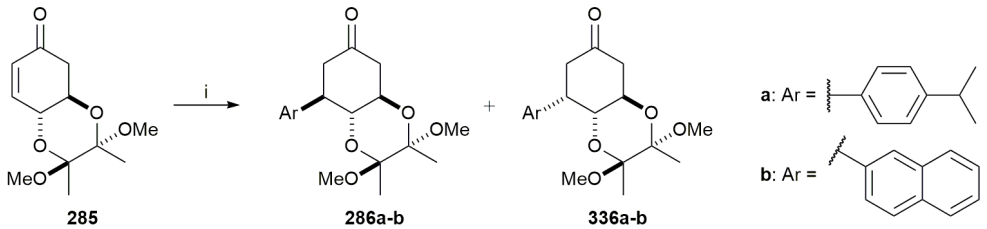

285 **286a-b** **336a-b**

Ar	Crude *anti*:*syn* (**286**:**336**) ratio†	Yield (%)
4-isopropylphenyl (**a**)	1:2	93 % (**286a** and **336a**)‡
2-naphthyl (**b**)	1:3	20 % (**286b**), 38 % (**336b**)

The rigid *trans*-decalin nature of BDA enone **285** resulted in negligible facial selectivity in the addition of the aryl boronic acid, affording a mixture of both *anti* and *syn* diastereomers. In both cases, the undesired *syn* diastereomer was the major product from the reaction. The adducts **286b** and **336b** were separated by normal phase HPLC, with considerable loss of product due to poor separation. For the desired 4-isopropenylphenyl adduct **286a**, no significant separation could be achieved using analytical normal-phase HPLC. The poor diastereoselectivity of both conjugate addition reactions signifies the advantage of using the iodo keto *cis*-diol route, which yielded *anti*-diastereomer **240a** exclusively.

In an effort to improve the diastereoselectivity, two alternative approaches were used. The first employed a chiral ligand to influence the selectivity. Uncertain regarding the ligand chirality that would be compatible with the system, both (*S*)- and (*R*)-BINAP were applied in the conjugate addition of 2-naphthylboronic acid using similar conditions as those described by Hayashi (**Table 18**).[145]

Table 18: Results of the addition of (*S*)/(*R*)-BINAP on diastereoselectivity. *Reagents and conditions*: (i) 2-naphthylboronic acid, $[RhCl(cod)]_2$ (5 mol %), (*S*) or (*R*)-BINAP, Et_3N, dioxane:H_2O (10:1), RT, 18 h.

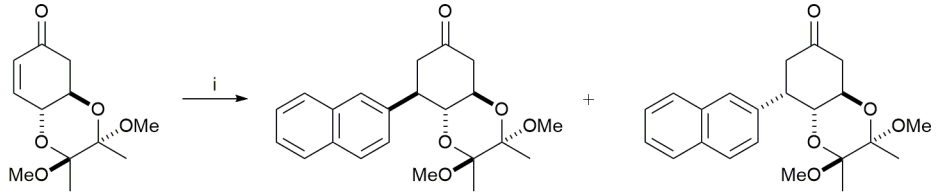

285 **286b** **336b**

Ligand (% loading)	Crude *anti*:*syn* ratio
(*S*)-BINAP (10 %)	1:7
(*R*)-BINAP (10 %)	1:3

The addition of the atropisomers of BINAP had no beneficial influence on the formation of the desired *anti*-diastereomer **286b**. It has been shown that enone **285** inherently favours the formation of the *syn* stereoisomer for the 4-isopropylphenyl and 2-naphthyl systems (**Table 17**). In light of this and the results shown in **Table 18**, the addition of a chiral ligand to an already biased system was deemed to be unsuccessful and was abandoned in favour of an alternative approach.

It was envisaged that removing the butan-1,2-diacetal of enone **285** to yield *trans*-diol **287** may provide a system with an inherent property to direct the incoming nucleophile during

the conjugate addition. At the onset it was unclear how the two hydroxyl groups would influence the diastereoselectivity (**Scheme 81**).

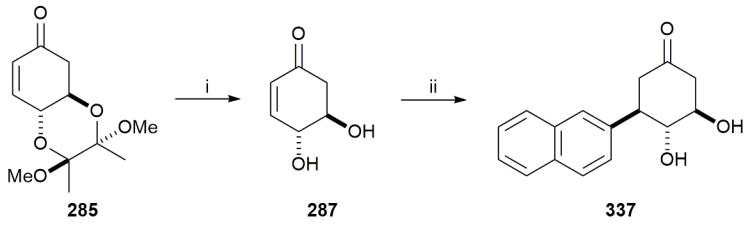

Scheme 81: *Reagents and conditions*: (i) TFA, distilled H_2O, CH_2Cl_2, RT, 18 h, 70 %; (ii) 2-naphthylboronic acid, $[RhCl(cod)]_2$, Et_3N, dioxane:H_2O (10:1), RT, 18 h, 24 %.

The rhodium catalysed conjugate addition to unprotected alcohols has precedent in the literature and showcases the functional group tolerance of this reaction.[146, 147] Based on the compatibility of the previously described reaction conditions, the conjugate addition of 2-naphthylboronic acid was trialled on TFA deprotected enone **287**.

Interestingly, one of the isolated products from the reaction mixture, following flash silica chromatography, suggested that the conjugate addition had selectively formed *anti*-adduct **337** (**Figure 49**).

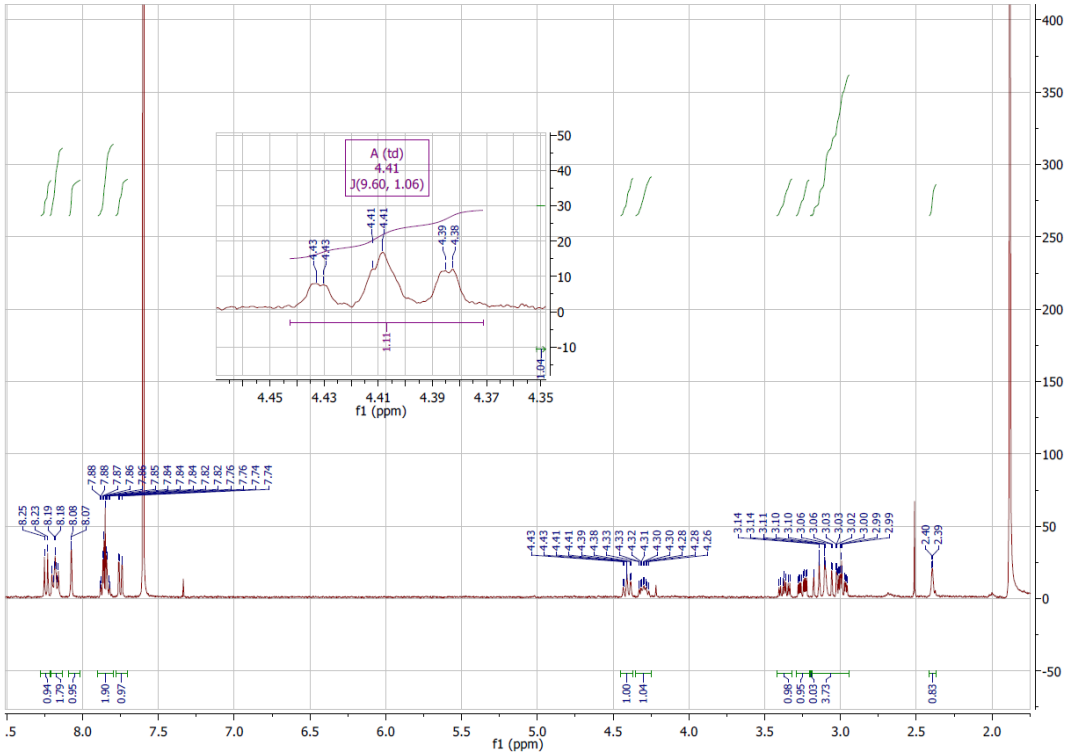

Figure 49: The ^1H NMR spectrum of the suggested *trans*-diol adduct **337** following flash silica chromatography. Solvent: $CDCl_3$.

The indicative coupling constant for the C4-hydrogen, a triplet of doublets at 4.41 ppm, was 9.6 Hz, which is within the expected range for a diaxial arrangement. On comparison with the coupling constant from the analogous hydrogen in protected *anti*-adduct **286b**, (10.1 Hz), it was concluded that the similarity between the two values suggests that *anti*-adduct **337** was formed.

Despite the promising nature of this reaction, the instability of *trans*-diol **287** and presence of an unidentified side-product made this approach problematic. On exposure to the reaction conditions, *trans*-diol **287** readily aromatised to form hydroquinone (**224**). Furthermore, the ^{1}H NMR spectrum of the unidentified impurity indicated aromatic functionality and an overall peak pattern that bared close resemblance to the ^{1}H NMR spectrum of product **337**. In summary, the reaction proved to be capricious and isolation of the suspected *trans*-adduct **337** was difficult. Nevertheless, this research showed a promising avenue for controlling the diastereoselectivity using the butan-1,2-diacetal protected (-)-quinic acid synthetic route.

2.4.6 Copper Catalysed Conjugate Addition

In 2007, Bräse and co-workers reported the conjugate addition of several aliphatic organocuprates to acetonide enone ***ent*-239** with varying success (**Table 19**). Nonetheless, all the reported conjugate additions proceeded with excellent *anti* diastereoselectivity (>99:1 *anti*:*syn*), due to the acetonide protecting group blocking *syn*-attack.[148]

Table 19: The organocuprate addition results as reported by Bräse and co-workers. *Reagents and conditions*: (i) $R_2CuMgBr.SMe_2$, THF, Me_2S, -50 °C, 14 h. † = Product unstable towards column chromatography, no yield was obtained.

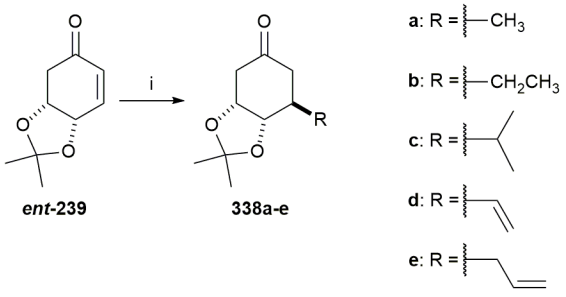

Adduct	Yield
338a	73 %
338b	66 %
338c	0 %
338d	-†
338e	4 %

Notably, for vinylcuprates **338d** and **338e** Bräse and co-workers reported poor yields. For the latter, the authors noted that in consequence of the basic reaction conditions and the propensity of the allyl cuprate to decompose rapidly, enone ***ent*-239** slowly eliminated to form hydroquinone (**224**). Subsequently, hydroquinone (**224**) underwent a conjugate addition with enone ***ent*-239** affording hydroquinone adduct **339** (**Figure 50**).

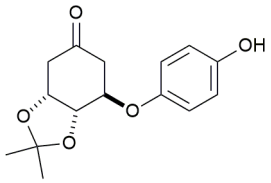

339

Figure 50: The structure of hydroquinone adduct **339**, as reported by Bräse and co-workers.

In addition to this, the conjugate adducts were observed to undergo elimination of the acetonide moiety to form the respective hydroxyenone (**335**). Nevertheless, previous work by the Whitehead group has utilised the procedure developed by Kornienko and co-workers for aryl cuprates with good success.[149] Satisfied that acetonide enone ***ent*-239** was compatible with a cuprate addition, these conditions were applied for the preparation of isopropenyl adduct ***ent*-240c** (**Scheme 82**).

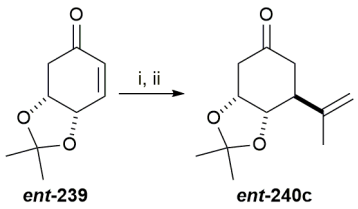

***ent*-239** ***ent*-240c**

Scheme 82: *Reagents and conditions*: (i) CuI, CH_2=C(CH_3)MgBr (0.5 M in THF), THF, -42 °C, 1 h; (ii) ***ent*-239**, TMSCl, THF, -42 °C, 3 h, 87 %.

The reaction proceeded in an excellent yield of 87 %. Contrary to the results obtained by Bräse and co-workers, there was no observed formation of the hydroquinone adduct or hydroxyenone products. Rather, the difficulty with this reaction was the hydrolysis of TMS complex **340**, which required prolonged stirring with a mixture of sat. $NH_4Cl_{(aq)}$:$NH_{3(aq)}$ (9:1) to liberate conjugate adduct ***ent*-240c** (**Figure 51**).

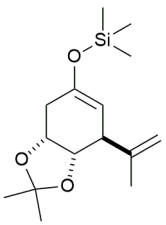

340

Figure 51: The structure of the coordinated TMS complex **340**.

The organocuprate addition to BDA enone **285** proved to be problematic due to the lack of inherent facial selectivity of the molecule. There have, however, been attempts reported in the literature to elucidate the diastereoselectivity of reactions of this type. Previous work by Corey and Boaz investigated the diastereoselectivity of the conjugate addition of lithium dimethylcuprate to spirocyclic enone **341** (**Figure 52**).[150]

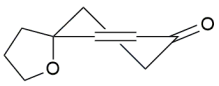

341

Figure 52: The structure of spirocyclic enone **341**.

Corey and Boaz's original hypothesis predicted that the *anti*-product would be favoured at the β-position, due to the γ-heteroatom withdrawing electron density away from the Cu(III) species via hyperconjugation. The maximum stabilisation therefore would be achieved via an *anti* geometry. The experimental data however showed a stronger preference for the *syn* addition (92:8, *syn*:*anti*): the proposed explanation for this result was that the reaction proceeded via rapid reversible formation of a copper-enone complex, in which the *syn* pathway led to faster product formation (**Scheme 83**).

To test this hypothesis, the reaction was repeated in the presence of 5.0 equivalents of chlorotrimethylsilane. Aside from an accelerated reaction time, only *anti*-product **345** was isolated from this reaction.

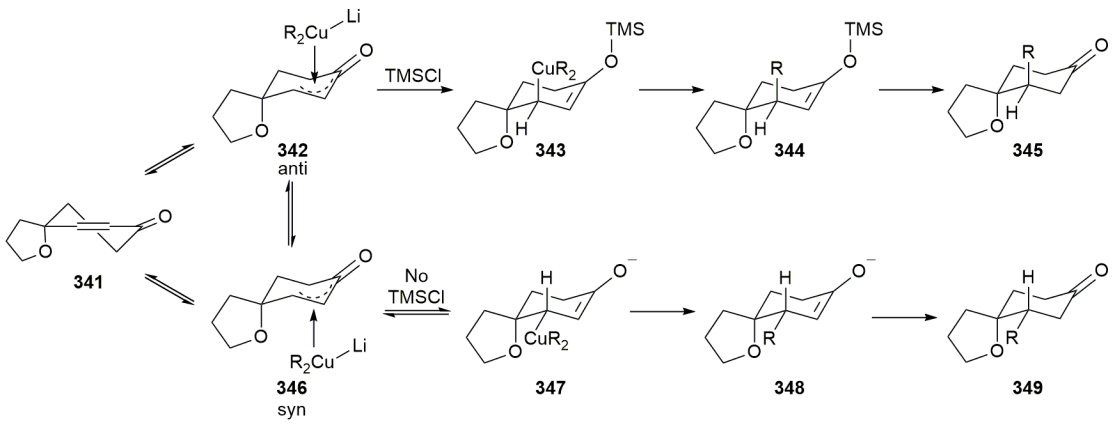

Scheme 83: The proposed mechanism for *anti*-selectivity as proposed by Corey and Boaz.[150]

The reaction of spiroenone **341** with the lithium cuprate resulted in the formation of π* copper(III) adducts **342** and **346**. The *cis* and *trans* copper(III) π* complexes **342** and **346** were suggested to rapidly interconvert, with *cis*-complex **346** predominating and leading to conjugate adduct **349**. The authors proposed that this selectivity may be due to steric reasons. When the reaction was conducted in the presence of TMSCl however, *trans*-complex **342** was trapped as TES enolate **343** and was prevented from interconverting. This led to the stereoselective formation of *anti*-conjugate adduct **345**. Frantz and Singleton used kinetic isotope effect studies to support the hypothesis by Corey and Boaz, which suggests that the TMSCl traps an intermediate π complex. This result was consistent with the experimental observations and the theoretical predictions.[151]

Despite the promising stereoselectivity exerted by the TMSCl coordination, previous work by the Whitehead group has indicated the capricious nature of the BDA enone system towards organocuprate addition.[152] It has been determined that the diastereoselectivity of the copper mediated conjugate addition is unpredictable, and in some instances the addition of TMSCl had no effect on the stereochemical outcome. Nevertheless, it transpired that temperature control was the most significant factor in influencing the diastereoselectivity. With this in mind, the Gilman cuprate conjugate additions of 2-naphthyl, 2-propenyl and 4-isopropylphenyl were conducted on enone **285**, and the most promising results are shown **Table 20.**

Table 20: The results for the organocuprate addition to BDA enone **285** using CuI and the corresponding Grignard reagent.

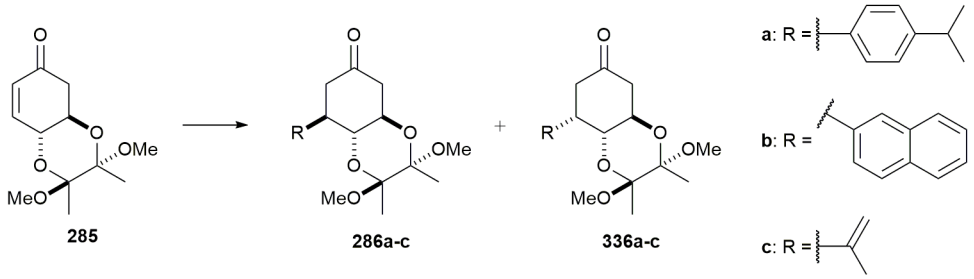

Reaction conditions	Crude *anti*:*syn* ratio	Yield
(4-^{i}Pr-C_6H_4)$_2$CuMgBr, TMSCl, 0 °C to RT, THF, 5 h	1:1	43 % (**286a** and **336a**)
(2-naphthyl)$_2$CuMgBr, TMSCl, -78 °C, THF, 6 h	1:1	12 % (**286b** and **336b**)
(2-propenyl)$_2$CuMgBr, TMSCl, -42 °C, THF, 3 h	3:1	51 % (**286c**)

The conjugate addition of the 2-propenyl moiety favoured the formation of *anti*-diastereomer **286c**, which could be easily purified by column chromatography. This however was not the case for the 4-isopropylphenyl and 2-naphthyl adducts, which afforded both diastereomers **286a-b** and **336a-b** in equal amounts. Efforts were made to investigate the effect of temperature control for the 4-isopropylphenyl conjugate addition, and the results showed that decreasing the reaction temperature led to an increase in the *syn*-product formation (**336a)**. In comparison to the rhodium catalysed process, the organocuprate addition delivered a better diastereoselectivity ratio, however the poor yields following purification limited the application of this methodology.

2.4.7 Dimerisation

The conjugate adducts ***ent*-240a-c** obtained using acetonide protected (-)-quinic acid **197** were dimerised, utilising a one pot procedure involving prolonged exposure to basic conditions to afford the respective incarviditone analogues ***ent*-237a-c** (**Scheme 84**). The dimerisation proceeds through a hydroxyenone (***ent*-266a-c**) intermediate and the mechanism is described in **Section 2.3.3**, **Scheme 58**.

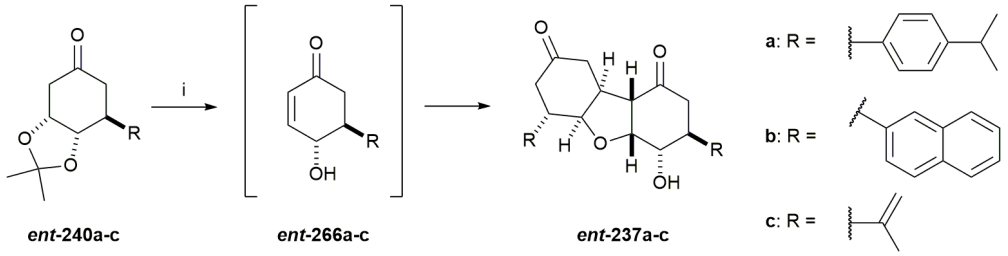

Scheme 84: *Reagents and conditions*: (i) 0.5 M $NaOH_{(aq)}$, THF, RT, 18 h, 60 % (**ent-237a**), 71 % (***ent*-237b**), 30 % (***ent*-237c**).

The dimerisation proceeded well for analogues ***ent*-237a** and ***ent*-237b**, however the yield for isopropenyl analogue ***ent*-237c** was poor. This was attributed to an unknown impurity unique to the dimerisation of adduct ***ent*-240c** when using NaOH and is explored further in **Section 2.6.3**. This impurity was also observed in the synthesis of the corresponding enantiomer **237c** described below.

To validate the hypothesis that the one-pot dimerisation proceeds via a hydroxyenone intermediate (***ent*-266**), isopropylphenyl hydroxyenone ***ent*-266a** was isolated and dimerised by utilising the previously stated reaction conditions (**Scheme 85**).

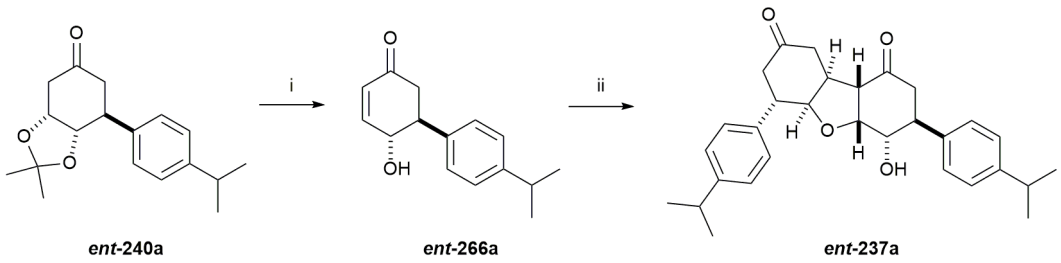

Scheme 85: *Reagents and conditions*: (i) 0.5 M $NaOH_{(aq)}$, THF, RT, 1 h, 85 %; (ii) 0.5 M $NaOH_{(aq)}$, THF, RT, 18 h, 66 %.

With an overall yield of 56 % over the two steps, the isolation of analogue ***ent*-237a** satisfied the aim of confirming the intermediate role of a hydroxyenone in the dimerisation mechanism.

The dimerisation of the BDA adducts **286b** and **286c** proceeded in a similar manner to the acetonide protected compounds described above, however an initial acid mediated deprotection was required to remove the diacetal protecting group (**Scheme 86**). From here, the resulting hydroxyenones **266b** and **266c** were dimerised under basic conditions to afford the antipodal incarviditone analogues **237b** and **237c**.

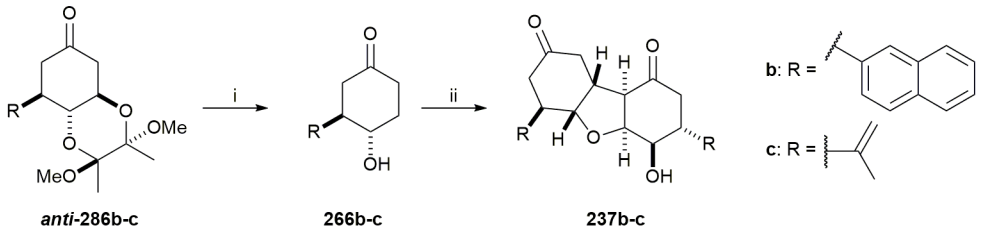

Scheme 86: *Reagents and conditions*: (i) TFA, distilled H_2O, CH_2Cl_2, RT, 18 h, 62 % (**266b**), 67 % (**266c**); (ii) 0.5 M $NaOH_{(aq)}$, THF, RT, 18 h, 56 % (**237b**), 42 % (**237c**).

The dimerisation of hydroxyenones **266b** and **266c** proceeded in a similar yield to their enantiomer adduct counterparts shown in **Scheme 84**. The synthesis of the unsubstituted incarviditone core **237d** was also achieved successfully by applying the modified route shown in **Scheme 87**.

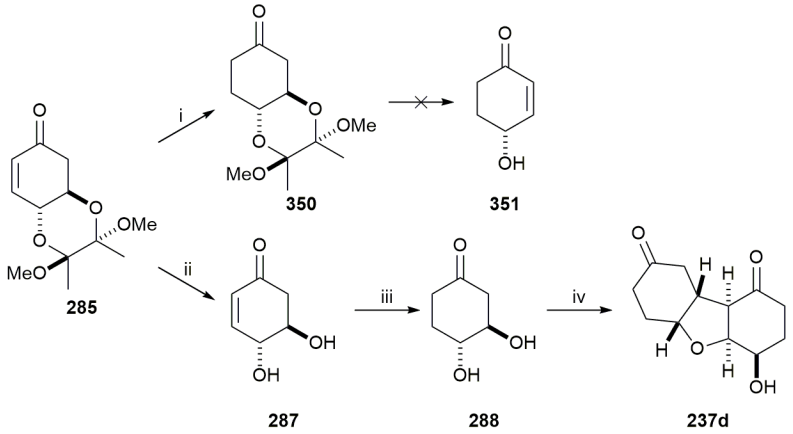

Scheme 87: *Reagents and conditions*: (i) 5 % Pd/C, EtOAc, RT, 18 h, 79 %; (ii) TFA, distilled H_2O, CH_2Cl_2, RT, 18 h, 70 %; (iii) 5 % Pd/C, EtOAc, RT, 18 h, 65 %; (iv) 0.5 M $NaOH_{(aq)}$, THF, RT, 48 h, 10 %.

Initially, BDA enone **285** was subjected to a hydrogenation reaction to afford cyclohexanone **350**. From here, it was envisaged that the BDA moiety could be removed using TFA and the resulting γ-hydroxyenone **351** dimerised to afford core analogue **237d**. Despite the hydrogenation proceeding well, the TFA deprotection resulted in a significant amount of decomposition of the desired product **351** to hydroquinone (**224**) due to its acid sensitivity. This observation concurred with the results reported by Danishefsky and co-workers, whereby the γ-hydroxyl of **351** was protected *in-situ* to prevent decomposition.[139]

An alternative approach was therefore pursued, which involved the removal of the BDA moiety prior to hydrogenation. Both the deprotection and hydrogenation steps proceeded in reasonable yields and the hydrogenated *trans*-diol **288** was dimerised to afford analogue

237d. Unfortunately, the high polarities and similar chromatography elution properties of *trans*-diol **288** and analogue **237d** resulted in the loss of products during the purification stage. The enantiomer of core dimer **237d** was synthesised by Y. Song and all the analogues were taken through to biological testing.[61]

Additionally, efforts were made to utilise *syn*-naphthyl adduct **336b** described in **Section 2.4.5**. Previous work by Kelly Ayton, a fourth year student, had alluded to the presence of an unidentified product arising from the dimerisation of phenyl *syn*-hydroxyenone **352** (**Figure 53**), however no formal isolation was achieved.[153]

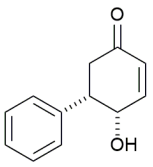

352

Figure 53: The structure of phenyl *syn*-hydroxyenone adduct **352**.

In order to investigate this further, *syn*-adduct **336b** was deprotected under acidic conditions (**Scheme 88**).

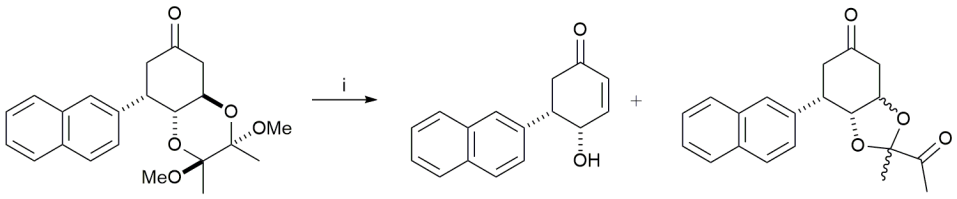

336b **353** **354**

Scheme 88: *Reagents and conditions*: (i) TFA, distilled H_2O, CH_2Cl_2, RT, 18 h, 24 % (**353**), 31 % (**354**).

The deprotection to hydroxyenone **336b** was initially assumed to have proceeded in a low yield. The analysis of the major product however suggested the formation of ketal **354**. Infra-red and ^{13}C NMR spectroscopy of the suspected side-product **354** indicated the presence of two chemically inequivalent carbonyl functional groups, and the accurate mass analysis corresponded to the chemical formula consistent with structure **354**. What is remarkable, however, is that the ^{1}H NMR spectrum indicated a single stereoisomer, which suggested that this side-product was formed diastereoselectively. The absolute configuration of the newly formed ketal carbon, however, could not be fully identified using ^{1}H NMR. The structural suggestion for side-product **354** originated from consideration of key intermediates formed during the BDA deprotection mechanism, and

based on this information, a possible mechanism of formation was suggested (**Scheme 89**).[154]

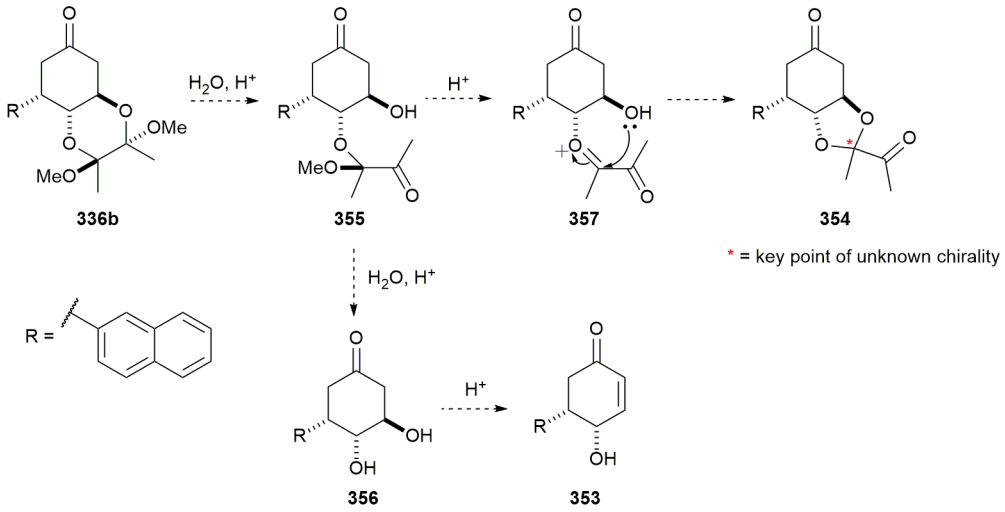

Scheme 89: The suggested key intermediates in the deprotection of *syn* adduct **366b** under acidic conditions to give **353** and **354**. The key centre of unknown chirality is indicated on ketal **354**.

No mechanistic studies were conducted as part of the investigations; however, it was suggested that the ketal of adduct **366b** is partially cleavage to afford β-hydroxy intermediate **355**. It was proposed that from here, two alternative pathways could occur to give the desired hydroxyenone **353** or side-product **354**. For the former, it is believed that the ketal is cleaved to give diol **356**, which is then subjected to acid mediated elimination to afford the desired hydroxyenone **353**. For side-product **354**, it was suggested that the methoxy group, from the BDA protecting group, is eliminated to form an oxycation (**357**). The carbonyl carbon is then attacked by the β-hydroxy to afford the five-membered ketal ring and thus **354**. Analysis of the ^{1}H NMR gave no indication of the potential stereochemistry of the unassigned stereocentre.

With *syn*-hydroxyenone **353** in hand, the dimerisation was attempted using the previously stated conditions (see **Scheme 86**). The dimerisation reaction produced a complex reaction profile, with six partially purified products isolated after column chromatography in relatively low yields. The ^{1}H NMR spectra of the two major products of unknown identities from the reaction are shown in **Figure 54** and **Figure 55**.

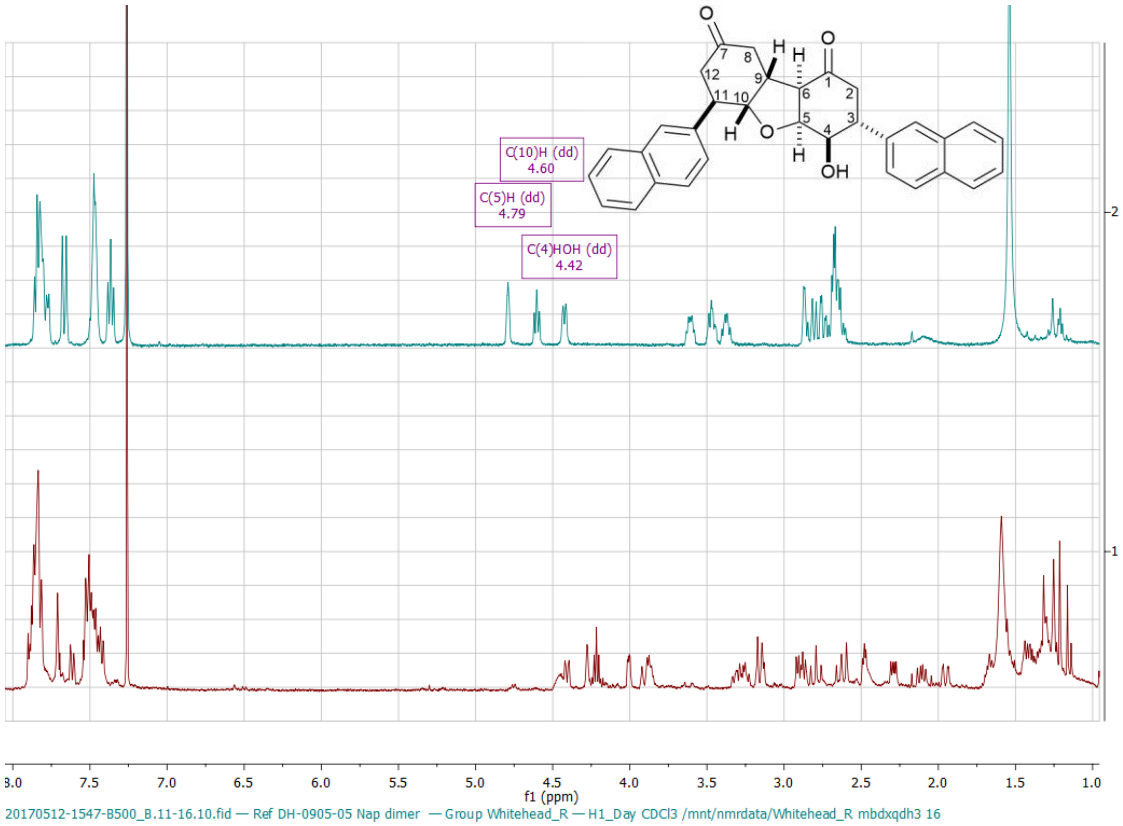

Figure 54: The ^{1}H NMR spectra comparison of one of the major isolated products from the dimerisation of *syn*-hydroxyenone **353** with naphthyl dimer **237b**. Cyan = naphthyl dimer **237b** ^{1}H NMR; red = product isolated from the dimerisation of *syn*-hydroxyenone **353**. Solvent: $CDCl_3$.

Analysis of the incarviditone analogues previous synthesised in the Whitehead group has showed that the hydrogen atoms adjacent to oxygen, C(5)H and C(10)H, consistently appear in region of 4.0-5.0 ppm in the ^{1}H NMR. For naphthyl analogue **237b** (see **Figure 54**, cyan), these peaks are present at 4.79 ppm and 4.60 ppm for C(5)H and C(10)H respectively. In the ^{1}H NMR spectrum of the partially purified product isolated from the dimerisation of *syn*-hydroxyenone **353**, there is presence of multiple peaks between 4.0-4.5 ppm. This is suggestive for hydrogen atoms adjacent to a tetrahydrofuran oxygen in a dimeric structure related to the incarviditone analogues. Furthermore, the presence of many aromatic signals indicated that the naphthyl functionality may be present. The ^{1}H NMR of the second major partially purified product and starting material **353** are shown in **Figure 55**.

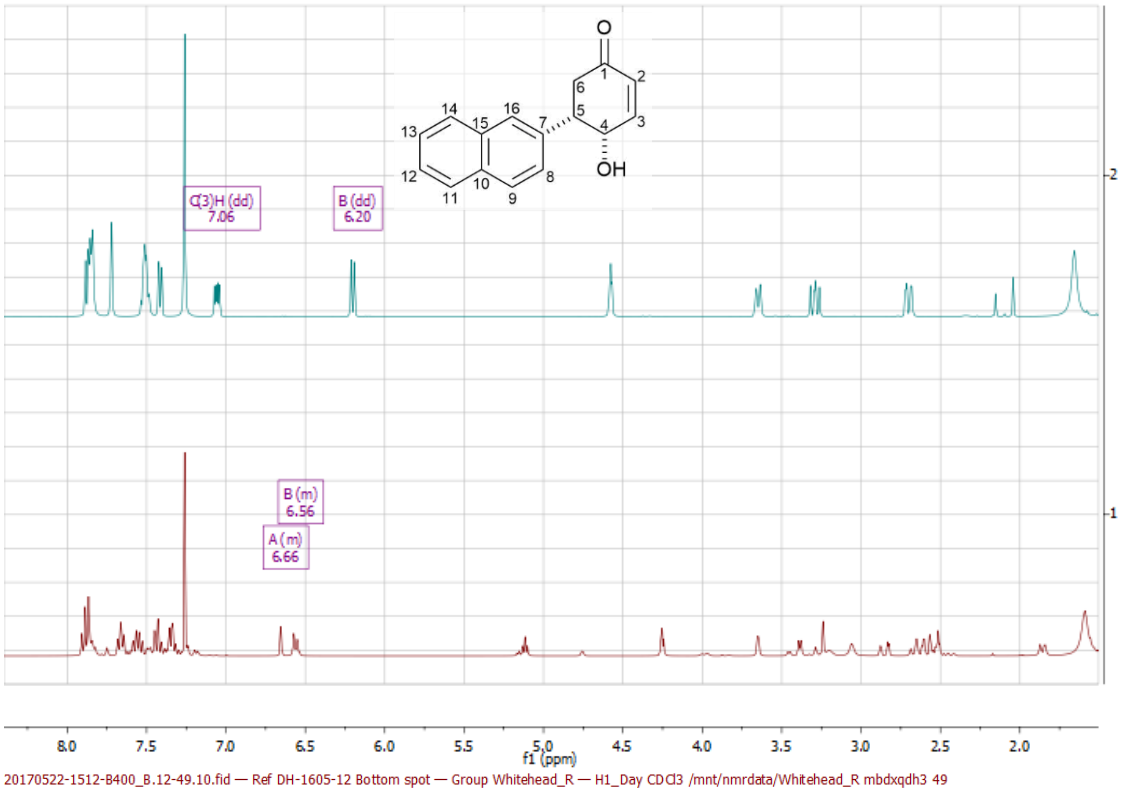

Figure 55: The ^{1}H NMR spectra comparison of one of the major isolated products from the dimerisation of *syn*-hydroxyenone **353** with the starting material **353**. Cyan = naphthyl *syn*-hydroxyenone **353** ^{1}H NMR; red = product isolated from the dimerisation of the *syn*-hydroxyenone. Solvent: $CDCl_3$.

For the second major product isolated from the reaction, there appeared to be an alkene hydrogen representative for an enone system (6.56 ppm, 6.65 ppm), which is not related to starting material **353** (6.20 ppm, 7.06 ppm, C(2)H and C(3)H respectively). Furthermore, as before, there is significant complexity within the aromatic region, which may be attributed to the naphthyl functionality.

This line of work was not pursued further due to the uncontrolled nature of the dimerisation and difficulty in purification. Nevertheless, the results of this investigation were indicative of the formation of structurally related compounds.

2.5 Modification of the (-)-Naphthyl Analogue

On account of the relatively potent biological activity of naphthyl analogue ***ent*-237b** against the lung cancer cell line A549 (see **Section 2.9.3.2**) and straightforward synthesis, studies were commenced to investigate structure-activity relationships by modifying the key functionalities highlighted in **Scheme 90**.

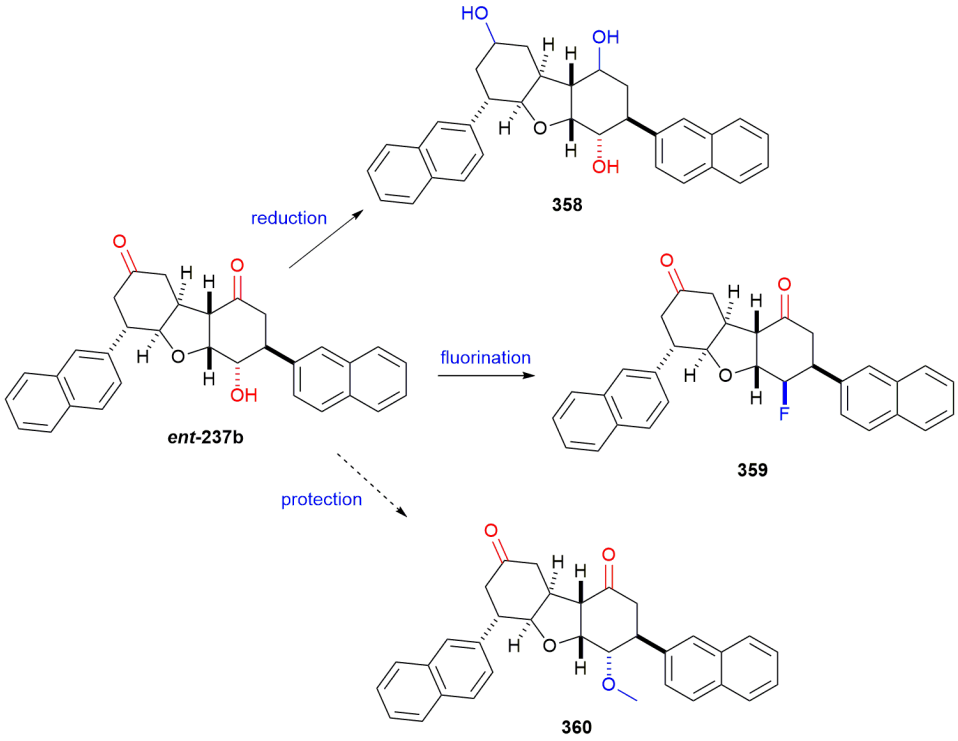

Scheme 90: The sites of diversification for (-)-naphthyl analogue ***ent*-237b**.

2.5.1 Reduction

The importance of the carbonyl functionalities in analogue ***ent*-237b** with regards to the biological activity was investigated by attempted reduction to the corresponding secondary alcohols (**Scheme 91**).

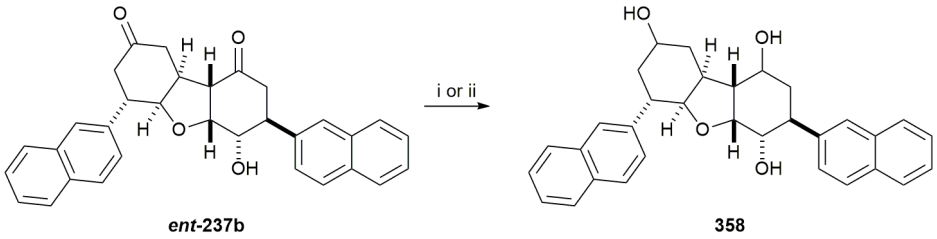

Scheme 91: *Reagents and conditions*: (i) $NaBH_4$ (10.0 eq.), MeOH, RT, 18 h; (ii) DIBAL (1 M in hexane, 2.4 eq.), anhydr. THF, -78 °C, 4 h.

Based on the crystal structure of *tert*-butylphenyl incarviditone analogue **361** (**Figure 56)** published by the Whitehead group in 2014, it was suggested that stereocontrol of the carbonyl reduction may be possible due to the compound's 3D structure.[66]

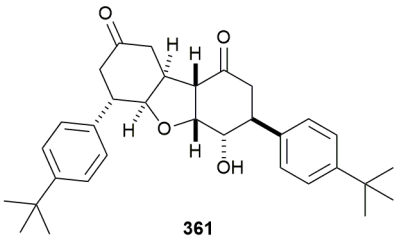

361

Figure 56: Structure of *tert*-butylphenyl incarviditone analogue **361**.

This was not the case when using $NaBH_4$ as the reductant; seven partially purified products were isolated from the reaction after column chromatography. The analysis of the ^{1}H and ^{13}C spectra revealed that in some instances, only one carbonyl group had been reduced, which indicated that the reaction had not gone to completion. The data, however, was suggestive of the formation of reduced analogue **358,** as supported by the infra-red spectrum of the partially purified product, which showed a broad O-H stretch and no carbonyl stretch.

In view of the troublesome purification and multitude of products, the reduction was trialled using the bulkier reductant DIBAL, in the hope that this may result in better stereocontrol based on the previously stated hypothesis (**Scheme 91**). The result was a notably less complicated reaction profile. Infra-red spectroscopic analysis indicated the presence of a hydroxyl group at 3382 cm^{-1} and the absence of both carbonyl functionalities, which supports the desired reduction of the carbonyls (**see Section 8.0 – Appendix**). The ^{1}H NMR spectrum of the sample following purification is shown in **Figure 57**, with the ^{1}H NMR spectrum of starting material ***ent*-237b** for comparison.

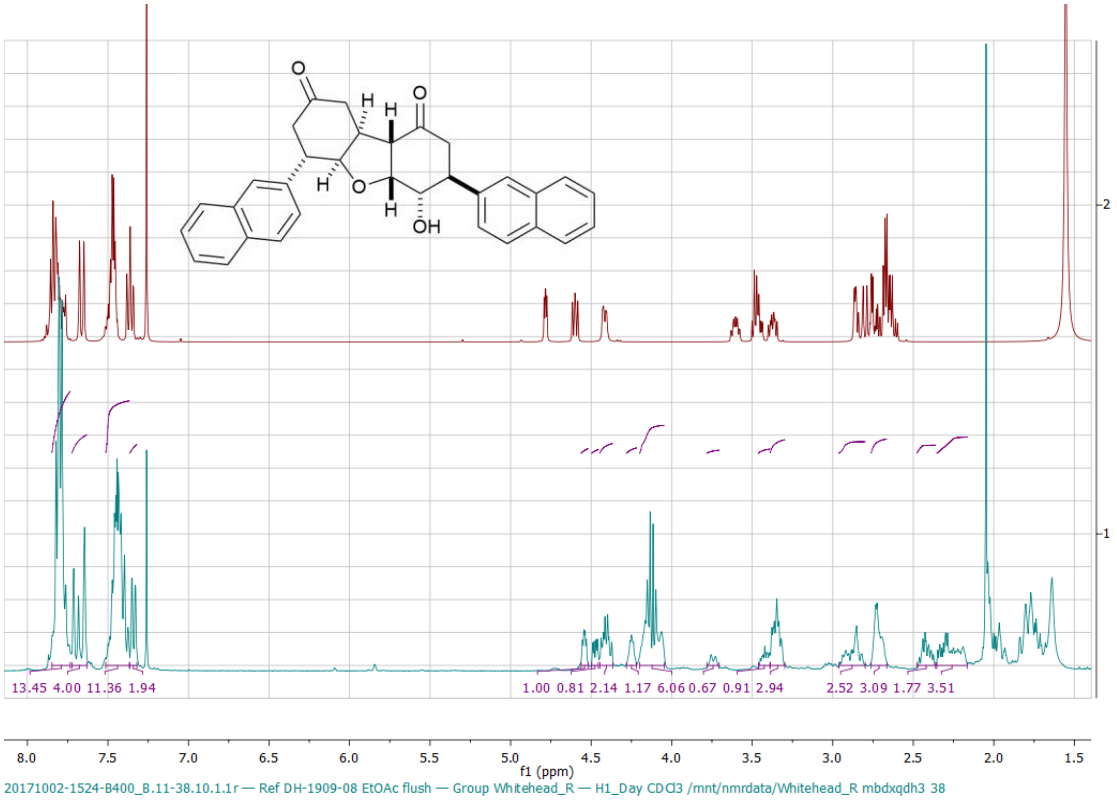

Figure 57: The ^{1}H NMR spectra of starting material ***ent*-237b** and the reduced sample following purification. Red = starting material ***ent*-237b**; cyan = isolated sample from the reduction reaction using DIBAL. Solvent: $CDCl_3$

The similarity between the ^{1}H NMR spectra of starting material ***ent*-237b** and the isolated sample, in combination with the infra-red spectrum, suggested that analogue ***ent*-237b** had successfully been reduced. It appeared however that complete stereocontrol was not achieved and the sample contained at least two structurally related products as shown by the integration values. The electrospray mass spectrometry analysis confirmed that the sample was comprised of products possessing the same molecular mass at 503, which corresponds to the $[M+Na]^+$ ion for triol **358**. Further analysis using accurate mass spectrometry supported this result. In consideration of the acquired data and the inability to separate the products via column chromatography, it was suggested that the sample was a mixture of diastereomers. In conclusion, the reduction was not pursued further, as any disparity in the biological assay of triol **358** in comparison to analogue ***ent*-237b** would not be attributable to a single compound.

2.5.2 Fluorination

With the intention to modify the hydrogen bonding properties of analogue ***ent*-237b**, DAST (**362**) was employed to fluorinate compound ***ent*-237b** at the hydroxyl position,

with the expectation that the stereochemistry would also be inverted at this position (**Scheme 92**).

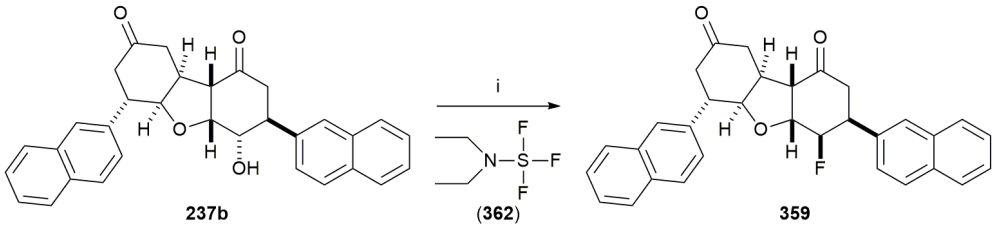

Scheme 92: *Reagents and conditions*: (i) DAST (1.2 eq.), anhydr. CH_2Cl_2, - 78 °C to RT, 4 h.

The isolation of one apparent spot by TLC following column chromatography revealed a mixture of different products, which possessed similar polarities. The ^{1}H NMR spectrum obtained after purification is shown in **Figure 58**.

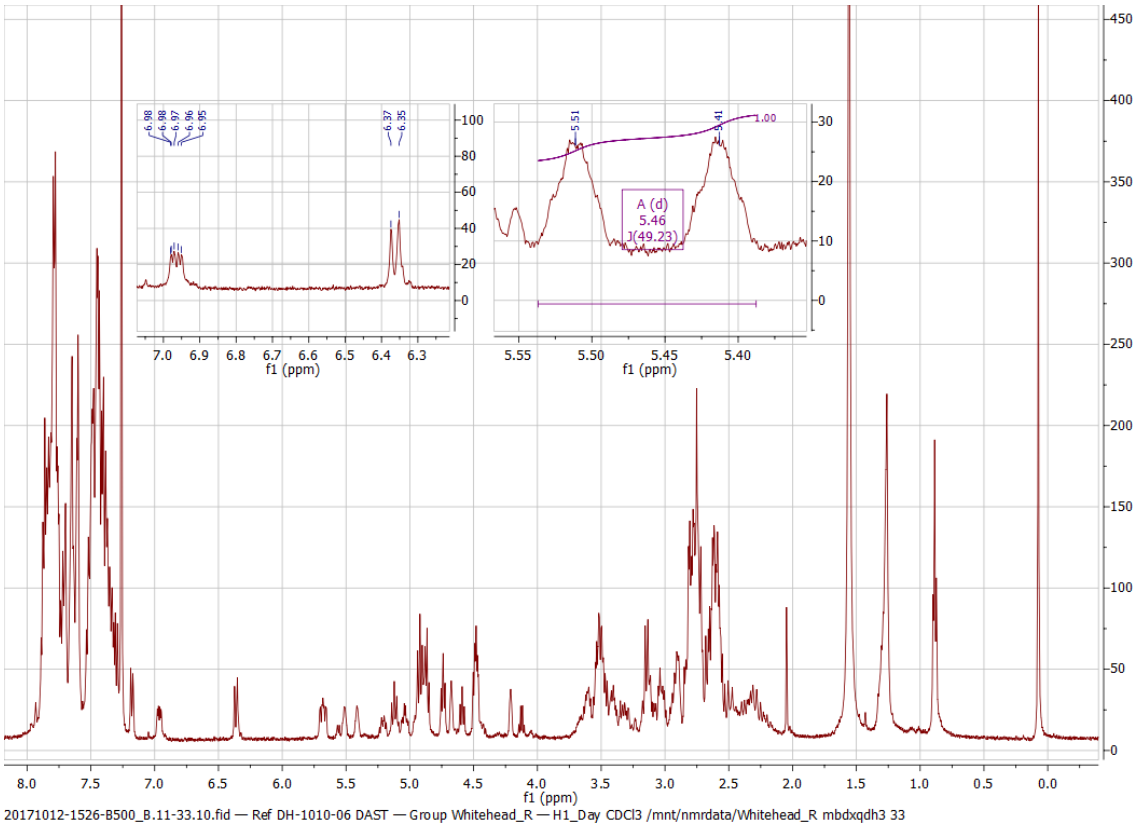

Figure 58: The ^{1}H NMR spectrum of the products from the fluorination reaction of analogue ***ent*-237b** at room temperature after column chromatography. Solvent: $CDCl_3$.

Despite the complexity of the ^{1}H NMR spectrum, there was indication of fluorination by the peak centred at 5.46 ppm, which possessed a coupling constant of 49.2 Hz, indicative of a $^2J_{F\text{-}H}$ coupling. There were, however, signs of elimination, which can be an undesirable side-reaction of DAST reactions: the resulting alkene signals can be seen at

6.36 ppm and 6.97 ppm.[155] Further analysis of the ^{13}C spectrum revealed the loss of both carbonyl functional groups, which indicated that fluorination may have occurred at these positions as well. This was supported by the ^{19}F NMR spectrum, which exhibited multiple fluorine environments present within the sample.

In an effort to control the unwanted side-reactions, the fluorination was repeated using the reaction conditions described in **Scheme 92**; however, the temperature was maintained at -78 °C for 4 hours in the hope that formation of eliminated products would be disfavoured. ^1H NMR analysis of the concentrated reaction mixture showed that starting material ***ent*-237b** went mostly unreacted; however, peaks corresponding to fluorinated and eliminated products were also present.

The identities of the products obtained from the reaction could not be fully realised due to the similar polarities and complex ^1H NMR spectra; however, later work by Francesco Zirilli, a fourth-year student, provided an insight into the possible reaction outcomes. Zirilli and co-workers reported two unexpected products when attempting to fluorinate *tert*-butyl hydroxyenone **363** using DAST (**362**) (see **Scheme 93**).[156]

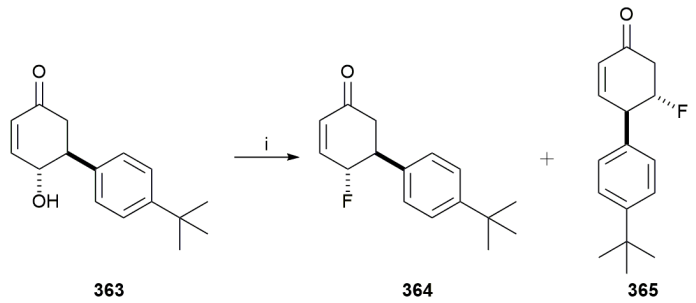

Scheme 93: *Reagents and conditions* as reported by F. Zirilli: (i) DAST, CH_2Cl_2, -78°C, 3.5 h.

Typically, DAST fluorination reactions proceed with inversion of stereochemistry because of S_N2 attack by the incoming fluoride ion. In this example, however, the fluorination proceeded with retention of stereochemistry to afford hydroxyenone **364** as the major product. In addition, a second structurally related hydroxyenone product (**365**) was isolated from the reaction; notably, the fluorine was now positioned at C-3, whereas the *tert*-butyl phenyl side-chain had moved to the adjacent C-4 position. The mechanism for the formation of hydroxyenones **364** and **365** is unknown; however, a plausible pathway was suggested (see **Scheme 94**).

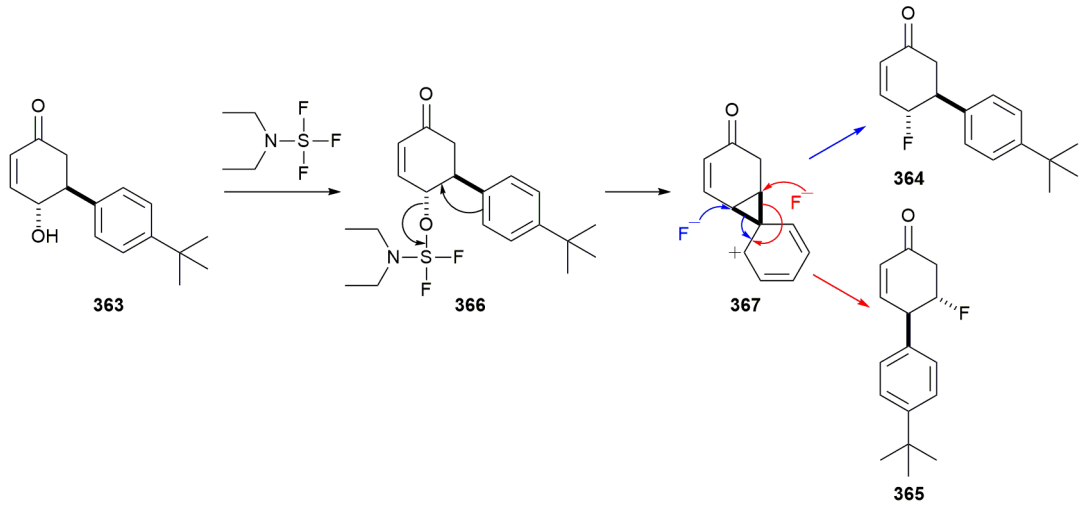

Scheme 94: The suggested mechanism for the formation of hydroxyenones **364** and **365**.

To account for the observed product formation, Zirilli and co-workers suggested that the reaction may proceed via arenium ion **367**, which can either fluorinate at C3 or C4. It is possible that such a mechanism may be occurring in the fluorination of naphthyl dimer ***ent*-237b** (see **Scheme 92**), which may account for the multiple products observed.

In light of the inability to control the reaction and difficult purification, fluorinated analogue **359** was not pursued further.

2.5.3 Protection as Methyl Ether

Based on the same reasoning as that used for the fluorinated analogue, the protection of the hydroxyl moiety of ***ent*-237b** was attempted in order to alter the hydrogen bonding properties at this position. Previous studies by the Whitehead group have shown however that the hydroxyl functionality of the incarviditone analogues can be relatively unreactive. With that in mind, the protection was attempted on the hydroxyenone precursor ***ent*-266b** with the view to attempt dimerisation with the protecting group in place (**Scheme 95**).

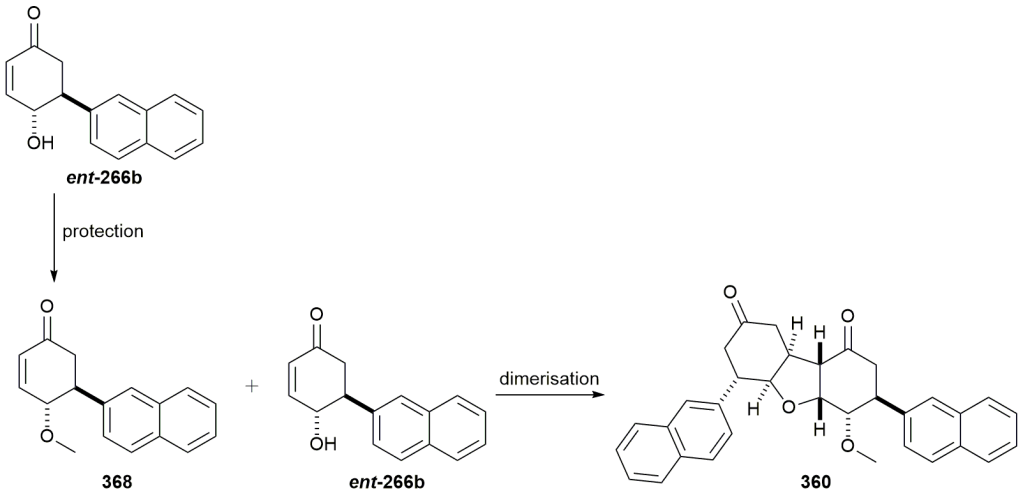

Scheme 95: The proposed synthetic route for the synthesis of the methylated analogue **360**.

The synthetic route proposed above would also allow evaluation of whether the dimerisation could be stereocontrolled. It was suggested that methylating the hydroxyl group would prevent the initial oxa-Michael addition of the protected molecule **368**, thereby forcing the free hydroxy of molecule ***ent*-266b** to act as the incoming nucleophile. If successfully demonstrated, it would have a significant implication on the synthesis of enantiomerically pure incarvilleatone analogues (**Section 2.6**) and unsymmetrical incarviditone analogues. The methoxy protecting group was selected as a consequence of a previous result using TES-protected hydroxyenone **369** (**Scheme 96**).

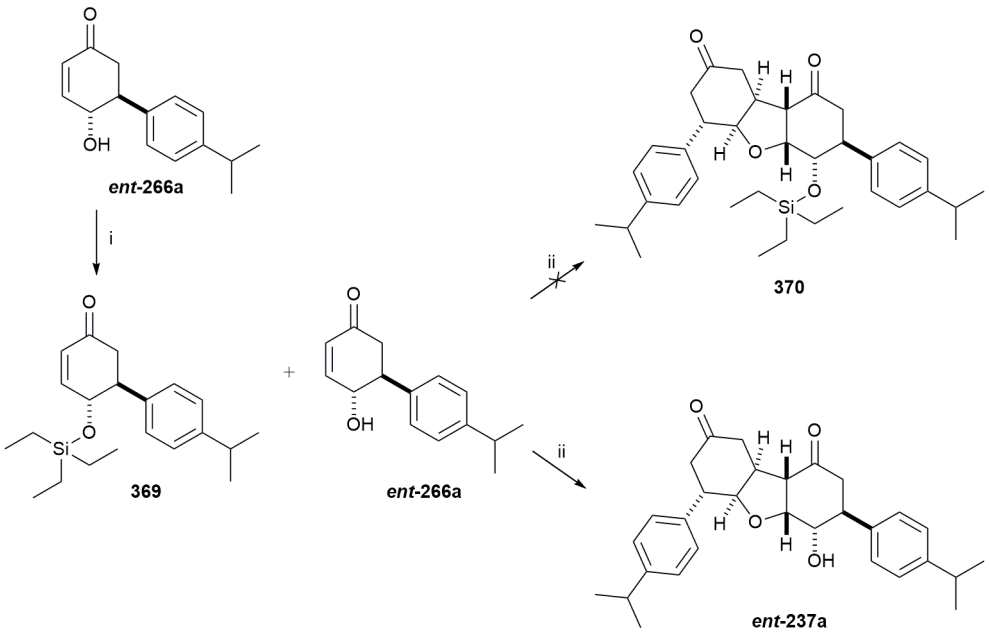

Scheme 96: *Reagents and conditions*: (i) 2,6-lutidine, TESOTf, CH_2Cl_2, -78 °C, 30 min, 89 %; (ii) 0.5 M $NaOH_{(aq)}$, THF, RT, 18 h.

The attempted dimerisation using TES protected hydroxyenone **369** yielded analogue ***ent*-237a** exclusively. This product was a result of the homodimerisation of hydroxyenone ***ent*-266a** under the basic conditions. At the time, it was proposed that the failure of this route could be due to two reasons: steric hindrance and/or disruption of hydrogen bonding. The addition of a bulky TES protecting group to an already sterically crowded position could have prevented the dimerisation. Alternatively, in consideration of the transition state proposed by Wu, Tang and co-workers (**Section 1.2.1**, **Scheme 24**), the TES group may have prevented a key hydrogen bond interaction between the two monomers. In consequence of this, the methylether functionality was selected based on its smaller size and ability to retain the oxygen atom's hydrogen bonding acceptor properties. The results for the methylation of the γ-hydroxyl of naphthyl hydroxyenone ***ent*-266b** under different reaction conditions are shown in **Table 21**.

Table 21: Methylation conditions for the attempted protection of the hydroxyl moiety of ***ent*-240b** or ***ent*-266b**. All reactions were conducted at room temperature.

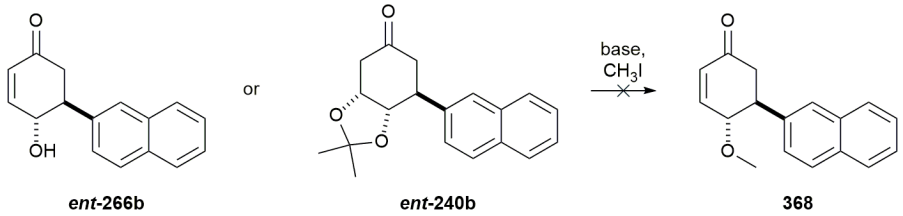

***ent*-266b** ***ent*-240b** **368**

Entry	Compound	Base (eq.)	Equivalents of methyl iodide (eq.)	Anhydrous solvent	Reaction time (h)
1	***ent*-240b**	DBU (3.0)	1.2	CH_2Cl_2	5
2	***ent*-240b**	DBU (7.0)	5.0	CH_2Cl_2	5
3	***ent*-266b**	NaH (1.1)	1.1	THF	4
4	***ent*-266b**	K_2CO_3 (1.2)	5.0	CH_3CH_2OH	4
5	***ent*-266b**	K_2CO_3 (1.2)	5.0	THF	18

Entries **1** and **2** were trialled with the hope that a one-pot procedure starting from conjugate adduct ***ent*-240b** could be achieved. The reaction however produced only hydroxyenone ***ent*-266b** and this result was consistent irrespective of the amount of methyl iodide added. To ensure that complete deprotonation occurred during the reaction, DBU was replaced with sodium hydride (entry **3**). This however proved to be too strong a base, and resulted in the aromatisation and degradation of hydroxyenone ***ent*-266b**. Further reaction conditions were scoped with K_2CO_3 (entries **4** and **5**), however no formation of the desired product **368** was observed. Despite this, the conditions in entry **4** proved to ideal for the dimerisation of hydroxyenone ***ent*-266b** to analogue ***ent*-237b**, affording a clean reaction

profile as determined by the ^{1}H NMR spectrum of the concentrated reaction mixture. In conclusion, no reaction conditions could be developed that resulted in the successful methylation of the hydroxyl in compound **368**.

2.6 Preparation of the (±)-Isopropenyl Incarvilleatone Analogue

As discussed in **Sections 1.2** and **1.3**, the homodimerisation (+/+, -/-) and heterodimerisation (+/-, -/+) of two rengyolone monomers yields two differing dimeric products, incarviditone (**124**) and incarvilleatone (**137**) respectively. With that in mind, it was envisaged that the heterodimerisation of the hydroxyenone intermediates would afford the first reported incarvilleatone analogues. Efforts to develop a methodology that would allow for stereocontrol however have yet to be developed (see **Section 2.5.3**), and as such the analogue was synthesised as a racemic mixture.

2.6.1 Heterodimerisation

To achieve the dimerisation, isopropenyl hydroxyenones ***ent*-266c** and **266c** were selected based on the ease of obtaining multigram quantities of each enantiomer. The heterodimerisation was accomplished using the reaction conditions applied to the incarviditone analogues, however improvements were made by substituting sodium hydroxide with the weaker base DBU (**Scheme 97**).

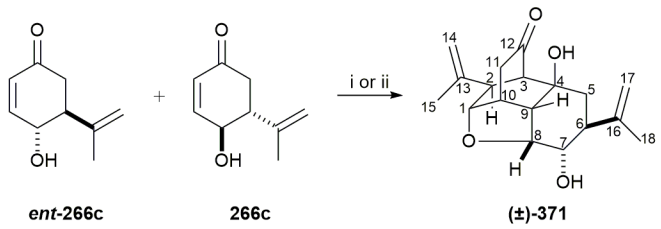

Scheme 97: *Reagents and conditions*: (i) 0.5 M $NaOH_{(aq)}$, THF, RT, 24 h, 10 %; (ii) DBU, CH_2Cl_2, RT, 4 days, 26 %.

The decision to employ a weaker base was the result of the presence of an unknown impurity of a similar polarity to product **371** when using sodium hydroxide, which made the purification challenging. This was observed in the synthesis of hydroxyenone ***ent*-266c** as well as incarviditone analogues **237c** and ***ent*-237c.** This impurity appeared to be unique to the isopropenyl substituted compounds and was not observed in other systems, suggesting that this side-chain has a propensity to undergo an undesired side-reaction. In light of this, sodium hydroxide was replaced with DBU, which led to a cleaner conversion and no formation of the unknown impurity. Analysis of the ^{1}H NMR spectrum of the

concentrated reaction mixture and isolated yields from the reaction indicated that the ratio of incarviditone:incarvilleatone formation was 3:1, hence the low yield of 26 % for heterodimer **371** after purification. To further understand the heterodimerisation, timed ^{1}H NMR experiments were conducted and are discussed in **Section 2.6.3**.

2.6.2 Structure Determination

Following the isolation of **371**, investigations began to confirm the structure of the isolated product. This was to unequivocally determine whether the heterodimerisation to give incarvilleatone analogue **371** was successful rather than affording a structural isomer, such as the examples reported by Spivey and co-workers (**Section 1.2.2**, **Scheme 32**).[68]

Initially, the ^{1}H NMR spectra of both the isolated product **371** and the incarvilleatone natural product **137** were compared.[69] The structural differences between the two products meant however that this method was unreliable and further analysis methods were required. Mass spectrometry analysis suggested that a dimeric species had formed as indicated by the doubling of mass units. Infra-red spectroscopy also confirmed the presence of the carbonyl and hydroxyl functionalities. The latter was further supported by a ^{1}H NMR D_2O shake experiment, which established the presence of two hydroxyl groups. Notably, the D_2O experiment also revealed that the hydroxyl located at C-4 underwent deuterium exchange at a faster rate than the C-7 hydroxyl (**Scheme 97**). To rule out the formation of an incarviditone related structure, a DEPT-135 experiment was conducted with the view that the number of methylene environments between the two structures differs (**371**: 4 and **237c**: 5). The experiment confirmed the presence of four CH_2 environments, therefore supporting the formation of the structure shown in **Scheme 97**.

Finally, in combination with a MM2 (force field calculation, Chem3D™ v17.0) minimised energy structure of analogue **371** (**Figure 59**), a ^{1}H-^{1}H NOESY experiment was conducted in order to identify the key through space interactions in the proposed caged structure (**Table 22**).

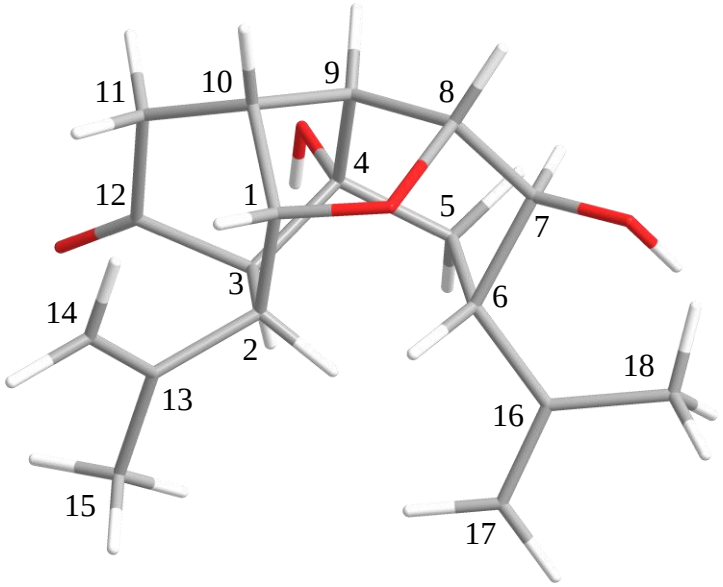

Figure 59: The MM2 energy minimised structure of analogue **371**.

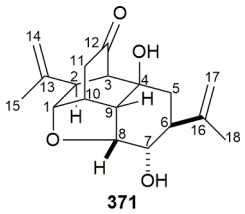

371

Table 22: The ^{1}H NMR assignments, chemical shifts, multiplicities and NOESY correlations for **371**.

Assignment	Chemical shift (ppm)	Multiplicity (*J*, Hz)	NOESY Correlation
C(1)H	4.60	d (4.3)	C(2)H, C(10)H
C(2)H	2.69	d (4.2)	C(1)H, C(3)H, C(15)H_3
C(3)H	2.550	d (4.2)	C(2)H, C(4)HOH, C(15)H_3
C(5)H_2	1.87-2.04	m	C(6)H, C(7)HOH, C(17)H_2
C(6)H	2.58-2.63	m	C(2)H, C(5)H_2, C(17)H_2
C(7)HOH	3.70	dd (10.6, 2.9)	C(5)H_2, C(6)H, C(8)H, C(9)H, C(17)H_2, C(18)H_3
C(8)H	4.40	dd (4.3, 2.9)	C(7)H, C(9)H, C(10)H
C(9)H	2.36	t (4.3)	C(8)H, C(10)H, C(11)H_2
C(10)H	2.83	tt (4.3, 3.4)	C(1)H, C(8)H, C(9)H, C(11)H_2
C(11)H_2	2.21, 2.545	dd (19.7, 3.4), dd (19.7, 3.4)	C(10)H, C(14)H_2
C(14)H_2	4.65, 4.87	s, s	C(11)H_2, C(15)H_3
C(17)H_2	4.93, 4.97	s, t (1.7)	C(6)H, C(18)H_3

Overall, the NOESY assignments correlated well with the proposed structure. One of the key interactions for the structural proposal, as illustrated by **Figure 59**, was between the C(2)H and C(6)H hydrogens, which was observed in the NOESY experiment. Furthermore, the minimised structure predicted an approximate 90° angle between C(1)H and C(2)H, which is reflected in the multiplicity, with no apparent coupling between these two hydrogen atoms. In summary, based on the disclosed evidence the proposed structure of isopropenyl analogue **371** is considered to be correct and this result has been independently replicated.[157]

2.6.3 ^{1}H NMR Reaction Monitoring

In an effort to understand the mechanism for the heterodimerisation of hydroxyenones **266c** and ***ent*-266c**, the dimerisation was monitored by ^{1}H NMR using sodium deuteroxide/D_2O in deuterated THF (**Scheme 98**).

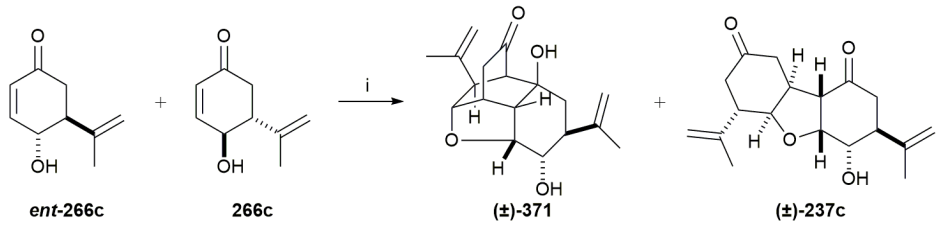

Scheme 98: *Reagents and conditions*: (i) 0.5 M NaOD in D_2O, THF-d_8, 24 h, RT.

The purpose of this experiment was to observe the rate of formation of the two products (±)-**371** and (±)-**237c** and to determine if the reaction is reversible. ^{1}H NMR spectra were recorded at hourly intervals and a summary of the results is shown in **Figure 61**. It is important to note that the following spectra appear simplified due to analogues (±)-**371** and (±)-**237c** containing several enolisable centres. This resulted in proton-deuterium exchange, with the deuterated structures shown in **Figure 60** for reference. The reference spectra for compounds: **266c**, **371** and **237c** in THF-d_8 can be found in **Section 8.0 – Appendix**.

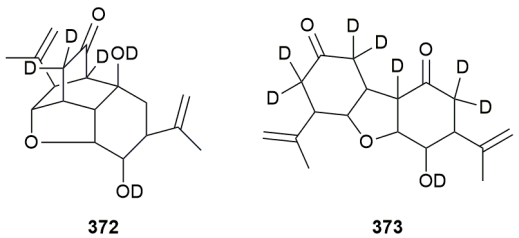

Figure 60: The structures of the deuterated 2-propenyl incarviditone **372** and incarvilleatone **373** analogues.

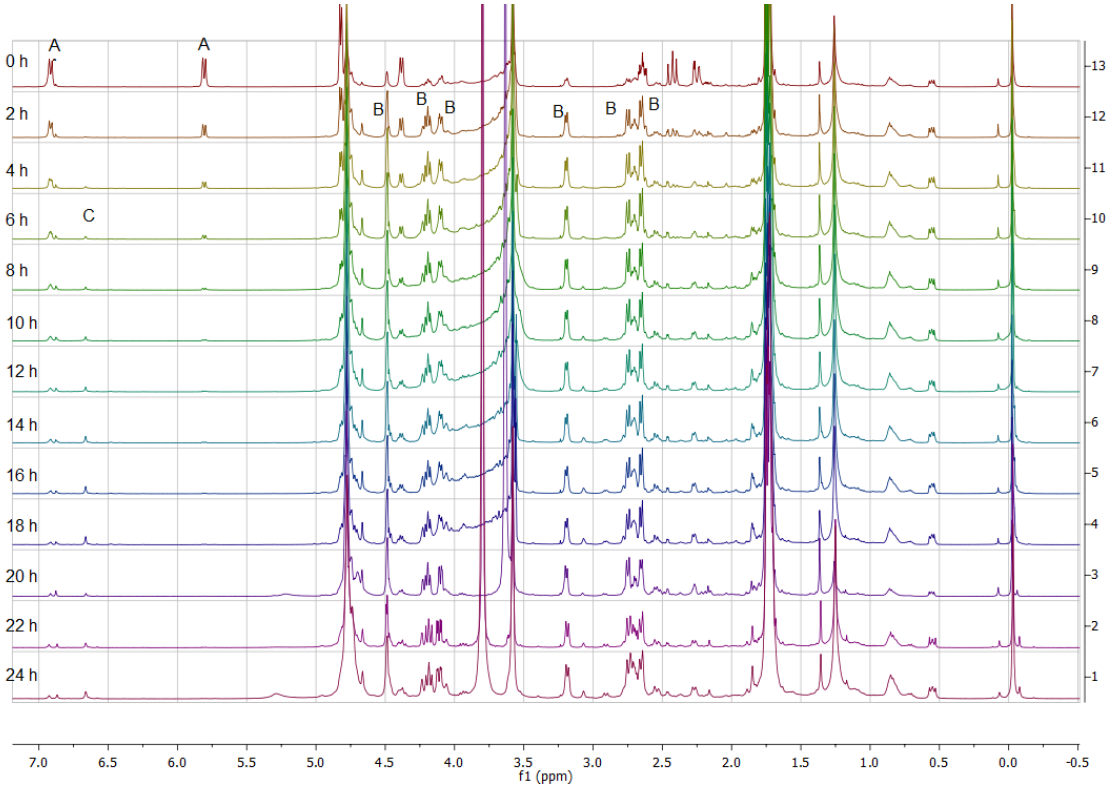

Figure 61: The ^{1}H NMR spectra at 2 hour intervals (for clarity). Solvent: THF-d_8. A = hydroxyenones **266c**/***ent*-266c**; B = incarviditone analogue **373** and C = unknown impurity.

It is evident from this experiment that homodimerisation (B: **373**) occurred at a faster rate than heterodimerisation. The evidence for the formation of product **373** as a result of the homodimerisation was observed at 0 hour, indicating that the homocoupling reaction took place before the completion of the ^{1}H NMR acquisition. As a consequence of the predominant formation of incarviditone analogue **373**, the spectral resolution for incarvilleatone analogue **372** was poor, which obscured the peak integrals and prevented a quantitative analysis. In addition to this, an unknown impurity (C) was shown to form from 4 hours onwards. The identity of this peak could not be linked to any potential product from the reaction, and therefore it was presumed to represent the close running impurity consistently observed when analogues containing the isopropenyl side-chain functionality were exposed to NaOH.

As a result of deuterium exchange (**Figure 60**) and limited NMR resolution, it was difficult to determine which peaks corresponded to incarvilleatone analogue **373**. As a consequence, the ratio of rates of formation of the homo- and heterodimers could not be established. In an effort to pursue this investigation, the NMR sample was enriched with analogue **371**; it was hoped that this would amplify the signals belonging to analogue **372**

and allow for a comparison to be made between analogues **372** and **373**. The results are shown in **Figure 62**.

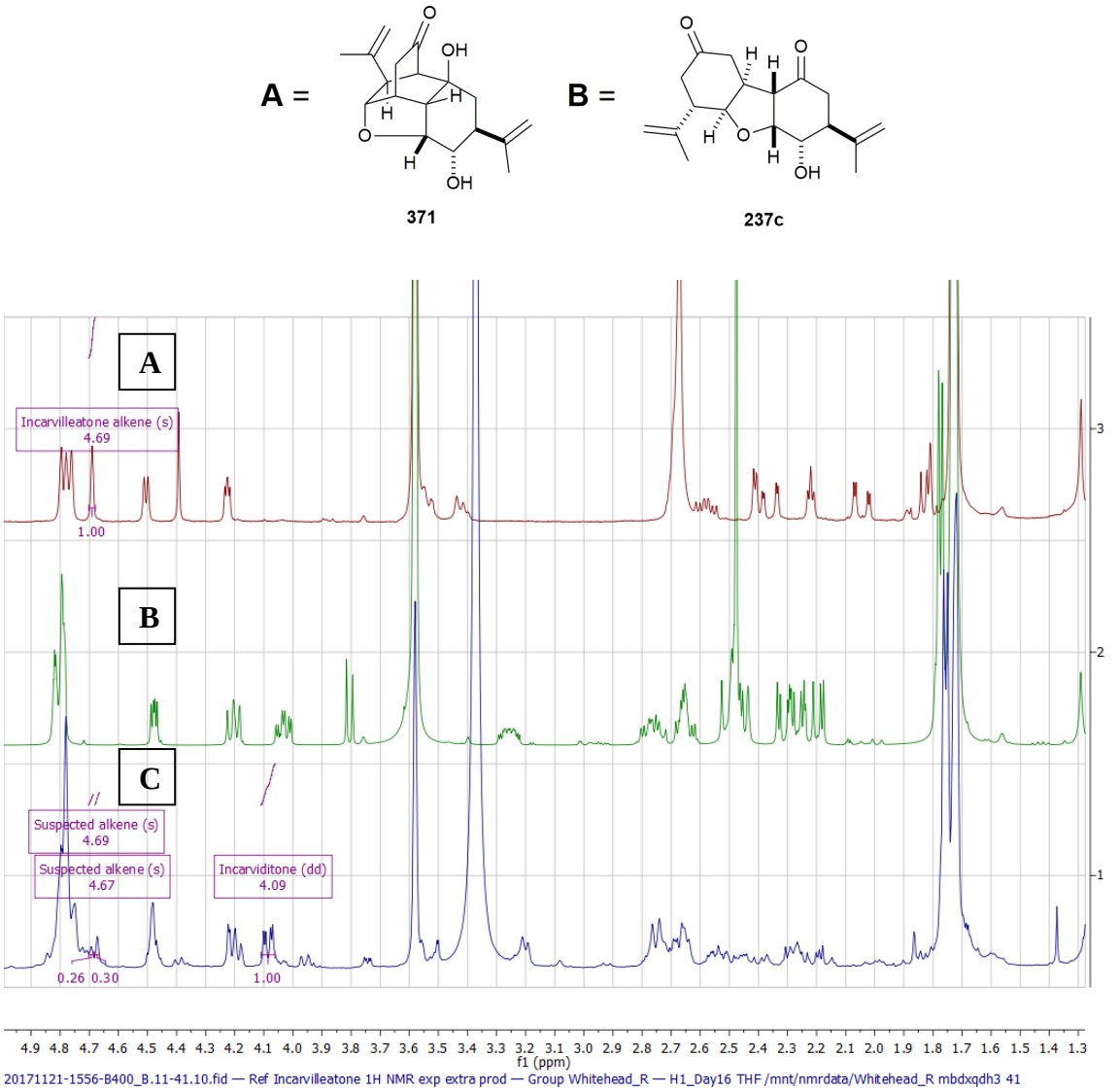

Figure 62: The superimposed ^{1}H NMR spectra of the NMR reaction and the two dimeric products **371** and **237c**. **A** = isopropenyl incarvilleatone analogue **371**; **B** = isopropenyl incarviditone analogue **237c**; **C** = ^{1}H NMR experiment enriched with analogue **371**. Solvent: THF-d_8.

Only a small improvement in the overall resolution was gained during the enrichment, as it became apparent that the reaction medium had reached its saturation point. Nevertheless, it appeared that one of the alkene peaks from incarvilleatone analogue **372** appeared at 4.67 or 4.69 ppm. The certainty of this peak could not be established due to the basic reaction conditions displacing the chemical shifts in relation to the THF-d_8 reference spectra. As a result, both peaks were included in the integration comparison with the C(4)H incarviditone analogue **372** peak at 4.09 ppm. This comparison was suggestive for a ratio

of 1:3 for heterodimerisation:homodimerisation, which is aligned with the result obtained from the ^{1}H NMR analysis of the concentrated reaction mixture discussed in **Section 2.6.1**.

In conclusion, monitoring the dimerisation of the two hydroxyenone enantiomers **266c** and ***ent*-266c** by ^{1}H NMR indicated that in this system, the homodimerisation occurred at a faster rate. No evidence was observed for the dimerisation processes being reversible; however, this cannot be concluded with certainty due to resolution limitations.

2.7 Preparation of the 4-Isopropylphenyl COTC Analogue

Further investigations into the synthetic applications for iodo keto *cis*-diol **117** included the synthesis of antheminone A and COTC hybrid analogues. Extensive research has already been conducted by the Whitehead group, and a library of these analogues has been biologically evaluated for their anti-proliferative activities.[60, 61, 112, 152, 158]

Based on the pre-existing biological data, which is discussed in **Section 2.9.3.1**, the trend indicates a higher potency for compounds with non-polar side-chain functionalities. In an effort to investigate this hypothesis and to demonstrate a potential synthetic route which could be applicable to diol **117**, the 4-isopropylphenyl antheminone A (**374**) and COTC/antheminone A hybrid (**375**) analogues were prepared using (-)-quinic acid (**194**) (**Figure 63**).

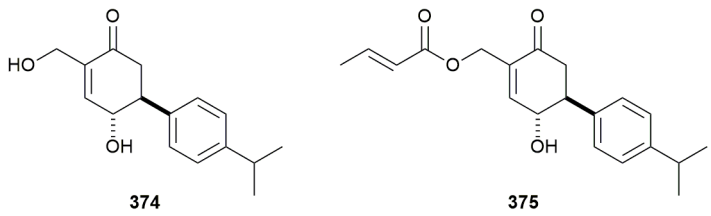

Figure 63: The structures of the 4-isopropylphenyl antheminone A analogue **374** and antheminone A/COTC hybrid analogue **375**.

2.7.1 TES Protection

The synthetic approach to analogues **374** and **375** can be considered an extension of the synthesises previously described in **Section 2.4**. For this reason, the route commences with the TES protection of 4-isopropylphenyl hydroxyenone ***ent*-266a** (**Scheme 99**).

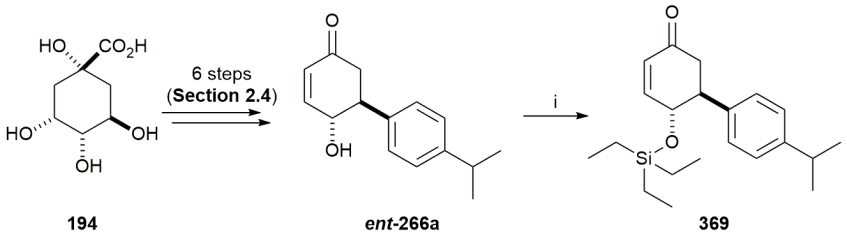

Scheme 99: *Reagents and conditions*: (i) 2,6-lutidine, TESOTf, CH_2Cl_2, -78 °C, 30 min, 89 %.

The protection to afford product **369** proceeded in excellent yield of 89 %, provided there was adequate pre-mixing of 2,6-lutidine and TESOTf at -78 °C prior to the addition of hydroxyenone ***ent*-266a**. Failure to pre-mix the two reagents resulted in the formation of diene **376** via the suggested mechanism shown in **Scheme 100**.

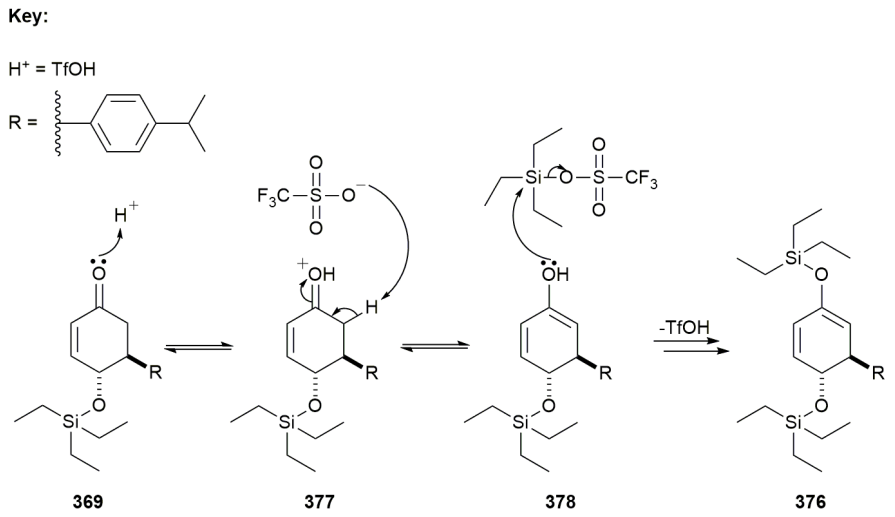

Scheme 100: The suggested mechanism for the formation of the diene **376**.

The formation of diene **376** is believed to be due to the presence of trace amounts of triflic acid in the TESOTf reagent. TES enone **369** undergoes enolisation catalysed by triflic acid (**377**), and the resulting hydroxyl **378** is subsequently protected by a second TES group, forming diene **376**. The prior neutralisation of triflic acid by 2,6-lutidine prevented the formation of the undesired side-product **376**.

2.7.2 Morita-Baylis Hillman Reaction

Following the TES protection, the hydroxymethyl side-chain was introduced at the C-2 position using a DMAP catalysed Morita-Baylis Hillman reaction (MBH), which proceeded in good yield (**Scheme 101**).

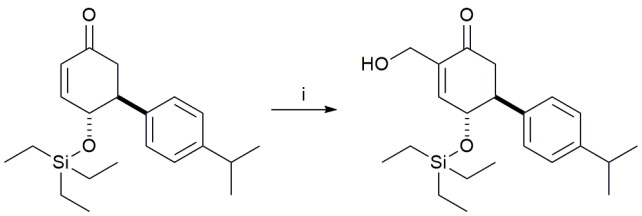

369 **379**

Scheme 101: *Reagents and conditions*: (i) DMAP, formaldehyde (37 % in H_2O), SDS, H_2O, RT, 18 h, 75 %.

The origins of the MBH reaction were first established by Morita and co-workers in 1968. A tricyclohexylphosphine catalyst was utilised to react various aldehydes with electron-deficient alkenes.[159] Following this pioneering work, Baylis and Hillman demonstrated an amine catalysed variant in 1972.[160] The various proposed mechanisms for this reaction are shown in **Scheme 102**.

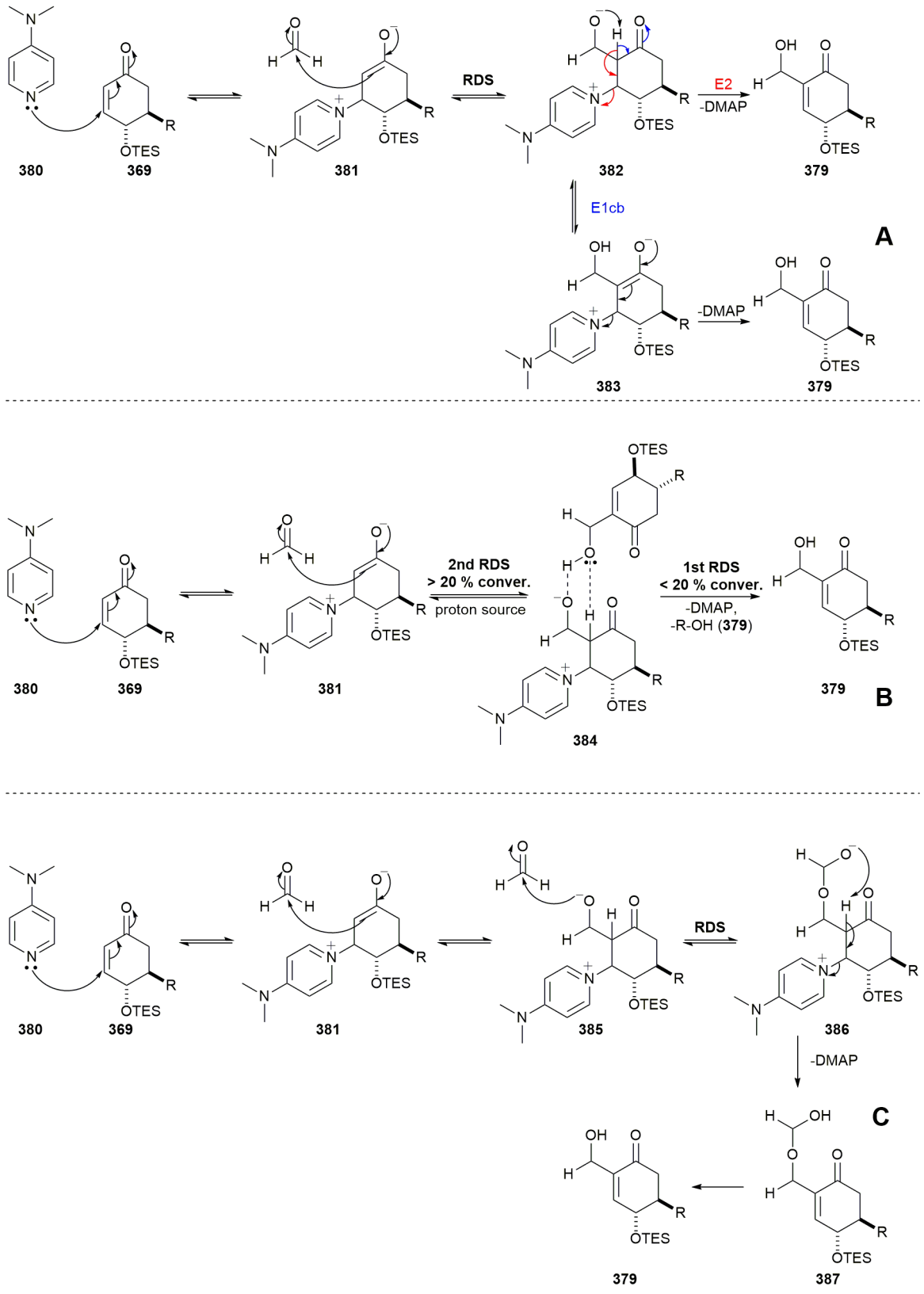

Scheme 102: The proposed mechanisms and rate-determining steps (RDS) for the MBH reaction. **A** = Hoffman and Rabe; **B** = Lloyd-Jones and co-workers; **C** = McQuade and co-workers.[161, 162, 163]

The earliest proposed mechanism was by Hoffman and Rabe in 1983 (**A**); their original hypothesis was also supported by kinetic data reported by Hill and Isaacs.[164] Hoffman and

Rabe hypothesised that the catalytic process initiates with the conjugate addition of a tertiary amine (e.g. DMAP (**380**)) to an electron deficient alkene (**369**) to afford a zwitterionic adduct (**381**). The zwitterion (**381**) then undergoes an aldol style addition with an aldehyde reagent to afford an alkoxide (**382**). From here, the mechanism concludes via an E2 or E1cB elimination, which liberates the product (**379**) and tertiary amine (**380**). The latter can then participate in another reaction cycle. Kinetic studies by Hill and Isaacs suggested that the aldol reaction between the aldehyde reagent and zwitterion (**381** to **382**) was the rate determining step in this mechanism. Later studies by Lloyd-Jones and co-workers in 2005 (**B**) however, suggested a more intricate kinetic profile for the MBH reaction, which involved two rate-determining steps. Their proposal suggested that the concluding proton-transfer to form the product (**379**) from the alkoxide generated by the aldol reaction, is facilitated by another molecule of the MBH product (**384**). As a result, the rate-determining step is the proton-transfer when the product concentration is < 20 %. As the product concentration increases (> 20 %), the rate-determining step reverts to the aldol reaction (**381**) as suggested by Hill and Isaacs. Lloyd-Jones and co-workers' hypothesis also explains the autocatalytic effect observed for the MBH reaction in the absence of proton-donors. In 2005, McQuade and co-workers (**C**) also suggested a revised mechanism for the MBH reaction; they proposed that the alkoxide resulting from the aldol reaction, reacts with a second molecule of aldehyde (**385**). The resulting intermediate (**386**) can then facilitate the elimination of the catalytic tertiary amine (DMAP, **380**) and subsequent proton transfer. The rate-determining step for this hypothesis was determined to be the proton-transfer by kinetic studies, which shares similarity with Lloyd-Jones and co-workers' mechanism (**B**). In 2009, mass spectrometry studies conducted by Eberlin, Coelho and co-workers found evidence for intermediates from both pathways (**B** and **C**) and concluded that the MBH proceeded in a dualistic fashion.[165]

Previous examples of the MBH reaction in the literature using structurally related compounds to **379** have typically suffered from long reaction times. The first reported MBH reaction catalysed by the pyridine derivative DMAP was in 1998 by Rezgui and El Gaïed, who used simple substituted cyclohexenones in combination with formaldehyde (**Scheme 103**).[166] This reaction proceeded slowly and took 6 days to reach completion. Further examples of the DMAP catalysed MBH reaction were later reported by Kim and co-workers in 2002.[167]

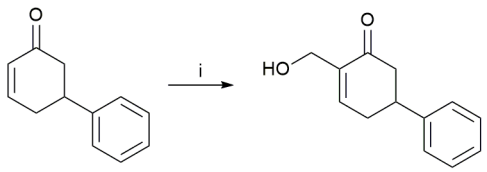

388 389

Scheme 103: *Reagents and conditions* as reported by Rezgui and El Gaïed: (i) formaldehyde (4.0 eq.), DMAP (20 mol %), RT, 6 days, 71 %.

Notably, Rezgui and El Gaïed also reported that this reaction did not proceed with DABCO, which has been supported by extensive past research by the Whitehead group using their own cyclohexenone systems.[60, 61, 158] Previous work by the Whitehead group has also investigated the imidazole catalysed MBH reaction first reported by El Gaïed and Gatri (**Scheme 104**).[168] Despite proceeding in an excellent yield, the reaction time was excessively prolonged (i.e. 17 days) for the conversion of cyclohexenone (**244**) to MBH product **390**.

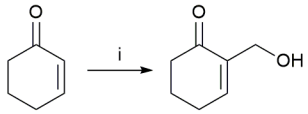

244 390

Scheme 104: *Reagents and conditions* as investigated by the Whitehead group: (i) imidazole (20 mol %), THF, H_2O, RT, 17 days, 93 %.[60]

In 2005, Williams and co-workers reported a methodology that significantly increased the rate of reaction whilst maintaining good yields using cyclohexenone substrates as examples.[169] By introducing a surfactant into the reaction medium and using water as the solvent, reaction times were in the order of hours rather than days at room temperature. This approach also had the additional benefit of avoiding organic co-solvents, thus providing a green chemistry alternative. These conditions were adopted by the Whitehead group with significant success, providing the enone was sufficiently lipophilic. The reasoning for the rate acceleration proposed by Williams and co-workers is shown in **Scheme 105**.

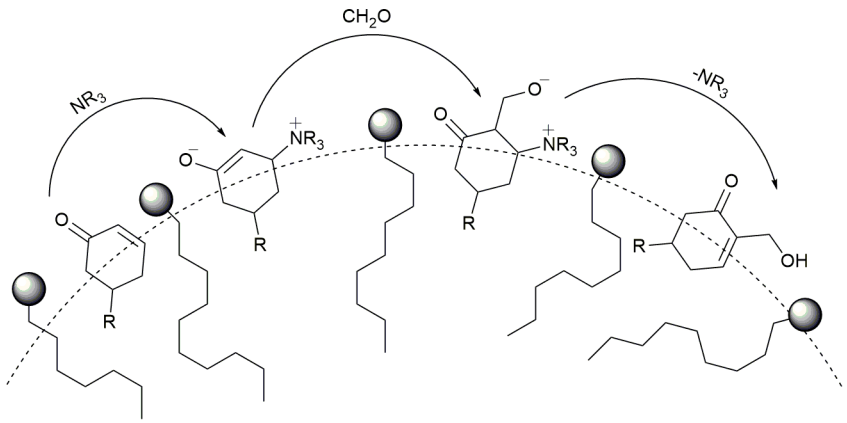

Scheme 105: The proposed mechanism for the surfactant mediated MBH reaction as reported by Williams and co-workers.

It was hypothesised that the non-polar side-chain, in this instance 4-isopropylphenyl, would reside in the hydrophobic regions of micelles formed from the surfactant, whereas the more polar functionalities would be in the hydrophilic regions. Furthermore, due to the zwitterionic nature of the intermediates (e.g. **381**) present in the MBH reaction mechanism, additional stabilisation could be achieved by the interaction of these entities with the polar head groups of the surfactant.

2.7.3 Deprotection and Crotonylation

In order to synthesise the 4-isopropylphenyl substituted analogue **374** of antheminone A, MBH adduct **379** was deprotected under acidic conditions (**Scheme 106**).

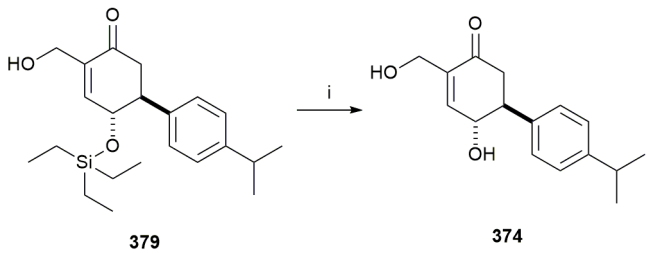

Scheme 106: *Reagents and conditions*: (i) TFA:H_2O (7:1), RT, 30 min, 39 %.

Following the successful preparation of antheminone A analogue **374**, efforts were made to synthesise COTC/antheminone A hybrid analogue **375**. This was accomplished by the crotonylation of the hydroxyl side chain of **379,** followed by an acid mediated deprotection (**Scheme 107**).

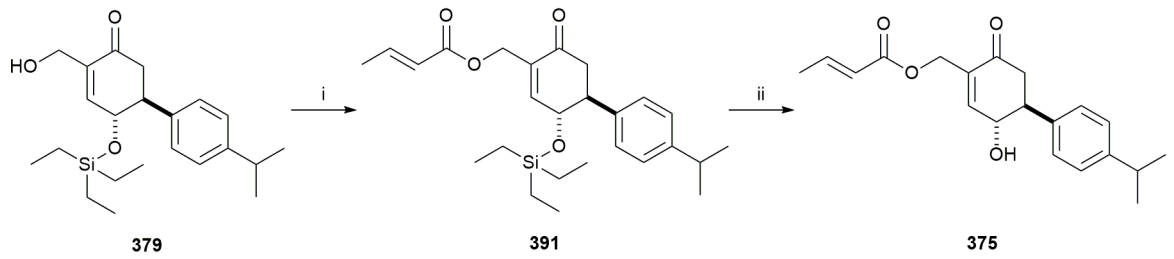

379 391 375

Scheme 107: *Reagents and conditions*: (i) crotonic anhydride, DMAP, pyridine, CH_2Cl_2, RT, 5 h; (ii) TFA:H_2O (7:1), RT, 30 min, 51 % (over two steps).

Crotonate ester **391** was purified by column chromatography; however, an unidentified close running impurity co-eluted. As a consequence, **391** was carried through without additional purification to the acid deprotection, after which product **375** could be isolated as pure.

With the syntheses of analogues **374** and **375** complete, biological testing commenced on both compounds, which is discussed in **Section 2.9.3.1**.

2.8 Pseudohygrophorone Synthesis Development

The discovery of pseudohygrophorones (**Figure 64**) by Arnold and co-workers in 2016 (see **Section 1.4**) has meant that no synthetic approaches to these newly identified natural products have been reported.[71] As a result, the aim of this section of the project was to develop synthetic methodologies that could be applied to iodo keto *cis*-diol **117** for the preparation of the pseudohygrophorone natural products. The pseudohygrophorones are of particular interest as they share key structural similarities with *cis*-diol **117**, namely the stereochemistry of the hydroxy groups and cyclohexenone core.

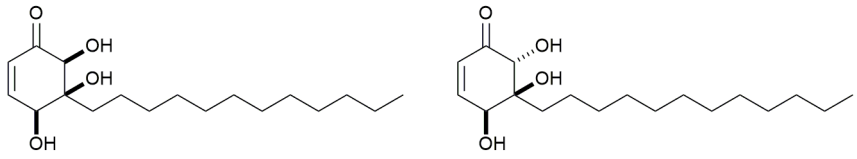

pseudohygrophorone A 168 pseudohygrophorone B 169

Figure 64: Structures of pseudohygrophorones A (**168**) and B (**169**) discovered by Arnold and co-workers.

2.8.1 3-Iodocyclohexenone

With a view to developing these synthetic methodologies, a model compound related to iodo keto *cis*-diol **117** was prepared using the reaction conditions described by Piers and co-workers in 1981 (**Scheme 108**).[170]

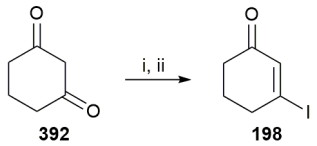

Scheme 108: *Reagents and conditions*: (i) PPh_3, I_2, MeCN, RT, 4 hours then; (ii) 1,3-cyclohexanedione, Et_3N, RT, 4 days, 81 %.

Prior to Piers' and co-workers' research, reports of synthetic approaches to β-iodo α,β-unsaturated ketones were rare within the literature. Rather, much of the focus was on developing methodologies towards the β-chloro and to a lesser extent, the β-bromo enone systems.[171, 172] The suggested mechanism for this reaction is shown in **Scheme 109**.[170, 173]

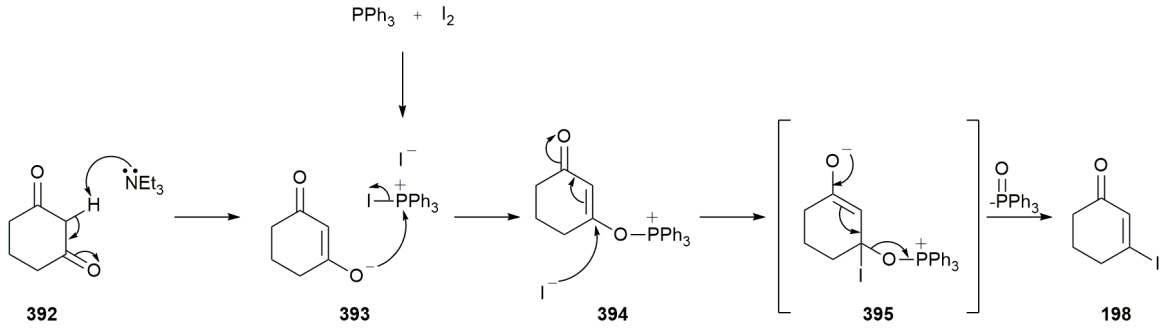

Scheme 109: The suggested mechanism for the formation of β-iodo cyclohexenone **198**.

The driving force for this reaction is considered to be the formation of the triphenylphosphine oxide by-product, which was formed upon elimination from intermediate **395**.

2.8.2 Cross-coupling

Initial investigations began with the cross-coupling of phenyl and naphthyl aromatic side chains using two approaches: copper catalysed Grignard and rhodium catalysed boronic acid coupling reactions. It was thought that the aromatic coupling partners would provide a simple system for development of the reaction conditions. The optimised reaction conditions could then be applied to the installation of long-chain aliphatic substituents. The proposed synthetic route is illustrated in **Scheme 110**.

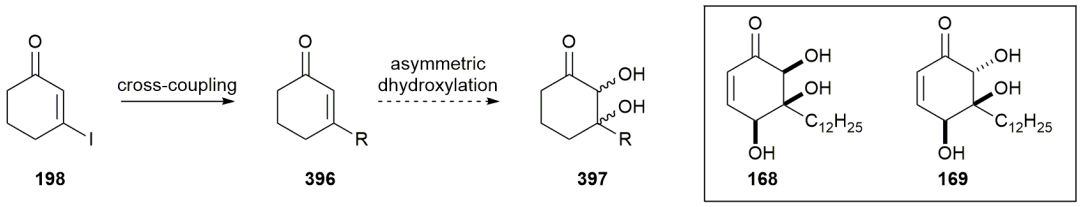

Scheme 110: The proposed synthetic procedure for the iodo keto *cis*-diol **117** mimic system using 3-iodocyclohexenone (**198**).

It was envisaged that the cross-coupling would result in the functionalisation at the β-position without removing the alkene functionality (**396**). This would then allow for an enantioselective dihydroxylation across the double bond to afford the desired diol (**397**).

The cross-coupling conditions for the phenyl side-chain are shown in **Table 23**. The copper catalysed conditions utilised the methodology developed by Procter and co-workers.[174] The rhodium catalysed conditions were the same as the conjugate addition reactions discussed in **Section 2.4.5**. Both approaches have a basis within the literature.[175, 176]

Table 23: The cross-coupling results for the phenyl side-chain functionality. General procedure for the copper catalysed cross-coupling: CuTC, **398** (1 M in THF), THF. General procedure for the rhodium catalysed cross-coupling: $[RhCl(cod)]_2$, **251**, Et_3N (1.0 eq.), dioxane:H_2O (10:1). CuTC = Copper thiophene-2-carboxylate. † = No reaction observed; ‡ = A small amount of product formation was observed by ^1H NMR.

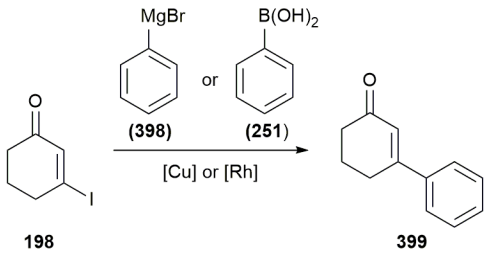

Catalyst (loading)	Coupling Reagent (eq.)	Reaction Temperature (°C)	Reaction Time (h)	Yield
CuTC (10 mol %)	**398** (1.2)	0	5 h	-†
CuTC (10 mol %)	**398** (1.2)	0 to RT	18 h	41 %
CuTC (20 mol %)	**398** (1.2)	0 to RT	18 h	44 %
$[RhCl(cod)]_2$ (5 mol %)	**251** (2.0)	RT	18 h	-‡
$[RhCl(cod)]_2$ (5 mol %)	**251** (6.0)	RT	18 h	-‡
$[RhCl(cod)]_2$ (5 mol %)	**251** (6.0)	RT	72 h	76 %

The copper catalysed cross-coupling proceeded in satisfactory yield of 41 %, which was achieved by increasing the reaction temperature slowly from 0 °C to room temperature. Doubling the catalyst loading from 10 mol % to 20 mol % led to a negligible increase in yield to 44 %. The 'Suzuki-like' rhodium catalysed cross-coupling, however, proceeded in excellent yield of 76 % at the expense of reaction time, which took 3 days. It should be noted that to achieve this transformation 6.0 equivalents of boronic acid had to be used. Nevertheless, the promising outlook of the rhodium catalysed approach led to the attempted reaction of 2-naphthylboronic acid with cyclohexenone **198** (**Scheme 111**).

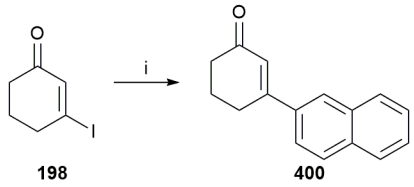

Scheme 111: *Reagents and conditions*: (i) $[RhCl(cod)]_2$ (5 mol %), 2-naphthylboronic acid (3.0 eq.), Et_3N, dioxane:H_2O (10:1), RT, 3 days, 47 %.

In an effort to improve the efficiency and to test the viability of this method, the boronic acid loading was decreased to 3.0 equivalents. The reaction proceeded, albeit in a satisfactory yield of 47 % after 3 days. The successful development of the cross-coupling reaction conditions for the aromatic coupling agents provided a basis to trial the coupling of a long-chain alkyl boronic acid, in this instance pentylboronic acid (**Scheme 112**, (i)).

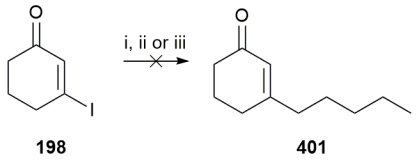

Scheme 112: *Reagents and conditions*: (i) $[RhCl(cod)]_2$ (5 mol %), pentylboronic acid (6.0 eq.), Et_3N, dioxane:H_2O (10:1), RT, 7 days; (ii) CuTC (20 mol %), pentylmagnesium bromide (2 M in Et_2O), THF, 0 °C to RT, 18 h; (iii) $ZnCl_2$.TMEDA, pentylmagnesium bromide (2 M in Et_2O), THF, -80 °C, 5 h.

The reaction was left for seven days on account of the long reaction time observed for the aromatic boronic acids; however, no product formation was observed by ^1H NMR. The likely reason for this result was the rapid decomposition of the pentyl boronic acid reagent via β-hydrogen elimination.[177]

Attention was turned back to the copper catalysed cross-coupling; however, this also failed to afford the pentyl coupled product **401** (**Scheme 112**, (ii)). Previous work conducted by Williams within the Whitehead group reported good success using triorganozincates to

transfer an alkyl group via a conjugate addition reaction to cyclic enones.[158] Furthermore, similar methodology has been reported within the literature, which involves a zinc catalysed cross-coupling.[178] This therefore prompted the trial cross-coupling reaction using $ZnCl_2$.TMEDA and pentylmagnesium bromide with enone **198**; however, no product formation was observed (**Scheme 112**, (iii)).

In summary, no reaction conditions were developed for the cross coupling of 3-iodocylohexenone (**198**) with a linear pentyl side-chain. Further possible methodologies are discussed in **Section 3.2**.

2.9 MTT Assay Results

2.9.1 MTT Cell Viability Assay

In 1983, Mosmann developed a rapid and quantitative colorimetric assay that was capable of handling large datasets for the determination of mammalian cell survival and proliferation.[179] Prior to this research, previous methods relied on manual cell counting and radioactive isotope labelling, which could not meet the demand for a large number of samples. The methodology described by Mosmann utilised (3-(4,5-dimethylthiazol-2-yl)-2,5-diphenyl tetrazolium bromide (MTT, **402**), a pale-yellow substrate, which is cleaved by the enzyme mitochondrial succinate dehydrogenase to afford purple formazan (**403**) crystals (**Scheme 113**). This process only occurs in metabolically active cells, and therefore the amount of formazan produced is proportional to the amount of living cells.

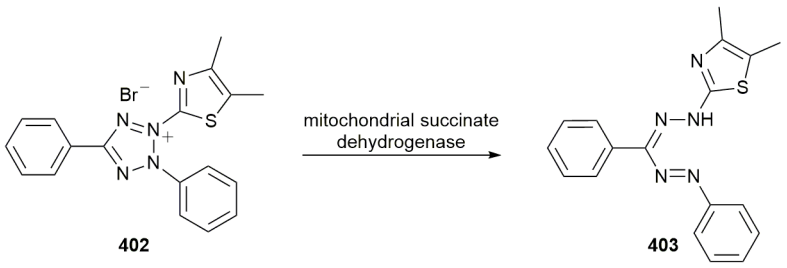

Scheme 113: The cleavage of MTT (**402**) to formazan (**403)** catalysed by mitochondrial succinate dehydrogenase.

The procedure for this colorimetric assay involved dissolving the MTT salt in phosphate buffered saline (PBS, 5 mg/mL) and incubating for 4 hours following addition to cell cultures. This was enough time for mitochondrial succinate dehydrogenase to cleave MTT (**402**) to afford formazan (**403**) crystals, which were reported to be only partially soluble in the cell medium. The amount of formazan produced during this process was proportional

to the number of living cells. To calculate the overall cell growth, Mosmann dissolved the formazan crystals in a solution of isopropyl alcohol and 0.04 M HCl before recording the optical densities (OD) using a scanning multiwall spectrophotometer at a wavelength of 570 nm.[180]

In 1987, Carmichael and co-workers assessed the MTT assay for use in chemosensitivity tests. The authors concluded that the MTT assay is rapid and reproducible, with a good standard error of deviation in measurements (± 5 %). Furthermore, Carmichael and co-workers optimised Mosmann's original procedure by switching isopropyl alcohol for DMSO. It was noted that the reduced formazan product (**403**) was poorly soluble in the acidic isopropyl alcohol used previously, whereas DMSO improved the solubility and absorption characteristics. The λ_{max} of formazan (**403**) varies greatly depending on what solvent is used; therefore, the optical densities were measured at 540 nm when solubilised in DMSO. Additionally, it was determined that the optimal assay duration for human cancer cell lines should be 4 days to compensate for cell death, loss of dehydrogenase activity and transport of a drug into the cell. This also avoided the need to refeed the cells with fresh media during the assay. The shortcomings of this assay, however, include the inability to distinguish between cytostatic and cytocidal effects on the cell. Moreover, compounds with reducing properties can react with MTT (**402**) to give a false result, and drugs that interact with the mitochondria may not be compatible with the assay.[181]

2.9.2 Cell Lines

The test compounds were assessed for their anti-proliferative activity against four cell lines, which are shown in **Table 24**. The cell lines were obtained from the American Type Culture Collection (ATCC). A549, MDA-MB-231 and FaDu were selected to give a diverse panel of cancer cell lines for biological evaluation, and PNT2, a healthy prostate cell line, was added for comparison.

Table 24: The cell lines used in the MTT assay.

Cell Line	Topography	Disease
A549	Human lung	Adenocarcinoma
MDA-MB-231	Mammary breast derived from metastatic site	Adenocarcinoma
FaDu	Human pharynx	Squamous cell carcinoma
PNT2	Human prostate	Normal prostate

The assays were conducted using the procedure described by Stratford and co-workers.[182,] Further information regarding this methodology can be found in **Section 6.2**. For each compound and each cell line, the assay was repeated a minimum of four times, and the results discussed in this chapter are the average values obtained from these experiments. The standard deviation was calculated from the results of each individual assay.

2.9.3 MTT Assay Results

In the following sections, the MTT assay results are described for the natural products discussed in the previous sections. The hydroxyenone ***ent*-266a**, antheminone A **374** and COTC hybrid **375** analogues were tested against the A549 cell line. All the synthesised incarviditone analogues (***ent*-237a-c** and **237a-d**) in addition to incarvilleatone analogue **(±)-371,** were tested against A549, MDA-MB-231 and FaDu. Selected incarviditone analogues (***ent*-237a** and **237a**) were also tested against the PNT2 cell line.

2.9.3.1 Hydroxyenone, Antheminone A and COTC

The antheminone A and COTC hybrid analogues **374** and **375** have been shown to inhibit GSH and therefore were tested against the A549 cell line, which has an elevated level of the GSH tripeptide.[183] As discussed in **Section 1.5**, the biological cytotoxic mechanism of this class of compounds is hypothesised to proceed via a conjugate addition of GSH to the analogue, followed by the displacement of the side-chain attached to C-2. Hydroxyenone ***ent*-266a**, which can be considered an analogue of incarviditone precursor, rengyolone (**125**), was also assayed for comparison with the antheminone A and COTC analogues. The lack of a side-chain leaving group in ***ent*-266a** makes for a useful comparison for investigation of the structure-activity relationships. The obtained IC_{50} results are shown in **Table 25**, alongside previously tested analogues reported by Y. Song and S. Christou.[60, 61]

Table 25: The MTT assay results for hydroxyenone ***ent*-266a**, antheminone A **374** and COTC hybrid **375** analogues against the A549 cell line. S. Christou tested: **405a**, **405b**, **405d**, **406a**, **406b** and **406d**; all the remaining analogues excluding **375** were tested by Y. Song. NA = not active >100 μM.

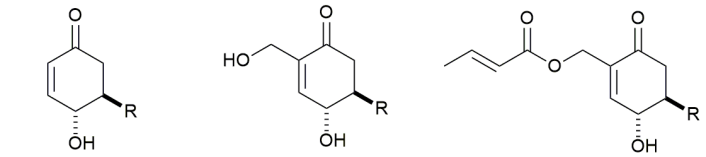

***ent*-266a** and **404a-d** **374** and **405a-d** **375** and **406a-d**

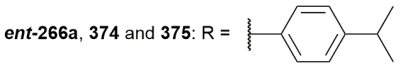

***ent*-266a**, **374** and **375**: R =

For **404**-**406**:

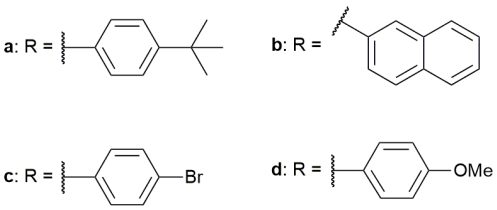

a: R = **b**: R = **c**: R = Br **d**: R = OMe

Compound	IC_{50} (μM)	miLogP
COTC/Antheminone A Hybrid Analogues		
406a	3.60 ± 3.2	3.96
375	3.25 ± 0.49	3.76
406b	2.47 ± 0.28	2.73
406c	2.97 ± 0.16	2.35
406d	3.17 ± 0.22	2.31
Antheminone A Analogues		
405a	19.0 ± 5.0	2.57
374	NA	2.37
405b	15.3 ± 0.22	2.04
405c	16.5 ± 1.6	1.67
405d	40.8 ± 5.4	0.92
Hydroxyenone Analogues		
404a	1.96 ± 0.38	3.26
***ent*-266a**	3.54 ± 0.18	3.07
404b	1.93 ± 0.39	2.74
404c	5.46 ± 0.49	2.37
404d	6.95 ± 0.33	1.61

From this dataset, the following observations can be made:

i. The 4-isopropylphenyl COTC/antheminone A hybrid analogue **375** showed similar activity to the wider data set against the A549 cell line (3.25 ± 0.49 μM). The overall data suggests that side-chain functionality has little influence on the observed activity.

ii. The 4-isopropylphenyl antheminone A analogue **374** showed an anomalous result (not active >100 μM) in relation to the previously tested antheminone A analogues. Additional assays were conducted, which confirmed this result and no plausible explanation can be suggested for this result. The result for 4-methoxyphenyl compound **405d** suggests that a decreasing milogP value is associated with lesser potency; however, further analogues are required to substantiate this trend and confirm whether the result for analogue **374** is an anomaly.

iii. The 4-isopropylphenyl hydroxyenone analogue ***ent*-266a** showed a similar trend of activity with regards to the dataset (3.54 ± 0.18 μM). The data suggests a correlation between hydrophobicity and anti-proliferative activity, with compounds possessing a high milogP value exhibiting the highest potency.

iv. Overall, the presence of a good leaving group in the hybrid analogues was reflected by a higher potency. This is closely followed by the hydroxyenone compounds, for which the biological mechanism is suggested to be a result of alkylation by the cellular components. This conclusion is in light of the absence of a side-chain leaving group and a propensity to undergo the Michael addition reaction. Finally, the anti-proliferative activities of the antheminone A analogues are much lower when compared to the hybrid analogues, suggesting that the leaving ability of the side-chain moiety is critical for bioactivity. In comparison to the hydroxyenones, the lesser potency of the antheminone A analogues may be associated with lower hydrophobicity.

2.9.3.2 Incarviditone and Incarvilleatone Analogues

The cytotoxic properties of incarviditone (**124)** described in **Section 1.2,** prompted the evaluation of the anti-proliferative activities of its analogues. The MTT assay results for the A549, MDA-MB-231 and FaDu cell lines are shown in **Table 26**. The data from previously synthesised analogues by the Whitehead group are also shown for comparison.

Table 26: The MTT assay results for the incarviditone analogues derived from acetonide/cyclohexylidene protected (-)-quinic acid **196** and **197**. NA = not active >100 µM. [a] = Synthesised by A. Edwards;[66] [b] = Tested by Y. Song; [c] = Synthesised by F. Zirilli;[156] [d] = Synthesised and tested by Y. Song;[61] [e] = Synthesised by M. Usher.[116]

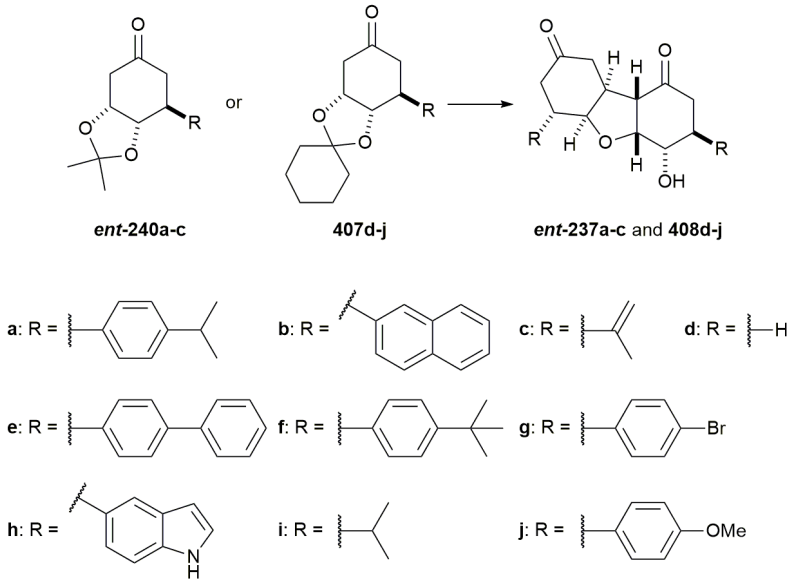

	IC_{50} (µM)			
Compound	A549	MDA-MB-231	FaDu	milogP
408e[a, b]	NA	NA	4.20 ± 0.58	6.83
408f[c]	12.0 ± 1.6	13.3 ± 0.14	NA	6.65
***ent*-237a**	83.4 ± 9.2	16.6 ± 1.2	88.7 ± 9.0	6.26
***ent*-237b**	13.4 ± 1.4	NA	NA	5.60
408g[d]	NA	11.3 ± 0.83	21.1 ± 2.5	4.86
408h[d]	NA	NA	NA	3.63
408i[e]	NA	NA	NA	3.60
408j[d]	NA	NA	NA	3.35
***ent*-237c**	83.6 ± 10.0	NA	NA	2.23
408d[d]	NA	NA	NA	-0.36

From this dataset, the following observations can be made:

i. For this set of results, the biological activity is negligible for compounds with a milogP value less than 4.0. This suggests that hydrophobicity may be a factor in the underlying mechanism of action.

ii. The presence of a hydrogen bonding donor in compound **408h** resulted in no activity. More datasets are required to determine if this characteristic has an effect on activity.

iii. MilogP values of greater than 4.8 gave variable results across the three cancer cell lines and showed no overall trend. The most potent compound was biphenyl analogue **408e** on the FaDu cell line (4.20 ± 0.58 µM), however this compound was inactive towards

the lung cancer and breast cancer cell lines A549 and MDA-MB-231 respectively. Comparatively, the naphthyl analogue ***ent*-237b** was one of the more potent compounds against A549 (13.4 ± 1.4 μM) but was inactive towards the MDA-MB-231 and FaDu cancer cell lines.

iv. There were significant differences in activities between *tert*-butylphenyl **408f** and isopropylphenyl ***ent*-237a** towards the A549 cell line (12.0 ± 1.6 μM and 83.4 ± 9.2 μM respectively), despite the similarity with regards to their milogP values and overall structures. The biological results were similar for the two compounds against the MDA-MB-231 and FaDu cell lines. This may suggest that A549 relies on a critical biological entity for cell survival, which is not as important in the MDA-MB-231 and FaDu cell lines, and thus has a greater sensitivity towards *tert*-butylphenyl **408f** over isopropylphenyl compound ***ent*-237a**.

v. Overall, *tert*-butylphenyl analogue **408f** exhibited the most potent biological activity, which was consistent across more than one cell-line (A549 and MDA-MB-231).

The successful development of the methodology utilising iodo keto *cis*-diol **117** and BDA protection of (-)-quinic acid (**Section 2.4**), allowed for the synthesis of both enantiomers of the incarviditone analogues as well as the preparation of isopropenyl incarvilleatone analogue (±)-**371**. All the resulting compounds were subjected to the MTT assay, and the results of which are shown in **Table 27**.

Table 27: The MTT assay results for enantiomeric pairs of incarviditone analogues, in addition to isopropenyl incarvilleatone analogue (±)-**371**. NA = not active >100 µM. [a] Synthesised and tested by Y. Song.[61]

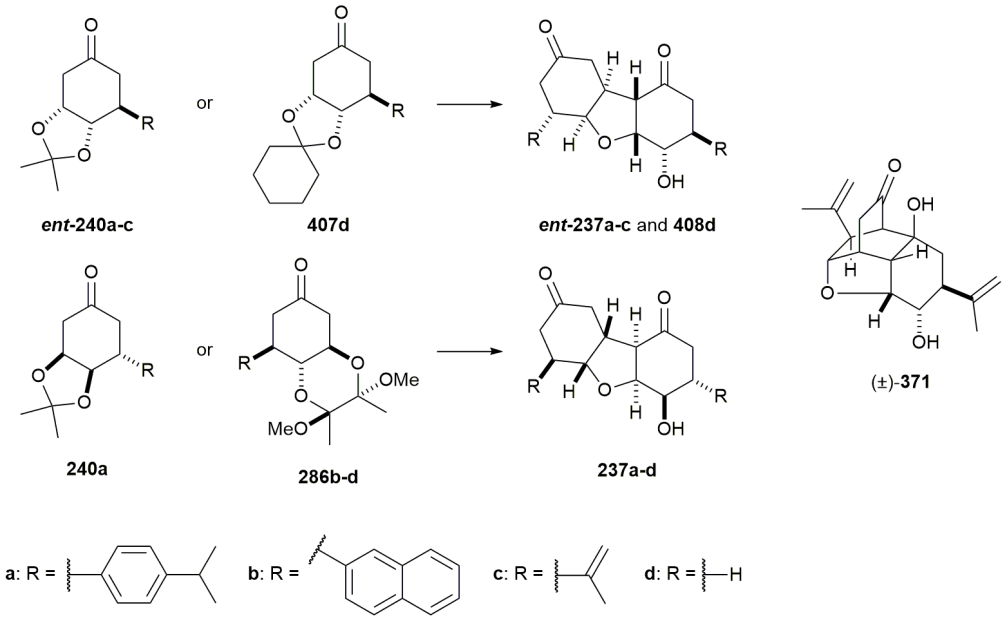

	IC_{50} (µM)			
Compound	A549	MDA-MB-231	FaDu	milogP
***ent*-237a**	83.4 ± 9.2	16.6 ± 1.2	88.7 ± 9.0	6.26
237a	NA	27.1 ± 0.80	75.6 ± 3.1	
***ent*-237b**	13.4 ± 1.4	NA	NA	5.60
237b	5.27 ± 1.5	3.51 ± 0.40	3.98 ± 0.30	
***ent*-237c**	83.6 ± 10.0	NA	NA	2.23
237c	NA	NA	NA	
408d[a]	NA	NA	NA	-0.36
237d	NA	NA	NA	
(±)-**371**	NA	NA	NA	2.44

From this dataset, the following observations can be made:

i. The enantiomers of the incarviditone analogues that possess a milogP value below 4.0 do not show any difference in biological activity and remain inactive (IC_{50} >100 µM).

ii. No significant difference was observed between the enantiomers for 4-isopropylphenyl analogue ***ent*-237a** and **237a** across the three cancer cell lines.

iii. A notable difference in anti-proliferative activity was observed between naphthyl enantiomers ***ent*-237b** and **237b**. Enantiomer ***ent*-237b** showed no activity against the MDA-MB-231 and FaDu cell lines; however, the antipodal compound **237b** exhibited

the most potent IC_{50} data recorded for an incarviditone analogue (MDA-MB-231: 3.51 ± 0.40 μM, FaDu: 3.98 ± 0.30 μM). Furthermore, testing of 4-isopropylphenyl incarviditone analogues ***ent*-237a** and **237a** against the PNT2, healthy prostate, cell line indicated further differences between enantiomers (**Table 28**). The healthy cell line was selected as a control so that general toxicity could be assessed for the incarviditone analogues.

Table 28: The MTT assay results for 4-isopropylphenyl incarviditone enantiomers ***ent*-237a** and **237a** against the PNT2 cell line.

Compound	IC_{50} (μM)
***ent*-237a**	17.4 ± 1.36
237a	86.3 ± 10.2

This data shows that the anti-proliferative activities of naphthyl and 4-isopropylphenyl analogues ***ent*-237a**/**237a** and ***ent*-237b**/**237b** is not due to general toxicity, as it would be expected that a similar IC_{50} would be observed for both enantiomers. Rather, it suggests that the analogues are interacting with an unidentified biological target, as the absolute stereochemistry has an effect on the IC_{50} values.

iv. The 2-propenyl incarvilleatone analogue **(±)-371** showed no activity against any of the cancer cell lines tested. Further analogues are required to substantiate whether the incarvilleatone analogues are generally inactive against the tested cancer cell lines.

3.0 Conclusion and Future Work

3.1 Computational Docking

A computational docking model was developed for the toluene dioxygenase enzyme with O_2 mapped into the active site. The model exhibited excellent correlation between the predicted docking outcome and the observed experimental results with regards to the monocyclic substrates. The results, however, are otherwise tentative without experimental validation. Of the 12 monocyclic substrates docked, the model was able to predict 70 % of the major poses. The weakness of this model however, appeared to be the determination of the likely bioproducts from the bicyclic substrates, with the model predicting the major pose for only 50 % of the sample substrates. The identification of a potential rotation pocket however, dubbed the 'His-311 pocket' could allow for a more accurate computational model. The significance of this rotation pocket has been demonstrated

computationally by the key interaction between the Met_{220} and His_{311} residues, which is believed to manifest in the binding of phenolic substrates. Incorporating this rotation into the model also led to a small increase in the correlation between the theoretical and experimental results for the bicyclic compounds, suggesting that further unidentified amino acid transpositions are likely to occur in the binding mode of these substrates.

Further work is required to substantiate the importance of the 'His-311 pocket'. This would include computationally mutating Gly_{264} to Ala. The methyl side-chain of alanine would be predicted to prevent the rotation of $His_{311,}$ and subsequent docking could therefore be used to show the effect this would have on the binding mode of phenolic substrates. This approach would require the application of molecular dynamics (e.g. Amber™) to allow the protein to relax to its lowest theoretical energy state following the mutation. It would also be appropriate to apply a molecular dynamics approach to TDO with the bicyclic substrates. Furthermore, it would be essential to investigate the effect of changing His_{311} through mutagenesis studies. The computational docking studies on bicyclic substrates indicated that the published crystal structure does not allow for a full and accurate representation of the binding poses for this larger substrate class.[7] A molecular dynamics simulation with TDO and a free bicyclic substrate would predict the lowest energy binding pose, and would give a possible indication of the torsional angles of the amino acid residues within the active site. This would allow for the identification of flexible amino acid side-chains, which could be subsequently incorporated into the docking model. Finally, the computational docking model was used to predict the biotransformation outcome for 4'-isopropyl-[1,1'-biphenyl]-3-ol (**272**) (**Scheme 114**).

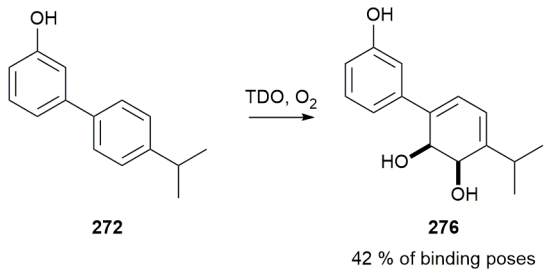

Scheme 114: The major predicted metabolite for 4'-isopropyl-[1,1'-biphenyl]-3-ol (**272**) **(Section 2.3.5**).

Further studies would focus on carrying out the *P. putida* UV4 catalysed biotransformation using substrate **272** to determine the validity of this model at predicting the outcome of unknown substrates.

3.2 Application of the Iodo Keto *cis*-Diol

The TDO catalysed biotransformation of 3-iodophenol (**115**) yielded iodo keto *cis*-diol **117**, which was successfully applied in the synthesis of incarviditone analogue **237a** (**Scheme 115**).

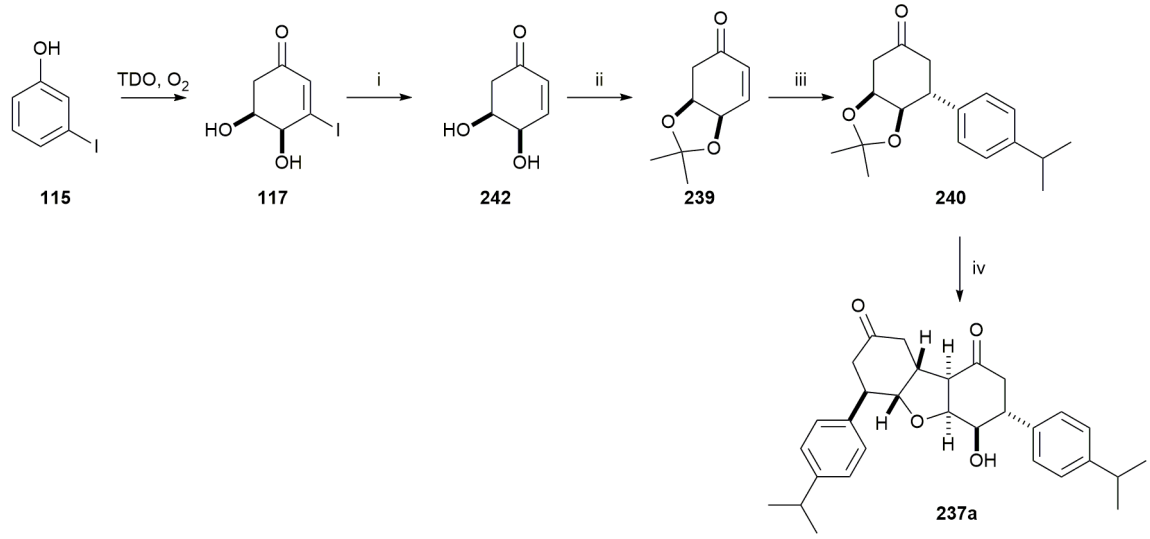

Scheme 115: The synthesis of 4-isopropylphenyl incarviditone analogue **237a** using iodo keto *cis*-diol **117**. *Reagents and conditions*: (i) 5 % Pd/C, H_2, Et_3N, MeOH, RT, 11 min, 69 %; (ii) 2,2-DMP, CSA, acetone, 0 °C, 75 min, 62 %; (iii) $[RhCl(cod)]_2$, 4-isopropylphenyl boronic acid, Et_3N, dioxane:H_2O (10:1), RT, 18 h, 62 %; (iv) 0.5 M $NaOH_{(aq)}$, THF, RT, 19 h, 73 %.

The synthesis of analogue **237a** demonstrated the synthetic application of iodo keto *cis*-diol **117**. Furthermore, alternative synthetic routes that resulted in the same stereochemical outcome as diol **117** were explored to serve as a comparison (**Scheme 116**).

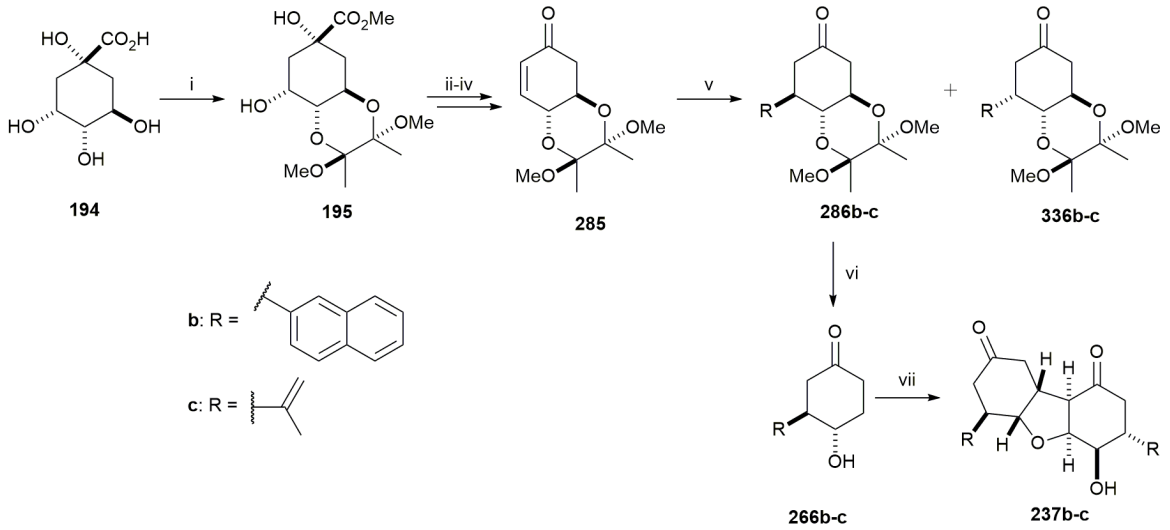

Scheme 116: The alternative synthetic route to incarviditone analogues **237b**, **237c** using butan-1,2-diacetal protected (-)-quinic acid **195**. *Reagents and conditions*: (i) butan-2,3-dione, trimethyl orthoformate, CSA, MeOH, reflux, 18 h, 88 %; (ii) $NaBH_4$, MeOH, 0 °C to RT, 18 h; (iii) $NaIO_4$, silica gel, CH_2Cl_2, RT. 2 h, 85 % (over two steps); (iv) MsCl, Et_3N, CH_2Cl_2, 0 °C to RT, 4 h, 83 %; (v) For **286b**: $[RhCl(cod)]_2$, naphthyl boronic acid, Et_3N, dioxane:H_2O (10:1), RT, 18 h, 20 %; for **286c**: CuI, isopropenyl magnesium bromide (0.5 M in THF), TMSCl, THF, -42 °C, 3 h, 51 %; (vi) TFA, H_2O, CH_2Cl_2, RT, 18 h, 62 % (**266b**), 67 % (**266c**); (vii) 0.5 M $NaOH_{(aq)}$, THF, RT, 18 h, 56 % (**237b**), 42 % (**237c**).

The alternative methodology to incarviditone analogues **237b** and **237c** involved utilising butan-1,2-diacetal protected (-)-quinic acid **195**, which proceeded with notable synthetic challenges. In addition to the longer synthetic route, the diastereoselectivity of the conjugate addition was worse and the adducts required extensive purification. This is in stark contrast to the iodo keto *cis*-diol **117** route, which proceeded with excellent diastereoselectivity due to the inherent directing acetonide moiety. In conclusion, the comparison of these two synthetic routes exemplifies the practicality of using the iodo keto *cis*-diol bioproduct **117**.

During this project, the major weakness of iodo bioproduct **117** was the biotransformation yield (ca. 18 %). The project collaborators, however, have since optimised the biotransformation conditions using an *E. coli* clone capable of removing the debilitating catechol **113** from the biotransformation mixture. For future applications, this should therefore result in a more abundant supply of bioproduct **117**. In light of this, future research would focus on applying diol **117** in the synthesis of novel natural product analogues, such as the anti-fungal agents pseudohygrophorones described in **Section 1.4**. Preliminary work described in this thesis attempted to develop reaction conditions towards analogues of pseudohygrophorones using a mimic system (**Scheme 117**).

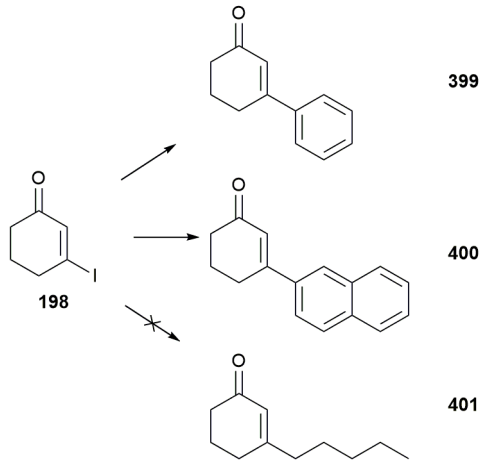

Scheme 117: The applications of 3-iodocyclohexenone (**198**) as a mimic system for iodo keto *cis*-diol **117**.

The successful cross-coupling reactions using phenyl and 2-naphthyl boronic acid and rhodium catalysis were demonstrated, however no reaction conditions were developed for the desired pentyl alkyl chain. Future cross-coupling reactions would involve investigation into the reaction conditions developed by Comasseto and co-workers (**Scheme 118**).[175]

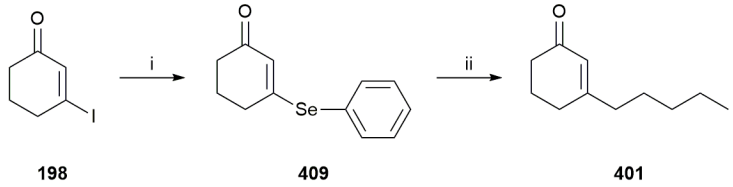

Scheme 118: *Reagents and conditions* as reported by Comasseto and co-workers: (i) $(C_6H_5Se)_2$, $NaBH_4$, acetic acid, EtOH, RT, 6 h, 75 %; (ii) *n*-$C_5H_{11}MgBr$ (1.2 eq.), $H_2SO_{4(aq)}$ (5 %), RT, 24 h, 46 %.

Furthermore, future applications for iodo keto *cis*-diol **117** would include the synthesis of further analogues of incarviditone and incarvilleatone based on their promising biological activity (see **Section 3.3**). Finally, the synthetic route to analogues of the natural products COTC and antheminone A have been demonstrated. This synthetic route would now be applied using iodo keto *cis*-diol **117** to show further examples of natural product analogues accessible by using bioproduct **117**.

3.3 Incarviditone and Incarvilleatone

The project satisfied the aim to investigate the biological activity of enantiomeric pairs of incarviditone analogues, which was accomplished by the successful synthesis of the following analogues (**Figure 65**).

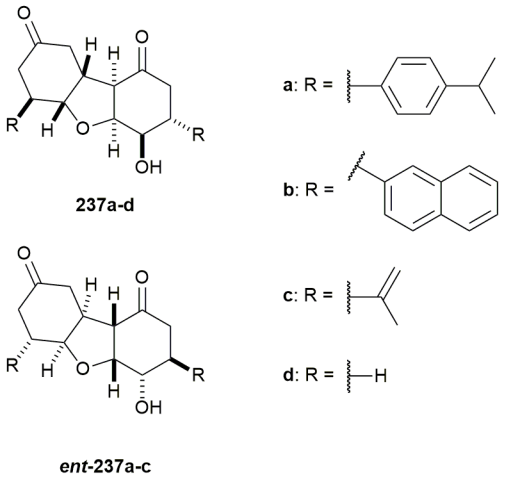

Figure 65: The synthesised incarviditone analogues.

The MTT assays of the synthesised compounds suggested the following:

i. Incarviditone analogues with a milogP < 4 were inactive, suggesting a link between the anti-proliferative activity and hydrophobicity.

ii. The biological mode of action of these class of compounds is not due to general toxicity. This is suggested based on the significant differences in the IC_{50} values of 4-isopropylphenyl enantiomers **237a** and ***ent*-237a**; and naphthyl enantiomers **237b** and ***ent*-237b** (**Table 29**).

Table 29: The summary of the differences in anti-proliferative activities between naphthyl and 4-isopropylphenyl incarviditone analogues ***ent*-237a-b** and **237a-b**. NA = not active.

	Compounds and IC_{50} (μM)	
Cell Line	***ent*-237b**	**237b**
MDA-MB-231	NA	3.51 ± 0.40
FaDu	NA	3.98 ± 0.30
	***ent*-237a**	**237a**
PNT2	17.4 ± 1.36	86.3 ± 10.2

The data implies that the chirality of incarviditone analogues ***ent*-237b** and **237b** influences the anti-proliferative activity, suggesting that the compound is acting on an unidentified biological target.

In addition to the incarviditone analogues formed by homodimerisation, the first reported incarvilleatone analogue was synthesised via heterodimerisation of two enantiomers of isopropenyl hydroxyenone (***ent*-266c** and **266c**, **Scheme 119**).

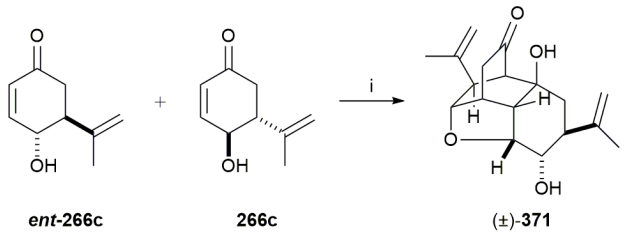

ent-**266c** **266c** (±)-**371**

Scheme 119: The synthesis of racemic isopropenyl incarvilleatone analogue **371**. *Reagents and conditions*: (i) DBU, CH_2Cl_2, RT, 4 days, 26 %.

The biological testing against the A549, MDA-MB-231 and FaDu cancer cell lines indicated no activity > 100 µM for compound **(±)-371**.

Future work regarding the incarviditone analogues would focus on investigating the enantiomeric differences further. The next appropriate enantiomer target therefore would be *tert*-butyl phenyl analogue **410**; the enantiomer **408f** which showed relatively potent activity against the A549 (12.0 ± 1.6 µM) and MDA-MB-231 (13.3 ± 0.14 µM) cell lines (**Figure 66**).

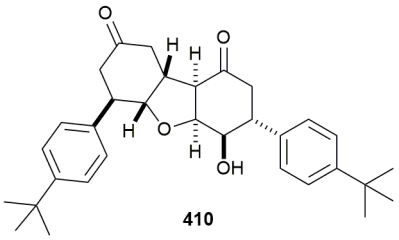

410

Figure 66: The structure of *tert*-butyl phenyl incarviditone analogue **410**.

Further studies would also continue to investigate the structure-activity relationship described in **Section 2.5**. This would involve the synthesis of the oxime incarviditone analogue **411** (**Figure 67**).

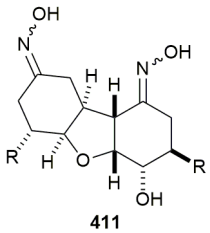

411

Figure 67: The structure of the oxime incarviditone analogue **411**.

It was suggested that the carbonyl functionalities of incarviditone analogues could play a prominent role in the biological mechanism due to their reactive nature. The less electrophilic oxime functional group would therefore probe this hypothesis.[184]

Concerning the incarvilleatone analogues, efforts would be made to control the stereoselectivity of the heterodimerisation, with the aim to produce enantiomerically pure analogues. To achieve this, investigations would continue to focus on the protection of the γ-hydroxyl from the hydroxyenone compounds using a moiety which would not disrupt the hydrogen bonding interaction. Taking into account the failed attempts to protect the hydroxyl using methyl iodide to form the methyl ester, attention would turn to using either methoxymethyl ether (MOM) or ethoxyethyl ether (MEM) protecting groups (**Figure 68**).

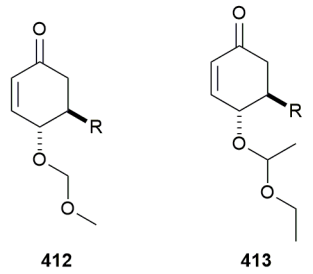

Figure 68: The structures of methoxymethyl ether (MOM) and ethoxyethyl ether (MEM) protected hydroxyenones **412** and **413** respectively.

Finally, biological testing on an expanded library of incarvilleatone analogues would be continued, in order to collect a large enough dataset to investigate any biological trend. In addition to this, LPS-induced RAW 264.7 macrophage assays measuring the nitric oxide inhibition would be conducted as a result of the promising biological activity of the incarvilleatone natural product, which exhibited a difference in activity between the two enantiomers on the inhibition of nitric oxide production (see **Section 1.3**).

4.0 Experimental

Chemical Structures

All chemical structures and chemical names were generated using ChemBioDraw v15.1. The chemical structures are numbered according to the general structures outlined below. The structures are numbered in relation to (-)-quinic acid (**194**), which is numbered in accordance to shikimic acid. If a double bond is present, this takes the highest priority and the numbering is changed accordingly.

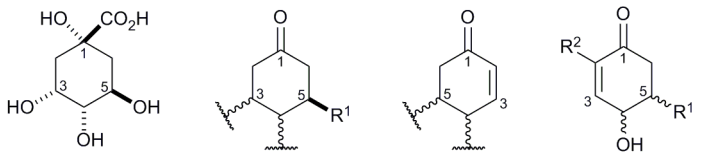

Solvent and Reaction Conditions

All the reactions were carried out under dry conditions, using an inert nitrogen atmosphere unless stated otherwise. The nitrogen atmosphere was applied using a nitrogen balloon. The glassware was pre-dried before use. All chemicals and solvents were purchased from Sigma Aldrich, Fluorochem, Fisher or Alfa-Aesar.

The solvents were evaporated on an IKA RV-10-B-S99 rotary evaporator equipped with an IKA HB-10 water bath or a Buchi R114 rotary evaporator equipped with a Buchi B-481 water bath.

Thin Layer Chromatography

TLC was performed using standard silica 60 pre-coated polyester sheets (Macherey-Nagel). UV active compounds were visualised using a fluorescent indicator at 254 nm. Plate visualisation was carried out using: iodine crystals, phosphomolybdic acid stain or potassium permanganate stain. The plate was heated via a heat gun to aid in visualisation.

Flash Silica Column Chromatography

Flash silica chromatography was performed using silica gel (Sigma Aldrich) 40-63 µm 60 Å. The solvent system used on the column is stated in each experimental procedure.

General Measuring Equipment

Braun Injekt®-F tuberculin 1 mL syringes accurate to 0.01 mL were used; values below 100 µL were measured using a VWR microsyringe (100 µL) or VWR microsyringe (50 µL). All weights were measured on a Sartorius CPA225D balance, accurate to 0.01 mg from 0 – 100 g and 0.1 mg from 120 g to 200 g.

Nuclear Magnetic Resonance

The ^{1}H and ^{13}C spectra were recorded using a B400 Bruker Avance III 400 or a B500 Bruker Avance II+ 500. All the chemical shifts (δ_H, δ_C) are reported in parts per million (ppm) to the nearest 0.01 ppm and referenced to the residual non-deuterated solvent peak.

For ^{1}H spectra, all the coupling constants (*J*) are reported to the nearest 0.1 Hz. The spectral data is reported in the following order: chemical shifts, integration, multiplicity (s, singlet; d, doublet; t, triplet; m, multiplet etc.; or as a combination of these, such as dd, dt etc.). The ~ symbol denotes a peak of apparent multiplicity.

All proton and carbon assignments were supported by 2D ^{1}H-^{1}H COSY, 2D ^{13}C-^{1}H HSQC, ^{13}C-^{1}H HMBC, ^{13}C DEPT-90 and ^{13}C DEPT-135.

Melting Point

Melting points were recorded on a Sanyo Gallenkamp MPD350 heater.

Infra-Red Spectroscopy

The IR spectra were recorded on a Perkin Elmer FT-IR instrument. Absorption (ν_{max}) is quoted in wavenumbers (cm^{-1}) and the peak intensities are described as: strong (s), medium (m), weak (w) or broad (br).

Mass Spectrometry

The mass spectrometry was performed by the staff at the School of Chemistry, University of Manchester in the Mass Spectrometry Laboratory department. The low-resolution mass spectra were measured using the Micromass Platform II apparatus with electrospray ionisation. Only the molecular ions, fractions from molecular ions and major peaks are reported as mass/charge (*m/z*) ratios. The reported mass values are within ±5 ppm mass units.

Optical Rotations ($[\alpha]_D^T$)

The optical rotations were performed using an automatic polarimeter AA-100 with a sodium D light (λ = 589 nm). The $[\alpha]_D^T$ values are reported in (deg·mL)/(g·dm) and were calculated using the following equation:

$$[\alpha]_D^T = \frac{100\alpha}{l \times c}$$

α = Observed angle of rotation

l = Length of cell (the cell used was 0.25 dm)

c = Concentration of sample (g/100 mL)

T = Temperature measurement was taken at (°C).

Ten recordings were taken, and the average of these values was used as the observed angle of rotation.

HPLC

The normal phase HPLC was performed on an Agilent 1260 Infinity machine using HPLC grade solvents. The column used was the Ace 10 Sil (10 µM particle size, 100 Å pore size). The flow rate was set at 15 mL/min.

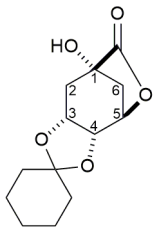

196

$C_{13}H_{18}O_5$; M_w = 254.28 g/mol

(3a'*R*,4'*R*,7'*S*,8a'*R*)-7'-Hydroxytetrahydrospiro[cyclohexane-1,2'-[4,7]methano[1,3]dioxolo[4,5-c]oxepin]-6'(4'*H*)-one (196):

A solution of (-)-quinic acid (5.00 g, 26.0 mmol) and cyclohexanone (15.9 mL, 15.1 g, 156 mmol) in toluene (50 mL) was heated at reflux using a Dean and Stark apparatus and was stirred for 30 minutes under a N_2 atmosphere. After cooling the solution to room temperature, Amberlite® resin IR 120 H^+ (5.00 g, pre-washed with MeOH (30 mL) and Et_2O (2 × 30 mL) and dried under vacuum) was added and the reaction mixture was heated at reflux for 6 hours under a N_2 atmosphere. The resin was removed by filtration and the organic filtrate was washed with sat. $NaHCO_{3(aq)}$ (20 mL), distilled water (20 mL) and brine (20 mL). 40-60 Petroleum ether was added to the combined organic layers to form a white precipitate, which was filtered and washed with 40-60 petroleum ether (2 × 20 mL) to afford the title compound **196** as a white solid (2.87 g, 43 %). m.p. 146-147 °C [Lit.[117] 139-141 °C]; $[\alpha]_D^{25}$ -35.8 (*c* 1.00 in CH_2Cl_2) [Lit.[117] $[\alpha]_D^{22}$ -33.0 (*c* 1.05 in $CHCl_3$)]; ν_{max} /cm^{-1} 3429br (O-H), 2950m, 2932m, 2853m (C-H), 1766s (C=O); δ_H (400 MHz; $CDCl_3$) 1.41-1.72 (10H, m, 5 × (C$\underline{H}_2$) of cyclohexane), 2.20 (1H, dd, *J* 13.9, 2.9, C(2)$\underline{H}_{eq}$), 2.28-2.39 (2H, m, C(2)$\underline{H}_{ax}$ and one of C(6)$\underline{H}_2$), 2.68 (1H, d, *J* 12.2, one of C(6)$\underline{H}_2$), 4.32 (1H, dt, *J* 6.7, 1.2, C(4)$\underline{H}$), 4.49 (1H, td, *J* 6.7, 2.9, C(3)$\underline{H}$), 4.75 (1H, dd, *J* 6.7, 2.4, C(5)$\underline{H}$); δ_C (100 MHz; $CDCl_3$) 23.5, 24.0, 25.0, 33.7 (4 × $\underline{C}H_2$ of cyclohexane), 34.4 ($\underline{C}$(6)H_2), 36.9 ($\underline{C}H_2$ of cyclohexane), 38.5 ($\underline{C}$(2)H_2), 71.1 ($\underline{C}$(3)H), 71.6 ($\underline{C}$(1)), 71.8 ($\underline{C}$(4)H), 76.0 ($\underline{C}$(5)H), 110.6 ($\underline{C}$ of cyclohexane), 178.9 ($\underline{C}$=O); *m/z* (+ES) 277 ($[M+Na]^+$, 100 %).

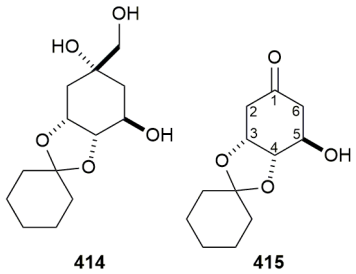

414 415

$C_{12}H_{18}O_4$; M_w = 226.27 g/mol

(3a*S*,4*R*,7a*R*)-4-Hydroxytetrahydrospiro[benzo[*d*][1,3]dioxole-2,1'-cyclohexan]-6(3a*H*)-one (415):

The lactone **196** (1.13 g, 4.44 mmol) was dissolved in MeOH (60 mL) and the solution was cooled to 0 °C. Sodium borohydride (1.68 g, 44.4 mmol) was added portion-wise to the solution and then stirred until effervescence ceased. The reaction mixture was allowed to warm up to room temperature and was stirred for 20 hours under a N_2 atmosphere. The reaction was quenched by the addition of sat. $NH_4Cl_{(aq)}$ (10 mL) and concentrated *in vacuo* to afford a white solid. The resulting crude solid was washed with EtOAc (3 × 30 mL) and the combined organic filtrate was dried over $MgSO_4$, filtered and concentrated *in vacuo* to afford crude triol **414** as an off-white gum (1.56 g), which was carried through to the next step.

To a solution of sodium *meta*-periodate (3.23 g, 15.1 mmol) in hot water (5 mL) was added silica gel (8.00 g). The resulting slurry was mixed until a free-flowing powder was obtained. To the resulting powder were added CH_2Cl_2 (20 mL) and a solution of crude triol **414** (1.56 g) in CH_2Cl_2 (20 mL). The reaction mixture was stirred at room temperature for 2 hours under a N_2 atmosphere. The silica was filtered and washed with CH_2Cl_2 (4 × 20 mL). The combined filtrate was dried over $MgSO_4$, filtered and concentrated *in vacuo* to afford the title compound **415** as a colourless oil (1.07 g, 65 % over two steps). m.p. 99-101 °C [Lit.[185] 97-98 °C]; $[\alpha]_D^{25}$ +79.2 (*c* 1.00 in CH_2Cl_2) [Lit.[185] $[\alpha]_D^{29}$ 100.3 (*c* 0.44 in MeOH)]; ν_{max} /cm^{-1} 3454br (O-H), 2939m, 2859w (C-H), 1709s (C=O); δ_H (400 MHz; $CDCl_3$) 1.38-1.58 (10H, 5 × C$\underline{H}_2$ of cyclohexane), 2.31 (1H, br s, O$\underline{H}$), 2.45 (1H, ddd, *J* 17.6, 3.0, 1.7, C(6)$\underline{H}_{ax}$), 2.66 (1H, ~t, *J* 3.2, C(2)$\underline{H}_{eq}$), 2.70 (1H, ~t, *J* 3.0, C(6)$\underline{H}_{eq}$), 2.81 (1H, dd, *J* 17.5, 3.2, C(2)$\underline{H}_{ax}$), 4.25 (1H, ~q, *J* 3.0, C(5)$\underline{H}$), 4.31 (1H, dt, *J* 7.0, 2.1, C(4)$\underline{H}$) 4.70 (1H, dt, *J* 7.0, 3.2, C(3)$\underline{H}$); δ_C (100 MHz; $CDCl_3$) 23.2, 23.6, 24.9, 33.0, 36.0 (5 × $\underline{C}H_2$ of cyclohexane), 40.0 ($\underline{C}$(2)H_2), 41.4

(C(6)H_2), 68.1 (C(5)HOH), 71.5 (C(3)H), 74.4 (C(4)H), 109.3 (C of cyclohexane), 207.8 (C=O); *m/z* (+ES) 249 ([M+Na]$^+$, 100 %).

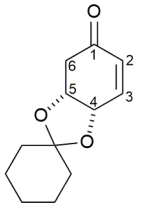

416

$C_{12}H_{16}O_3$; M_w = 208.26 g/mol

(3a*R*,7a*S*)-3a,7a-Dihydrospiro[benzo[*d*][1,3]dioxole-2,1'-cyclohexan]-5(4*H*)-one (416):

The hydroxyketone **415** (1.62 g, 7.16 mmol) was dissolved in CH_2Cl_2 (30 mL) and the solution was cooled to 0 °C. Triethylamine (2.59 mL, 1.88 g, 18.6 mmol) and methanesulfonyl chloride (0.64 mL, 947 mg, 8.27 mmol) were added sequentially to the solution. The reaction mixture was allowed to warm up to room temperature and was stirred for 4 hours under a N_2 atmosphere. The reaction was quenched by the addition of distilled water (10 mL) and partitioned with CH_2Cl_2 (20 mL). The organic layer was separated and the aqueous layer was extracted with CH_2Cl_2 (2 × 20 mL). The combined organic layers were washed with distilled water (20 mL), brine (20 mL), dried over $MgSO_4$, filtered and concentrated *in vacuo* to afford a brown solid. The crude material was purified by flash silica chromatography, eluting with 40-60 petroleum ether:EtOAc (5:1) to afford the title compound **416** as an off-white solid (1.29 g, 87 %). m.p. 66-68 °C [Lit.[185] 55-58 °C]; $[\alpha]_D^{25}$ +128 (*c* 1.00 in CH_2Cl_2) [Lit.[185] $[\alpha]_D^{25}$ +100 (*c* 0.44 in MeOH)]; ν_{max} /cm^{-1} 2944m (C-H), 1675s (C=O), 1661w (C=C); δ_H (400 MHz; $CDCl_3$) 1.57-1.61 (10H, m, 5 × C$\underline{H}_2$ of cyclohexane), 2.68 (1H, dd, *J* 17.6, 3.9, one of C(6)$\underline{H}_2$), 2.95 (1H, ddd, *J* 17.6, 2.4, 0.9, one of C(6)$\underline{H}_2$), 4.67-4.72 (2H, m, C(5)$\underline{H}$ and C(4)$\underline{H}$), 6.02 (1H, dd, *J* 10.4, 0.9, C(2)$\underline{H}$), 6.65 (1H, dt, *J* 10.4, 2.4, C(3)$\underline{H}$); δ_C (100 MHz; $CDCl_3$) 24.1, 24.2, 25.2, 36.3, 37.8 (5 × $\underline{C}H_2$ of cyclohexane), 39.2 (C(6)H_2), 71.0 (C(5)H), 73.3 (C(4)H), 110.9 (C of cyclohexane), 129.1 (C(2)H), 146.4 (C(3)H), 195.9 (C=O); *m/z* (+ES) 249 ([M+Na]$^+$, 100 %).

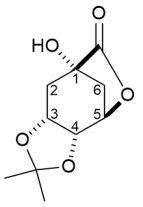

197

$C_{10}H_{14}O_5$; M_w = 214.22 g/mol

(3a*R*,4*R*,7*S*,8a*R*)-7-Hydroxy-2,2-dimethyltetrahydro-4,7-methano[1,3]dioxolo[4,5-c]oxepin-6(4*H*)-one (**197**):

(-)-Quinic acid (10.0 g, 52.0 mmol) was dissolved in acetone (150 mL). 2,2-Dimethoxypropane (25.6 mL, 21.7 g, 208 mmol) and *p*-toluenesulfonic acid monohydrate (990 mg, 5.20 mmol) were added sequentially to the solution. The reaction mixture was heated at reflux and stirred for 6 hours under a N_2 atmosphere. The reaction was quenched by the addition of triethylamine (1 mL) and concentrated *in vacuo* to afford a brown oil. The resulting crude oil was dissolved in EtOAc (200 mL) and washed with distilled water (3 × 50 mL). The organic layer was dried over $MgSO_4$, filtered and concentrated *in vacuo* to give a crude brown solid, which was stirred in pentane (300 mL) for 4 hours to afford the title compound **197** as a white solid (8.62 g, 77 %). m.p. 147-148 °C [Lit.[186] 143-144 °C]; $[\alpha]_D^{25}$ -33.6 (*c* 1.00 in CH_2Cl_2) [Lit.[187] $[\alpha]_D^{19}$ -36.0 (*c* 0.8 in $CHCl_3$)]; ν_{max} /cm^{-1} 3417br (O-H), 2978w, 2923w (C-H), 1772s (C=O); δ_H (400 MHz; $CDCl_3$) 1.34 (3H, s, C$\underline{H}_3$ of acetonide), 1.53 (3H, s, C$\underline{H}_3$ of acetonide), 2.19 (1H, dd, *J* 14.9, 2.8, C(2)$\underline{H}_{eq}$), 2.29-2.40 (2H, m, C(2)$\underline{H}_{ax}$ and one of C(6)$\underline{H}_2$), 2.66 (1H, d, *J* 11.7, one of C(6)$\underline{H}_2$), 4.31 (1H, ddd, *J* 6.8, 2.6, 1.2, C(4)$\underline{H}$), 4.50 (1H, td, *J* 6.8, 2.8, C(3)$\underline{H}$), 4.73 (1H, dd, *J* 6.1, 2.6, C(5)$\underline{H}$); δ_C (100 MHz; $CDCl_3$) 24.4 (C$\underline{H}_3$ of acetonide), 27.1 (C$\underline{H}_3$ of acetonide), 34.4 (C$\underline{(6)}H_2$), 38.4 (C$\underline{(2)}H_2$), 71.7 (C$\underline{(3)}$H), 72.2 (C$\underline{(4)}$H), 76.0 (C$\underline{(5)}$H), 77.4 (C$\underline{(1)}$), 109.9 (C of acetonide), 178.9 (C$\underline{=O}$); *m/z* (+ES) 237 ($[M+Na]^+$, 100 %); HRMS calculated for $C_{10}H_{14}O_5Na$, ($[M+Na]^+$): 237.0739, found: 237.0744.

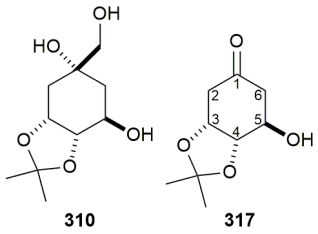

310 **317**

$C_9H_{14}O_4$; M_w = 186.21 g/mol

(3a*R*,7*R*,7a*S*)-7-Hydroxy-2,2-dimethyltetrahydrobenzo[*d*][1,3]dioxol-5(4*H*)-one (317):

The lactone **197** (2.33 g, 10.8 mmol) was dissolved in EtOH (45 mL) and the solution was cooled to 0 °C. Sodium borohydride (4.10 g, 108 mmol) was added portion-wise to the solution and then stirred until effervescence ceased. The reaction mixture was allowed to warm up to room temperature and was stirred for 20 hours under a N_2 atmosphere. The reaction was quenched by the addition of brine (20 mL) and was left to stir for a further 20 hours at room temperature. The solution was concentrated *in vacuo* to afford a crude white solid, which was washed with $CHCl_3$:MeOH (90 mL, 2:1). The organic filtrate was concentrated *in vacuo* to afford crude triol **310** as a colourless oil (4.45 g), which was carried through to the next step.

To a solution of sodium *meta*-periodate (5.79 g, 27.1 mmol) in hot water (12 mL) was added silica gel (12.0 g). The resulting slurry was mixed until a free-flowing powder was obtained. To the resulting powder were added $CHCl_3$ (35 mL) and a solution of crude triol **310** (2.36 g, 10.8 mmol) in $CHCl_3$ (35 mL). The reaction mixture was stirred at room temperature for 2 hours under a N_2 atmosphere. The silica was removed by filtration and washed with Et_2O (3 × 30 mL). The combined filtrate was dried over $MgSO_4$, filtered and concentrated *in vacuo* to afford the title compound **317** as a colourless oil, which solidified on freezing (1.72 g, 85 % over 2 steps). m.p. 73-74 °C [Lit.[188] 80-81 °C]; $[\alpha]_D^{25}$ +101 (*c* 1.00 in CH_2Cl_2) [Lit.[187] $[\alpha]_D^{19}$ +135 (*c* 0.92 in $CHCl_3$)]; ν_{max} /cm^{-1} 3426br (O-H), 2990w, 2975w, 2911w (C-H), 1715s (C=O); δ_H (400 MHz; $CDCl_3$) 1.37 (3H, s, C$\underline{H}_3$ of acetonide), 1.45 (3H, s, C$\underline{H}_3$ of acetonide), 1.75 (1H, br s, O$\underline{H}$), 2.46 (1H, ddd, *J* 17.9, 3.9, 1.8, one of C(6)$\underline{H}_2$), 2.65-2.68 (1H, m, one of C(6)$\underline{H}_2$), 2.70-2.71 (1H, m, one of C(2)$\underline{H}_2$), 2.81 (1H, dd, *J* 17.5, 3.8 one of C(2)$\underline{H}_2$), 4.24-4.26 (1H, m, C(5)$\underline{H}$OH), 4.31 (1H, ddd, *J* 7.1, 2.7, 1.9 C(4)$\underline{H}$), 4.70-4.73 (1H, m, C(3)$\underline{H}$); δ_C (100 MHz; $CDCl_3$) 24.1 ($\underline{C}H_3$ of acetonide), 26.5 ($\underline{C}H_3$ of acetonide), 40.3 ($\underline{C}$(2)H_2), 41.7 ($\underline{C}$(6)H_2), 68.4 ($\underline{C}$(5)HOH), 72.4 ($\underline{C}$(3)H), 75.1

(C(4)H), 109.0 (C of acetonide), 207.7 (C=O); *m/z* (+ES) 209 ([M+Na]$^+$, 100 %); HRMS calculated for $C_9H_{15}O_4$, ([M+H]$^+$): 187.0970, found: 187.0978.

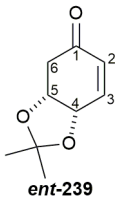

***ent*-239**

$C_9H_{12}O_3$; M_w = 168.19 g/mol

(3a*R*,7a*S*)-2,2-Dimethyl-3a,7a-dihydrobenzo[*d*][1,3]dioxol-5(4*H*)-one (*ent*-239):

The hydroxyketone **317** (1.70 g, 9.13 mmol) was dissolved in CH_2Cl_2 (35 mL) and the solution was cooled to 0 °C. Triethylamine (3.31 mL, 2.40 g, 23.7 mmol) and methanesulfonyl chloride (0.81 mL, 1.20 g, 10.5 mmol) were added sequentially to the solution and the reaction mixture was stirred at room temperature for 5 hours under a N_2 atmosphere. The reaction was quenched by the addition of distilled water (15 mL) and partitioned with CH_2Cl_2 (10 mL). The organic layer was separated and the aqueous layer was extracted with CH_2Cl_2 (2 × 10 mL). The organic layers were combined, dried over $MgSO_4$, filtered and concentrated *in vacuo* to afford a brown oil. The crude product was purified by flash silica chromatography, eluting with 40-60 petroleum ether:EtOAc (5:1) to afford the title compound ***ent*-239** as a colourless oil that solidified to a white solid on freezing (1.17 g, 76 %). m.p. 40-41 °C [Lit.[189] 39-40 °C]; $[\alpha]_D^{25}$ +148 (*c* 1.00 in CH_2Cl_2) [Lit.[189] $[\alpha]_D$ +148 (*c* 0.48 in $CHCl_3$)]; ν_{max} /cm^{-1} 2987w, 2880w (C-H), 1681s (C=O), 1667m (C=C); δ_H (400 MHz; $CDCl_3$) 1.38 (3H, s, C$\underline{H}_3$ of acetonide), 1.39 (3H, s, C$\underline{H}_3$ of acetonide), 2.69 (1H, dd, *J* 17.6, 4.5, one of C(6)$\underline{H}_2$), 2.93 (1H, ddd, *J* 17.6, 2.5, 1.3, one of C(6)$\underline{H}_2$), 4.68 (1H, ~tt, *J* 4.5, 2.5, C(5)$\underline{H}$), 4.72 (1H, ddd, *J* 4.5, 2.5, 1.3, C(4)$\underline{H}$), 6.03 (1H, dt, *J* 10.4, 1.3, C(2)$\underline{H}$), 6.65 (1H, dt, *J* 10.4, 2.5, C(3)$\underline{H}$); δ_C (100 MHz; $CDCl_3$) 26.8 (C$\underline{H}_3$ of acetonide), 27.9 (C$\underline{H}_3$ of acetonide), 38.9 (C(6)$\underline{H}_2$), 71.2 (C(4)H), 73.5 (C(5)H), 110.1 (C of acetonide), 129.0 (C(2)H), 146.0 (C(3)H), 195.4 (C(1)); *m/z* (+ES) 191 ([M+Na]$^+$, 100 %); HRMS calculated for $C_9H_{12}O_3Na$, ([M+Na]$^+$): 191.0684, found: 191.0686.

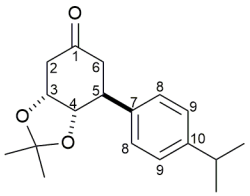

***ent*-240a**

$C_{18}H_{24}O_3$; M_w = 288.39 g/mol

(3a*R*,7*S*,7a*S*)-7-(4-Isopropylphenyl)-2,2-dimethyltetrahydrobenzo[*d*][1,3]dioxol-5(4*H*)-one (*ent*-240a):

The enone ***ent*-239** (181 mg, 1.08 mmol) was dissolved in dioxane:water (2 mL, 10:1). 4-Isopropylphenylboronic acid (354 mg, 2.16 mmol), $[RhCl(cod)]_2$ (25.0 mg, 0.05 mmol) and triethylamine (0.15 mL, 109 mg, 1.08 mmol) were added sequentially to the solution. The reaction mixture was stirred at room temperature for 18 hours under a N_2 atmosphere when it was concentrated *in vacuo* to afford a brown solid. Purification by flash silica chromatography, eluting with 40-60 petroleum ether:EtOAc (10:1 to 9:1) afforded the title compound ***ent*-240a** as a white solid (195 mg, 76 %). m.p. 49-50 °C; $[\alpha]_D^{26}$ -86.0 (*c* 1.00 in CH_2Cl_2); ν_{max} /cm^{-1} 2965w, 2895w (C-H), 1711s (C=O), 1597m, 1578m (C=C aromatic); δ_H (400 MHz; C_6D_6) 1.13 (6H, d, *J* 6.9, (C$\underline{H}_3$)$_2$ of isopropyl), 1.15 (3H, s, C$\underline{H}_3$ of acetonide), 1.40 (3H, s, C$\underline{H}_3$ of acetonide), 2.25 (1H, dd, *J* 17.6, 9.6, C(6)$\underline{H}_{ax}$), 2.37 (1H, dd, *J* 16.6, 5.3, one of C(2)$\underline{H}_2$), 2.51 (1H, ~d, *J* 5.3, one of C(2)$\underline{H}_2$), 2.54-2.58 (1H, m, C(6)$\underline{H}_{eq}$), 2.70 (1H, hept, *J* 6.9, C$\underline{H}$ of isopropyl), 3.11 (1H, ddd, *J* 9.6, 6.8, 4.5, C(5)$\underline{H}$), 3.93 (1H, dt, *J* 6.8, 5.3, C(3)$\underline{H}$), 4.12 (1H, t, *J* 6.8, C(4)$\underline{H}$), 6.98 (2H, d, *J* 8.2, C(8)$\underline{H}$), 7.05 (2H, d, *J* 8.2, C(9)$\underline{H}$); δ_C (100 MHz; C_6D_6) 24.2 ((C$\underline{H}_3$)$_2$ of isopropyl), 24.5 (C$\underline{H}_3$ of acetonide), 27.3 (C$\underline{H}_3$ of acetonide), 34.1 (C$\underline{H}$ of isopropyl), 41.3 (C$\underline{(6)}H_2$), 42.6 (C$\underline{(5)}$H), 42.7 (C$\underline{(2)}H_2$), 72.7 (C$\underline{(3)}$H), 78.3 (C$\underline{(4)}$H), 108.4 (C of acetonide), 126.9 (C$\underline{(9)}$H), 127.9 (C$\underline{(8)}$H), 138.5 (C$\underline{(7)}$), 147.5 (C$\underline{(10)}$), 206.4 (C$\underline{(1)}$); *m/z* (+ES) 311 ([M+Na]$^+$, 100 %); HRMS calculated for $C_{18}H_{24}O_3Na$, ([M+Na]$^+$): 311.1623, found: 311.1637.

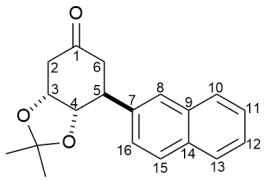

***ent*-240b**

$C_{19}H_{20}O_3$; M_w = 296.37 g/mol

(3a*R*,7*S*,7a*S*)-2,2-Dimethyl-7-(naphthalen-2-yl)tetrahydrobenzo[*d*][1,3]dioxol-5(4*H*)-one (*ent*-240b):

The enone ***ent*-239** (323 mg, 1.92 mmol) was dissolved in dioxane:water (4 mL, 10:1). 2-Naphthylboronic acid (660 mg, 3.84 mmol), $[RhCl(cod)]_2$ (49.0 mg, 0.10 mmol) and triethylamine (0.13 mL, 94.4 mg, 0.93 mmol) were added sequentially to the solution. The reaction mixture was stirred at room temperature for 18 hours under a N_2 atmosphere when it was concentrated *in vacuo* to give a dark red solid. Purification by flash silica chromatography, eluting with 40-60 petroleum ether:EtOAc (10:1) afforded the title compound ***ent*-240b** as a white solid (403 mg, 71 %). m.p. 85-86 °C; $[\alpha]_D^{25}$ -73.8 (*c* 2.00 in CH_2Cl_2); ν_{max} /cm^{-1} 2987w, 2932w, 2906w (C-H), 1713s (C=O), 1620w, 1596w (C=C aromatic); δ_H (400 MHz; $CDCl_3$) 1.38 (3H, s, C$\underline{H}_3$ of acetonide), 1.55 (3H, s, C$\underline{H}_3$ of acetonide), 2.69 (1H, dd, *J* 16.8, 5.2, one of C(2)$\underline{H}_2$), 2.73 (1H, dd, *J* 17.7, 8.7, C(6)$\underline{H}_{ax}$), 2.76 (1H, dd, *J* 16.8, 5.2, one of C(2)$\underline{H}_2$), 2.83 (1H, dd, *J* 17.7, 6.8 C(6)$\underline{H}_{eq}$), 3.58 (1H, dt, *J* 8.7, 6.8 C(5)$\underline{H}$), 4.64 (1H, dt, *J* 6.8, 5.2, C(3)$\underline{H}$), 4.74 (1H, t, *J* 6.8, C(4)$\underline{H}$), 7.41 (1H, dd, *J* 8.5, 1.9, C(16)$\underline{H}$), 7.44-7.51 (2H, m, C(12)$\underline{H}$ and C(13)$\underline{H}$), 7.62 (1H, dd, *J* 1.9, 0.9, C(8)$\underline{H}$), 7.78-7.83 (2H, m, C(10)$\underline{H}$ and C(11)$\underline{H}$), 7.84 (1H, d, *J* 8.5, C(15)$\underline{H}$); δ_C (100 MHz; $CDCl_3$) 24.5 ($\underline{C}H_3$ of acetonide), 27.2 ($\underline{C}H_3$ of acetonide), 41.1 ($\underline{C}(6)H_2$), 42.5 ($\underline{C}(2)H_2$), 42.9 ($\underline{C}(5)H$), 72.7 ($\underline{C}(3)H$), 77.8 ($\underline{C}(4)H$), 108.9 ($\underline{C}$ of acetonide), 125.9 ($\underline{C}(16)H$), 126.0 ($\underline{C}(8)H$), 126.2 ($\underline{C}(12)H$ or $\underline{C}(13)H$), 126.6 ($\underline{C}(12)H$ or $\underline{C}(13)H$), 127.7 ($\underline{C}(10)H$ or $\underline{C}(11)H$), 127.9 ($\underline{C}(10)H$ or $\underline{C}(11)H$), 128.8 ($\underline{C}(15)H$), 132.6 ($\underline{C}(9)$), 133.5 ($\underline{C}(14)$), 137.6 ($\underline{C}(7)$), 208.7 ($\underline{C}(1)$); *m/z* (+ES) 239 (100 %), 319 ([M+Na]$^+$, 80 %); HRMS calculated for $C_{19}H_{20}O_3Na$, ([M+Na]$^+$): 319.1305, found: 319.1302.

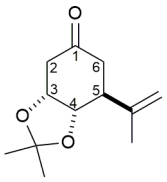

***ent*-240c**

$C_{12}H_{18}O_3$; M_w = 210.27 g/mol

(3a*R*,7*S*,7a*S*)-2,2-Dimethyl-7-(prop-1-en-2-yl)tetrahydrobenzo[*d*][1,3]dioxol-5(4*H*)-one (*ent*-240c):

Copper iodide (823 mg, 4.32 mmol) was stored in an oven dried flask under vacuum for 30 minutes and suspended in anhydrous THF (5 mL). The suspension was placed under a N_2 atmosphere and was cooled to -42 °C using a dry ice/acetonitrile bath. Isopropenyl magnesium bromide (0.5 M in THF) (17.3 mL, 16.2 g, 8.64 mmol) was added drop-wise to the suspension, which was stirred at -42 °C for 1 h to form the Gilman cuprate. To the cuprate reaction mixture was added chlorotrimethylsilane (1.82 mL, 1.56 g, 14.4 mmol), followed by the drop-wise addition of a solution of enone ***ent*-239** (484 mg, 2.88 mmol) in anhydrous THF (14 mL). The reaction mixture was stirred at -42 °C for 3 hours when it was quenched by the addition of sat. $NH_4Cl_{(aq)}$:$NH_{3(aq)}$ (20 mL, 9:1) and extracted with Et_2O (3 × 50 mL). The combined organic extracts were washed with brine (20 mL), dried over $MgSO_4$, filtered and concentrated *in vacuo* to give a brown solid. The crude product was purified by flash silica chromatography, eluting with 40-60 petroleum ether:EtOAc (5:1) to afford the title compound ***ent*-240c** as a colourless oil (531 mg, 87 %). $[\alpha]_D^{26}$ -49.0 (*c* 0.50 in CH_2Cl_2); ν_{max} /cm^{-1} 2982w, 2939w, 2906w, 2882w, (C-H), 1707s (C=O), 1646m (C=C); δ_H (400 MHz; $CDCl_3$) 1.38 (3H, s, C$\underline{H}_3$ of acetonide), 1.49 (3H, s, C$\underline{H}_3$ of acetonide), 1.82 (3H, s, C$\underline{H}_3$ of isopropenyl), 2.39 (1H, ddd, *J* 17.6, 7.2, 1.0, C(6)$\underline{H}_{ax}$), 2.60 (1H, dd, *J* 17.6, 5.6, C(6)$\underline{H}_{eq}$), 2.61 (1H, dd, *J* 17.2, 4.9, one of C(2)$\underline{H}_2$), 2.70 (1H, dd, *J* 17.2, 4.9, one of C(2)$\underline{H}_2$), 2.71-2.76 (1H, m, C(5)$\underline{H}$), 4.50 (1H, ddd, *J* 7.1, 5.0, 1.0, C(4)$\underline{H}$), 4.56-4.60 (1H, m, C(3)$\underline{H}$), 4.73 (1H, s, one of C$\underline{H}_2$ of isopropenyl), 4.95 (1H, s, one of C$\underline{H}_2$ of isopropenyl); δ_C (100 MHz; $CDCl_3$) 21.8 (C$\underline{H}_3$ of isopropenyl), 24.3 (C$\underline{H}_3$ of acetonide), 26.9 (C$\underline{H}_3$ of acetonide), 39.4 (C(6)$\underline{C}H_2$), 41.6 (C(2)$\underline{C}H_2$), 44.2 (C(5)$\underline{C}$H), 72.5 (C(3)$\underline{C}$H), 74.5 (C(4)$\underline{C}$H), 108.4 ($\underline{C}$ of acetonide), 113.0 ($\underline{C}H_2$ of isopropenyl), 143.9 ($\underline{C}$ of isopropenyl), 208.9 ($\underline{C}$(1)); *m/z* (+ES) 233 ([M+Na]$^+$, 100 %); HRMS calculated for $C_{12}H_{18}O_3Na$, ([M+Na]$^+$): 233.1148, found: 233.1143.

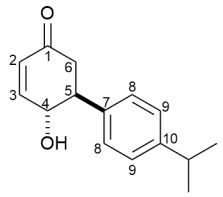

***ent*-266a**

$C_{15}H_{18}O_2$; M_w = 230.31 g/mol

(1*S*,6*R*)-6-Hydroxy-4'-isopropyl-1,6-dihydro-[1,1'-biphenyl]-3(2H)-one (*ent*-266a):

The conjugate adduct ***ent*-240a** (392 mg, 1.36 mmol) was dissolved in THF (10 mL) and placed under a N_2 atmosphere. 0.5 M $NaOH_{(aq)}$ (0.03 mL) was added to the solution and the reaction mixture was stirred at room temperature for 1 hour when it was quenched by the addition of sat. $NH_4Cl_{(aq)}$ (20 mL) and extracted with CH_2Cl_2 (3 × 60 mL). The organic layers were combined, dried over $MgSO_4$, filtered and concentrated *in vacuo* to give a light brown solid. The resulting crude product was purified by flash silica chromatography, eluting with 40-60 petroleum ether:EtOAc (4:1 to 3:1) to afford the title compound ***ent*-266a** as colourless crystals (266 mg, 85 %). m.p. 107-108 °C; $[\alpha]_D^{26}$ -124 (*c* 1.00 in CH_2Cl_2); ν_{max} /cm^{-1} 3387br (O-H), 3011w, 2953w (C-H), 1677s (C=O), 1512w (C=C); δ_H (400 MHz; $CDCl_3$) 1.26 (6H, d, *J* 6.9, (C<u>H</u>$_3$)$_2$ of isopropyl), 2.67-2.70 (2H, m, C(6)<u>H</u>$_2$), 2.92 (1H, hept, *J* 6.9, C<u>H</u> of isopropyl), 3.22 (1H, ddd, *J* 11.0, 9.8, 6.9, C(5)<u>H</u>), 4.65 (1H, dt, *J* 9.8, 2.3, C(4)<u>H</u>OH), 6.06 (1H, ddd, *J* 10.2, 2.3, 0.8, C(2)<u>H</u>), 7.00 (1H, dd, *J* 10.2, 2.3, C(3)<u>H</u>), 7.22 (2H, d, *J* 8.5, C(8)<u>H</u>), 7.25 (2H, d, *J* 8.5, C(9)<u>H</u>); δ_C (100 MHz; $CDCl_3$) 24.1 ((<u>C</u>H$_3$)$_2$ of isopropyl), 33.9 (<u>C</u>H of isopropyl), 43.2 (<u>C</u>(6)H$_2$), 50.5 (<u>C</u>(5)H), 72.1 (<u>C</u>(4)HOH), 127.4 (<u>C</u>(9)H), 127.8 (<u>C</u>(8)H), 129.1 (<u>C</u>(2)H), 136.8 (<u>C</u>(7)), 148.8 (<u>C</u>(10)), 152.3 (<u>C</u>(3)H), 198.4 (<u>C</u>(1)); *m/z* (-ES) 229 ([M-H]$^-$, 100 %); HRMS calculated for $C_{15}H_{19}O_2$, ([M+H]$^+$): 231.1380, found: 231.1379.

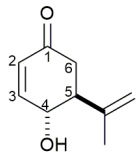

***ent*-266c**

$C_9H_{12}O_2$; M_w = 152.19 g/mol

(4*R*,5*S*)-4-Hydroxy-5-(prop-1-en-2-yl)cyclohex-2-en-1-one (*ent*-266c):

The conjugate adduct ***ent*-240c** (140 mg, 0.67 mmol) was dissolved in CH_2Cl_2 (2 mL) and placed under a N_2 atmosphere. DBU (0.10 mL, 102 mg, 0.67 mmol) was added to the solution and the reaction mixture was stirred at room temperature for 3 hours when it was quenched by the addition of sat. $NH_4Cl_{(aq)}$ (10 mL) and extracted with CH_2Cl_2 (3 × 50 mL). The organic layers were combined, dried over $MgSO_4$, filtered and concentrated *in vacuo* to afford a brown oil. The crude product was purified by flash silica chromatography, eluting with Et_2O:hexane (1:1) to afford the title compound ***ent*-266c** as a colourless oil (53.0 mg, 52 %). $[\alpha]_D^{27}$ -171 (*c* 1.00 in CH_2Cl_2); ν_{max} /cm^{-1} 3387br (O-H), 2968m, 2933m, 2877m, (C-H), 1671s (C=O), 1645m (C=C); δ_H (500 MHz; $CDCl_3$) 1.78 (3H, s, C$\underline{H}_3$ of isopropenyl), 2.42 (1H, dd, *J* 16.4, 13.7, C(6)$\underline{H}_{ax}$), 2.51 (1H, ddd, *J* 16.4, 4.0, 1.2, C(6)$\underline{H}_{eq}$), 2.75 (1H, ddd, *J* 13.7, 9.8, 4.0, C(5)$\underline{H}$), 4.49 (1H, dt, *J* 9.8, 2.3, C(4)$\underline{H}$OH), 4.99 (1H, s, one of C$\underline{H}_2$ of isopropenyl), 5.03 (1H, s, one of C$\underline{H}_2$ of isopropenyl), 5.99 (1H, ddd, *J* 10.2, 2.3, 1.2, C(2)$\underline{H}$), 6.97 (1H, dd, *J* 10.2, 2.3, C(3)$\underline{H}$); δ_C (125 MHz; $CDCl_3$) 19.1 ($\underline{C}H_3$ of isopropenyl), 41.0 ($\underline{C}(6)H_2$), 52.6 ($\underline{C}(5)H$), 68.4 ($\underline{C}(4)HOH$), 115.3 ($\underline{C}H_2$ of isopropenyl), 128.8 ($\underline{C}(2)H$), 143.0 ($\underline{C}$ of isopropenyl), 152.4 ($\underline{C}(3)H$), 198.3 ($\underline{C}(1)$); *m/z* (-ES) 151 ([M-H]$^-$, 100 %); HRMS calculated for $C_9H_{11}O_2$, ([M-H]$^-$): 151.0765, found: 151.0747.

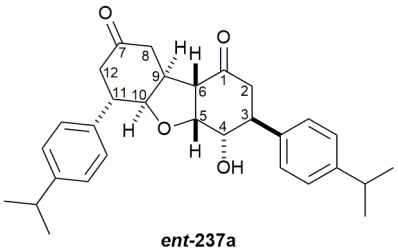

***ent*-237a**

$C_{30}H_{36}O_4$; M_w = 460.61 g/mol

3*S*,4*S*,4a*R*,5a*R*,6*S*,9a*S*,9b*S*)-4-Hydroxy-3,6-bis(4-isopropylphenyl)octahydrodibenzo[*b,d*]furan-1,8(2*H*,5a*H*)-dione (*ent*-237a):

Method 1:

The conjugate adduct ***ent*-240a** (321 mg, 1.11 mmol) was dissolved in THF (7 mL). 0.5 M $NaOH_{(aq)}$ (0.05 mL) was added to the solution and the reaction mixture was stirred at room temperature under a N_2 atmosphere. An additional 0.35 mL of 0.5 M $NaOH_{(aq)}$ was added to the reaction mixture in 0.05 mL portions at regular intervals over 18 hours. The reaction was quenched by the addition of sat. $NH_4Cl_{(aq)}$ (20 mL) and extracted with CH_2Cl_2 (3 × 30 mL). The organic layers were combined, dried over $MgSO_4$, filtered and concentrated *in vacuo* to give a brown solid. The crude material was purified by flash silica chromatography, eluting with 40-60 petroleum ether:EtOAc (4:1 to 1:1) to afford the title compound ***ent*-237a** as a white solid (154 mg, 60 %).

Method 2:

The hydroxyenone ***ent*-266a** (121 mg, 0.53 mmol) was dissolved in THF (3.2 mL). 0.5 M $NaOH_{(aq)}$ (0.20 mL) was added to the solution and the reaction mixture was stirred at room temperature for 18 hours under a N_2 atmosphere. The reaction was quenched by the addition of sat. $NH_4Cl_{(aq)}$ (10 mL) and extracted with CH_2Cl_2 (3 × 20 mL). The organic layers were combined, dried over $MgSO_4$, filtered and concentrated *in vacuo* to give a brown solid. The crude material was purified by flash silica chromatography, eluting with 40-60 petroleum ether:EtOAc (3:1 to 1:1) to afford the title compound ***ent*-237a** as a white solid (80.0 mg, 66 %).

m.p. 135-136 °C; $[\alpha]_D^{25}$ -168 (*c* 1.00 in CH_2Cl_2); ν_{max} /cm^{-1} 3454br (O-H), 2962w, 2901w, 2856w (C-H), 1701s (C=O), 1519m (C=C aromatic); δ_H (400 MHz; $CDCl_3$) 1.23 (6H, d, *J* 6.9, $(C\underline{H}_3)_2$ of isopropyl), 1.25 (6H, d, *J* 6.9, $(C\underline{H}_3)_2$ of isopropyl), 2.08 (1H, d, *J* 8.0,

C(4)HOH), 2.54-2.60 (4H, m, C(8)H_2 and C(12)H_2), 2.64-2.67 (2H, m, C(2)H_2), 2.79 (1H, dd, *J* 5.1, 2.2, C(6)H), 2.90 (1H, hept, *J* 6.9, CH of isopropyl), 2.90 (1H, hept, *J* 6.9, (CH of isopropyl), 3.17 (1H, ddd, *J* 10.0, 9.5, 5.0, C(11)H), 3.29 (1H, td, *J* 10.4, 7.2, C(3)H), 3.48-3.51 (1H, m, C(9)H), 4.28 (1H, ddd, *J* 10.4, 8.0, 3.3, C(4)HOH), 4.43 (1H, dd, *J* 9.5, 7.4, C(10)H), 4.71 (1H, dd, *J* 5.1, 3.3, C(5)H), 7.14 (4H, dd, *J* 8.3, 1.8, Ar-CH), 7.21 (4H, dd, *J* 8.3, 1.8, Ar-CH); δ_C (100 MHz; $CDCl_3$) 24.10 ((CH_3)$_2$ of isopropyl), 24.12 ((CH_3)$_2$ of isopropyl), 33.8 (CH of isopropyl), 33.9 (CH of isopropyl), 37.2 (C(9)H), 40.6 (C(8)H_2), 42.9 (C(11)H), 43.0 (C(12)H_2), 44.2 (C(3)H), 45.2 (C(2)H_2), 56.9 (C(6)H), 73.0 (C(4)HOH), 78.6 (C(5)H), 81.8 (C(10)H), 127.0 (Ar-CH), 127.2 (Ar-CH), 127.4 (Ar-CH), 127.5 (Ar-CH), 137.3 (Ar-C), 138.6 (Ar-C), 147.9 (Ar-C), 148.2 (Ar-C), 206.8 (C(1)), 209.9 (C(7)); *m/z* (+ES) 483 $[M+Na]^+$, 100 %); HRMS calculated for $C_{30}H_{36}O_4Na$, ($[M+Na]^+$): 483.2511, found: 483.2522.

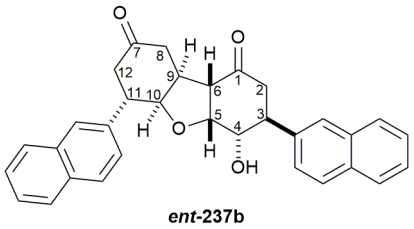

***ent*-237b**

$C_{32}H_{28}O_4$; M_w = 476.57 g/mol

(3*S*,4*S*,4a*R*,5a*R*,6*S*,9a*S*,9b*S*)-4-Hydroxy-3,6-di(naphthalen-2-yl)octahydrodibenzo[b,d]furan-1,8(2H,5aH)-dione (*ent*-237b):

The conjugate adduct ***ent*-240b** (61.0 mg, 0.21 mmol) was dissolved in THF (1 mL). 0.5 M $NaOH_{(aq)}$ (0.10 mL) was added to the solution and the reaction mixture was stirred at room temperature under a N_2 atmosphere. An additional 0.50 mL of 0.5 M $NaOH_{(aq)}$ was added to the reaction mixture in 0.05 mL portions over 18 hours. The reaction was quenched by the addition of sat. $NH_4Cl_{(aq)}$ (10 mL) and extracted with CH_2Cl_2 (3 × 30 mL). The organic layers were combined, dried over $MgSO_4$, filtered and concentrated *in vacuo* to give a brown solid. The crude product was purified by flash silica chromatography, eluting with 10 % to 15 % (3:1 EtOAc:EtOH) in 40-60 petroleum ether to afford the title compound ***ent*-237b** as a white solid (35.0 mg, 71 %). m.p. 214-215 °C; $[\alpha]_D^{26}$ -93.3 (*c* 0.6 in $CHCl_3$); ν_{max} /cm^{-1} 3443br (O-H), 3050w, 2961w, 2923w, 2885w (C-H), 1711s (C=O), 1633w, 1600w, 1509w (C=C aromatic); δ_H (500 MHz; $CDCl_3$) 2.60-2.69 (4H, m, C(8)H_2 and C(12)H_2), 2.74 (1H, dd, *J* 14.9, 4.4, C(2)H_{eq}), 2.81 (1H, dd, *J* 14.9, 11.7, C(2)H_{ax}), 2.86

(1H, dd, *J* 5.1, 2.1, C(6)H), 3.37 (1H, dt, *J* 9.8, 6.4, C(11)H), 3.44-3.50 (1H, m, C(3)H), 3.60 (1H, dtd, *J* 14.0, 7.0, 2.1, C(9)H), 4.42 (1H, dd, *J* 10.1, 3.3, C(4)HOH), 4.60 (1H, dd, *J* 9.8, 7.0, C(10)H), 4.78 (1H, dd, *J* 5.1, 3.3, C(5)H), 7.36 (2H, ddd, *J* 10.4, 8.4, 1.8, Ar-CH), 7.43-7.53 (4H, m, Ar-CH), 7.65 (1H, s, Ar-CH), 7.68 (1H, s, Ar-CH), 7.74-7.90 (6H, m, Ar-CH); δ_C (125 MHz; $CDCl_3$) 37.3 (C(9)H), 40.5 (C(8)H_2), 43.1 (C(12)H_2), 43.6 (C(11)H), 44.7 (C(3)H), 45.2 (C(2)H_2), 57.0 (C(6)H), 72.9 (C(4)HOH), 78.8 (C(5)H), 81.9 (C(10)H), 125.3 (Ar-CH), 125.6 (Ar-CH), 126.1 (Ar-CH), 126.2 (Ar-CH), 126.3 (Ar-CH), 126.52 (Ar-CH), 126.54 (Ar-CH), 126.7 (Ar-CH), 127.8 (Ar-CH and Ar-CH), 127.87 (Ar-CH), 127.91 (Ar-CH), 128.8 (Ar-CH), 128.9 (Ar-CH), 132.8 (Ar-C), 132.9 (Ar-C), 133.6 (Ar-C and Ar-C), 137.4 (Ar-C), 138.7 (Ar-C), 206.5 (C(1)), 209.5 (C(7)); *m/z* (+ES) 301 (100 %), 499 ($[M+Na]^+$, 40 %); HRMS calculated for $C_{32}H_{27}O_4$, ($[M-H]^-$): 475.1904, found: 475.1904.

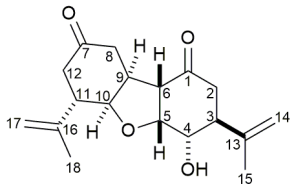

***ent*-237c**

$C_{18}H_{24}O_4$; M_w = 304.39 g/mol

(3*S*,4*S*,6*S*)-4-Hydroxy-3,6-di(prop-1-en-2-yl)octahydrodibenzo[*b*,*d*]furan-1,8(2*H*,5a*H*)-dione (*ent*-237c):

The conjugate adduct ***ent*-240c** (117 mg, 0.56 mmol) was dissolved in THF (3.4 mL). 0.5 M $NaOH_{(aq)}$ (0.10 mL) was added to the solution and the reaction mixture was stirred at room temperature under a N_2 atmosphere. An additional 0.50 mL of 0.5 M $NaOH_{(aq)}$ was added to the reaction mixture in 0.05 mL portions at regular intervals over 18 hours. The reaction was quenched by the addition of sat. $NH_4Cl_{(aq)}$ (10 mL) and extracted with CH_2Cl_2 (3 × 30 mL). The organic layers were combined, dried over $MgSO_4$, filtered and concentrated *in vacuo* to give a brown solid. The crude product was purified by silica chromatography, eluting with hexane:EtOAc (2:1) to afford the title compound ***ent*-237c** as a fine, white solid (25.0 mg, 30 %). m.p. 123-124 °C, $[\alpha]_D^{24}$ -126 (*c* 0.4 in CH_2Cl_2); ν_{max} /cm^{-1} 3376br (O-H), 2928w, 2924w, 2922w (C-H), 1702s, 1698s (C=O), 1646w (C=C); δ_H (400 MHz; $CDCl_3$) 1.77 (3H, s, C(18)H_3), 1.79 (3H, s, C(15)H_3), 2.25 (1H, dd, *J* 17.4,

12.7, C(12)H$_{ax}$), 2.39 (1H, dd, *J* 17.4, 3.8, C(12)H$_{eq}$), 2.39-2.52 (4H, m, C(2)H$_2$, C(8)H$_2$), 2.60-2.66 (2H, m, C(6)H and C(11)H), 2.84 (1H, td, *J* 10.0, 4.7, C(3)H), 3.36 (1H, dtd, *J* 12.9, 7.3, 2.9, C(9)H), 4.12 (1H, dd, *J* 10.0, 3.3, C(4)HOH), 4.25 (1H, dd, *J* 8.9, 7.3, C(10)H), 4.59 (1H, dd, *J* 5.3, 3.3, C(5)H), 4.82 (1H, s, one of C(17)H$_2$), 4.89 (1H, s, one of C(14)H$_2$), 4.90 (1H, s, one of C(17)H$_2$), 4.96 (1H, s, one of C(14)H$_2$); δ_C (100 MHz; $CDCl_3$) 19.5 (C(15)H$_3$), 20.6 (C(17)H$_3$), 37.1 (C(9)H), 40.3 (C(8)H$_2$), 41.2 (C(12)H$_2$), 43.0 (C(2)H$_2$), 44.5 (C(11)H), 45.6 (C(3)H), 56.7 (C(6)H), 70.2 (C(4)HOH), 78.5 (C(5)H), 79.0 (C(10)H), 113.1 (C(17)H$_2$), 114.2 (C(14)H$_2$), 143.6 (C(13)), 144.4 (C(16)), 207.1 (C(1)), 209.9 (C(7)); *m/z* (+ES) 327 ($[M+Na]^+$, 100 %); HRMS calculated for $C_{18}H_{24}O_4Na$, ($[M+Na]^+$): 327.1567, found: 327.1566.

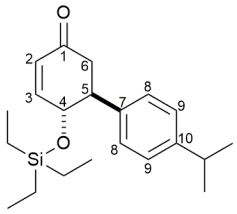

369

$C_{21}H_{32}O_2Si$; M_w = 344.57 g/mol

(1*S*,6*R*)-4'-Isopropyl-6-((triethylsilyl)oxy)-1,6-dihydro-[1,1'-biphenyl]-3(2H)-one (369):

2,6-Lutidine (0.12 mL, 110 mg, 1.03 mmol) and TESOTf (0.17 mL, 199 mg, 0.75 mmol) in CH_2Cl_2 (3 mL) were pre-mixed at -78 °C for 15 minutes under a N_2 atmosphere. A solution of the hydroxyketone ***ent*-266a** (96.0 mg, 0.33 mmol) in CH_2Cl_2 (3 mL) was added dropwise to the pre-mixed solution and the reaction mixture was stirred at -78 °C for 30 minutes. The reaction was quenched by the addition of sat. $NH_4Cl_{(aq)}$ (15 mL) and extracted with CH_2Cl_2 (3 × 50 mL). The organic layers were combined, dried over $MgSO_4$, filtered and concentrated *in vacuo* to give a brown oil. The crude product was purified by flash silica chromatography, eluting with 40-60 petroleum ether:CH_2Cl_2 (3:1 to 100 %) to afford the title compound **369** as a colourless oil (102 mg, 89 %). $[\alpha]_D^{25}$ -55.2 (*c* 1.00 in CH_2Cl_2); ν_{max} /cm^{-1} 2813w, 2749w (C-H), 1684s (C=O), 1534w (C=C); δ_H (400 MHz; $CDCl_3$) 0.19-0.39 (6H, m, (CH$_2$)$_3$ of TES), 0.73 (9H, t, *J* 7.9, (CH$_3$)$_3$ of TES), 1.22 (6H, d, *J* 6.9, (CH$_3$)$_2$ of isopropyl), 2.66 (1H, ddd, *J* 16.6, 4.4, 1.2, C(6)H$_{eq}$), 2.75 (1H, ddd, *J* 16.6, 13.4, C(6)H$_{ax}$), 2.88 (1H, hept, *J* 6.9, CH of isopropyl), 3.22 (1H, ddd, *J* 13.4, 9.3, 4.4, C(5)H), 4.51 (1H, dt, *J* 9.3, 2.0, C(4)H), 6.01 (1H, ddd, *J* 10.2, 2.0, 1.2, C(2)H), 6.83 (1H,

dd, *J* 10.2, 2.0, C(3)H), 7.16 (2H, d, *J* 8.7, C(8)H), 7.19 (2H, d, *J* 8.7, C(9)H); δ_C (100 MHz; $CDCl_3$) 4.5 ((CH_2)$_3$ of TES), 6.8 ((CH_3)$_3$ of TES), 24.2 ((CH_3)$_2$ of isopropyl), 34.0 (CH of isopropyl), 42.9 (C(6)H_2), 50.5 (C(5)H), 73.1 (C(4)H), 126.6 (C(9)H), 128.1 (C(8)H), 128.6 (C(2)H), 138.3 (C(7)), 148.3 (C(10)), 154.1 (C(3)H), 198.9 (C(1)); *m/z* (+ES) 367 ([M+Na]$^+$, 100 %); HRMS calculated for $C_{21}H_{33}O_2Si$, ([M+H]$^+$): 345.2244, found: 345.2245.

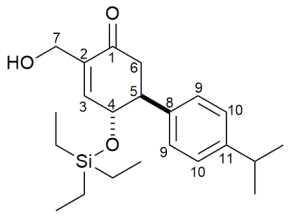

379

$C_{22}H_{34}O_3Si$; M_w = 374.60 g/mol

(1*S*,6*R*)-4-(Hydroxymethyl)-4'-isopropyl-6-((triethylsilyl)oxy)-1,6-dihydro-[1,1'-biphenyl]-3(2H)-one (379):

The TES enone **369** (50.0 mg, 0.15 mmol) was suspended in water (0.60 mL). SDS (12.0 mg, 0.04 mmol) was added to the suspension and was stirred at room temperature for 5 minutes to form an emulsion. DMAP (43.0 mg, 0.35 mmol) and formaldehyde (37 % in H_2O) (0.17 mL, 185 mg, 2.09 mmol) were added sequentially to the emulsion and the reaction mixture was stirred at room temperature for 18 hours under a N_2 atmosphere. The reaction was quenched by the addition of brine (5 mL) and extracted with EtOAc (3 × 20 mL). The organic layers were combined, dried over $MgSO_4$, filtered and concentrated *in vacuo* to give a brown solid. The crude product was purified by flash silica chromatography, eluting with 40-60 petroleum ether:acetone (10:1) to afford the title compound **379** as colourless crystals (41.0 mg, 75 %). m.p. 64-65 °C; $[\alpha]_D^{26}$ -102 (*c* 1.00 in CH_2Cl_2); ν_{max} /cm^{-1} 3410br (O-H), 2965w, 2923w, 2880w (C-H), 1673s (C=O), 1586w, 1574w (C=C); δ_H (400 MHz; $CDCl_3$) 0.18-0.36 (6H, m, (CH_2)$_3$ of TES), 0.74 (9H, t, *J* 7.9, (CH_3)$_3$ of TES), 1.23 (6H, d, *J* 6.9, (CH_3)$_2$ of isopropyl), 2.69 (1H, dd, *J* 16.6, 4.6, C(6)H_{eq}), 2.78 (1H, dd, *J* 16.6, 13.3, C(6)H_{ax}), 2.89 (1H, hept, *J* 6.9, CH of isopropyl), 3.21 (1H, ddd, *J* 13.3, 9.5, 4.6, C(5)H), 4.24 (1H, dt, *J* 13.5, 1.2, C(7)H_a), 4.37 (1H, dt, *J* 13.5, 1.2, C(7)H_b), 4.53 (1H, ddt, *J* 9.5, 2.2, 1.2, C(4)H), 6.75 (1H, dt, *J* 2.2, 1.2, C(3)H), 7.15 (2H, d, *J* 8.4, C(9)H), 7.19 (2H, d, *J* 8.4, C(10)H); δ_C (100 MHz; $CDCl_3$) 4.5 ((CH_2)$_3$ of TES), 6.8 ((CH_3)$_3$ of TES), 24.2 ((CH_3)$_2$ of isopropyl), 34.0 (CH of isopropyl), 43.1

(C(6)H_2), 50.5 (C(5)H), 61.6 (C(7)H_2), 73.1 (C(4)H), 126.6 (C(10)H), 128.1 (C(9)H), 137.0 (C(8)), 137.9 (C(2)), 148.4 (C(11)), 149.9 (C(3)H), 199.6 (C(1)); *m/z* (+ES) 375 ($[M+H]^+$, 100 %); HRMS calculated for $C_{22}H_{35}O_3Si$, ($[M+H]^+$): 375.2350, found: 375.2351.

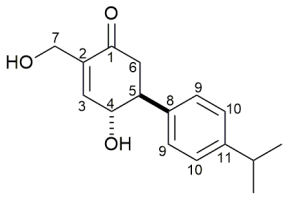

374

$C_{16}H_{20}O_3$; M_w = 260.33 g/mol

(1*S*,6*R*)-6-Hydroxy-4-(hydroxymethyl)-4'-isopropyl-1,6-dihydro-[1,1'-biphenyl]-3(2*H*)-one (374):

The hydroxylated enone **379** (85.0 mg, 0.23 mmol) was dissolved in TFA:H_2O (1.8 mL, 7:1) and placed under a N_2 atmosphere. The reaction mixture was stirred at room temperature for 30 minutes when it was concentrated *in vacuo* to give a brown oil. Purification by flash silica chromatography, eluting with 40-60 petroleum ether:EtOAc (1:1 to 100 %) afforded the title compound **374** as an off-white gum (20.0 mg, 39 %). m.p. 157-158 °C; $[\alpha]_D^{24}$ -78.7 (*c* 1.2 in CH_2Cl_2); ν_{max} /cm^{-1} 3022br (O-H), 2963w, 2924w, 2913w (C-H), 1676s (C=O), 1624w, 1528w (C=C); δ_H (400 MHz; $CDCl_3$) 1.25 (6H, d, *J* 6.9, (CH_3)$_2$ isopropyl), 2.68-2.73 (2H, m, C(6)H_2), 2.91 (1H, hept, *J* 6.9, CH of isopropyl), 3.21 (1H, ddd, *J* 11.3, 9.9, 6.8, C(5)H), 4.29 (1H, d, *J* 13.7, C(7)H_a), 4.37 (1H, d, *J* 13.7, C(7)H_b), 4.68 (1H, dd, *J* 9.9, 1.9, C(4)HOH), 6.93-6.95 (1H, m, C(3)H), 7.21 (2H, d, *J* 8.1, C(9)H), 7.25 (2H, d, *J* 8.1, C(10)H); δ_C (100 MHz; $CDCl_3$) 24.1 ((CH_3)$_2$ of isopropyl), 33.9 (CH of isopropyl), 43.5 (C(6)H_2), 50.5 (C(5)H), 61.3 (C(7)H_2), 72.1 (C(4)HOH), 127.4 (C(10)H), 127.7 (C(9)H), 136.5 (C(8)), 137.7 (C(2)), 148.0 (C(3)H), 148.8 (C(11)), 199.0 (C(1)); *m/z* (+ES) 283 ($[M+Na]^+$, 100 %); HRMS calculated for $C_{16}H_{20}O_3Na$, ($[M+Na]^+$): 283.1305, found: 283.1293.

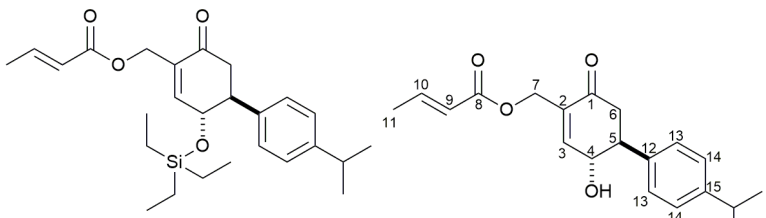

391 375

$C_{20}H_{24}O_4$; M_w = 328.41 g/mol

((1*S*,6*R*)-6-Hydroxy-4'-isopropyl-3-oxo-1,2,3,6-tetrahydro-[1,1'-biphenyl]-4-yl)methyl (*E*)-but-2-enoate (375):

The hydroxylated enone **379** (121 mg, 0.32 mmol) was dissolved in CH_2Cl_2 (3.2 mL). Crotonic anhydride (0.11 mL, 114 mg, 0.74 mmol), DMAP (4.0 mg, 0.03 mmol) and pyridine (0.24 mL, 235 mg, 2.97 mmol) were added sequentially to the solution and the reaction mixture was stirred at room temperature for 5 hours under a N_2 atmosphere. The reaction was quenched by the addition of sat. $NaHCO_{3(aq)}$ (10 mL) and extracted with CH_2Cl_2 (3 × 40 mL). The organic layers were combined, dried over $MgSO_4$, filtered and concentrated *in vacuo* to give a brown solid. The crude product was purified by flash silica chromatography, eluting with 40-60 petroleum ether:acetone (24:1) to afford the crude compound **391** as an off-white solid (98.0 mg), which was carried through to the next step.

The crotonylated TES enone **391** (98.0 mg, 0.22 mmol) was dissolved in TFA:H_2O (1.8 mL, 7:1) and placed under a N_2 atmosphere. The reaction mixture was stirred at room temperature for 30 minutes when it was concentrated *in vacuo* to give a brown oil. Purification by flash silica chromatography, eluting with hexane:EtOAc (7:1) afforded the title compound **375** as a colourless oil (54.0 mg, 51 % over two steps). $[\alpha]_D^{30}$ -64.0 (*c* 1.6 in CH_2Cl_2); ν_{max} /cm^{-1} 3430br (O-H), 2991w, 2962w, 2926w (C-H), 1723s (C=O), 1681s (C=O), 1679m, 1624w (C=C); (400 MHz; $CDCl_3$) 1.26 (6H, d, *J* 6.9, (C$\underline{H}_3$)$_2$ of isopropyl), 1.90 (3H, dd, *J* 6.9, 1.8, C(11)$\underline{H}_3$), 1.99 (1H, br s, C(4)HO$\underline{H}$), 2.71-2.74 (2H, m, C(6)$\underline{H}_2$), 2.92 (1H, hept, *J* 6.9, C$\underline{H}$ of isopropyl), 3.22 (1H, ddd, *J* 18.1, 9.8, 8.3, C(5)$\underline{H}$), 4.68 (1H, dd, *J* 9.8, 2.4, C(4)$\underline{H}$OH), 4.84 (1H, d, *J* 14.3, C(7)$\underline{H}_a$), 4.91 (1H, d, *J* 14.3, C(7)$\underline{H}_b$), 5.89 (1H, dq, *J* 15.6, 1.8, C(9)$\underline{H}$), 6.95 (1H, d, *J* 2.4, C(3)$\underline{H}$), 7.04 (1H, dq, *J* 15.6, 6.9, C(10)$\underline{H}$), 7.21 (2H, d, *J* 8.3, C(13)$\underline{H}$), 7.26 (2H, d, *J* 8.3, C(14)$\underline{H}$); δ_C (100 MHz; $CDCl_3$) 18.3 (C(11)$\underline{C}H_3$), 24.1 ((C$\underline{H}_3$)$_2$ of isopropyl), 33.9 (C$\underline{H}$ of isopropyl), 43.4 (C(6)$\underline{C}H_2$), 50.4 (C(5)$\underline{C}$H), 60.3 (C(7)$\underline{C}H_2$), 72.1 (C(4)$\underline{C}$HOH), 122.3 (C(9)$\underline{C}$H), 127.4 (C(14)$\underline{C}$H), 127.7 (C(13)$\underline{C}$H), 134.2 (C(2)$\underline{C}$), 136.5 (C(12)$\underline{C}$), 145.9 (C(10)$\underline{C}$H), 148.3 (C(3)$\underline{C}$H), 148.8 (C(15)$\underline{C}$), 166.1 (C(8)$\underline{C}$),

196.7 (C(1)); *m/z* (+ES) 351 ([M+Na]$^+$, 100 %); HRMS calculated for $C_{20}H_{24}O_4Na$, ([M+Na]$^+$): 351.1567, found: 351.1553.

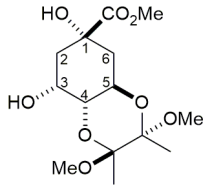

195

$C_{14}H_{24}O_8$; M_w = 320.34 g/mol

Methyl (2*S*,3*S*,4a*R*,6*S*,8*R*,8a*R*)-6,8-dihydroxy-2,3-dimethoxy-2,3-dimethyloctahydrobenzo[b][1,4]dioxine-6-carboxylate (195):

(-)-Quinic acid (5.00 g, 26.0 mmol) was dissolved in MeOH (125 mL). Butan-2,3-dione (5.48 mL, 5.37 g, 62.4 mmol), trimethylorthoformate (22.8 mL, 22.1 g, 208 mmol) and camphorsulfonic acid (664 mg, 2.86 mmol) were added sequentially and the reaction mixture was heated at reflux and stirred for 18 hours under a N_2 atmosphere. The reaction mixture was allowed to cool to room temperature and was quenched by the addition of triethylamine (7 mL). The reaction mixture was concentrated *in vacuo* and solubilised in EtOAc (30.0 mL). The solution was decolourised with activated charcoal and filtered through Celite®. The organic filtrate was concentrated *in vacuo* to give a tan solid, which was recrystallised from hot EtOAc:cold 40-60 petroleum ether (1:1) to afford the title compound **195** as an off-white solid (7.36 g, 88 %). m.p. 137-138 °C [Lit.[190] 138-140 °C]; $[\alpha]_D^{25}$ +105 (*c* 1.00 in CH_2Cl_2) [Lit.[190] $[\alpha]_D^{20}$ +116 (*c* 1.06 in CH_2Cl_2)]; δ_H (400 MHz; $CDCl_3$) 1.30 (3H, s, C$\underline{H}_3$ of BDA), 1.34 (3H, s, C$\underline{H}_3$ of BDA), 1.92 (1H, t, *J* 12.6, C(6)$\underline{H}_{ax}$), 2.04 (1H, ddd, *J* 14.8, 3.0, 1.2, one of C(2)$\underline{H}_2$), 2.10 (1H, ddd, *J* 12.6, 4.6, 3.0, C(6)$\underline{H}_{eq}$), 2.18 (1H, dt, *J* 14.8, 3.0, one of C(2)$\underline{H}_2$), 3.06 (1H, dd, *J* 3.5, 1.2, C(3)HO$\underline{H}$), 3.26 (3H, s, OC$\underline{H}_3$ of BDA), 3.26 (3H, s, OC$\underline{H}_3$ of BDA), 3.62 (1H, dd, *J* 10.1, 2.9, C(4)$\underline{H}$), 3.79 (3H, s, C(1)$CO_2C\underline{H}_3$), 4.14-4.22 (1H, m, C(3)$\underline{H}$OH), 4.20 (1H, s, C(1)O$\underline{H}$), 4.31 (1H, ddd, *J* 12.6, 10.1, 4.6, C(5)$\underline{H}$); δ_C (100 MHz; $CDCl_3$) 17.9 ($\underline{C}H_3$ of BDA), 18.0 ($\underline{C}H_3$ of BDA), 37.6 ($\underline{C}$(2)H_2), 38.8 ($\underline{C}$(6)H_2), 48.1 (O$\underline{C}H_3$ of BDA), 48.1 (O$\underline{C}H_3$ of BDA), 53.1 (C(1)$CO_2\underline{C}H_3$), 62.6 ($\underline{C}$(5)H), 69.4 ($\underline{C}$(3)HOH), 72.9 ($\underline{C}$(4)H), 76.0 ($\underline{C}$(1)OH), 100.0 ($\underline{C}$ of BDA), 100.5 ($\underline{C}$ of BDA), 174.5 ($\underline{C}$=O); *m/z* (+ES) 343 ([M+Na]$^+$, 100 %).

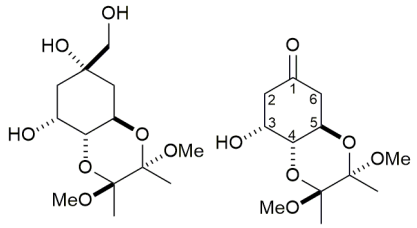

$C_{12}H_{20}O_6$; M_w = 260.29 g/mol

(2*S*,3*S*,4a*R*,8*R*,8a*R*)-8-Hydroxy-2,3-dimethoxy-2,3-dimethylhexahydrobenzo[b][1,4]dioxin-6(5H)-one (318):

The BDA ester **195** (7.35 g, 23.0 mmol) was dissolved in MeOH (150 mL) and the solution was cooled to 0 °C. Sodium borohydride (8.68 g, 230 mmol) was added portion-wise to the solution and then stirred until effervescence ceased. The reaction mixture was allowed to warm up to room temperature and was stirred for 20 hours under a N_2 atmosphere. The reaction was quenched by the addition of sat. $NH_4Cl_{(aq)}$ (50 mL) and concentrated *in vacuo* to give a crude white solid. The organic material was extracted from the solid by washing with EtOAc (250 mL) and the organic filtrate was dried over $MgSO_4$, filtered and concentrated *in vacuo* to afford crude triol **311** as a white, foamy solid, which was carried through to the next step.

To a solution of sodium *meta*-periodate (12.3 g, 57.4 mmol) in hot water (42 mL) was added silica gel (32.0 g). The resulting slurry was mixed until a free-flowing powder was obtained. To the resulting powder were added CH_2Cl_2 (50 mL) and a solution of crude triol **311** (6.71 g, 23.0 mmol) in CH_2Cl_2 (100 mL). The reaction mixture was stirred at room temperature for 2 hours under a N_2 atmosphere. The silica was removed by filtration and washed with CH_2Cl_2 (250 mL). The organic filtrate was dried over $MgSO_4$, filtered and concentrated *in vacuo* to afford the title compound **318** as an off-white solid (3.83 g, 64 % over two steps). m.p. 150-151 °C [Lit.[191] 163-165 °C]; $[\alpha]_D^{25}$ +136 (*c* 1.00 in CH_2Cl_2) [Lit.[191] $[\alpha]_D^{20}$ +160 (*c* 0.59 in CH_2Cl_2)]; δ_H (400 MHz; $CDCl_3$) 1.30 (3H, s, C$\underline{H}_3$ of BDA), 1.34 (3H, s, C$\underline{H}_3$ of BDA), 2.49-2.52 (3H, m, one of C(2)$\underline{H}_2$, one of C(6)$\underline{H}_2$ and C(3)HO$\underline{H}$), 2.63-2.68 (2H, m, one of C(2)$\underline{H}_2$ and C(6)$\underline{H}_2$), 3.23 (3H, s, OC$\underline{H}_3$ of BDA), 3.30 (3H, s, OC$\underline{H}_3$ of BDA), 3.88 (1H, dd, *J* 9.9, 2.5, C(4)$\underline{H}$), 4.23-4.31 (2H, m, C(3)$\underline{H}$OH and C(5)$\underline{H}$); δ_C (100 MHz; $CDCl_3$) 17.7 ($\underline{C}H_3$ of BDA), 17.9 ($\underline{C}H_3$ of BDA), 44.9 ($\underline{C}$(2)H_2 or $\underline{C}$(6)H_2), 46.3 ($\underline{C}$(2)H_2 or $\underline{C}$(6)H_2), 48.1 (O$\underline{C}H_3$ of BDA), 48.3 (O$\underline{C}H_3$ of BDA), 63.4

(C(3)HOH or C(5)H), 67.8 (C(3)HOH or C(5)H), 72.4 (C(4)H), 99.4 (C of BDA), 100.4 (C of BDA), 205.6 (C(1)); *m/z* (+ES) 283 ([M+Na]$^+$, 100 %).

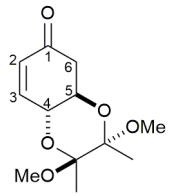

285

$C_{12}H_{18}O_5$; M_w = 242.27 g/mol

(2*S*,3*S*,4a*R*,8a*R*)-2,3-Dimethoxy-2,3-dimethyl-2,3,4a,8a-tetrahydrobenzo[b][1,4]dioxin-6(5H)-one (285):

The hydroxyketone **318** (932 mg, 3.58 mmol) was dissolved in CH_2Cl_2 (20 mL) and the solution was cooled to 0 °C. Methanesulfonyl chloride (0.33 mL, 488 mg, 4.26 mmol) and triethylamine (1.30 mL, 942 mg, 9.31 mmol) were added sequentially to the solution and the reaction mixture was stirred at room temperature for 4 hours under a N_2 atmosphere. The reaction was quenched by the addition of distilled water (50 mL) and partitioned with CH_2Cl_2 (50 mL). The organic layer was separated, and the aqueous layer was extracted with CH_2Cl_2 (2 × 50 mL). The organic layers were combined, dried over $MgSO_4$, filtered and concentrated *in vacuo* to give a brown oil. The crude product was purified by flash silica chromatography, eluting with 40-60 petroleum ether:EtOAc (4:1) to afford the title compound **285** as a white solid (718 mg, 83 %). m.p. 181-182 °C [Lit.[191] 182-184 °C]; $[\alpha]_D^{26}$ +62.8 (*c* 1.00 in CH_2Cl_2) [Lit.[191] $[\alpha]_D^{20}$ +64.4 (*c* 0.39 in CH_2Cl_2)]; δ_H (400 MHz; $CDCl_3$) 1.33 (3H, s, C$\underline{H}_3$ of BDA), 1.37 (3H, s, C$\underline{H}_3$ of BDA), 2.49 (1H, dd, *J* 16.4, 13.5, C(6)$\underline{H}_{ax}$), 2.74 (1H, ddd, *J* 16.4, 4.9, 1.2, C(6)$\underline{H}_{eq}$), 3.26 (3H, s, OC$\underline{H}_3$ of BDA), 3.32 (3H, s, OC$\underline{H}_3$ of BDA), 4.05 (1H, ddd, *J* 13.5, 9.1, 4.9, C(5)$\underline{H}$), 4.50 (1H, ddd, *J* 9.1, 2.8, 1.7, C(4)$\underline{H}$), 6.00 (1H, ddd, *J* 10.1, 2.8, 1.2, C(2)$\underline{H}$), 6.87 (1H, dd, *J* 10.1, 1.7, C(3)$\underline{H}$); δ_C (100 MHz; $CDCl_3$) 17.8 (C$\underline{H}_3$ of BDA), 17.9 (C$\underline{H}_3$ of BDA), 42.2 (C(6)$\underline{C}H_2$), 48.3 (OC$\underline{H}_3$ of BDA), 48.4 (OC$\underline{H}_3$ of BDA), 68.2 (C(5)$\underline{C}$H), 69.4 (C(4)$\underline{C}$H), 99.8 (C of BDA), 100.9 (C of BDA), 130.2 (C(2)$\underline{C}$H), 148.7 (C(3)$\underline{C}$H), 197.0 (C(1)$\underline{C}$); *m/z* (+ES) 265 ([M+Na]$^+$, 100 %).

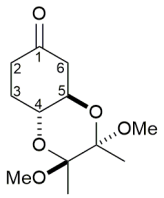

350

$C_{12}H_{20}O_5$; M_w = 244.29 g/mol

(2*S*,3*S*,4a*R*,8a*R*)-2,3-Dimethoxy-2,3-dimethylhexahydrobenzo[b][1,4]dioxin-6(5H)-one (350):

The BDA enone **285** (400 mg, 1.65 mmol) was dissolved in EtOAc (34 mL). 5 % Pd on carbon (64.0 mg) was added to the solution and the reaction mixture was placed under a H_2 atmosphere and was stirred at room temperature for 18 hours. The reaction mixture was filtered through Celite® and the organic filtrate was evaporated to afford the title compound **350** as colourless crystals (319 mg, 79 %). m.p. 158-159 °C; $[\alpha]_D^{16}$ +168 (*c* 0.4 in CH_2Cl_2) [Lit.[191] $[\alpha]_D^{20}$ +153 (*c* 0.49 in CH_2Cl_2)]; ν_{max} /cm^{-1} 2955w, 2889w, 2833w (C-H), 1718s (C=O); δ_H (400 MHz; $CDCl_3$) 1.32 (3H, s, C$\underline{H}_3$ of BDA), 1.33 (3H, s, C$\underline{H}_3$ of BDA), 1.68 (1H, ddd, *J* 13.3, 11.9, 5.2, C(3)$\underline{H}_{ax}$) 2.03 (1H, dddd, *J* 13.3, 6.5, 4.3, 2.4, C(3)$\underline{H}_{eq}$), 2.34 (1H, dd, *J* 15.6, 6.5, one of C(2)$\underline{H}_2$), 2.46 (1H, ddt, *J* 15.6, 5.2, 2.4, one of C(2)$\underline{H}_2$), 2.50-2.54 (1H, m, C(6)$\underline{H}_{ax}$), 2.60 (1H, ddd, *J* 14.3, 5.4, 2.4, C(6)$\underline{H}_{eq}$), 3.24 (3H, s, OC$\underline{H}_3$ of BDA), 3.32 (3H, s, OC$\underline{H}_3$ of BDA), 3.75 (1H, ddd, *J* 12.6, 9.6, 5.4, C(5)$\underline{H}$), 3.89 (1H, ddd, *J* 11.9, 9.6, 4.3, C(4)$\underline{H}$); δ_C (100 MHz; $CDCl_3$) 17.85 (C$\underline{H}_3$ of BDA), 17.91 (C$\underline{H}_3$ of BDA), 25.9 (C$\underline{(3)}H_2$), 39.3 (C$\underline{(2)}H_2$), 44.9 (C$\underline{(6)}H_2$), 48.18 (OC$\underline{H}_3$ of BDA), 48.24 (OC$\underline{H}_3$ of BDA), 68.9 (C$\underline{(5)}$H), 69.9 (C$\underline{(4)}$H), 99.4 (C$\underline{}$ of BDA), 99.8 (C$\underline{}$ of BDA), 207.1 (C$\underline{(1)}$); *m/z* (-ES) 261 ($[M-H+H_2O]^-$, 100 %); HRMS calculated for $C_{13}H_{24}O_6Na$, ($[M+Na+MeOH]^+$): 299.1465, found: 299.1463.

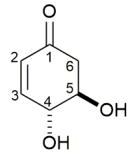

287

$C_6H_8O_3$; M_w = 128.13 g/mol

(4*R*,5*R*)-4,5-Dihydroxycyclohex-2-en-1-one (287):

The BDA enone **285** (300 mg, 1.24 mmol) was dissolved in CH_2Cl_2 (5 mL). TFA (0.19 mL, 281 mg, 2.46 mmol) and distilled water (0.03 µL, 30.0 mg, 1.67 mmol) were added to the solution and the reaction mixture was stirred at room temperature for 18 hours under a N_2 atmosphere. The reaction mixture was loaded directly onto silica and purified by flash silica chromatography, eluting with 100 % EtOAc to afford a colourless oil. To the resulting crude oil was added Et_2O (100 mL), which was evaporated *in vacuo* to afford the title compound **287** as a white solid (111 mg, 70 %). m.p. 93-94 ºC; $[\alpha]_D^{28}$ -141 (*c* 2.00 in MeOH); ν_{max} /cm^{-1} 3268br (O-H), 2947w, 2837w (C-H), 1666s (C=O), 1521w (C=C); δ_H (400 MHz; $CDCl_3$) 2.45 (1H, dd, *J* 16.3, 12.3, C(6)H$_{ax}$), 2.86 (1H, ddd, *J* 16.3, 4.9, 1.3, C(6)H$_{eq}$), 4.00 (1H, ddd, *J* 12.3, 8.4, 4.9, C(5)HOH), 4.42 (1H, dt, *J* 8.4, 2.2, C(4)HOH), 6.02 (1H, ddd, *J* 10.2, 2.2, 1.3, C(2)H), 6.87 (1H, dd, *J* 10.2, 2.2, C(3)H); δ_C (100 MHz; $CDCl_3$) 44.7 (C(6)H_2), 73.0 (C(5)HOH), 73.2 (C(4)HOH), 130.0 (C(2)H), 150.0 (C(3)H), 196.0 (C(1)); *m/z* (+ES) 139 (100 %), 151 ([M+Na]$^+$, 90 %); HRMS calculated for $C_6H_9O_3$, ([M+H]$^+$): 129.0551, found: 129.0548.

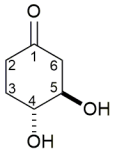

288

$C_6H_{10}O_3$; M_w = 130.14 g/mol

(3*R*,4*R*)-3,4-Dihydroxycyclohexan-1-one (288):

The enone diol **287** (98.0 mg, 0.77 mmol) was dissolved in EtOAc (16 mL). 5 % Pd on carbon (30.0 mg) was added to the solution and the reaction mixture was placed under a H_2 atmosphere and was stirred at room temperature for 18 hours. The reaction mixture was filtered through Celite® and the organic filtrate was evaporated to afford the title compound **288** as colourless crystals (65.0 mg, 65 %). m.p. 85-86 °C; $[\alpha]_D^{27}$ -24.8 (*c* 0.5 in MeOH); ν_{max} /cm^{-1} 3350br (O-H), 2972w, 2932w, 2909w (C-H), 1688s (C=O); δ_H (400 MHz; CD_3OD) 1.74-1.85 (1H, m, C(3)H$_{eq}$), 2.18 (1H, dddd, *J* 14.1, 9.1, 5.4, 3.3, C(3)H$_{ax}$),

2.29 (1H, dddd, *J* 14.7, 7.2, 5.4, 1.8, C(2)H$_{eq}$), 2.35 (1H, ddd, *J* 14.5, 6.5, 1.8, C(6)H$_{ax}$), 2.53 (1H, dddd, *J* 14.7, 9.1, 5.7, 1.6, C(2)H$_{ax}$), 2.76 (1H, ddd, *J* 14.5, 4.3, 1.6, C(6)H$_{eq}$), 3.83 (1H, dt, *J* 6.1, 3.3, C(4)HOH), 3.91-3.95 (1H, m C(5)HOH); δ_C (100 MHz; CD_3OD) 29.2 (C(3)H_2), 38.0 (C(2)H_2), 46.5 (C(6)H_2), 71.0 (C(4)HOH), 74.1 (C(5)HOH), 212.2 (C(1)); *m/z* (+APCI) 113 ([M-OH]$^+$, 100 %); HRMS calculated for $C_6H_{11}O_3$, ([M+H]$^+$): 131.0703, found: 131.0700.

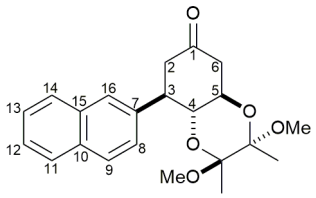

286b

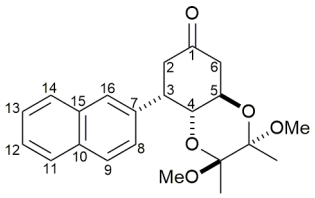

336b

$C_{22}H_{26}O_5$; M_w = 370.44 g/mol

(2*S*,3*S*,4a*R*,8*R*,8a*R*)-2,3-Dimethoxy-2,3-dimethyl-8-(naphthalen-2-yl)hexahydrobenzo[b][1,4]dioxin-6(5*H*)-one (286b):

The enone **285** (500 mg, 2.06 mmol) was dissolved in dioxane:water (15 mL, 10:1). 2-Naphthylboronic acid (1.06 g, 6.18 mmol), triethylamine (0.29 mL, 211 mg, 2.08 mmol) and $[RhCl(cod)]_2$ (49.0 mg, 0.10 mmol) were added sequentially. The reaction mixture was stirred at room temperature for 18 hours under a N_2 atmosphere when it was concentrated *in vacuo* to give a brown solid. The resulting crude product was purified by flash silica chromatography, eluting with 5 % (3:1, EtOAc:EtOH) in 40-60 petroleum ether to afford a 3:1 mixture of *syn*:*anti* diastereoisomers **336b** and **286b** as an off-white solid. The diastereoisomers were separated by normal phase preparative HPLC using an Ace 10 Sil column, eluting with hexane:EtOAc (4:1) to afford the titled products **336b** (287 mg, 38 %) and **286b** (150 mg, 20 %) as white solids. *Syn* R_t = 15.6 min, *Anti* R_t = 16 min.

Data for 286b:

m.p. 214-215 °C; $[\alpha]_D^{28}$ +201 (*c* 0.3 in CH_2Cl_2); ν_{max} /cm^{-1} 3051w, 3028w, 2966w, 2925w, 2883w, 2842w (C-H), 1712s (C=O), 1601w, 1503w (C=C aromatic); δ_H (400 MHz; $CDCl_3$) 1.12 (3H, s, CH$_3$ of BDA), 1.30 (3H, s, CH$_3$ of BDA), 2.64 (1H, dd, *J* 15.2, 5.2, C(2)H$_{eq}$), 2.69-2.80 (3H, m, C(2)H$_{ax}$ and C(6)H$_2$), 2.94 (3H, s, OCH$_3$ of BDA), 3.17 (1H, dd, *J* 12.1, 10.1, 5.2, C(3)H), 3.28 (3H, s, OCH$_3$ of BDA), 3.99 (1H, ddd, *J* 11.1, 10.1, 7.6,

C(5)H), 4.26 (1H, t, *J* 10.1, C(4)H), 7.43 (1H, d, *J* 8.7, C(8)H), 7.46-7.50 (2H, m, C(12)H and C(14)H), 7.72 (1H, s, C(16)H), 7.78-7.80 (1H, m, C(13)H), 7.82-7.84 (2H, C(9)H and C(11)H); δ_C (100 MHz; $CDCl_3$) 17.7 (CH_3 of BDA), 17.8 (CH_3 of BDA), 43.5 (C(3)H), 45.2 ($C(6)H_2$), 47.8 ($C(2)H_2$), 48.2 (OCH_3 of BDA), 48.2 (OCH_3 of BDA), 68.7 (C(5)H), 73.5 (C(4)H), 99.7 (C of BDA), 100.0 (C of BDA), 125.2 (Ar-CH), 125.9 (Ar-CH), 126.3 (Ar-CH), 127.1 (Ar-CH), 127.8 (Ar-CH), 127.8 (Ar-CH), 128.3 (Ar-CH), 132.8 (C(15)), 133.5 (C(10)), 137.3 (C(7)), 205.7 (C(1)); *m/z* (+ES) 149 (100 %), 371 ($[M+H]^+$, 40 %); HRMS calculated for $C_{22}H_{27}O_5$, ($[M+H]^+$): 371.1853, found: 371.1852.

Data for 336b:

m.p. 103-105 °C; $[\alpha]_D^{28}$ +19.3 (*c* 0.5 in CH_2Cl_2); ν_{max} /cm^{-1} 3057w, 2951w, 2831w (C-H), 1713s (C=O), 1601w, 1506w (C=C aromatic); δ_H (400 MHz; $CDCl_3$) 1.23 (3H, s, CH_3 of BDA), 1.27 (3H, s, CH_3 of BDA), 2.60 (1H, dd, *J* 15.4, 12.0, C(6)H_{ax}), 2.71-2.76 (1H, m, C(6)H_{eq}), 2.86 (1H, dd, *J* 16.0, 6.5, one of $C(2)H_2$), 2.91 (1H, s, OCH_3 of BDA), 3.03 (1H, d, *J* 16.0, one of $C(2)H_2$), 3.41 (1H, s, OCH_3 of BDA), 3.69 (1H, t, *J* 6.5, C(3)H), 3.81 (1H, td, *J* 12.0, 6.5, C(5)H), 4.25 (1H, dd, *J* 12.0, 6.5, C(4)H), 7.44-7.47 (2H, m, C(12)H and C(13)H), 7.48 (1H, d, *J* 8.5, C(8)H), 7.59 (1H, s, C(16)H), 7.74 (1H, d, *J* 8.5, C(9)H), 7.79 (1H, d, *J* 5.0, C(12)H), 7.81 (1H, d, *J* 5.0, C(14)H); δ_C (100 MHz; $CDCl_3$) 17.7 (CH_3 of BDA), 17.8 (CH_3 of BDA), 40.8 (C(3)H), 45.2 ($C(2)H_2$), 45.4 ($C(6)H_2$), 47.8 (OCH_3 of BDA), 48.3 (OCH_3 of BDA), 63.9 (C(5)H), 71.8 (C(4)H), 98.9 (C of BDA), 99.9 (C of BDA), 125.8 (Ar-CH), 125.9 (Ar-CH), 127.2 (Ar-CH), 127.2 (Ar-CH), 127.5 (Ar-CH), 128.2 (Ar-CH), 128.5 (Ar-CH), 132.4 (C(15)), 133.1 (C(10)), 137.0 (C(7)), 208.3 (C(1)); *m/z* (+ES) 221 (100 %), 393 ($[M+Na]^+$, 60 %); HRMS calculated for $C_{22}H_{26}O_5Na$, ($[M+Na]^+$): 393.1672, found: 393.1663.

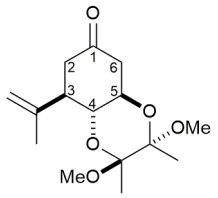

286c

$C_{15}H_{24}O_5$; M_w = 284.35 g/mol

(2*S*,3*S*,4a*R*,8*R*,8a*R*)-2,3-dimethoxy-2,3-dimethyl-8-(prop-1-en-2-yl)hexahydrobenzo[*b*][1,4]dioxin-6(5*H*)-one (286c):

Copper iodide (588 mg, 3.09 mmol) was stored in an oven dried flask under vacuum for 1 hour and suspended in anhydrous THF (9 mL). The suspension was placed under a N_2 atmosphere and cooled to -42 °C using a dry ice/acetonitrile cooling bath. Isopropenyl magnesium bromide (0.5 M in THF) (12.4 mL, 11.6 g, 6.18 mmol) was added drop-wise to the suspension, which was stirred at -42 °C for 1 hour to form the Gilman cuprate. To the cuprate mixture was added chlorotrimethylsilane (1.31 mL, 1.12 g, 10.3 mmol), followed by the drop-wise addition of a solution of enone **285** (500 mg, 2.06 mmol) in anhydrous THF (9 mL). The reaction mixture was stirred at -42 °C for 3 hours when it was quenched by the addition of sat. $NH_4Cl_{(aq)}$:$NH_{3(aq)}$ (20 mL, 9:1) and extracted with Et_2O (3 × 50 mL). The combined organic extracts were washed with brine (50 mL), dried over $MgSO_4$, filtered and concentration *in vacuo* to afford a colourless oil. The crude product was purified by flash silica chromatography, eluting with 40-60 petroleum ether:EtOAc (5:1) to afford the title compound **286c** as a colourless solid (298 mg, 51 %). m.p. 109-110 °C; $[\alpha]_D^{22}$ +198 (*c* 1.15 in CH_2Cl_2); ν_{max} /cm^{-1} 3585br (O-H), 2993w, 2981w, 2948w, 2916w (C-H stretch), 1719s (C=O), 1651w (C=C); δ_H (400 MHz; $CDCl_3$) 1.31 (6H, s, 2 × C$\underline{H}_3$ of BDA), 1.79 (3H, s, C$\underline{H}_3$ of isopropenyl), 2.29 (1H, dd, *J* 12.3, 4.8, C(2)$\underline{H}_{eq}$), 2.35 (1H, t, *J* 12.3, C(2)$\underline{H}_{ax}$), 2.42 (1H, ddd, *J* 12.3, 9.8, 4.8, C(3)$\underline{H}$), 2.51-2.53 (2H, m, C(6)$\underline{H}_2$), 3.24 (3H, s, OC$\underline{H}_3$ of BDA), 3.29 (3H, s, OC$\underline{H}_3$ of BDA), 3.75 (1H, ddd, *J* 10.9, 9.8, 7.4, C(5)$\underline{H}$), 3.84 (1H, t, *J* 9.8, C(4)$\underline{H}$), 4.88 (1H, s, one of C$\underline{H}_2$ of isopropenyl), 4.92 (1H, s, one of C$\underline{H}_2$ of isopropenyl); δ_C (100 MHz; $CDCl_3$) 17.9 (2 × $\underline{C}H_3$ of BDA), 20.3 ($\underline{C}H_3$ of isopropenyl), 44.3 ($\underline{C}$(3)H), 45.0 ($\underline{C}$(6)H_2), 45.4 ($\underline{C}$(2)H_2), 48.2 (O$\underline{C}H_3$ of BDA), 48.5 (O$\underline{C}H_3$ of BDA), 68.6 ($\underline{C}$(5)H), 72.3 ($\underline{C}$(4)H), 99.6 ($\underline{C}$ of BDA), 99.9 ($\underline{C}$ of BDA), 113.3 ($\underline{C}H_2$ of isopropenyl), 143.2 ($\underline{C}$ of isopropenyl), 206.5 ($\underline{C}$(1)); *m/z* (-ES) 283 ([M-H]$^-$, 100 %); HRMS calculated for $C_{15}H_{28}O_5N$, ([M+NH_4]$^+$): 302.1962, found: 302.1948.

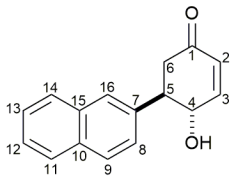

266b

$C_{16}H_{14}O_2$; M_w = 238.29 g/mol

(4*S*,5*R*)-4-Hydroxy-5-(naphthalen-2-yl)cyclohex-2-en-1-one (266b):

The conjugate adduct **286b** (133 mg, 0.36 mmol) was dissolved in CH_2Cl_2 (1 mL). TFA (0.15 mL, 222 mg, 1.94 mmol) and distilled water (0.01 mL, 10.0 mg, 0.56 mmol) were added to the solution and the reaction mixture was stirred at room temperature for 18 hours under a N_2 atmosphere, when it was concentrated *in vacuo* to give a brown oil. The crude product was purified by flash silica chromatography, eluting with 10 % (3:1, EtOAc:EtOH) in 40-60 petroleum ether to afford the title compound **266b** as a colourless oil (53.0 mg, 62 %). $[\alpha]_D^{25}$ +93.6 (*c* 0.5 in CH_2Cl_2); ν_{max} /cm^{-1} 3379br (O-H), 3055w, 2922w (C-H), 1668s (C=O), 1600w, 1509w (C=C); δ_H (400 MHz; $CDCl_3$) 2.77 (1H, ddd, *J* 16.6, 4.9, 1.1, C(6)$\underline{H}_{eq}$), 2.84 (1H, dd, *J* 16.6, 13.1, C(6)$\underline{H}_{ax}$), 3.43 (1H, ddd, *J* 13.1, 9.8, 4.9, C(5)$\underline{H}$), 4.81 (1H, dt, *J* 9.8, 2.1, C(4)$\underline{H}$OH), 6.12 (1H, ddd, *J* 10.3, 2.1, 1.1, C(2)$\underline{H}$), 7.05 (1H, dd, *J* 10.3, 2.1, C(3)$\underline{H}$), 7.43 (1H, dd, *J* 8.5, 1.9, C(8)$\underline{H}$), 7.52 (1H, t, *J* 6.0, C(12)$\underline{H}$), 7.52 (1H, d, *J* 7.3, C(14)$\underline{H}$), 7.76 (1H, s, C(16)$\underline{H}$), 7.83-7.87 (2H, m, C(11)$\underline{H}$ and C(13)$\underline{H}$), 7.90 (1H, d, *J* 8.5, C(9)$\underline{H}$); δ_C (100 MHz; $CDCl_3$) 43.2 ($\underline{C}$(6)H_2), 51.1 ($\underline{C}$(5)H), 72.0 ($\underline{C}$(4)HOH), 125.1 ($\underline{C}$(8)H), 126.5 ($\underline{C}$(12)H or $\underline{C}$(14)H), 126.8 ($\underline{C}$(12)H or $\underline{C}$(14)H), 127.2 ($\underline{C}$(16)H), 127.9 ($\underline{C}$(11)H or $\underline{C}$(13)H), 127.9 ($\underline{C}$(11)H or $\underline{C}$(13)H), 129.2 ($\underline{C}$(2)H), 129.3 ($\underline{C}$(9)H), 133.1 ($\underline{C}$(15)), 133.6 ($\underline{C}$(10)), 136.7 ($\underline{C}$(7)), 152.4 ($\underline{C}$(3)H), 198.4 ($\underline{C}$(1)); *m/z* (+ES) 261 ([M+Na]$^+$, 30 %), 283 ([M+2Na-H]$^+$, 100 %); HRMS calculated for $C_{16}H_{15}O_2$, ([M+H]$^+$): 239.1067, found: 239.1058.

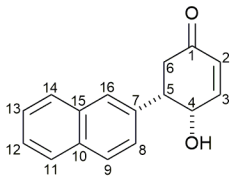

353

$C_{16}H_{14}O_2$; M_w = 238.29 g/mol

(4*S*,5*S*)-4-Hydroxy-5-(naphthalen-2-yl)cyclohex-2-en-1-one (353):

The conjugate adduct **336b** (294 mg, 0.79 mmol) was dissolved in CH_2Cl_2 (3 mL). TFA (0.58 mL, 857 mg, 7.52 mmol) and distilled water (0.02 mL, 20.0 mg, 1.11 mmol) were added to the solution and the reaction mixture was stirred at room temperature for 18 hours under a N_2 atmosphere when it was concentrated *in vacuo* to give a brown oil. The crude product was purified by flash silica chromatography, eluting with 10 % (3:1 EtOAc:EtOH) in 40-60 petroleum ether to afford the title compound **353** as a colourless oil (46.0 mg, 24 %). $[\alpha]_D^{25}$ + 240 (*c* 0.2 in CH_2Cl_2); ν_{max} /cm^{-1} 3404br (O-H), 3054w, 2958w, 2907w (C-H), 1675s (C=O), 1632m, 1600w, 1507w (C=C); δ_H (500 MHz; $CDCl_3$) 2.70 (1H, dd, *J* 16.2, 4.0, C(6)$\underline{H}_{eq}$), 3.29 (1H, dd, *J* 16.2, 12.8, C(6)$\underline{H}_{ax}$), 3.65 (1H, dt, *J* 12.8, 4.0, C(5)$\underline{H}$), 4.58 (1H, t, *J* 4.0, C(4)$\underline{H}$OH), 6.20 (1H, d, *J* 10.0, C(2)$\underline{H}$), 7.06 (1H, dd, *J* 10.0, 4.0, C(3)$\underline{H}$), 7.41 (1H d, *J* 8.5, C(8)$\underline{H}$), 7.46-7.53 (2H, m, C(12)$\underline{H}$ and C(14)$\underline{H}$), 7.72 (1H, s, C(16)$\underline{H}$), 7.84-7.88 (3H, m, C(9)$\underline{H}$, C(11)$\underline{H}$ and C(13)$\underline{H}$); δ_C (125 MHz; $CDCl_3$) 37.9 (C(6)$\underline{C}H_2$), 45.3 (C(5)$\underline{C}$H), 66.7 (C(4)$\underline{C}$HOH), 126.37 (C(8)$\underline{C}$H), 126.39, 126.7 (C(12)$\underline{C}$H and C(14)$\underline{C}$H), 127.0 (C(16)$\underline{C}$H), 127.8, 128.0, 128.9 (C(9)$\underline{C}$H, C(11)$\underline{C}$H and C(13H)$\underline{C}$), 131.0 (C(2)$\underline{C}$H), 132.9, 133.6 (C(10)$\underline{C}$ and C(15)$\underline{C}$), 136.9 (C(7)$\underline{C}$), 147.1 (C(3)$\underline{C}$H), 199.3 (C(1)$\underline{C}$); *m/z* (-ES) 113 (100 %), 219.1 ([M-H_2O-H]$^-$, 40 %); HRMS calculated for $C_{16}H_{15}O_2$, ([M+H]$^+$): 239.1067, found: 239.1067.

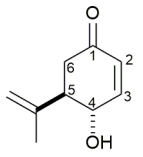

266c

$C_9H_{12}O_2$; M_w = 152.19 g/mol

(4*S*,5*R*)-4-Hydroxy-5-(prop-1-en-2-yl)cyclohex-2-en-1-one (266c):

The conjugate adduct **286c** (204 mg, 0.72 mmol) was dissolved in CH_2Cl_2 (16 mL). TFA (0.74 mL, 1.09 g, 9.59 mmol) and distilled water (0.03 mL, 30.0 mg, 1.67 mmol) were added to the solution and the reaction mixture was stirred at room temperature for 18 hours under a N_2 atmosphere. The reaction was quenched by the addition of sat. $NaHCO_{3(aq)}$ (15 mL) and the resulting suspension was filtered and washed with CH_2Cl_2 (3 × 50 mL). The organic layer was dried over $MgSO_4$, filtered and concentrated *in vacuo* to give an orange oil. The resulting crude product was purified by flash silica chromatography, eluting with 40-60 petroleum ether:EtOAc (1:1) to afford the title compound **266c** as a colourless oil (73.0 mg, 67 %). $[\alpha]_D^{27}$ +164 (*c* 1.00 in CH_2Cl_2); ν_{max} /cm^{-1} 3403br (O-H), 2971w, 2936w, 2889w (C-H), 1679s (C=O), 1668m, 1441w (C=C); δ_H (500 MHz; $CDCl_3$) 1.78 (3H, s, C$\underline{H}_3$ of isopropenyl), 2.42 (1H, dd, *J* 16.5, 13.7, C(6)$\underline{H}_{ax}$), 2.51 (1H, ddd, *J* 16.5, 4.1, 1.2, C(6)$\underline{H}_{eq}$), 2.75 (1H, ddd, *J* 13.7, 9.8, 4.1, C(5)$\underline{H}$), 4.49 (1H, dt, *J* 9.8, 2.2, C(4)$\underline{H}$OH), 4.99 (1H, s, one of C$\underline{H}_2$ of isopropenyl), 5.03 (1H, t, *J* 1.6, one of C$\underline{H}_2$ of isopropenyl), 5.99 (1H, ddd, *J* 10.2, 2.2, 1.2, C(2)$\underline{H}$), 6.97 (1H, dd, *J* 10.2, 2.2, C(3)$\underline{H}$); δ_C (125 MHz; $CDCl_3$) 19.1 ($\underline{C}H_3$ of isopropenyl), 41.0 ($\underline{C}$(6)H_2), 52.6 ($\underline{C}$(5)H), 68.4 ($\underline{C}$(4)HOH), 115.3 ($\underline{C}H_2$ of isopropenyl), 128.8 ($\underline{C}$(2)H), 143.0 ($\underline{C}$ of isopropenyl), 152.4 ($\underline{C}$(3)H), 198.3 ($\underline{C}$(1)); *m/z* (-ES) 151 ([M-H]$^-$, 100 %); HRMS calculated for $C_9H_{11}O_2$, ([M-H]$^-$): 151.0754, found: 151.0747.

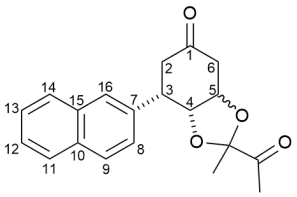

354

$C_{20}H_{20}O_4$; M_w = 324.38 g/mol

(3a*S*,7*S*,7a*R*)-2-Acetyl-2-methyl-7-(naphthalen-2-yl)tetrahydrobenzo[d][1,3]dioxol-5(4*H*)-one (354):

The conjugate adduct **336b** (287 mg, 0.78 mmol) was dissolved in CH_2Cl_2 (1.4 mL). TFA (0.36 mL, 532 mg, 4.67 mmol) and distilled water (0.02 mL, 20.0 mg, 1.11 mmol) were added to the solution and the reaction mixture was stirred at room temperature for 18 hours under a N_2 atmosphere, when it was concentrated *in vacuo* to give a brown solid. The crude product was purified by flash silica chromatography, eluting with 6 % (3:1 EtOAc:EtOH) in 40-60 petroleum ether to afford the title compound **354** as a white solid (79.0 mg, 31 %). m.p. 137-138 °C; $[\alpha]_D^{28}$ -32.3 (*c* 0.47 in MeOH); ν_{max} /cm^{-1} 3056w, 2991w, 2938w, 2913w (C-H), 1728s, 1714s (C=O), 1601w, 1506w (C=C aromatic); δ_H (500 MHz; $CDCl_3$) 1.59 (3H, s, C$\underline{H}_3$), 2.15 (3H, s, C$\underline{H}_3$), 2.61 (1H, dd, *J* 18.3, 3.9, C(2)$\underline{H}_{eq}$), 2.66 (1H, dd, *J* 16.9, 3.9, one of C(6)$\underline{H}_2$), 2.86 (1H, dd, *J* 16.9, 2.1, one of C(6)$\underline{H}_2$), 2.97 (1H, dd, *J* 18.3, 13.8, C(2)$\underline{H}_{ax}$), 3.38 (1H, dt, *J* 13.8, 3.9, C(3)$\underline{H}$), 4.68-4.70 (1H, m, C(4)$\underline{H}$), 4.73 (1H, ddd, *J* 7.8, 3.9, 2.1, C(5)$\underline{H}$), 7.45 (1H, dd, *J* 8.4, 1.9, C(8)$\underline{H}$), 7.47-7.49 (1H, m, C(12)$\underline{H}$), 7.50 (1H, dd, *J* 6.8, 1.7, C(14)$\underline{H}$), 7.73 (1H, d, *J* 1.7, C(16)$\underline{H}$), 7.82-7.85 (3H, m, C(9)$\underline{H}$, C(11)$\underline{H}$ and C(13)$\underline{H}$); δ_C (125 MHz; $CDCl_3$) 20.7 ($\underline{C}H_3$), 24.9 ($\underline{C}H_3$), 39.3 ($\underline{C}(2)H_2$), 41.8 ($\underline{C}(3)H$), 42.0 ($\underline{C}(6)H_2$), 74.6 ($\underline{C}(5)H$), 76.9 ($\underline{C}(4)H$), 107.4 ($\underline{C}(CH_3)$), 126.1, 126.3, 126.4 ($\underline{C}(8)H$, $\underline{C}(12)H$ and $\underline{C}(14)H$), 126.9 ($\underline{C}(16)H$), 127.8, 128.0, 128.5 ($\underline{C}(9)H$, $\underline{C}(11)H$, $\underline{C}(13)H$), 132.8, 133.6 ($\underline{C}(10)$ and $\underline{C}(15)$), 136.7 ($\underline{C}(7)$), 205.6 ($(CH_3)\underline{C}$=O), 208.0 ($\underline{C}(1)$); *m/z* (+ES) 347 ([M+Na]$^+$, 100 %); HRMS calculated for $C_{21}H_{21}O_4$, ([M+H]$^+$): 325.1434, found: 325.1432.

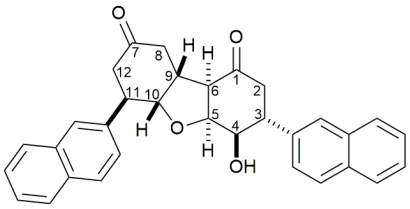

237b

$C_{32}H_{28}O_4$; M_w = 476.57 g/mol

(3*S*,4*S*,4a*R*,5a*R*,6*S*,9a*S*,9b*S*)-4-Hydroxy-3,6-di(naphthalen-2-yl)octahydrodibenzo[b,d]furan-1,8(2H,5aH)-dione (237b):

The hydroxyenone **266b** (82.0 mg, 0.34 mmol) was dissolved in THF (1 mL). 0.5 M $NaOH_{(aq)}$ (0.10 mL) was added to the solution and the reaction mixture was stirred at room temperature under a N_2 atmosphere. An additional 0.50 mL of 0.5 M $NaOH_{(aq)}$ was added to the reaction mixture in 0.05 mL portions at regular intervals over 18 hours. The reaction was quenched by the addition of sat. $NH_4Cl_{(aq)}$ (10 mL) and extracted with CH_2Cl_2 (3 × 30 mL). The organic layers were combined, dried over $MgSO_4$, filtered and concentrated *in vacuo* to give a brown solid. The crude product was purified by flash silica chromatography, eluting with 10 to 15 % (3:1, EtOAc:EtOH) in 40-60 petroleum ether to afford the title compound **237b** as a white solid (46.0 mg, 56 %). m.p. 215-216 °C; $[\alpha]_D^{24}$ +86.4 (*c* 0.5 in $CHCl_3$); ν_{max} /cm^{-1} 3337br (O-H), 2942w, 2832w (C-H), 1709s (C=O), 1600w, 1509w (C=C aromatic); δ_H (500 MHz; $CDCl_3$) 2.60-2.71 (4H, m, C(8)$\underline{H}_2$ and C(12)$\underline{H}_2$), 2.74 (1H, dd, *J* 14.7, 4.5, C(2)$\underline{H}_{eq}$), 2.81 (1H, dd, *J* 14.7, 11.1, C(2)$\underline{H}_{ax}$), 2.87 (1H, dd, *J* 5.1, 2.1, C(6)$\underline{H}$), 3.38 (1H, dt, *J* 9.6, 6.5, C(11)$\underline{H}$), 3.44-3.49 (1H, m, C(3)$\underline{H}$), 3.61 (1H, dtd, *J* 13.0, 6.9, 2.1 C(9)$\underline{H}$), 4.42 (1H, dd, *J* 10.2, 3.3, C(4)$\underline{H}$OH), 4.60 (1H, dd, *J* 9.6, 6.9, C(10)$\underline{H}$), 4.79 (1H, dd, 5.1, 3.3, C(5)$\underline{H}$), 7.36 (2H, t, *J* 9.4, Ar-C$\underline{H}$), 7.44-7.50 (4H, m, Ar-C$\underline{H}$), 7.65 (1H, s, Ar-C$\underline{H}$), 7.68 (1H, s, Ar-C$\underline{H}$), 7.76-7.86 (6H, m, Ar-C$\underline{H}$); δ_C (125 MHz; $CDCl_3$) 37.3 (C(9)H), 40.5 (C(8)H_2), 43.1 (C(12)H_2), 43.6 (C(11)H), 44.7 (C(3)H), 45.2 (C(2)H_2), 57.0 (C(6)H), 72.9 (C(4)HOH), 78.8 (C(5)H), 81.9 (C(10)H), 125.3 (Ar-CH), 125.6 (Ar-CH), 126.1 (Ar-CH), 126.2 (Ar-CH), 126.3 (Ar-CH), 126.52 (Ar-CH), 126.53 (Ar-CH), 126.7 (Ar-CH), 127.8 (Ar-CH and Ar-CH), 127.86 (Ar-CH), 127.91 (Ar-CH), 128.8 (Ar-CH), 128.9 (Ar-CH), 132.8 (Ar-C), 132.9 (Ar-C), 133.6 (Ar-C and Ar-C), 137.4 (Ar-C), 138.7 (Ar-C), 206.4 (C(1)), 209.5 (C(7)); *m/z* (+ES) 494 ($[M+NH_4]^+$, 100 %), 499 ($[M+Na]^+$, 90 %); HRMS calculated for $C_{32}H_{28}O_4Na$, ($[M+Na]^+$): 499.1880, found: 499.1881.

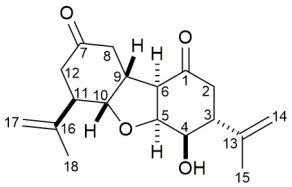

237c

$C_{18}H_{24}O_4$; M_w = 304.39 g/mol

(3*S*,4*S*,6*S*)-4-Hydroxy-3,6-di(prop-1-en-2-yl)octahydrodibenzo[*b*,*d*]furan-1,8(2*H*,5a*H*)-dione (237c):

The hydroxyenone **266c** (100 mg, 0.66 mmol) was dissolved in THF (6.6 mL). 0.5 M $NaOH_{(aq)}$ (0.10 mL) was added to the solution and the reaction mixture was stirred at room temperature for 18 hours under a N_2 atmosphere. The reaction was quenched by the addition of sat. $NH_4Cl_{(aq)}$ (20 mL) and extracted with CH_2Cl_2 (3 × 12 mL). The organic layers were combined, dried over $MgSO_4$, filtered and concentrated *in vacuo* to give a brown solid. The crude product was purified by flash silica chromatography, eluting with 40-60 petroleum ether:EtOAc (2:1) to afford the title compound **237c** as a white solid (42.0 mg, 42 %). m.p. 103-104 °C; $[\alpha]_D^{27}$ +131 (*c* 0.5 in CH_2Cl_2); ν_{max} /cm^{-1} 3390br (O-H), 2923w, 2853w (C-H), 1775s (C=O), 1645w (C=C); δ_H (400 MHz; $CDCl_3$) 1.77 (3H, s, C(18)$\underline{H}_3$), 1.80 (3H, s, C(15)$\underline{H}_3$), 2.26 (1H, dd, *J* 17.4, 12.7, C(12)$\underline{H}_{ax}$), 2.39 (1H, dd, *J* 17.4, 3.8, C(12)$\underline{H}_{eq}$), 2.39-2.53 (4H, m, C(2)$\underline{H}_2$ and C(8)$\underline{H}_2$), 2.61-2.67 (2H, m, C(6)$\underline{H}$ and C(11)$\underline{H}$), 2.85 (1H, td, *J* 10.4, 4.2, C(3)$\underline{H}$), 3.37 (1H, dtd, *J* 13.6, 7.5, 2.4, C(9)$\underline{H}$), 4.13 (1H, dd, *J* 10.4, 3.3, C(4)$\underline{H}$OH), 4.26 (1H, dd, *J* 8.6, 7.5, C(10)$\underline{H}$), 4.59 (1H, dd, *J* 5.2, 3.3, C(5)$\underline{H}$), 4.83 (1H, s, one of C(17)$\underline{H}_2$), 4.89 (1H, s, one of C(14)$\underline{H}_2$), 4.91 (1H, s, one of C(17)$\underline{H}_2$), 4.97 (1H, s, one of C(14)$\underline{H}_2$); δ_C (100 MHz; $CDCl_3$) 19.5 (C(15)H_3), 20.6 (C(18)H_3), 37.2 (C(9)H), 40.3 (C(8)H_2), 41.2 (C(12)H_2), 43.0 (C(2)H_2), 44.5 (C(11)H), 45.9 (C(3)H), 56.7 (C(6)H), 70.3 (C(4)HOH), 78.6 (C(5)H), 79.0 (C(10)H), 113.1 (C(17)H_2), 114.3 (C(14)H_2), 143.6 (C(13)), 144.4 (C(16)), 207.1 (C(1)), 209.9 (C(7)); *m/z* (+ES) 327 ($[M+Na]^+$, 100 %); HRMS calculated for $C_{18}H_{25}O_4$, ($[M+H]^+$): 305.1747, found: 305.1752.

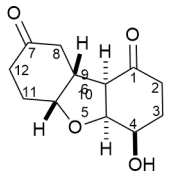

237d

$C_{12}H_{16}O_4$; M_w = 224.26 g/mol

(4*R*)-4-Hydroxyoctahydrodibenzo[b,d]furan-1,8(2H,5aH)-dione (237d):

The *trans*-diol **288** (133 mg, 1.02 mmol) was dissolved in THF (1.2 mL). 0.5 M $NaOH_{(aq)}$ (0.05 mL) was added to the solution and the reaction mixture was stirred at room temperature under a N_2 atmosphere. An additional 0.5 M $NaOH_{(aq)}$ (0.50 mL) was added to the reaction mixture in 0.05 mL portions at regular intervals over 48 hours until the reaction was complete. The reaction was quenched by the addition of sat. $NH_4Cl_{(aq)}$ (10 mL) and extracted with EtOAc (3 × 40 mL). The organic layers were combined, dried over Na_2SO_4, filtered and concentrated *in vacuo* to give a brown solid. The crude product was purified by flash silica chromatography, eluting with 40-60 petroleum ether:acetone (2:1) to afford the title compound **237d** as a white solid (11.0 mg, 10 %). m.p. 138-139 °C; $[\alpha]_D^{28}$ -68.0 (*c* 0.7 in MeOH); ν_{max} /cm^{-1} 3422br (O-H), 2953w, 2921w, 2892w (C-H), 1710s, 1696s (C=O); δ_H (400 MHz; $CDCl_3$) 1.93-2.00 (1H, m, one of C(3)$\underline{H}_2$), 2.05-2.17 (3H, m, one of C(3)$\underline{H}_2$ and C(11)$\underline{H}_2$), 2.23 (1H, dd, *J* 16.5, 6.1, C(12)$\underline{H}_{eq}$), 2.25-2.30 (1H, m, one of C(2)$\underline{H}_2$), 2.34 (1H, dd, *J* 15.4, 7.1, one of C(8)$\underline{H}_2$), 2.45 (1H, ddd, *J* 16.5, 8.9, 5.6, C(12)$\underline{H}_{ax}$), 2.52 (1H, dd, *J* 15.4, 7.1, one of C(8)$\underline{H}_2$), 2.56 (1H, ~d, *J* 8.8, one of C(2)$\underline{H}_2$), 2.59 (1H, dd, *J* 7.1, 4.6, C(6)$\underline{H}$), 3.29 (1H, ~qd, *J* 7.1, 4.6, C(9)$\underline{H}$), 4.20 (1H, dt, *J* 7.1, 3.5, C(4)$\underline{H}$OH), 4.34 (1H, ~q, *J* 5.6, C(10)$\underline{H}$), 4.55 (1H, dd, *J* 7.1, 3.5, C(5)$\underline{H}$); δ_C (100 MHz; $CDCl_3$) 25.7 (C(3)$\underline{C}H_2$), 27.2 (C(11)$\underline{C}H_2$), 34.5 (C(2)$\underline{C}H_2$), 35.2 (C(12)$\underline{C}H_2$), 39.5 (C(9)$\underline{C}$H), 41.5 (C(8)$\underline{C}H_2$), 56.5 (C(6)$\underline{C}$H), 67.2 (C(4)$\underline{C}$HOH), 76.5 (C(10)$\underline{C}$H), 80.3 (C(5)$\underline{C}$H), 208.1 ($\underline{C}$(1)), 210.9 ($\underline{C}$(7)); *m/z* (+ES) 247 ([M+Na]$^+$, 100 %); HRMS calculated for $C_{12}H_{16}O_4Na$, ([M+Na]$^+$): 247.0941, found: 247.0936.

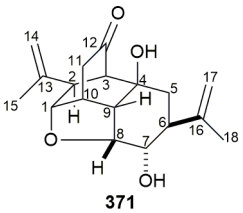

371

$C_{18}H_{24}O_4$; M_w = 304.39 g/mol

5a,8-Dihydroxy-7,9-di(prop-1-en-2-yl)octahydro-2*H*-2,5-methanonaphtho[1,8-bc]furan-4(2a1*H*)-one (371):

The isopropenyl hydroxyenones **266c** (60.0 mg, 0.39 mmol) and ***ent*-266c** (60.0 mg, 0.39 mmol) were dissolved in CH_2Cl_2 (1.2 mL). DBU (0.18 mL, 183 mg, 1.20 mmol) was added to the solution and the reaction mixture was stirred at room temperature for 4 days under a N_2 atmosphere. The reaction was quenched by the addition of sat. $NH_4Cl_{(aq)}$ (10 mL) and extracted with CH_2Cl_2 (3 × 50 mL). The organic layers were combined, dried over Na_2SO_4, filtered and concentrated *in vacuo* to give a brown solid. The crude product was purified by flash silica chromatography, eluting with 15 % (3:1 EtOAc:EtOH) in hexane to afford the title compound **371** as an off-white solid (31.0 mg, 26 %). m.p. 172-173 °C; ν_{max} /cm^{-1} 3391br, 3081br (O-H), 2956m, 2923m, 2859w (C-H), 1723s (C=O), 1645m (C=C); δ_H (400 MHz; $CDCl_3$) 1.76 (6H, s, C(15)$\underline{H}_3$ and C(18)$\underline{H}_3$), 1.87-2.04 (3H, m, C(5)$\underline{H}_2$ and C(7)HO$\underline{H}$), 2.21 (1H, dd, *J* 19.7, 3.4, one of C(11)$\underline{H}_2$), 2.36 (1H, t, *J* 4.3, C(9)$\underline{H}$), 2.545 (1H, dd, *J* 19.7, 3.4, one of C(11)$\underline{H}_2$), 2.550 (1H, d, *J* 4.2, C(3)$\underline{H}$), 2.58-2.63 (1H, m, C(6)$\underline{H}$), 2.64 (1H, br s C(4)HO$\underline{H}$), 2.69 (1H, d, *J* 4.2, C(2)$\underline{H}$), 2.83 (1H, tt, 4.3, 3.4, C(10)$\underline{H}$), 3.70 (1H, dd, *J* 10.6, 2.9, C(7)$\underline{H}$OH), 4.40 (1H, dd, *J* 4.3, 2.9, C(8)$\underline{H}$), 4.60 (1H, d, *J* 4.3, C(1)$\underline{H}$), 4.65 (1H, s, one of C(14)$\underline{H}_2$), 4.87 (1H, s, one of C(14)$\underline{H}_2$), 4.93 (1H, s, one of C(17)$\underline{H}_2$), 4.97 (1H, s, one of C(17)$\underline{H}_2$); δ_C (100 MHz; $CDCl_3$) 18.9, 23.1 ($\underline{C}$(15)H_3 and $\underline{C}$(18)H_3), 33.1 ($\underline{C}$(11)H_2), 40.2 ($\underline{C}$(10)H), 44.5 ($\underline{C}$(5)H_2), 44.7 ($\underline{C}$(6)H), 46.8 ($\underline{C}$(9)H), 48.6 ($\underline{C}$(2)H), 58.8 ($\underline{C}$(3)H), 70.8 ($\underline{C}$(7)HOH), 73.0 ($\underline{C}$(4)OH), 75.9 ($\underline{C}$(1)H), 79.5 ($\underline{C}$(8)H), 111.9 ($\underline{C}$(14)H_2), 114.4 ($\underline{C}$(17)H_2), 144.0 ($\underline{C}$(13)), 144.5 ($\underline{C}$(16)), 208.9 ($\underline{C}$(12)); *m/z* (-ES) 303 ([M-H]$^-$, 100 %); HRMS calculated for $C_{18}H_{24}{}^{35}ClO_4$, ([M+Cl]$^-$): 339.1369, found: 339.1360.

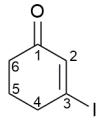

198

C_6H_7IO; M_w = 222.03 g/mol

3-Iodocyclohex-2-en-1-one (198):

Triphenylphosphine (1.29 g, 4.91 mmol) was dissolved in MeCN (45 mL). Iodine (1.24 g, 4.91 mmol) was added to the solution and the reaction mixture was stirred at room temperature for 4 hours under a N_2 atmosphere. 1,3-Cyclohexanedione (500 mg, 4.46 mmol) and triethylamine (0.68 mL, 494 mg, 4.88 mmol) were added to the reaction mixture, which was then stirred for 4 days at room temperature. The reaction mixture was concentrated *in vacuo* to give a dark yellow oil, which was purified by flash silica chromatography, eluting with 100 % Et_2O to afford the title compound **198** as a yellow oil (806 mg, 81 %). δ_H (400 MHz; $CDCl_3$) 2.00-2.06 (2H, m, C(5)$\underline{H}_2$), 2.41-2.45 (2H, m, C(6)$\underline{H}_2$), 2.89-2.93 (2H, m, C(4)$\underline{H}_2$), 6.82 (1H, t, *J* 1.8, C(2)$\underline{H}$); δ_C (100 MHz; $CDCl_3$) 24.2 ($\underline{C}$(5)H_2), 36.8 ($\underline{C}$(4)H_2), 40.8 ($\underline{C}$(6)H_2), 127.1 ($\underline{C}$(3)), 140.9 ($\underline{C}$(2)H), 195.3 ($\underline{C}$(1)); *m/z* (+ES) 222 ($[M+H]^+$, 100 %).[192]

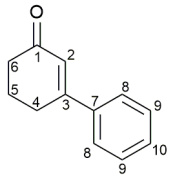

399

$C_{12}H_{12}O$; M_w = 172.23 g/mol

5,6-Dihydro-[1,1'-biphenyl]-3(4*H*)-one (399):

Method 1:

Copper(I)thiophene-2-carboxylate (17.0 mg, 0.09 mmol) was stored in an oven-dried flask under vacuum for 30 minutes and suspended in anhydrous THF (2.5 mL). The suspension was placed under a N_2 atmosphere and was cooled to 0 °C. Phenylmagnesium bromide (1.0 M in THF) (0.54 mL, 542 mg, 0.54 mmol) was added dropwise to the suspension, which was stirred at 0 °C for 15 minutes. A solution of iodo enone **198** (100 mg, 0.45 mmol) in anhydrous THF (2.5 mL) was added dropwise to the reaction mixture, which was

then stirred at room temperature for 18 hours. The reaction was quenched by the addition of sat. $NH_4Cl_{(aq)}$ (20 mL) and extracted with CH_2Cl_2 (3 × 25 mL). The organic layers were combined, dried over $MgSO_4$, filtered and concentrated *in vacuo* to give a brown oil. The crude product was purified by flash silica chromatography, eluting with 40-60 petroleum ether:EtOAc (11:1) to afford the title compound **399** as an off-white solid (34.0 mg, 44 %).

Method 2:

The iodo enone **198** (100 mg, 0.45 mmol) was dissolved in dioxane:water (2 mL, 10:1). Phenylboronic acid (329 mg, 2.70 mmol), $[RhCl(cod)]_2$ (10.0 mg, 0.02 mmol) and triethylamine (0.06 mL, 43.6 mg, 0.43 mmol) were added sequentially to the solution and the reaction mixture was stirred at room temperature for 3 days under a N_2 atmosphere when it was concentrated *in vacuo* to give a brown solid. The crude product was purified by flash silica chromatography, eluting with 40-60 petroleum ether:EtOAc (11:1) to afford the title compound **399** as an off-white solid (59.0 mg, 76 %). m.p. 68-69 °C [Lit.[193] 64-65 °C]; δ_H (400 MHz; $CDCl_3$) 2.13-2.21 (2H, m, C(5)$\underline{H}_2$), 2.48-2.51 (2H, m, C(6)$\underline{H}_2$), 2.77-2.80 (2H, m, C(4)$\underline{H}_2$), 6.42 (1H, t, *J* 1.5, C(2)$\underline{H}$), 7.38-7.25 (3H, m, C(8)$\underline{H}$ and C(10)$\underline{H}$), 7.50-7.56 (2H, m, C(9)$\underline{H}$); δ_C (100 MHz; $CDCl_3$) 23.0 ($\underline{C}(5)H_2$), 28.3 ($\underline{C}(4)H_2$), 37.4 ($\underline{C}(6)H_2$), 125.6 ($\underline{C}(2)H$), 126.2 ($\underline{C}(9)H$), 128.9 ($\underline{C}(8)H$), 130.1 ($\underline{C}(10)H$), 139.0 ($\underline{C}(7)$), 159.9 ($\underline{C}(3)$), 200.1 ($\underline{C}(1)$); *m/z* (+ES) 173 ($[M+H]^+$, 100 %).

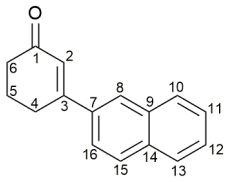

400

$C_{16}H_{14}O$; M_w = 222.29 g/mol

3-(Naphthalen-2-yl)cyclohex-2-en-1-one (400):

The iodo enone **198** (100 mg, 0.45 mmol) was dissolved in dioxane:water (2 mL, 10:1). 2-Naphthylboronic acid (232 mg, 1.35 mmol), $[RhCl(cod)]_2$ (10.0 mg, 0.02 mmol) and triethylamine (0.06 mL, 43.6 mg, 0.43 mmol) were added sequentially to the solution and the reaction mixture was stirred at room temperature for 3 days under a N_2 atmosphere when it was concentrated *in vacuo* to give a brown solid. The crude product was purified by flash silica chromatography, eluting with 40-60 petroleum ether:EtOAc (10:1) to afford

the title compound **400** as a white solid (47.0 mg, 47 %). m.p. 101-102 °C [Lit.[194] 89-90 °C]; δ_H (400 MHz; $CDCl_3$) 2.19-2.25 (2H, m, C(5)$\underline{H}_2$), 2.52-2.55 (2H, m, C(6)$\underline{H}_2$), 2.90-2.94 (2H, m, C(4)$\underline{H}_2$), 7.26 (1H, s, C(2)$\underline{H}$), 7.50-7.56 (2H, m, C(10)$\underline{H}$ or C(13)$\underline{H}$ and C(11)$\underline{H}$ or C(12)$\underline{H}$)), 7.66 (1H, dd, *J* 8.7, 1.9, C(16)$\underline{H}$), 7.83-7.90 (3H, m, C(15)$\underline{H}$, C(10)$\underline{H}$ or C(13)$\underline{H}$ and C(11)$\underline{H}$ or C(12)$\underline{H}$), 8.02 (1H, d, *J* 1.9, C(8)$\underline{H}$); δ_C (100 MHz; $CDCl_3$) 23.0 ($\underline{C}(5)H_2$), 28.3 ($\underline{C}(4)H_2$), 37.5 ($\underline{C}(6)H_2$), 123.5 ($\underline{C}$(16)H), 125.9 ($\underline{C}$(2)H), 126.3 ($\underline{C}$(8)H), 126.9, 127.3 ($\underline{C}$(10)H or $\underline{C}$(13)H and $\underline{C}$(11)H or $\underline{C}$(12)H), 127.8, 128.6, 128.8 ($\underline{C}$(10)H or $\underline{C}$(13)H, $\underline{C}$(11)H or $\underline{C}$(12)H and $\underline{C}$(15)H), 133.2, 134.1, 136.1 ($\underline{C}$(7), $\underline{C}$(9) and $\underline{C}$(14)), 159.2 ($\underline{C}$(3)), 200.1 ($\underline{C}$(1)); *m/z* (+ES) 245 ([M+Na], 100 %).

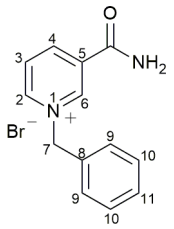

247

$C_{13}H_{13}BrN_2O$; M_w = 293.16 g/mol

1-Benzyl-3-carbamoylpyridin-1-ium bromide (247):

Nicotinamide (2.44 g, 20.0 mmol) was dissolved in anhydrous MeCN (30 mL). Benzyl bromide (2.38 mL, 3.42 g, 20.0 mmol) was added to the solution and the reaction mixture was heated at reflux for 15 hours under a N_2 atmosphere, during which a white precipitate formed. The reaction mixture was allowed to cool to room temperature and Et_2O (35 mL) was added to promote further precipitation. The white solid was filtered and washed with Et_2O (3 × 20 mL) to afford the title compound **247** as a white solid (5.76 g, 98 %). m.p. 216-217 °C [Lit.[195] 205 °C]; δ_H (400 MHz; CD_3OD) 5.94 (2H, s, C(7)$\underline{H}_2$), 7.48-7.53 (3H, m, C(10)$\underline{H}$ and C(11)$\underline{H}$), 7.54-7.56 (2H, m, C(9)$\underline{H}$), 8.23 (1H, dd, *J* 8.1, 6.2, C(3)$\underline{H}$), 9.00 (1H, dt, *J* 8.1, 1.5, C(4)$\underline{H}$), 9.18 (1H, dt, *J* 6.2, 1.5, C(2)$\underline{H}$), 9.53 (1H, t, *J* 1.5, C(6)$\underline{H}$); δ_C (100 MHz; CD_3OD) 66.2 ($\underline{C}(7)H_2$), 129.6 ($\underline{C}$(3)H), 130.3 ($\underline{C}$(9)H), 130.8 ($\underline{C}$(10)H or $\underline{C}$(11)H), 131.2 ($\underline{C}$(10)H or $\underline{C}$(11)H), 134.2 ($\underline{C}$(8)), 136.2 ($\underline{C}$(5)), 145.3 ($\underline{C}$(4)H), 146.1 ($\underline{C}$(6)H), 147.5 ($\underline{C}$(2)H), 165.0 ($\underline{C}$=O); *m/z* (+ES) 213 ($[M]^+$, 100 %).[196]

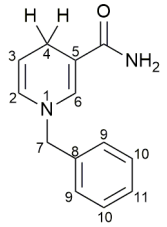

248

$C_{13}H_{14}N_2O$; M_w = 214.27 g/mol

1-Benzyl-1,4-dihydropyridine-3-carboxamide (248):

The compound **247** (2.92 g, 10.0 mmol) was dissolved in distilled water (60 mL). $NaHCO_3$ (4.20 g, 50.0 mmol) was added to the solution, followed by the portion-wise addition of sodium dithionite (8.81 g, 50.0 mmol). The reaction mixture was stirred at room temperature for 3 hours under a N_2 atmosphere in darkness, during which a yellow precipitate formed. The yellow precipitate was filtered and washed with ice cold distilled water (3 × 10 mL) to afford the title compound **248** as a yellow solid (1.82 g, 85 %). m.p. 120-121 °C; δ_H (400 MHz; CD_3OD) 3.10-3.12 (2H, m, C(4)$\underline{H}_2$), 4.35 (2H, s, C(7)$\underline{H}_2$), 4.76-4.80 (1H, m, C(3)$\underline{H}$), 5.86 (1H, dt, *J* 8.1, 1.6, C(2)$\underline{H}$), 7.12 (1H, t, *J* 1.6, C(6)$\underline{H}$), 7.27-7.32 (3H, m, $\underline{C}$(10)H and $\underline{C}$(11)H), 7.34-7.38 (2H, m, $\underline{C}$(9)H); δ_C (100 MHz; CD_3OD) 23.3 ($\underline{C}$(4)H_2), 58.1 ($\underline{C}$(7)H_2), 99.8 ($\underline{C}$(5)), 104.5 ($\underline{C}$(3)H), 128.4 ($\underline{C}$(10)H or $\underline{C}$(11)H), 128.7 ($\underline{C}$(10)H or $\underline{C}$(11)H), 129.8 ($\underline{C}$(9)H), 130.1 ($\underline{C}$(2)H), 139.3 ($\underline{C}$(8)), 141.3 ($\underline{C}$(6)H), 173.6 ($\underline{C}$=O); *m/z* (+ES) 213 (100 %), 237 ($[M+Na]^+$, 90 %).[197]

5.0 Biotransformation of 3-Iodophenol and Bromobenzene using *P. putida* UV4

5.1 Solutions Preparation

100 mL of the necessary stock solutions were prepared as follows:

1.5 M PBS solution:

0.75 M Na_2HPO_4 and 0.75 M KH_2PO_4 were dissolved in doubly distilled (dd) H_2O (100 mL). The pH was adjusted to 7.4 and the solution was autoclaved for 30 minutes.

Nitrogen and magnesium source solution:

15 g of NH_4Cl and 2 g of $MgSO_4$ were dissolved in ddH_2O (100 mL). The pH was adjusted to 6.0 and the solution was autoclaved for 30 minutes.

Trace metal solution:

Ethylenediamine tetraacetic acid (5.00 g), $ZnSO_4 \cdot 7H_2O$ (2.20 g), $CaCl_2$ (554 mg), $MnCl_2 \cdot 4H_2O$ (506 mg), $FeSO_4 \cdot 7H_2O$ (499 mg), $(NH_4)_6Mo_7O_{24} \cdot 4H_2O$ (110 mg), $CuSO_4 \cdot 5H_2O$ (157 mg) and $CoCl_2 \cdot 6H_2O$ (161 mg) were dissolved in ddH_2O (100 mL).[198] The pH was adjusted to 6.0 and the solution was autoclaved for 30 minutes.

5.2 Preparation of minimum salt medium (MSM)

A 100 mL of MSM was prepared as follows:

1.00 g of glucose and 500 mg of sodium pyruvate were dissolved in 96 mL of ddH_2O in a 500 mL Erlenmeyer flask. The flask was plugged with cotton and covered in aluminium foil. The flask was autoclaved for 30 minutes. Under sterile conditions, 2 mL of 1.5 M PBS solution, 2 mL of nitrogen and magnesium source solution and 200 µL of trace metal solution were added.

5.3 Indole Test

Prior to the inoculation, the activity of the strain was tested using the indole test.

Two 500 mL Erlenmeyer flasks each containing 200 mg of glucose dissolved in 100 mL ddH_2O were prepared. To each flask was added 1.60 g of agar and the solution was autoclaved for 30 minutes. Under sterile conditions, 200 µL of trace metal solution, 2 mL

1.5 M PBS solution and 2 mL of nitrogen and magnesium source solution were added. To one of the flasks was added indole at a concentration of 1mM. The stock solution of indole was prepared by dissolving 234 mg of indole in 1 mL of MeOH. For 100 mL of MSM, 50 µL of stock was added. Both flasks were mixed gently, and each flask was poured into 5 petri dishes. The petri dishes were dried at room temperature overnight.

Both sets of MSM plates were divided into eight areas. A single colony from the LB plate containing *P. putida* UV4, as prepared by Patrick Höering in Belfast, was used to streak four lines on the MSM plate prepared without indole. The same sterile pick was then used to spot the MSM plate containing the indole. The last two steps were repeated for each area of the MSM plate. Both plates were incubated at 30 °C overnight. A blue colour was observed on the indole MSM plates which contained active *P. putida* UV4 colonies.

5.4 Preparation of the Iodo Keto *Cis*-Diol

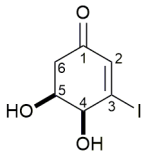

117

$C_6H_7IO_3$; M_w = 254.02 g/mol

(4*S*,5*S*)-4,5-Dihydroxy-3-iodocyclohex-2-en-1-one (117):

A single active colony of *P. putida* UV4, from the MSM plate not containing indole, was used to inoculate 100 mL of MSM. The cells were incubated overnight at 30 °C and 150 rpm. The pH was adjusted to 7.0 and 1 g of glucose was added. The cells were incubated for 1 hour at 30 °C and 150 rpm. The pH was adjusted to 7.0 and the OD_{600} was measured. OD samples were prepared by diluting 10 µL of the sample in 990 µL of ddH_2O. Once the OD > 4, the substrate 3-iodophenol was added at a concentration of 0.5 mg/mL (100 mg, 0.455 mmol) and the cells were incubated for 2 hours at 30 °C and 150 rpm. The pH was adjusted to 7.0 after 1 hour. The reaction was monitored by LCMS at hourly intervals using the method outlined below:

Solution A: 95 % MeOH, 0.1 % formic acid

Solution B: 5 % MeOH, 0.1 % formic acid

Table 30: LCMS method. Solution A: 95 % MeOH, 0.1 % formic acid; solution B: MeOH, 0.1 %, formic acid.

Time (min)	Solution B (%)	Flow (ml/min)
0	100	0.5
1	100	0.5
15	5	0.5
25	5	0.5
27	100	0.5

After 2 hours, the biotransformation was stopped by increasing the PBS concentration to 100 mM. The cell pellets were removed by centrifugation (4000 rpm, 30 minutes, 4 °C). The aqueous solution was extracted with EtOAc (3 × 100 mL), dried over $MgSO_4$, filtered and concentrated *in vacuo* to afford the crude biotransformation product as a brown oil. The crude product was analysed by ^1H NMR with a ratio of 1:1.7:0.7 of product:starting material:catechol. Patrick Hoering at Queens Belfast University prepared iodo keto *cis*-diol **117** on a large scale (>100 g) and provided the material for the synthesises described herein. The Queens Belfast group was also responsible for the optimisation of the biotransformations carried out by *P. putida* UV4.

The whole cell biotransformation using *P. putida* UV4 was carried out by Patrick Höering at Queens Belfast University to afford the crude product as a brown oil. The crude product was purified by flash silica chromatography, eluting with 40-60 petroleum ether:EtOAc (1:1 to 1:2) to afford the title compound **117** as an off-white solid. m.p. 98-99 °C [Lit.[56] 98-100 °C]; $[\alpha]_D^{24}$ -26.4 (*c* 1.00 in MeOH) [Lit. $[\alpha]_D$ -38.0 (*c* 0.91 in MeOH)]; ν_{max} /cm^{-1} 3410br, 3398br (O-H), 1639s (C=O), 1586m (C=C); δ_H (400 MHz; $CDCl_3$) 2.48 (1H, d, *J* 4.6, C(5)HOH), 2.65 (1H, ddd, *J* 16.7, 3.4, 1.3, one of C(6)H_2), 2.82 (1H, dd, *J* 16.7, 5.9, one of C(6)H_2), 2.94 (1H, d, *J* 6.2, C(4)HOH), 4.42 (1H, ddt, *J* 5.9, 4.6, 3.4, C(5)HOH), 4.53 (1H, ddd, *J* 6.2, 3.4, 1.3, C(4)HOH), 6.90 (1H, t, *J* 1.3, C(2)H); δ_C (125 MHz; $CDCl_3$) 42.5 (C(6)H_2), 67.9 (C(5)HOH), 73.6 (C(4)HOH), 130.2 (C(3)), 141.1 (C(2)H), 192.6 (C(1)); *m/z* (+ES) 276 ($[M+Na]^+$, 100 %); HRMS calculated for $C_6H_7IO_3Na$, ($[M+Na]^+$): 276.9348, found: 276.9346.

5.4.1 Utilising the Iodo Keto *Cis*-Diol in the Synthesis of the Isopropyl Incarviditone Analogue

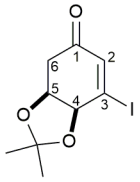

238

$C_9H_{11}IO_3$; M_w = 294.09 g/mol

(3a*S*,7a*S*)-7-Iodo-2,2-dimethyl-3a,7a-dihydrobenzo[*d*][1,3]dioxol-5(4*H*)-one (238):

The iodo keto *cis*-diol **117** (197 mg, 0.78 mmol) was dissolved in anhydrous acetone (4 mL) and the solution was cooled to 0 °C. 2,2-Dimethoxypropane (0.14 mL, 119 mg, 1.14 mmol) and *p*-toluenesulfonic acid monohydrate (3.80 mg, 0.02 mmol) were added to the solution and the reaction mixture was placed under a N_2 atmosphere and then stirred for 1 hour and 15 minutes. The reaction was quenched by the addition of triethylamine (0.50 mL) and concentrated *in vacuo* to give a colourless oil. The crude material was purified by flash silica chromatography, eluting with 40-60 petroleum ether:EtOAc (5:1 to 4:1) to afford the title compound **238** as a white solid (148 mg, 65 %). m.p. 133-134 °C; $[\alpha]_D^{25}$ +47.7 (*c* 1.00 in CH_2Cl_2); ν_{max} /cm^{-1} 2928w, 2895w (C-H), 1672s (C=O), 1596m (C=C); δ_H (500 MHz; $CDCl_3$) 1.41 (3H, s, C$\underline{H}_3$ of acetonide), 1.43 (3H, s, C$\underline{H}_3$ of acetonide), 2.73 (1H, dd, *J* 17.7, 3.8, one of C(6)$\underline{H}_2$), 2.98 (1H, ddd, *J* 17.7, 2.5, 0.9, one of C(6)$\underline{H}_2$), 4.63 (1H, ddd, *J* 4.8, 3.8, 2.5, C(5)$\underline{H}$), 4.73 (1H, dd, *J* 4.8, 0.9, C(4)$\underline{H}$), 6.84 (1H, t, *J* 0.9, C(2)$\underline{H}$); δ_C (100 MHz; $CDCl_3$) 26.6 ($\underline{C}H_3$ of acetonide), 27.7 ($\underline{C}H_3$ of acetonide), 38.4 ($\underline{C}(6)H_2$), 73.0 ($\underline{C}(5)H$), 77.7 ($\underline{C}(4)H$), 110.7 ($\underline{C}$ of acetonide), 129.6 ($\underline{C}(3)$), 140.2 ($\underline{C}(2)H$), 190.3 ($\underline{C}(1)$); *m/z* (+ES) 317 ([M+Na]$^+$, 100 %); HRMS calculated for $C_9H_{11}IO_3Na$, ([M+Na]$^+$): 316.9651, found: 316.9649.

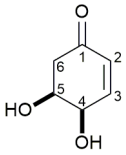

242

$C_6H_8O_3$; M_w = 128.13 g/mol

(4*R*,5*S*)-4,5-Dihydroxycyclohex-2-en-1-one (242):

The iodo keto *cis*-diol **117** (221 mg, 0.87 mmol) was dissolved in MeOH (18 mL). Triethylamine (0.14 mL, 102 mg, 1.00 mmol) and 5 % Pd on carbon (22.0 mg) were added to the solution and the reaction mixture was placed under a H_2 atmosphere and then was stirred at room temperature for 10 minutes. The reaction mixture was filtered through Celite® and the organic filtrate was concentrated *in vacuo* to give an off-white solid. The crude product was purified by flash silica chromatography, eluting with 40-60 petroleum ether:acetone (4:1 to 2:1) to afford the title compound **242** as a white solid (76.0 mg, 68 %). m.p. 73-74 °C [Lit.[56] 72-74 °C]; $[\alpha]_D^{26}$ -202 (*c* 1.00 in MeOH) [Lit.[5] $[\alpha]_D$ -217 (*c* 0.92 in MeOH)]; ν_{max} /cm^{-1} 3432br, 3358br (O-H), 2907w (C-H), 1659s (C=O), 1625w (C=C); δ_H (400 MHz; $CDCl_3$) 2.62 (1H, dd, *J* 16.7, 3.3, one of C(6)$\underline{H}_2$), 2.80 (1H, ddd, *J* 16.7, 5.5, 1.0, one of C(6)$\underline{H}_2$), 4.38 (1H, dtd, *J* 5.5, 3.3, 1.7, C(5)$\underline{H}$OH), 4.56 (1H, ~quin, *J* 2.3, C(4)$\underline{H}$OH), 6.08 (1H, ddd, *J* 10.3, 2.0, 1.0 C(2)$\underline{H}$), 6.77 (1H, ddd, *J* 10.3, 2.9, 1.7, C(3)$\underline{H}$); δ_C (100 MHz; $CDCl_3$) 43.4 ($\underline{C}$(6)H_2), 67.6 ($\underline{C}$(4)HOH), 69.7 ($\underline{C}$(5)HOH), 130.2 ($\underline{C}$(2)H), 147.8 ($\underline{C}$(3)H), 196.5 ($\underline{C}$(1)); *m/z* (+ES) 151 ([M+Na]$^+$, 100 %); HRMS calculated for $C_6H_8O_3Na$, ([M+Na]$^+$): 151.0371, found: 151.0365.

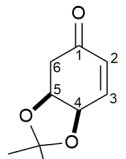

239

$C_9H_{12}O_3$; M_w = 168.19 g/mol

(3a*S*,7a*R*)-2,2-Dimethyl-3a,7a-dihydrobenzo[*d*][1,3]dioxol-5(4*H*)-one (239):

The *cis*-diol **242** (53.0 mg, 0.41 mmol) was dissolved in anhydrous acetone (3 mL) and the solution was cooled to 0 °C. 2,2-Dimethoxypropane (1.52 mL, 1.27 g, 12.4 mmol) and camphorsulfonic acid (2.30 mg, 0.01 mmol) were added to the solution and the reaction

mixture was stirred at 0 °C for 1 hour 12 minutes under a N_2 atmosphere. The reaction was quenched by the addition of triethylamine (2 µL) and concentrated *in vacuo* to give a brown oil. The crude product was purified by flash silica chromatography, eluting with 40-60 petroleum ether:EtOAc (5:1) to afford the title compound **239** as a white solid (43.0 mg, 62 %). m.p. 37-38 °C; $[\alpha]_D^{25}$ -152 (*c* 1.00 in CH_2Cl_2); ν_{max} /cm^{-1} 2987w, 2889w (C-H), 1680s (C=O), 1666m (C=C); δ_H (400 MHz; $CDCl_3$) 1.38 (3H, s, C<u>H</u>$_3$ of acetonide), 1.39 (3H, s, C<u>H</u>$_3$ of acetonide), 2.69 (1H, dd, *J* 17.6, 3.8, one of C(6)<u>H</u>$_2$), 2.93 (1H, ddd, *J* 17.6, 2.6, 1.2, one of C(6)<u>H</u>$_2$), 4.67-4.69 (1H, m, C(5)<u>H</u>), 4.73 (1H, ddd, *J* 4.1, 2.7, 1.2, C(4)<u>H</u>), 6.03 (1H, dt, *J* 10.4, 1.2, C(2)<u>H</u>), 6.65 (1H, ddd, *J* 10.4, 2.7, 2.0, C(3)<u>H</u>); δ_C (125 MHz; $CDCl_3$) 26.8 (<u>C</u>H$_3$ of acetonide), 27.9 (<u>C</u>H$_3$ of acetonide), 38.9 (<u>C</u>(6)H$_2$), 71.2 (<u>C</u>(4)H), 73.5 (<u>C</u>(5)H), 110.1 (<u>C</u> of acetonide), 129.0 (<u>C</u>(2)H), 146.0 (<u>C</u>(3)H), 195.5 (<u>C</u>(1)); *m/z* (+ES) 153 ($[M-CH_3]^+$, 100 %); HRMS calculated for $C_9H_{12}O_3Na$, ($[M+Na]^+$): 191.0684, found: 191.0678.

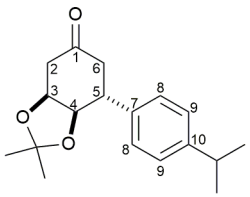

240a

$C_{18}H_{24}O_3$; M_w = 288.39 g/mol

(3a*S*,7*R*,7a*R*)-7-(4-Isopropylphenyl)-2,2-dimethyltetrahydrobenzo[d][1,3]dioxol-5(4*H*)-one (240a):

The enone **239** (35.0 mg, 0.21 mmol) was dissolved in dioxane:water (0.90 mL, 10:1). 4-Isopropylphenylboronic acid (68.2 mg, 0.42 mmol), $[RhCl(cod)]_2$ (5.00 mg, 0.01 mmol) and triethylamine (0.03 mL, 21.8 mg, 0.22 mmol) were added sequentially to the solution. The reaction mixture was stirred at room temperature for 18 hours under a N_2 atmosphere when it was concentrated *in vacuo* to give a brown solid. Purification by flash silica chromatography, eluting with 40-60 petroleum ether:EtOAc (10:1) afforded the title compound **240a** as a white solid (33.0 mg, 55 %). m.p. 48-49 °C; $[\alpha]_D^{29}$ +81.6 (*c* 1.00 in CH_2Cl_2); ν_{max} /cm^{-1} 2969w, 2929w (C-H), 1720s (C=O), 1576w (C=C aromatic); δ_H (400 MHz; $CDCl_3$) 1.24 (6H, d, *J* 6.8, (C<u>H</u>$_3$)$_2$ of isopropyl), 1.37 (3H, s, C<u>H</u>$_3$ of acetonide), 1.53 (3H, s, C<u>H</u>$_3$ of acetonide), 2.60 (1H, dd, *J* 17.8, 8.7, C(6)<u>H</u>$_{ax}$), 2.63 (1H, dd, *J* 17.1, 4.7, one of C(2)<u>H</u>$_2$), 2.71 (1H, dd, *J* 17.1, 4.4, one of C(2)<u>H</u>$_2$), 2.73 (1H, dd, *J* 17.8, 4.8,

C(6)H$_{eq}$), 2.89 (1H, hept, *J* 6.8, CH of isopropyl), 3.39 (1H, dt, *J* 8.7, 4.8, C(5)H), 4.56-4.64 (2H, m, C(3)H and C(4)H), 7.15 (2H, d, *J* 8.1, C(8)H), 7.20 (2H, d, *J* 8.1, C(9)H); δ_C (100 MHz; $CDCl_3$) 24.1 ((CH$_3$)$_2$ of isopropyl), 24.5 (CH$_3$ of acetonide), 27.2 (CH$_3$ of acetonide), 33.8 (CH of isopropyl), 41.0 (C(6)H$_2$), 42.3 (C(5)H), 42.4 (C(2)H$_2$), 72.6 (C(3)H), 77.9 (C(4)H), 108.7 (C of acetonide), 127.1 (C(9)H), 127.5 (C(8)H), 137.4 (C(7)), 147.8 (C(10)), 209.0 (C(1)); *m/z* (+ES) 311 ([M+Na]$^+$, 100 %); HRMS calculated for $C_{18}H_{24}O_3Na$, ([M+Na]$^+$): 311.1623, found: 311.1618.

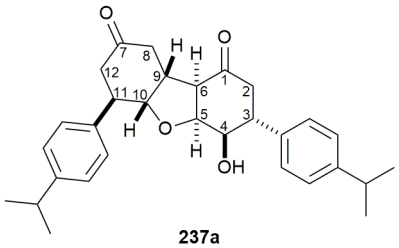

237a

$C_{30}H_{36}O_4$; M_w = 460.61 g/mol

(3*R*,4*R*,6*R*)-4-Hydroxy-3,6-bis(4-isopropylphenyl)octahydrodibenzo[b,d]furan-1,8(2H,5aH)-dione (237a):

The conjugate adduct **240a** (77.0 mg, 0.27 mmol) was dissolved in THF (1.6 mL). 0.5 M $NaOH_{(aq)}$ (0.03 mL) was added to the solution and the reaction mixture was stirred at room temperature under a N_2 atmosphere. An additional 0.15 mL of 0.5 M $NaOH_{(aq)}$ was added to the reaction mixture in 0.05 mL portions at regular intervals over 18 hours. The reaction was quenched by the addition of sat. $NH_4Cl_{(aq)}$ (10 mL) and extracted with CH_2Cl_2 (3 × 30 mL). The combined organic extracts were dried over $MgSO_4$, filtered and concentrated *in vacuo* to give a brown solid. The crude product was purified by flash silica chromatography, eluting with 40-60 petroleum ether:EtOAc (4:1 to 1:1) to afford the title compound **237a** as a white solid (45.0 mg, 73 %). m.p. 131-132 °C; $[\alpha]_D^{25}$ +171 (*c* 0.70 in CH_2Cl_2); ν_{max} /cm^{-1} 3585w (O-H), 2962w, 2929w, 2911w, 2868w (C-H), 1705s (C=O), 1515w (C=C aromatic); δ_H (400 MHz; $CDCl_3$) 1.23 (6H, d, *J* 6.9, (CH$_3$)$_2$ of isopropyl), 1.25 (6H, d, *J* 6.9, (CH$_3$)$_2$ of isopropyl), 2.09 (1H, d, *J* 8.0, C(4)HOH), 2.54-2.60 (4H, m, C(8)H$_2$ and C(12)H$_2$), 2.65-2.67 (2H, m, C(2)H$_2$), 2.79 (1H, dd, *J* 5.1, 2.2, C(6)H), 2.89 (1H, hept, *J* 6.9, CH of isopropyl), 2.89 (1H, hept, *J* 6.9, CH of isopropyl), 3.17 (1H, ddd, *J* 11.1, 9.3, 6.1, C(11)H), 3.29 (1H, td, *J* 10.2, 6.7, C(3)H), 3.45-3.55 (1H, m, C(9)H), 4.28 (1H, ddd, *J* 10.2, 8.0, 3.3, C(4)HOH), 4.43 (1H, dd, *J* 9.3, 7.4, C(10)H), 4.71 (1H, dd, *J* 5.1, 3.3, C(5)H), 7.14 (4H, dd, *J* 8.3, Ar-CH), 7.21 (4H, d, *J* 8.3, Ar-CH); δ_C (100 MHz;

$CDCl_3$) 24.10 (($\underline{C}H_3)_2$ of isopropyl), 24.13 (($\underline{C}H_3)_2$ of isopropyl), 33.8 (<u>C</u>H of isopropyl), 33.9 (<u>C</u>H of isopropyl), 37.1 (<u>C</u>(9)H), 40.5 (<u>C</u>(8)H_2), 42.9 (<u>C</u>(11)H), 43.0 (<u>C</u>(12)H_2), 44.2 (<u>C</u>(3)H), 45.3 (<u>C</u>(2)H_2), 56.9 (<u>C</u>(6)H), 73.0 (<u>C</u>(4)HOH), 78.6 (<u>C</u>(5)H), 81.8 (<u>C</u>(10)H), 127.0 (Ar-<u>C</u>H), 127.2 (Ar-<u>C</u>H), 127.4 (Ar-<u>C</u>H), 127.5 (Ar-<u>C</u>H), 137.3 (Ar-<u>C</u>), 138.6 (Ar-<u>C</u>), 147.9 (Ar-<u>C</u>), 148.1 (Ar-<u>C</u>), 206.8 (<u>C</u>(1)), 210.0 (<u>C</u>(7)); *m/z* (+ES) 483 ($[M+Na]^+$, 100 %); HRMS calculated for $C_{30}H_{36}O_4Na$, ($[M+Na]^+$): 483.2506, found: 483.2506.

5.5 Preparation of Bromobenzene *Cis*-Diol

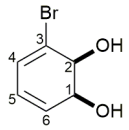

63

$C_6H_7BrO_2$; M_w = 191.02 g/mol

(1*S*,2*S*)-3-Bromocyclohexa-3,5-diene-1,2-diol (63):

A single active colony of *P. putida* UV4, from the MSM plate not containing indole, was used to inoculate 500 mL of MSM. The cells were incubated overnight at 30 °C and 150 rpm. The pH was adjusted to 7.0 and 5 g of glucose was added. The cells were incubated for 1 hour at 30 °C and 150 rpm. The pH was adjusted to 7.0 and the OD_{600} was measured. OD samples were prepared by diluting 10 µL of the sample in 990 µL of ddH_2O. Once the OD > 4, the substrate bromobenzene was added (239 µL, 356 mg, 2.27 mmol) and the cells were incubated for 3 hours at 30 °C and 150 rpm. The pH was adjusted to 7.0 at every hour. The reaction was monitored by LCMS at hourly intervals using the method outlined below:

Solution A: 95 % MeOH, 0.1 % formic acid

Solution B: 5 % MeOH, 0.1 % formic acid

Table 31: LCMS method. Solution A: 95 % MeOH, 0.1 % formic acid; solution B: MeOH, 0.1 %, formic acid.

Time (min)	Solution B (%)	Flow (ml/min)
0	100	0.5
1	100	0.5
15	5	0.5
25	5	0.5
27	100	0.5

After 3 hours, the biotransformation was stopped by increasing the PBS concentration to 100 mM. The cell pellets were removed by centrifugation (4000 rpm, 30 minutes, 4 °C). The aqueous solution was extracted with EtOAc (3 × 500 mL), dried over $MgSO_4$, filtered and concentrated *in vacuo* to afford the crude biotransformation product as a colourless oil. The crude product was purified by flash silica chromatography, eluting with hexane:EtOAc (1:1) to afford the title compound **63** as colourless crystals (120 mg, 28 %). m.p. 94-95 °C [Lit.[48] 91-94 °C]; $[\alpha]_D^{28}$ +43.6 (*c* 0.55 in CH_2Cl_2); ν_{max} /cm^{-1} 3261br, 3043br (O-H), 2916w, 2854w (C-H), 1654w (C=C); δ_H (400 MHz; $CDCl_3$) 2.32 (1H, br d, *J* 8.4, C(1)HOH), 2.42 (1H, br d, *J* 7.0, C(2)HOH), 4.29 (1H, t, *J* 7.0, C(2)HOH), 4.47-4.51 (1H, m, C(1)HOH), 5.85 (1H, ddd, *J* 9.0, 4.7, 1.6, C(5)H), 5.96 (1H, dd, *J* 9.4, 4.7, C(6)H), 6.38 (1H, d, *J* 9.0, C(4)H); δ_C (100 MHz; $CDCl_3$) 69.2 (C(1)HOH), 72.6 (C(2)HOH), 124.2 (C(5)H), 126.3 (C(3)), 127.0 (C(4)H), 129.4 (C(6)H); *m/z* (GC/MS) 172 ([M(^{79}Br)-H-OH]$^+$, 100 %), 174 ([M(^{81}Br)-H-OH]$^+$, 100 %); HRMS calculated for $C_6H_7{}^{79}BrO_2$ ([M]$^+$): 189.9624, found: 189.9620.

6.0 Biological Assays Methods and Materials

6.1 Cell Culture

All chemicals used for cell culturing were supplied by Sigma-Aldrich (Missouri, U.S.A.). All handlings of cells were performed under sterile conditions in a Class II laminar flow microbiological safety cabinet.

6.1.1 The Cell Lines

Information regarding the cell lines used in the MTT cell viability assays is listed in **Table 32**.

Table 32: Cell lines used in the MTT assay.

Cell line	Cell type	Type	Tissue of origin	Disease
A549	Epithelial	Human	Lung	Adenocarcinoma
MDA-MB-231	Epithelial	Human	Breast	Adenocarcinoma
FaDu	Epithelial	Human	Pharynx	Squamous cell carcinoma
PNT2	Epithelial	Human	Prostate	Healthy prostate

All cell lines were maintained in RPMI-1640 medium with 10 % fetal bovine serum (FBS) and 2 mM L-glutamine (1 %). All media used were free from mycoplasma contamination.

6.1.2 Sub-Culturing the Cell Line

The cell lines were cultured in T-75 tissue culture flasks (Falcon, Becton Dickinson, New Jersey, U.S.A.) and kept in a humidified incubator set at 37 °C with a 5 % CO_2 atmosphere.

Once the confluency of a cell line exceeded > 70 %, the cell line was sub-cultured. The growth medium in the flask was removed and the cells were washed with sterile phosphate buffered saline (PBS, pH = 7.4). The cells were trypsinised and incubated at 37 °C for 5 to 10 minutes. The Trypsin/EDTA was then neutralised by the addition of 8 mL of fresh growth medium. The cells were cultured into a new T-75 flask with fresh growth media. The overall dilution ratio varied from 1:2 to 1:4.

6.1.3 Cryopreservation of the Cell Line

The cell lines were preserved at -80 °C for further use. The freezing was performed when the confluency of the cells was >70 %. The cells were trypsinised, re-suspended in fresh growth medium and centrifuged at 1300 rpm (Megafuge 1.0, Heraeus, Hanau, Germany) for 5 minutes. The medium was removed, and the cell pellet was re-suspended in freezing medium (see **Table 33**). 1 mL of the resulting cell suspension was transferred into a 1.6 mL cryovial (Greiner bio-one, Frickenhausen, Germany). The cells were first transferred to a -20 °C freezer for 10 minutes before being transferred to a −80 °C freezer.

Table 33: Freezing medium components for each cell line.

Cell line	Components of freezing medium
A549	40 % RPMI-1640, 50 % FBS, 10 % DMSO
MDA-MB-231	70 % RPMI-1640, 20 % FBS, 10 % DMSO
FaDu	95 % RPMI-1640, 5 % DMSO
PNT2	90 % RPMI-1640, 10 % DMSO

6.1.4 Thawing Cells

Frozen cells were thawed at 37 °C. The resulting cell suspension was transferred into a universal tube (Medline Scientific, Chalgrove, U.K.) and 4 mL of growth medium was added. The tube was centrifuged for 5 minutes at 1300 rpm. The media was removed, and the cell pellet was re-suspended in 5 mL of fresh growth medium. The resulting cell suspension was transferred into a T-25 tissue culture flask (Falcon, Becton Dickinson, New Jersey, U.S.A.) containing fresh growth medium. The dilution ratio was 1:1. The cells were incubated at 37 °C within an atmosphere of 5 % CO_2 and were used for studies after two sub-culture passages.

6.2 MTT Cell Viability Assays

All chemicals used for the MTT cell viability assays were supplied by Sigma-Aldrich. All the assays were performed under sterile conditions in a Class II laminar flow microbiological safety cabinet.

6.2.1 Preparation of the MTT Solution

MTT powder (50.0 mg) was dissolved in 20.0 mL of PBS (pH = 7.4). The resulting solution was kept in a 50 mL Falcon tube wrapped in aluminium foil and stored at 4 °C.

6.2.2 Counting and Seeding Cells

The cells were seeded into 8 columns sextuplicately across the 96-well microtitre plates in 180 μL of culture media at a seeding density of 1000 cells/mL, incubated at 37 °C within a 5 % atmosphere of CO_2 for 24 hours prior to the drug treatments.

The concentration of the cell suspension was determined using a haemocytometer (Neubauer, Germany). A cover-slip was placed over the counting chamber of the haemocytometer and 10 μL of the cell suspension was transferred onto the chamber. The

chamber was placed under a light microscope and the cells in the four corner squares were counted in an order from 1 to 4 (see **Figure 69**).

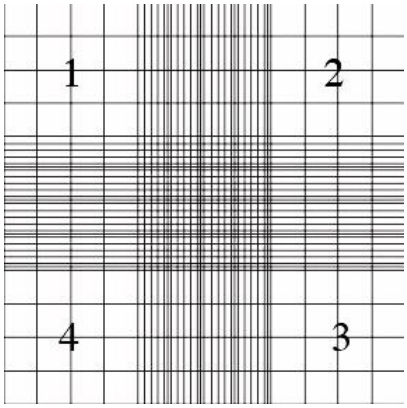

Figure 69: A representation of the counting chamber.

The amount of cell suspension (mL) was determined using the following equation:

$$\frac{5555.6 \times 20\ mL}{Mean\ number\ of\ cells\ counted \times 10^4}$$

Equation 2: Equation to determine the required amount of cell suspension for an approximate seeding density of 1000 cells/mL.

6.2.3 Treating Cells

A stock solution of the compound to be tested was made up in DMSO at a concentration of 25 mM. Five serial dilutions with concentrations at 2.5 mM, 0.25 mM, 250 µM, 25 µM and 2.5 µM were prepared from the stock solution. 40 µL of the stock solution and each serial dilution were added into 960 µL of growth media in a 6-well microtitre plate. 20 µL of each resulting new dilution was added to 180 µL of the cell suspension in an ascending order of concentration (i.e. Row 5 = 1 nM to Row 10 = 100 µM). The final drug concentrations were as followed: 1 nM, 10 nM, 100 nM, 1 µM, 10 µM and 100 µM. 40 µL of DMSO was added in row 4 as a solvent control group and row 3 was a blank control group (**Figure 70**). The plates were incubated at 37 °C within a 5 % CO_2 atmosphere for 96 hours.

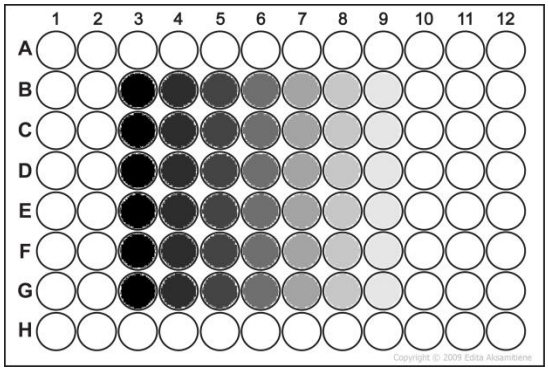

Figure 70: A representation of the 96-well plate used in the MTT assay.

6.2.4 Ending the MTT Viability Assay

50 µL of the MTT solution in PBS (2.5 mg/mL) was added to all the cell containing wells after 96 hours of incubation. The plate was incubated at 37 °C for 4 hours, after which the solution in each well was aspirated and 200 µL of DMSO was added to dissolve the resulting formazan crystals. The plate was gently shaken for 5 minutes prior to the absorbance readings. Absorbance for each well was read at a wavelength of 540 nm on a multi-well scanning spectrophtometer (µQuant Microplate Spectrophotometer, BioTek, Potton, U.K.) using the Gen5 software package (BioTek, Vermont, U.S.A.). The optical density (OD) values, which are proportional to the number of viable cells, were calculated using the average absorption values.

6.2.5 Calculating IC_{50} Concentrations

The OD values were used to determine the half maximal inhibitory concentration (IC_{50}) of the test compounds. With OD values, a dose-response curve (percentage of cell viability against the logarithm of concentration of compound (Log C)) could be generated using GraphPad Prism®. The IC_{50} could be hence obtained from the curve using the XY analysis 'Nonlinear regression (curve fit)', with the equation 'log(inhibitor) vs response – variable slope (four parameters)' within GraphPad Prism®.

7.0 Computational Methods

7.1 Preparation of Protein

The NDO (PDB code: 1O7N) and TDO (PDB code: 3EN1) X-ray crystal structures bound with O_2/indole and toluene respectively were obtained from the PDB database.

Prior to docking, all water molecules were removed and hydrogens were added to the crystal structures using PyMol (v 2.0.4). The files were then saved in the format .mol2.

7.2 Preparation of the O_2 bound TDO

The NDO and TDO crystal structures were overlaid in PyMol (v 2.0.4). The bound O_2 from NDO was extracted and saved within the TDO crystal structure retaining the same coordinates. All coordination bonds from the iron centre were removed as per the requirements of docking using Gold™.

7.3 Preparation of Ligand

Ligands were obtained from the ZINC database. Hydrogens were added and the files were saved in the .mol2 format using PyMol (v 2.0.4).

Ligands that were not available via the ZINC database were created within Chem3D (v. 15.0) and saved in the .mol2 format.

7.4 Docking

All docking was performed using Gold™ (v 5.3). The bound toluene was extracted from the crystal structure and used to define the docking cavity. Hydrogen addition was repeated within Gold™. The docking cavity was set as a sphere, with a radius of 10 Å from the bound toluene. The atom selection within the cavity was restricted to a solvent accessible surface and all hydrogen bond donors/acceptors were also treated as solvent accessible. The target substrate was loaded and 100 genetic algorithms were set. ChemPLP was used as the scoring function, no early termination was allowed, and the docking was set to allow for diverse solutions. The search efficiency was set to 200 %. All other settings were left as default.

7.5 Visualising Docked Results

All the docked results were visualised in GoldMine™. A histogram was generated using the Gold.PLP.Fitness descriptor and docked solutions were grouped in order of Fitness score and docked pose (R.M.S.D. set at 1.5 Å). A higher fitness score correlated with a better binding pose. All 100 genetic algorithms were analysed and visualised within Gold™, and the predicted bioproduct was determined by the minimum distance of the substrate to the mononuclear iron.

8.0 Appendix

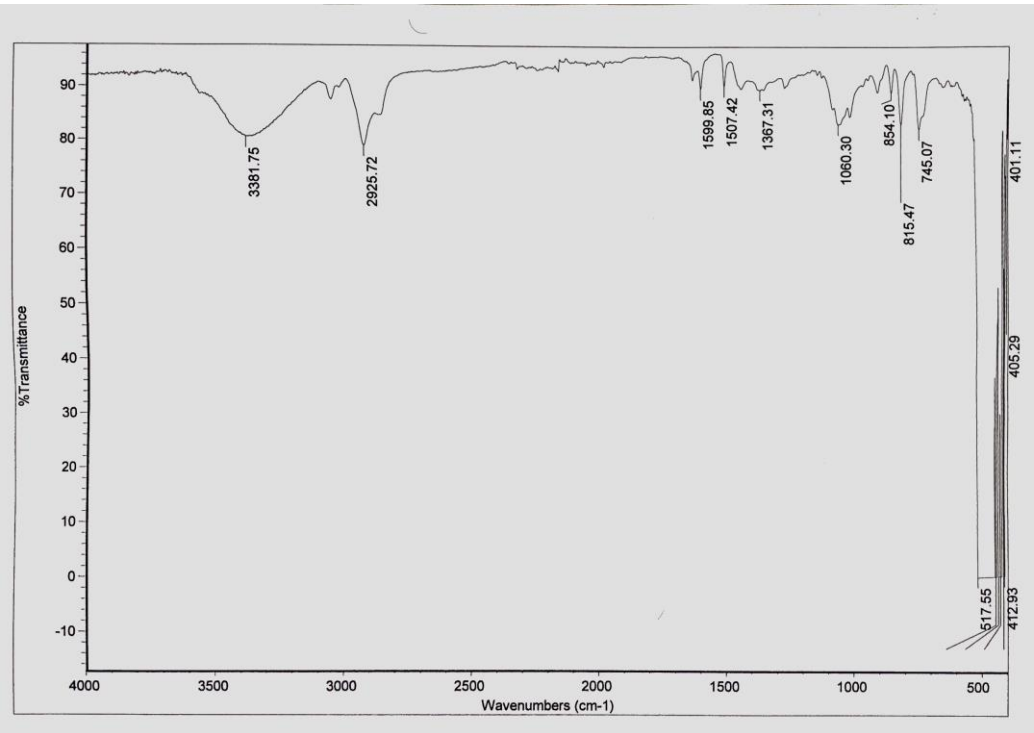

Figure 71: Infra-red spectrum of the sample obtained from the reduction of incarviditone analogue ***ent*-237b** using DIBAL following purification.

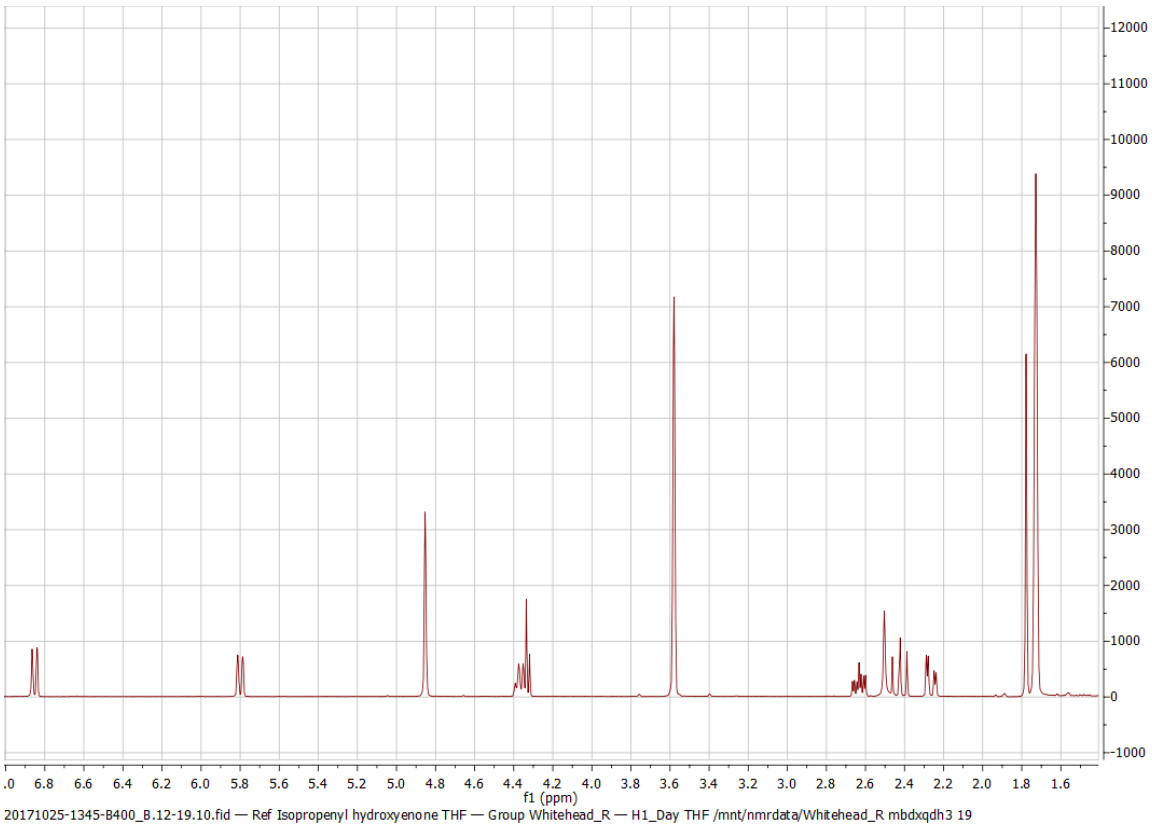

Figure 72: The isopropenyl hydroxyenone **266c** ^{1}H NMR spectrum in THF-d_8.

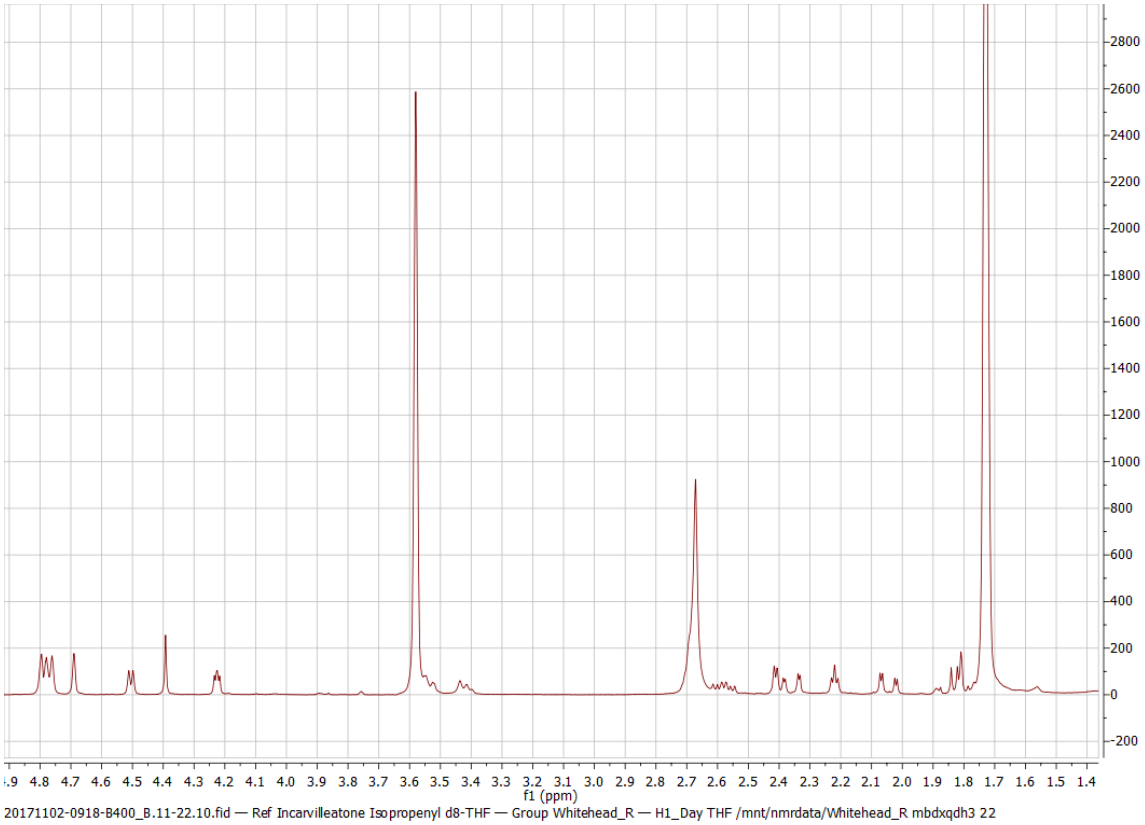

Figure 73: The isopropenyl incarvilleatone **371** ^{1}H NMR spectrum in THF-d_8.

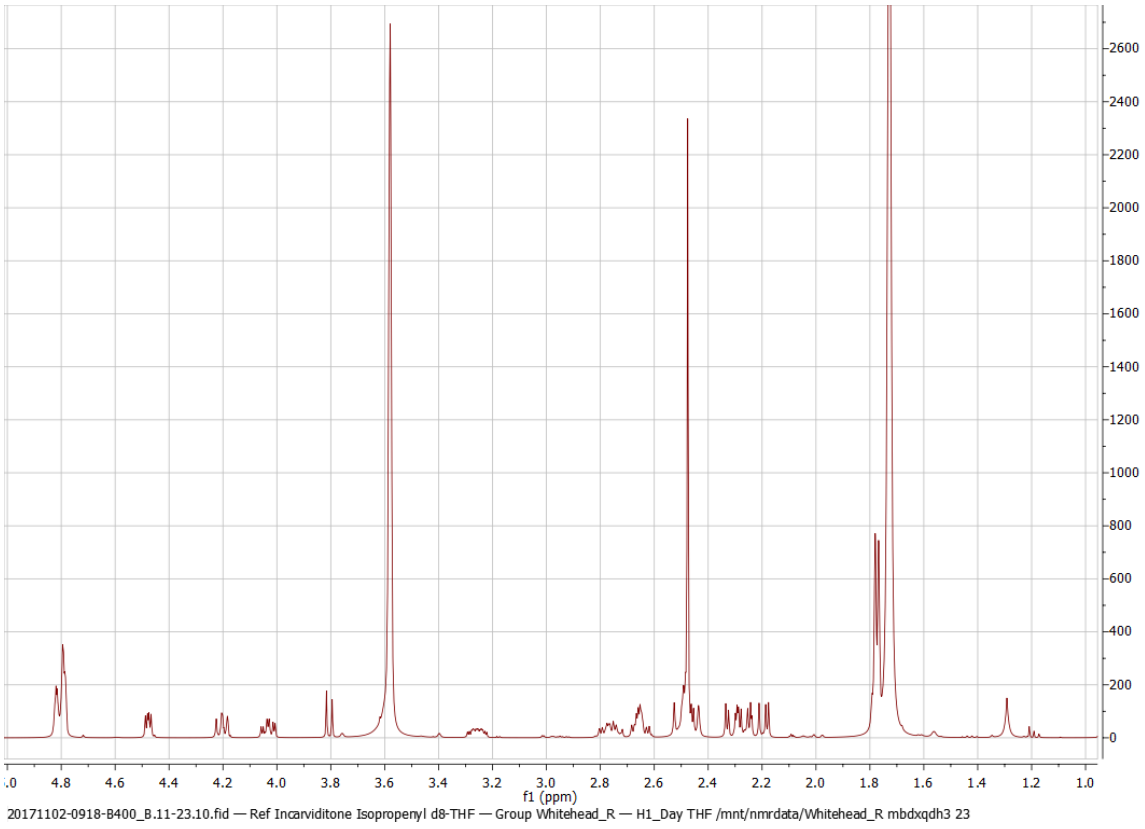

Figure 74: The isopropenyl incarviditone **237c** ^{1}H NMR spectrum in THF-d_8.

9.0 References

[1] D. J. Newman and G. M. Cragg, *J. Nat. Prod.*, 2016, **79**, 629-661.

[2] M. D. Truppo, *ACS Med. Chem. Lett.*, 2017, **8**, 476-480.

[3] The National Center for Biotechnology Information, https://www.ncbi.nlm.nih.gov/gene/3620 (accessed 6th Janurary 2018).

[4] T. D. H. Bugg, *Tetrahedron*, 2003, **59**, 7075-7101.

[5] O. Kweon, S. Kim, S. Baek, J. Chae, M. D. Adjei, D. Baek, Y. Kim and C. E. Cerniglia, *BMC Biochem.*, 2008, **9**, 1-20.

[6] D. T. Gibson and R. E. Parales, *Curr. Opin. Biotechnol.*, 2000, **11**, 236-243.

[7] R. Friemann, K. Lee, E. N. Brown, D. T. Gibson, H. Eklund and S. Ramaswamy, *Acta Crystallogr. D. Biol. Crystallogr.*, 2009, **65**, 24-33.

[8] D. R. Boyd and T. D. H. Bugg, *Org. Biomol. Chem.*, 2006, **4**, 181-192.

[9] P. I. Nikel, M. Chavarria, T. Fuhrer, U. Sauer and V. D. Lorenzo, *J. Biol. Chem*., 2015, **43**, 25920-25932.

[10] M. Chavarria, P. I. Nikel, D. Pérez-Pantoja and V. D. Lorenzo, *Environ. Microbiol.*, 2013, **6**, 1772-1785.

[11] N. Entner and M. Doudoroff, *J. Biol. Chem.*, 1952, **196**, 853-862.

[12] G. J. Zylstra, W. R. McCombie, D. T. Gibson and B. A. Finette, *Appl. Environ. Microbiol.*, 1988, **54**, 1498-1503.

[13] D. R. Boyd, N. D. Sharma, M. V. Berberian, M. Cleij, C. Hardacre, V. Ljubez, G. McConville, P. J. Stevenson, L. A. Kulakov and C. C. R. Allen, *Adv. Synth. Catal.*, 2015, **357**, 1881-1894.

[14] J. Zeyer and P. C. Kearney, *J. Argio. Food Chem.*, 1984, **32**, 238-242.

[15] E. Diaz and K. N. Timmis, *J. Biol. Chem*., 1995, **270**, 6403-6411.

[16] W. K. Yeh, D. T. Gibson and T. Liu, *Biochem. Biophys. Res. Commun.*, 1977, **78**, 401-410.

[17] V. Subramanian, T. Liu, W. K. Yeh and D. T. Gibson, *Biochem. Biophys. Res. Commun.*, 1979, **91**, 1131-1139.

[18] V. Subramanian, T. N. Liu, W. K. Yeh, M. Narro and D. T. Gibson, *J. Biol. Chem.*, 1981, **256**, 2723-2730.

[19] L. P. Wackett, L. D. Kwart and D. T. Gibson, *Biochem*., 1988, **27**, 1367-1373.

[20] V. Subramanian, T. Liu, W. K. Yeh, C. M. Serdar, L. P. Wackett and D. T. Gibson, *J. Biol. Chem.*, 1985, **260**, 2355-2363.

[21] B. Kauppi, K. Lee, E. Carredano, R. E. Parales, D. T. Gibson, H. Eklund and S. Ramaswamy, *Structure*, 1998, **6**, 571-586.

[22] E. L. Hegg and L. Que Jr, *Eur. J. Biochem.*, 1997, **250**, 625-629.

[23] D. R. Boyd, N. D. Sharma, N. I. Bowers, R. Boyle, J. S. Harrison, K. Lee, T. D. H. Bugg and D. T. Gibson, *Org. Biomol. Chem.*, 2003, **1**, 1298-1307.

[24] D. T. Gibson, G. E. Cardini, F. C. Maseles and R. E. Kallio, *Biochemistry*, 1970, **9**, 1631-1635.

[25] K. Lee, *J. Bacteriol.*, 1999, **181**, 2719-2725.

[26] M. D. Wolfe and J. D. Lipscomb, *J. Biol. Chem.*, 2003, **278**, 829-835.

[27] B. Meunier, S. P. de Visser and S. Shaik, *Chem. Rev.*, 2004, **104**, 3947-3980.

[28] M. D. Wolfe, J. V. Parales, D. T. Gibson and J. D. Lipscomb, *J. Biol. Chem.*, 2001, **276**, 1945-1953.

[29] B. J. Wallar and J. D. Lipscomb, *Chem. Rev.*, 1996, **96**, 2625-2657.

[30] A. Bassan, M. R. A. Blomberg and P. E. M. Siegbahn, *J. Biol. Inorg. Chem.*, 2004, **9**, 439-452.

[31] B. E. Haigler and J. C. Spain, *Appl. Environ. Microbiol.*, 1991, **57**, 3156-3162.

[32] E. Carredano, A. Karlsson, B. Kauppi, D. Choudhury, R. E. Parales, J. V. Parales, K. Lee, D. T. Gibson, H. Eklund and S. Ramaswamy, *J. Mol. Biol.*, 2000, **296**, 701-712.

[33] D. T. Gibson, J. R. Koch and R. E. Kallio, *Biochemistry*, 1968, **7**, 2653-2662.

[34] H. J. Heipieper, in *Bioremediation of Soils Contaminated with Aromatic Compounds*, Springer, Dordrecht, 1st edn, 2007, pp 105-124.

[35] E. Goldman and L. H. Green, in *Practical Handbook of Microbiology*, CRC Press, Boca Raton, 2nd edn, 2009, Ch. 18, pp. 240-241.

[36] M. Mulet, E. Garía-Valdés and J. Lalucat, *Res. Microbiol.*, 2013, **164**, 351-359.

[37] D. T. Gibson, M. Hensley, H. Yoshioka and T. J. Mabry, *Biochemistry*, 1970, **9**, 1626-1630.

[38] J. Lee, J. Roh and H. Kim, *Biotechnol. Bioeng.*, 1994, **43**, 1146-1152.

[39] H. Yu, B. J. Kim and B. E. Rittmann, *Biodegradation*, 2001, **12**, 455-463.

[40] D. G. H. Ballard, A. Courtis, I. M. Shirley and S. C. Taylor, *J. Chem. Soc., Chem. Commun.*, 1983, **0**, 954-955.

[41] R. O. Jenkins and S. C. Heald, *Appl. Microbiol. Biotechnol.*, 1996, **46**, 388-392.

[42] S. C. Heald and R. O. Jenkins, *Appl. Microbiol. Biotechnol.*, 1996, **45**, 56-62.

[43] T. Skvortsov, P. Hoering, K. Arkhipova, R. C. Whitehead, D. R. Boyd and C. C. R. Allen, *Genome Announc.*, 2018, **6**, 1-2.

[44] P. U. M. Raghavan and M. Vivekanandan, *Int. Biodeterior. Biodegradation*, 1999, **44**, 29-32.

[45] D. R. Boyd, N. D. Sharma, N. M. Llamas, C. R. O'Dowd and C. C. R. Allen, *Org. Biomol. Chem*., 2006, **4**, 2208-2217.

[46] D. R. Boyd, M. V. Hand, N. D. Sharma, J. Chima, H. Dalton and G. N. Sheldrake, *J. Chem. Soc., Chem. Commun.*, 1991, **0**, 1630-1632.

[47] M. A. Endoma, V. P. Bui, J. Hansen and T. Hudlicky, *Org. Process Res. Dev.*, 2002, **6**, 525-532.

[48] D. R. Boyd, N. D. Sharma, B. Bryne, M. V. Hand, J. F. Malone, G. N. Sheldrake, J. Blacker and H. Dalton, *J. Chem. Soc., Perkin Trans 1*, 1998, 1935-1943.

[49] J. L. Humphreys, D. J. Lowes, K. A. Wesson and R. C. Whitehead, *Tetrahedron*, 2006, **62**, 5099-5108.

[50] C. L. Arthurs, J. Raftery, H. L. Whitby, R. C. Whitehead, N. S. Wind and I. J. Stratford, *J. Bioorg. Med. Chem. Lett.*, 2007, **17**, 5974-5977.

[51] T. Hudlicky, U. Rinner, D. Gonzalez, H. Akgun, S. Schilling, P. Siengalewicz, T. A. Martinot and G. R. Pettit, *J. Org. Chem.*, 2002, **67**, 8726-8743.

[52] M. Kwit, J. Gawronski, D. R. Boyd, N. D. Sharma, M. Kaik, R. A. More O'Ferrall and J. S. Kudavalli, *Chem. Eur. J.*, 2008, **14**, 11500-11511.

[53] D. R. Boyd, N. D. Sharma, I. N. Brannigan, T. A. Evans, S. A. Haughey, B. T. McMurray, J. F. Malone, P. B. A. McIntyre, P. J. Stevenson and C. C. R. Allen, *Org. Biomol. Chem.*, 2012, **10**, 7292-7304.

[54] D. R. Boyd, N. D. Sharma, J. F. Malone, P. B. A. McIntyre, C. McRoberts, S. Floyd, C. C. R. Allen, A. Gohil, S. J. Coles, P. N. Horton and P. J. Stevenson, *J. Org. Chem.*, 2015, **80**, 3429-3439.

[55] V. Berberian, C. C. R. Allen, N. D. Sharma, D. R. Boyd and C. Hardacre, *Adv. Synth. Catal.*, 2007, **349**, 727-739.

[56] D. R. Boyd, N. D. Sharma, J. F. Malone and C. C. R. Allen, *Chem. Commun.*, 2009, 3633-3635.

[57] D. R. Boyd, N. D. Sharma, P. J. Stevenson, M. Blain, C. McRoberts, J. T. G. Hamilton, J. M. Argudo, H. Mundi, L. A. Kulakov and C. C. R. Allen, *Org. Biomol. Chem.*, 2011, **9**, 1479-1490.

[58] R. Friemann, K. Lee, E. N. Brown, D. T. Gibson, H. Eklund and S. Ramaswamy, *Acta. Cryst.*, 2009, **D65**, 24-33.

[59] Y. Chen, Y. Shen, Y. Su, L. Kong and W. Zhang, *Chem. Biodiversity*, 2009, **6**, 779-783.

[60] S. Christou, PhD thesis, University of Manchester, 2014.

[61] Y. Song, PhD thesis, University of Manchester, 2017.

[62] K. Zhao, G. Cheng, H. Yang, H. Shang, X. Zhang, Y. Wu and Y. Tang, *Org. Lett.*, 2012, **14**, 4878-4881.

[63] P. D. Brown, A. C. Willis, M. S. Sherburn and A. L. Lawrence, *Org. Lett.*, 2012, **14**, 4537-4539.

[64] C. Jiménez and R. Riguera, *Nat. Prod. Rep.*, 1994, **11**, 591-606.

[65] H. Yamamoto, M. Hori, H. Kuwajima and K. Inoue, *Planta*, 2003, **216**, 432-436.

[66] S. Christou, A. C. Edwards, R. G. Pritchard, P. Quayle, I. J. Stratford and R. W. Whitehead, *Synlett*, 2014, **25**, 1262-1266.

[67] M. C. Carreño and M. Ribagorda, *Org. Lett.*, 2003, **5**, 2425-2428.

[68] V. L. Paddock, R. J. Phipps, A. Conde-Angulo, A. Blanco-Martin, C. Giró-Mañas, L. J. Martin, A. J. P. White and A. C. Spivey, *J. Org. Chem.*, 2011, **76**, 1483-1486.

[69] Y. Gao, Y. Shen, S. Zang, J. Tian, H. Zeng, J. Ye, H. Li, L. Shan and W. Zhang, *Org. Lett.*, 2012, **14**, 1954-1957.

[70] J. N. Sharma, A. Al-Omran and S. S. Parvathy, *Inflammopharmacology*, 2007, **15**, 252-259.

[71] A. Otto, A. Prozel, J. Schmidt, W. Brandt, L. Wessjohann and N. Arnold, *J. Nat. Prod.*, 2016, **79**, 74-80.

[72] T. Lübken, J. Schmidt, A. Porzel, N. Arnold and L. Wessjohann, *Phytochemistry*, 2004, **65**, 1061-1071.

[73] A. Otto, A. Porzel, J. Schmidt, L. Wessjohann and N. Arnold, *Phytochemistry*, 2015, **118**, 174-180.

[74] T. Takeuchi, H. Chimura, M. Hamada, H. Umezawa, O. Yoshioka, N. Oguchi, Y.Takahashi and A. Matsuda, *J. Antibiot.*, 1975, **28**, 737-742.

[75] H. Chimura, H. Nakamura, T. Takita, T. Takeuchi and H. Umezawa, *J. Antibiot.*,1975, **28**, 743-748.

[76] P. J. Thornalley, *Mol. Aspects Med.*, 1993, **14**, 287-371.

[77] A. Pompella, A. Visvikis, A. Paolicchi, V. D. Tata and A. F. Casini, *Biochem. Pharmacol.*, 2003, **66**, 1499-1503.

[78] D. Kamiya, Y. Uchihata, E. Ichikawa, K. Kato and K. Umezawa, *Bioorg. Med. Chem. Lett.*, 2005, **15**, 1111-1114.

[79] A. L. Vahrmeijer, C. A. Snel, D. P. Steenvoorden, J. H. Beijnen, K. S. Pang, J. Schutrups, R. Tirona, H. J. Keizer, J. H. van Dierendonck, C. J. van der Velde and G. J. Mulder, *Cancer Res.*, 1996, **56**, 4709-4714.

[80] C. F. Huntley, D. S. Hamilton, D. J. Creighton and B. Ganem, *Org. Lett.*, 2000, **2**, 3143-3144.

[81] D. S. Hamilton, Z. Ding, B. Ganem and D. J. Creighton, *Org. Lett.*, 2002, **4**, 1209-1212.

[82] D. S. Hamilton, X. Zhang, Z. Ding, I. Hubatsch, B. Mannervik, K. N. Houk, B. Ganem and D. J. Creighton, *J. Am. Chem. Soc.*, 2003, **125**, 15049-15058.

[83] F. Collu, L. Bonsignore, M. Casu, C. Floris, J. Gertsch and F. Cottiglia, *Bioorg. Med. Chem. Lett.*, 2008, **18**, 1559-1562.

[84] P. Höering and C. C. R. Allen, Project Collaborators, Queens Belfast University.

[85] C. L. Arthurs, K. F. Lingley, M. Piacenti, I. J. Stratford, T. Tatic, R. C. Whitehead and N. S. Wind, *Tetrahedron Lett*., 2008, **49**, 2410-2413.

[86] Cambridge Crystallographic Data Centre, https://www.ccdc.cam.ac.uk/support-and-resources/ccdcresources/workcase_posepred.pdf, (accessed 31st Janurary 2018).

[87] O. Krb, T. Stützle and T. E. Exner, *J. Chem. Inf. Model*., 2009, **49**, 84-96.

[88] A. Karlsson, J. V. Parales, R. E. Parales, D. T. Gibson, H. Eklund and S. Ramaswamy, *Science*, 2003, **299**, 1039-1042.

[89] R. Anjana, M. K. Vaishnavi, D. Sherlin, S. P. Kumar, K. Naveen, P. S. Kanth and K. Sekar, *Bioinfromation*, 2012, **8**, 1220-1224.

[90] E. Cauët, M. Rooman, R. Wintjens, J. Liévin and C. Biot, *J. Chem. Theory Comput.*, 2005, **1**, 472-483.

[91] D. R. Boyd, M. R. J. Dorrity, M. V. Hand, J. F. Malone and N. D. Sharma, *J. Am. Chem. Soc*., 1991, **113**, 666-667.

[92] A. Bondi, *J. Phys. Chem*., 1964, **68**, 441-451.

[93] D. R. Boyd, N. D. Sharma, L. V. Modyanova, J. G. Carroll, J. F. Malone, C. C. R. Allen, J. T. G. Hamilton, D. T. Gibson, R. E. Parales and H. Dalton, *Can. J. Chem*., 2002, **80**, 589-600.

[94] P. Höering, K. Rothschild-Mancinelli, N. D. Sharma, D. R. Boyd and C. C. R. Allen, *J. Mol. Catal. B: Enzym.*, 2016, **134**, 396-406.

[95] J. C. Spain and D. T. Gibson, *Appl. Environ. Microbol.*, 1988, **54**, 1399-1404.

[96] P. Radivojac, Z. Obradovic, D. K. Smith, G. Zhu, S. Vucetic, C. J. Brown, J. D. Lawson and A. K. Dunker, *Protein Sci.*, 2004, **13**, 71-80.

[97] D. R. Boyd, N. D. Sharma, N. I. Bowers, J. Duffy, J. S. Harrison and H. Dalton, *J. Chem. Soc., Perkin Trans 1*, 2000, 1345-1350.

[98] D. R. Boyd, N. D. Sharma, P. B. A. McIntyre, P. J. Stevenson, W. C. McRoberts, A. Gohil, P. Hoering, and C. C. R. Allen, *Adv. Synth. Catal.*, 2017, **359**, 4002-4014.

[99] D. R. Boyd, N. D. Sharma, G. P. Coen, F. Hempenstall, V. Ljubez, J. F. Malone, C. C. R. Allen and J. T. G. Hamilton, *Org. Biomol. Chem.*, 2008, **6**, 3957-3966.

[100] P. Pentlavalli, PhD thesis, Queens Belfast University, 2015.

[101] Molinspiration, http://www.molinspiration.com/cgi-bin/properties, (accessed 27th February 2018).

[102] B. B. Bahule and Y. M. Nandurkar, *IOSR-JAC*, 2012, **3**, 28-29.

[103] R. Hekmatshoar, S. Sajadi and M. M. Heravi, *J. Chin. Chem. Soc.*, 2008, **55**, 616-618.

[104] S. Yasui, K. Nakamura, M. Fujii and A. Ohno, *J. Org. Chem.*, 1985, **50**, 3283-3287.

[105] N. Krause and A. Hoffmann-Röder, *Synthesis*, 2001, **2**, 171-196.

[106] I. H. Escher and A. Pfaltz, *Tetrahedron*, 2000, **56**, 2879-2888.

[107] T. Jerphagnon, M. G. Pizzuti, A. J. Minnard and B. L. Feringa, *Chem. Soc. Rev.*, 2009, **38**, 1039-1075.
[108] M. Sakai, H. Hayashi and N. Miyaura, *Organometallics*, 1997, **16**, 4229-4231.
[109] Y. Takaya, M. Ogasawara and T. Hayashi, *J. Am. Chem. Soc.*, 1998, **120**, 5579-5580.
[110] T. Hayashi, M. Takahashi, Y. Takaya and M. Ogasawara, *J. Am. Chem. Soc.*, 2002, **124**, 5052-5058.
[111] K. Fagnou and M. Lautens, *Chem. Rev.*, 2003, **103**, 169-196.
[112] S. Christou, A. C. Edwards, R. G. Pritchard, P. Quayle, Y. Song, I. J. Stratford, K. F. Williams and R. C. Whitehead, *Tetrahedron*, 2016, **72**, 5433-5443.
[113] U. K. Ohnemüller, C. F. Nising, A. Encinas and S. Bräse, *Synthesis*, 2007, **14**, 2175-2185.
[114] D. R. Boyd, N. D. Sharma, R. Boyle, B. T. McMurray, T. A. Evans, J. F. Malone, H. Dalton, J. Chima and G. N. Sheldrake, *J. Chem. Soc., Chem. Commun.*, 1993, 49-51.
[115] Patrick Höering, Queens Belfast University, 2018.
[116] M. Usher, MChem thesis, University of Manchester, 2016.
[117] D. Mercier, J. Leboul, J. Cleophax and S. D. Gero, *Carbohydr. Res.*, 1971, **20**, 299-304.
[118] V. H. Grewe and E. Nolte, *Justus Liebigs Ann. Chem.*, 1952, **575**, 1-11.
[119] M. Keizo, M. Takuya and N. Keiji, *Heterocycles*, 1998, **48**, 1213-1220.
[120] F. E. Critchfield and E. T. Bishop, *Anal. Chem.*, 1961, **33**, 1034-1035.
[121] A. Flores-Parra, D. M. Gutiérrez-Avella and R. Contreras, *Magn. Reson. Chem.*, 1989, **27**, 544-555.
[122] J. Montchamp, F. Tian, M. E. Hart and J. W. Frost, *J. Org. Chem.*, 1996, **61**, 3897-3899.
[123] S. V. Ley, H. W. M. Priepke and S. L. Warriner, *Angew. Chem., Int. Ed. Engl.*, 1994, **33**, 2290-2292.
[124] N. L. Douglas, S. V. Ley, H. M. I. Osborn, D. R. Owen, H. W. M. Priepke and S. L. Warriner, *Synlett*, 1996, **8**, 793-795.
[125] S. V. Ley, D. K. Baeschlin, D. J. Dixon, A. C. Foster, S. J. Ince, H. W. M. Priepke and D. J. Reynolds, *Chem. Rev.*, 2001, **101**, 53-80.
[126] E. Lence, L. Castedo and C. Gonzalez-Bello, *Chem. Soc. Rev.*, 2008, **37**, 1689-1708.
[127] Z. Wang and Y. Shi, *J. Org. Chem.*, 1997, **62**, 8622-8626.
[128] E. Schenker, *Angew. Chem.*, 1961, **73**, 81-107.
[129] H. Seki, K. Koga, H. Matuso, S. Ohki, I. Matuso and S. Yamada, *Chem. Pharm. Bull.*, 1965, **13**, 995-1000.
[130] V. Dalla, J. P. Catteau and P. Pale, *Tetrahedron Lett.*, 1999, **40**, 5193-5196.
[131] M. S. Brown and H. Rapoport, *J. Org. Chem.*, 1963, **28**, 3261-3263.
[132] R. E. Davis and J. A. Gottbrath, *J. Am. Chem. Soc.*, 1962, **84**, 895-898.
[133] Z. Wang, S. M. Miller, O. P. Anderson and Y. Shi, *J. Org. Chem.*, 1999, **64**, 6443-6458.
[134] B. Sklarz, *Quart. Rev.*, 1967, **21**, 3-28.
[135] D. H. Gupta, P. Hodge and J. E. Davies, *J. Chem. Soc., Perkin Trans. 1*, 1981, 2970-2973.
[136] M. Daumas, Y. Vo-Quang, L. Vo-Quang and F. L. Goffic, *Synthesis*, 1989, **1**, 64-65.
[137] Y. Zhong and T. K. M. Shing, *J. Org. Chem.*, 1997, **62**, 2622-2624.
[138] R. Criegee, L. Kraft and B. Rank, *Eur. J. Org. Chem.*, 1933, **507**, 159-197.
[139] J. E. Audia, L. Boisvert, A. D. Patten, A. Villalobos and S. J. Danishefsky, *J. Org. Chem.*, 1989, **54**, 3738-3740.

[140] M. S. Singh, in *Advanced Organic Chemistry Reaction and Mechanisms*, Dorling Kindersley, Delhi, 1st edn, 2007, ch. 4.4, pp. 136-137.

[141] W. E. Truce, R. W. Campbell and J. R. Norell, *J. Am. Chem. Soc.*, 1964, **86**, 288-288.

[142] J. F. King, J. Y. L. Lam and S. Skonieczny, *J. Am. Chem. Soc.*, 1992, **114**, 1743-1749.

[143] D. M. Knapp, E. P. Gillis and M. D. Burke, *J. Am. Chem. Soc.*, 2009, **131**, 6961-6963.

[144] Y. Wang, Masters in Research thesis, University of Manchester, 2016.

[145] T. Hayashi, *Synlett*, 2001, **0**, 879-887.

[146] C. Navarro, A. Moreno and A. G. Csákÿ, *J. Org. Chem.*, 2009, **74**, 466-469.

[147] G. de la Herán, M. Mba, M. C. Murcia, J. Plumet and A. G. Csákÿ, *Org. Lett*., 2005, **7**, 1669-1671.

[148] U. K. Ohnemüller, C. F. Nising, A. Encinas and S. Bräse, *Synthesis*, 2007, **14**, 2175-2185.

[149] A. S. Kireev, M. Manpadi and A. Kornienko, *J. Org. Chem.*, 2006, **71**, 2630-2640.

[150] E. J. Corey and N. W. Boaz, *Tetrahedron Lett.*, 1985, **26**, 6015-6018.

[151] D. E. Frantz and D. A. Singleton, *J. Am. Chem. Soc.*, 2000, **122**, 3288-3295.

[152] S. Christou, E. Ozturk, R. G. Pritchard, P. Quayle, I. J. Stratford, R. C. Whitehead and K. F. Williams, *Bioorg. Med. Chem. Lett*., 2013, **23**, 5066-5069.

[153] K. Ayton, MChem thesis, University of Manchester, 2015.

[154] A. A. Wiles, MPhil thesis, University of Manchester, 2010.

[155] M. K. Nielsen, C. R. Ugaz, W. Li and A. G. Doyle, *J. Am. Chem. Soc.*, 2015, **137**, 9571-9574.

[156] F. Zirilli, MChem Thesis, University of Manchester, 2018.

[157] R. Adams, University of Manchester, 2017, Personal Communication.

[158] K. F. Williams, *PhD Thesis*, University of Manchester, 2012.

[159] K. Morita, Z. Suzuki and H. Hirose, *Bull. Chem. Soc., Jpn.*, 1968, **41**, 2815-2815.

[160] A. B. Baylis and M. E. D. Hillman, German Pat., 6803364, 1968.

[161] H. M. R. Hoffmann and J. Rabe, *J. Angew. Chem., Int. Ed. Engl.*, 1983, **22**, 795-796.

[162] V. K. Aggarwal, S. Y. Fulford and G. C. Lloyd-Jones, *Angew. Chem., Int. Ed*., 2005, **44**, 1706-1708.

[163] K. E. Price, S. J. Broadwater, H. M. Jung and D. T. McQuade, *Org. Lett.*, 2005, **7**, 147-150.

[164] J. S. Hill and N. S. Isaacs, *J. Phys. Org. Chem*., 1990, **3**, 285-288.

[165] G. W. Amarante, H. M. S. Milagre, B. G. Vaz, B. R. Vilachâ Ferreira, M. N. Eberlin and F. Coelho, *J. Org. Chem*., 2009, **74**, 3031-3037.

[166] F. Rezgui and M. M. El Gaïed, *Tetrahedron Lett*., 1998, **39**, 5965-5966.

[167] K. Y. Lee, J. H. Gong and J. N. Kim, *Bull. Korean Chem. Soc.*, 2002, **23**, 659-660.

[168] R. Gatri and M. M. El Gaïed, *Tetrahedron Lett*., 2002, **43**, 7835-7836.

[169] A. Porzelle, C. M. Williams and B. D. Schwartz, *Synlett*, 2005, **19**, 2923-2926.

[170] E. Piers, J. R. Grierson, C. K. Lau and I. Nagakura, *Can. J. Chem*., 1982, **60**, 210-223.

[171] A. E. Pohland and W. R. Benson, *Chem. Rev*., 1966, **66**, 161-197.

[172] Y. Tamura, T. Miyamoto, T. Nishimura, J. Eiho and Y. Kita, *J. Chem. Soc., Perkin Trans. 1*, 1974, 102-104.

[173] F. A. Cotton and P. A. Kibala, *J. Am. Chem. Soc.*, 1987, **109**, 3308-3312.

[174] D. J. Procter and B. Ruscoe, University of Manchester, 2016, Personal Communication.

[175] J. V. Comasseto, L. W. Lo and N. Petragnani, *Tetrahedron*, 1997, **53**, 7445-7460.

[176] P. Schäfer, T. Palacin, M. Sidera and S. P. Fletcher, *Nat. Commun*., 2017, **8**, 1-8.

[177] R. Jana, T. P. Pathak and M. S. Sigman, *Chem. Rev*., 2011, **111**, 1417-1492.

[178] C. Studte and B. Breit, *Angew. Chem. Int. Ed.*, 2008, **47**, 5451-5455.

[179] T. Mosmann, *J. Immunol. Methods*, 1983, **65**, 55-63.

[180] F. Denizot and R. Lang, *J. Immunol. Methods*, 1986, **89**, 271-277.

[181] J. Carmichael, W. D. DeGraff, A. F. Gazdar, J. D. Minna and J. B. Mitchell, *Cancer Res.*, 1987, **47**, 936-942.

[182] N. Robertson, I. J. Stratford, S. Houlbrook, J. Carmichael and G. E. Adams, *Biochem. Pharmacol.*, 1992, **44**, 409-412.

[183] A. Russo, W. DeGraff, N. Friedman and J. B. Mitchell, *Cancer Res*., 1986, **46**, 2845-2848.

[184] R. Bloch, *Chem. Rev*., 1998, **98**, 1407-1438.

[185] J. Schulz, M. W. Beaton and D. Gani, *J. Chem. Soc., Perkin Trans.*, 2000, **1**, 943-954.

[186] B. M. Trost and A. G. Romero, *J. Org. Chem.*, 1986, **51**, 2332-2042.

[187] H. Kawashima, M. Sakai, Y. Kaneko and Y. Kobayashi, *Tetrahedron*, 2015, **71**, 2387-2392.

[188] J. E. Audia, L. Boisvert, A. D. Patten, A. Villalobos and S. J. Danishefsky, *J. Org. Chem.*, 1989, **54**, 3738-3740.

[189] M. T. Barros, C. D. Maycock and M. R. Ventura, *J. Org. Chem.*, 1997, **62**, 3984-3988.

[190] C. Alves, M. T. Barros, C. D. Maycock and M. R. Ventura, *Tetrahedron*, 1999, **55**, 8443-8456.

[191] M. T. Barros, C. D. Maycock and M. R. Ventura, *J. Chem. Soc., Perkin Trans.*, 2001, **1**, 166-173.

[192] D. A. Archer and B. W. Singer, *J. Chem. Soc., Perkin Trans. 1*, 1976, **0**, 2484-2488.

[193] M. Shibuya, M. Tomizawa and Y. Iwabuchi, *Org. Lett.*, 2008, **10**, 4715-4718.

[194] R. Yuan, D. Zhao, L. Zhang, X. Pan, Y. Yang, P. Wang, H. Li and C. Da, *Org. Biomol. Chem.*, 2016, **14**, 724-728.

[195] J. A. Gautier, *Compt. Rend.*, 1948, **226**, 1736-1738

[196] M. J. Haren, R. Taig, J. Kuppens, J. S. Torano, E. E. Moret, R. B. Parsons, D. Sartini, M. Emanuelli and N. I. Martin, *Org. Biomol. Chem.*, 2017, **15**, 6656-6667.

[197] M. Soetens, R. Drouet and O. Riant, *ChemCatChem*, 2017, **9**, 929-933.

[198] W. Vishniac and M. Santer, *Bacteriol Rev.*, 1957, **21**, 195-213.